Characterization of the Conformational States of Phospholamban and their Roles in Regulation of SR Calcium-ATPase

A Dissertation
SUBMITTED TO THE FACULTY OF
UNIVERSITY OF MINNESOTA
BY

Bengt Martin Gustavsson

IN PARTIAL FULFILLMENT OF THE REQUIREMENTS
FOR THE DEGREE OF
DOCTOR OF PHILOSOPHY

Adviser

Dr. Gianluigi Veglia

December 2012

Acknowledgements

First of all, I would like to thank my advisor, Dr. Gianluigi Veglia. Since the day I joined his lab he has been an excellent mentor. His support and constant excitement for research has inspired me to always strive to be a better scientist.

I would also thank all the past and present members of the Veglia group who have made the last five years a great experience. Especially Frank Chao, T. Gopinath, Kim Ha, Larry Masterson, Kaustubh Mote, Nate Traaseth and Raffaello Verardi. I thank them for all the discussions, collaborations and helpful comments.

Thanks to our collaborators in the Thomas lab for being helpful through discussions and sharing of protocols and instrumentation.

Finally, I would like to thank the people that have supported me outside the lab. My parents, grand-parents, siblings and nephews have always encouraged me to do what I want to do even when I decided to move all the way to Minnesota.

Last but not least, I thank Tina for always being there for me.

Abstract

Membrane proteins constitute 30% of the human genome but represent only a small fraction of the known three-dimensional protein structures. In this thesis I describe the characterization of the membrane protein complex between sarcoplasmic reticulum Ca^{2+}-ATPase (SERCA) and phospholamban (PLN). SERCA drives cardiac muscle relaxation by active transport of Ca^{2+} ions into the SR. PLN is a small membrane protein that consists of a helical trans-membrane domain connected to a cytoplasmic domain through a short loop, and inhibits SERCA through intra-membrane interactions. The cytoplasmic domain of PLN is in equilibrium between a helical, membrane-associated T state and an unfolded, membrane-dissociated R state. Here, I summarize the work to probe the structures of the T and R states and elucidate the role of the conformational equilibrium in regulation of SERCA. Using solution and solid state NMR in combination with biochemical assays I show that the structures of T and R state but not their relative populations are conserved in different lipid environments and sample conditions. Furthermore, the T/ R equilibrium has a central role in SERCA regulation and is crucial to relieve the inhibition of the enzyme. These findings provide new insights into SERCA/PLN function and offer a unique view of the role of conformational equilibria and multiple conformational states in membrane protein structure and function.

Table of contents

List of tables

List of figures

Chapter 1 - Introduction

Chapter 2 - Lipid-Mediated Folding/Unfolding of Phospholamban Cytoplasmic Domains as a Regulatory Mechanism for the Sarcoplasmic Reticulum Ca2+-ATPase

Chapter 1 - Introduction

1.1 Lipid membranes

Cells and organelles are surrounded by self-assembled phopsholipid bilayers referred to as membranes. Membranes create a barrier to the outside environment and are the site of many important cellular processes such as oxidative phosphorylation, photosynthesis and signaling. The majority of these functions are carried out by membrane proteins that are associated with or span the membrane bilayer. According to the classic “fluid mosaic model”, membranes can be depicted as two-dimensional entities where lipids and proteins can diffuse freely (1) (**Figure 1**). This view has later been challenged by the discovery of microdomains within the membrane of lipids and proteins referred to as “lipid rafts” and multiple anchoring interactions between membrane-associated proteins and the cell cytoskeleton (2). The lipid composition of the membrane varies between different organelles and organisms. For example, the eukaryotic endoplasmic reticulum (ER) membrane has an average chain length of ~18 carbons and is composed mainly of lipids with phosphocholine (PC) and phosphoethanolamine (PE) head groups while the most abundant lipids in yeast cell membranes are phosphoinositol (PI), phosphoserine (PS) and sphingomyelin (3).

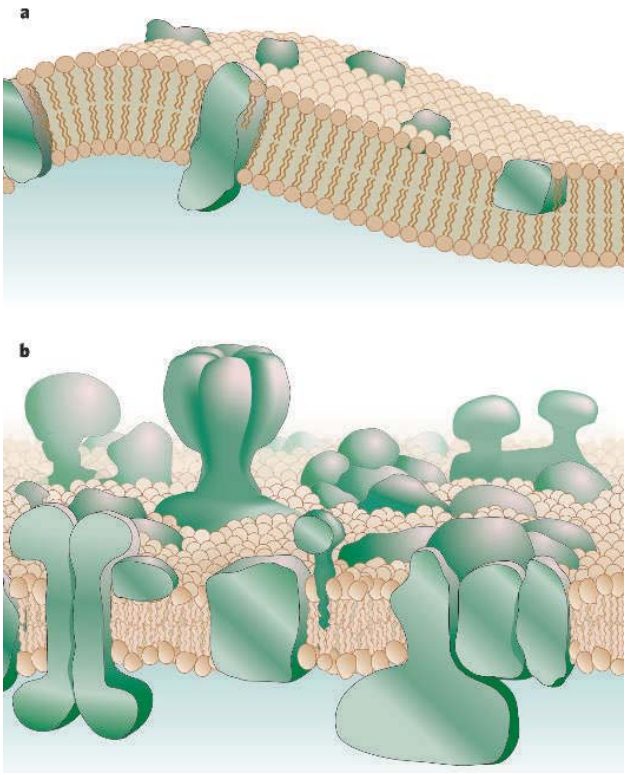

Figure 1. Fluid mosaic model of lipid membranes. *A.) Original model proposed by Singer et al.* (1) *B.) Revised model by Engelman*(2)*. Figure adapted from Engelman* (2)*.*

1.2 Membrane proteins

Membrane proteins constitute ~30% (4) of the proteins in the human genome and more than 50% of the available drug targets (5). Integral membrane proteins span the membrane bilayer one or several times either as β-strands or as trans-membrane (TM) α-helices. 8 to 24 β-strands fold into cylindrical β-barrels with hydrogen bonds between adjacent strands and hydrophilic side chains lining the inside of the barrel (6) (**Figure 2A**). This creates a hydrophilic pore through the bilayer and β-barrels mediate transport of compounds through the outer periplasmic membrane of prokaryotes and the outer membranes of mitochondria and chloroplasts of eukaryotic cells. Proteins with TM α-helices account for the rest of the integral membrane proteins (**Figure 2B**). They range from single-spanning, hydrophobic helices to multi-helical structures with as as many as 20 TM helices that form channels or other functional units (7). Helical TM domains have an abundance of amino acids with hydrophobic side chains, especially Val, Ile and Leu.

TM helices can therefore often be identified from the primary sequence of a protein due to the relative hydrophobicity of its amino acids (7).

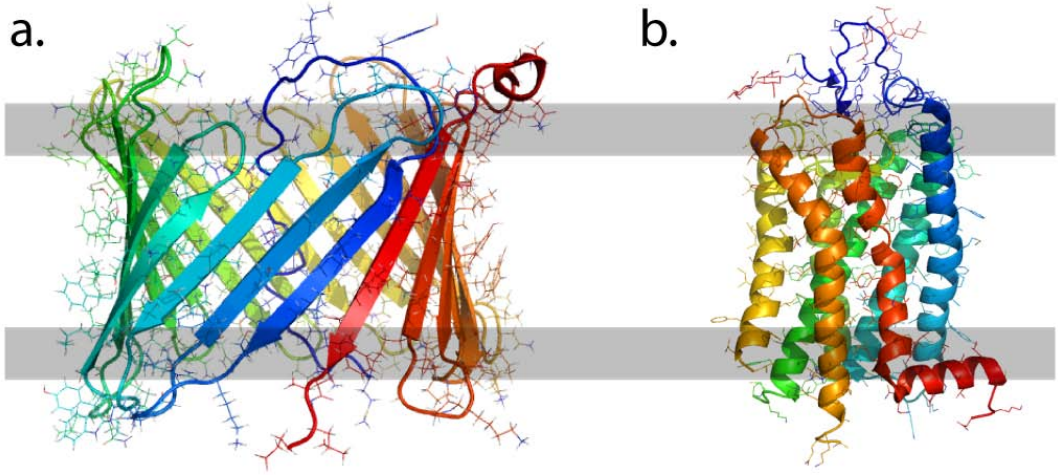

Figure 2. Membrane protein structures. *A.) β-barrel exemplified by the voltage-gated anion channel (VDAC) (PDB ID 2K4T). B.) α-helical rhodopsin with the typical seven TM helix fold of G-protein coupled receptors (PDB ID 1F88).*

In the last few decades there has been a near exponential growth of the number of protein structures deposited in the protein database, which currently contains ~80000 protein structures (www.pdb.org). However, membrane proteins make up only ~2% of these, and there are only ~ 300 unique membrane protein structures (http://blanco.biomol.uci.edu/membrane_proteins_xtal.html). The reason for the discrepancy between the number of membrane protein structures and the total number of known structures is that membrane proteins present a number of experimental challenges. They are typically difficult to over-express and frequently form inclusion bodies that are complicated to refold to regain the native three-dimensional protein structure. In addition, membrane proteins require a membrane-mimicking environment such as a micelle or a lipid bilayer to be solubilized. Solution nuclear magnetic resonance (NMR) and X-ray crystallography cannot be performed in lipid bilayers. Therefore, these techniques, which together contributed more than 99% of the structures in the PDB, are typically performed with proteins reconstituted into detergent micelles. Studies of detergent-solubilized protein have produced a number of groundbreaking results such as crystal structures of ion channels (8), G protein coupled receptors

(GPCRs) (9, 10) and translocons (11) and solution NMR structures of polytopic membrane proteins such as voltage-dependent anion channel VDAC (12), uncoupling protein 2 (13) and DsbB (14). However, detergent micelles are a poor mimic of the native membrane environment and can interfere with both protein structure and function. In contrast to solution NMR and X-ray crystallography, solid state NMR (ssNMR) experiments can be acquired in lipid bilayers and even whole cells (15). Thanks in part to this unique property, ssNMR has developed as a powerful tool to obtain high resolution structural information of membrane proteins in their natural environment (16, 17).

1.3 NMR spectroscopy

Certain atomic nuclei possess a spin and can therefore populate different spin states. In a magnetic field these states have degenerate energies, leading to a distribution of spins between the states according to the Boltzmann distribution. The excitation, manipulation and detection of nuclear spins form the basis of NMR spectroscopy. The two main NMR techniques are solution NMR and ssNMR. An important difference between these techniques is the nature of the samples. Solution NMR samples are characterized by molecules that tumble rapidly in solution, for example small soluble proteins. ssNMR samples, on the other hand, have restricted motion, such as fibrillar proteins or a membrane proteins in bilayers. The motional differences have significant effects on NMR observables such as chemical shifts and dipolar couplings. As a consequence, solution NMR and ssNMR differ both in the nature of the experiments and the information that can be obtained from them.

1.3.1 Chemical shifts

The electrons surrounding a nucleus give rise to magnetic fields that can either increase or decrease the static field of the NMR magnet. Each nucleus therefore experiences a local, “induced” field (B_{ind}) that is slightly different than the global field B_0. This effective magnetic field can be approximated as (18):

$$B_{ind} = \delta B_0$$

Where δ is a 3*3 matrix that is referred to as the chemical shift tensor and is different for each nucleus. The rapid molecular tumbling of a solution NMR sample gives isotropic chemical shift according to:

$$\delta_{iso} = \frac{\delta_{11} + \delta_{22} + \delta_{33}}{3}$$

Where δ_{11}, δ_{22} and δ_{33} represent the diagonal elements of the chemical shift tensor and are referred to as principal values (18). Under these conditions the chemical shift has no orientation-dependence and is sensitive to the local environment of the nucleus. For example, isotropic chemical shifts of C_α nuclei are excellent probes of secondary structure. In ssNMR samples, chemical shift are not motionally averaged and thus orientation-dependent. ssNMR therefore requires specific methods to acquire high resolution spectra but can also provide information about the orientation of molecules in a sample (see section 1.3.4).

1.3.2 Dipolar couplings

Nuclear spins act as magnetic dipoles that generate magnetic fields in the space surrounding the nucleus. The interactions between neighboring nuclei give rise to dipolar couplings that are fundamental in NMR experiments and generally provide the main contribution to relaxation of the NMR signal. Under the secular approximation, the heteronuclear dipolar coupling (D_{IS}) between two spins I and S is

$$D_{IS} = -\frac{\mu_0 \gamma_I \gamma_S \hbar}{4\pi r_{IS}^3}\left(\frac{3\cos^2\theta_{IS} - 1}{2}\right)$$

where θ_{IS} is the angle that the I-S bond vector makes with respect to the magnetic field, γ_I and γ_S are the gyromagnetic ratios of the two spins and r_{IS} is the inter-nuclear distance. In solution NMR samples, molecules tumble rapidly in solution, leading to motional averaging of the dipolar couplings to zero and sharp peaks in the NMR spectrum. Still, their distance-dependence makes dipolar couplings very important in solution NMR since non-secular parts of the dipolar coupling give rise to the nuclear Overhauser effect (nOe), which is the central tool for structure determination of proteins by solution NMR. ssNMR samples have restricted motion and thus non-zero dipolar couplings. Therefore,

ssNMR experiments generally utilize dipolar couplings to transfer magnetization by cross-polarization transfers that satisfy the Hartmann-Hahn condition

$$\gamma_I B_{1,I} = \gamma_S B_{1,S}$$

where $B_{1,I}$ and $B_{1,S}$ are the applied radio-frequency fields on nuclei I and S, respectively. In ssNMR, dipolar couplings are also frequently used to get information about both orientation and inter-nuclear distances (see section 1.3.4).

1.3.3 Paramagnetic relaxation enhancement

Due to the large gyromagnetic ratio of the electron, unpaired electrons give rise to local magnetic fields of significantly larger magnitude than those arising from nuclei. The dipolar interactions with these paramagnetic centers give increased relaxation rates of NMR signals and increased line widths of the peaks in the NMR spectrum (**Figure 3**). This effect, often referred to as paramagnetic relaxation enhancement (PRE), can be used to probe distances up to ~30Å. PRE has therefore evolved as an important complement to the nOe, which is limited to distances ~6Å, in structure determination of proteins. PRE has been implemented together with other restraints to determine structures of soluble proteins (19) and membrane proteins (13, 20) by solution NMR. Recent studies have also extended this method to structure determination of small microcrystalline proteins by ssNMR (21).

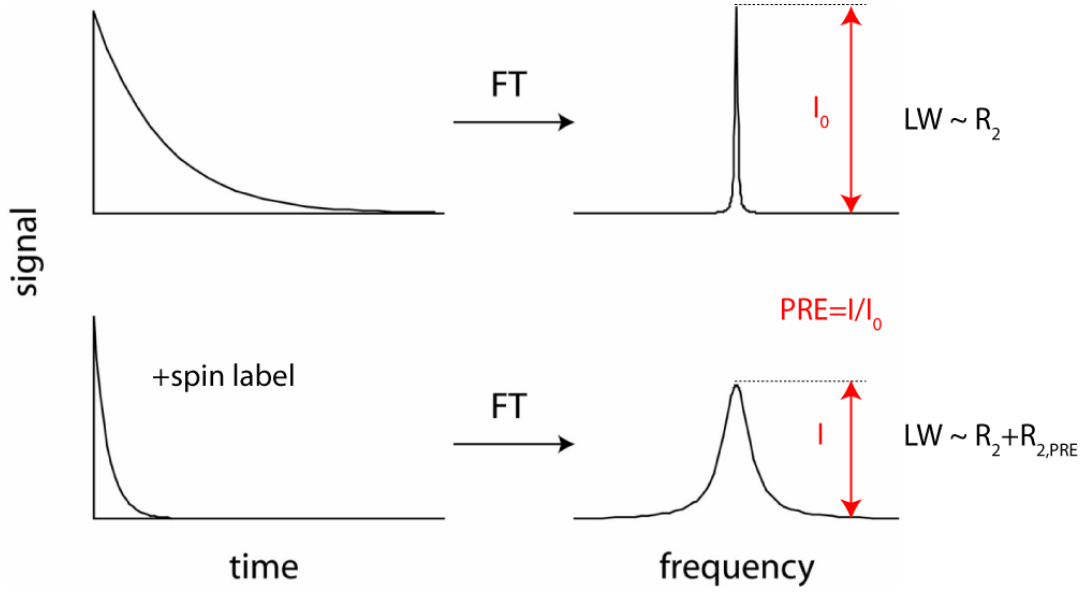

Figure 3. Paramagnetic relaxation enhancement. *Effect of spin label on NMR signal in the time domain and frequency domain. LW refers to the line width at half height.*

1.3.4 Solid state NMR

A crucial feature of a solution NMR sample is a rapid molecular reorientation with rotational correlation times on the ns time scale. Detergent-solubilized membrane proteins tumble rapidly in solution. This gives dipolar couplings that are motionally averaged to zero and the chemical shift take an isotropic value. Lipid vesicles typically have correlation times of several μs. Under these conditions the dipolar couplings and chemical shifts are orientation-dependent, which leads to broad powder patterns that represent all possible orientations of each nucleus in the sample (**Figure 4**).

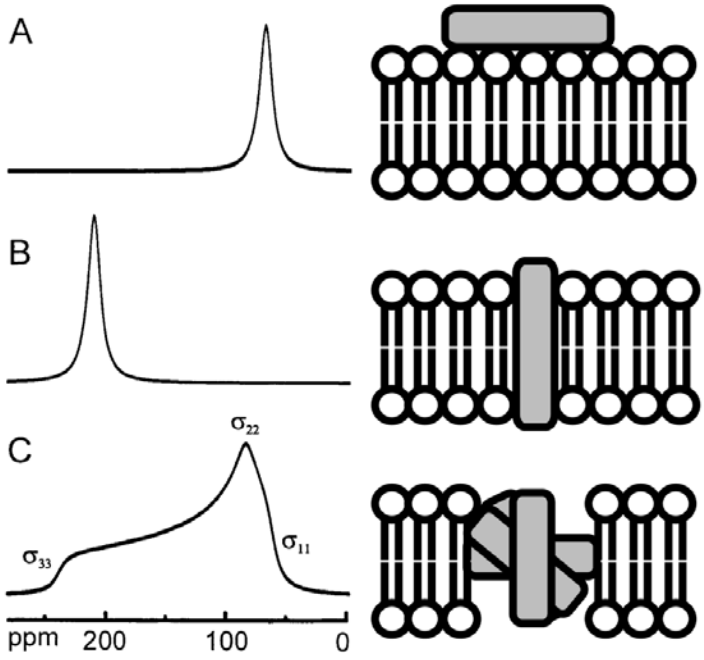

Figure 4. O-ssNMR of membrane proteins. *A.) and B.) Simulated spectra of an aligned TM helix with a single ^{15}N label. C.) Characteristic powder pattern of an unaligned protein.*

Thus, solution NMR experiments cannot be performed in lipid vesicles and ssNMR is the NMR method of choice for membrane proteins in lipid bilayers. ssNMR utilizes two main techniques, oriented ssNMR (O-ssNMR) and magic angle spinning (MAS) ssNMR, to produce high resolution spectra.

O-ssNMR: In O-ssNMR all molecules in the sample have a uniform alignment with respect to the static magnetic field of the magnet. As a consequence each nucleus gives rise to one peak in the NMR spectrum, and the position of the peak is orientation-dependent. The uniform alignment can be achieved by “mechanical alignment” where protein-containing lipid bilayers are stacked between thin glass slides. Alternatively, the sample can be oriented by “magnetic alignment” where proteins are reconstituted into bicelles, which are a mixture between short-chain and long-chain lipids that form a liquid crystalline phase and align spontaneously in a strong magnetic field. Orientation-dependent NMR observables offer a unique opportunity to orient membrane proteins in the lipid membrane. For example, the chemical shift of the amide nitrogen in a peptide bond is given by:

$$\delta_I = (\delta_{33} - \delta_{11}) \sin^2 \beta \cos^2(\alpha - 17) + (\delta_{11} - \delta_{22}) \sin^2 \beta + \delta_{22}$$

where the angles α and β are defined according to **figure 5** and the principal values of the chemical shift tensor are δ_{11} = 64 ppm, δ_{22} = 77 ppm, and δ_{33} = 225 ppm. The N-H dipolar coupling is:

$$D_{HN} = -\frac{\mu_0 \gamma_H \gamma_N \hbar}{4\pi r_{HN}^3} \left(\frac{3\cos^2 \theta_{HN} - 1}{2} \right)$$

where θ_{HN} is defined as the angle between the H-N bond vector and the magnetic field B_0 and r_{HN} is the distance between the amide nitrogen and amide proton.

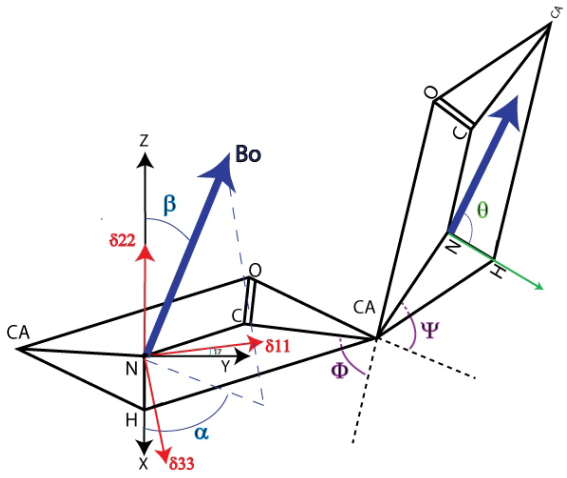

Figure 5. Principal components of the ^{15}N chemical shift tensor with respect to the peptide plane.

The orientation-dependence of NMR observables is frequently utilized in two-dimensional separated local field (SLF) experiments, such as the Polarization Inversion Spin Exchange at Magic Angle (PISEMA) experiment, that correlate chemical shifts and dipolar couplings. TM helices have 3.6 residues per helical turn and give rise to characteristic polarity indexed slant angle (PISA) wheels in the spectra with 3.6 peaks per turn of the wheel. The size and position of the PISA wheel is directly correlated to the angle between the helical axis and the bilayer normal and can therefore be utilized to orient the helix in the membrane (**Figure 6**). O-ssNMR has provided backbone structures of several membrane-spanning proteins (22, 23). In addition, a hybrid approach where O-ssNMR is combined with solution NMR in micelles has recently produced all-atom high resolution structures of both monomeric and pentameric forms of the membrane protein phospholamban (PLN) (24, 25).

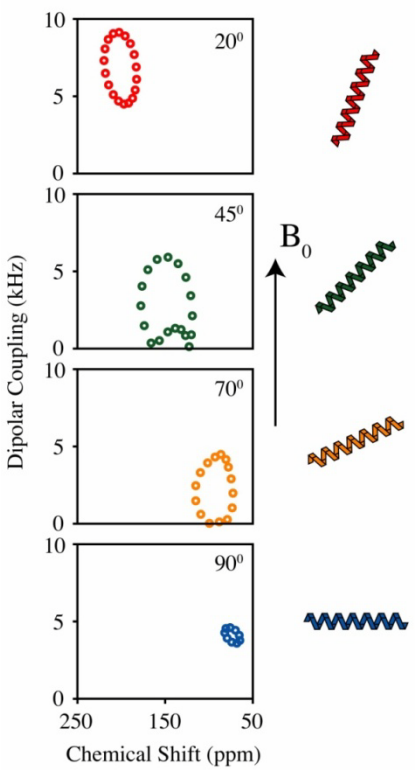

Figure 6. PISEMA spectra at different orientations of an α-helix.

MAS-ssNMR: In MAS-ssNMR, high resolution spectra are produced by spinning the sample around an axis which makes a 54.7° "magic" angle with respect to the magnetic field. The spinning averages out the secular contributions of the dipolar coupling and chemical shift, which gives isotropic chemical shifts and zero dipolar couplings (**Figure 7**) since

$$D_{IS} = -\frac{\mu_0 \gamma_I \gamma_S \hbar}{4\pi r_{IS}^3}\left(\frac{3\cos^2 54.7° - 1}{2}\right) = 0$$

There are a growing number of multidimensional MAS-ssNMR experiments that can be used for assignment of chemical shifts, measurement of inter-nuclear distances and internal dynamics (16, 17). MAS-ssNMR has been used to determine high resolution structures of micro-crystallized, soluble proteins like the α-spectrin SH3 domain (26) and ubiquitin (27). Notable MAS studies for membrane proteins include probing the mechanism of potassium channel (KcsA) gating (28), determining structure of the M2 channel of influenza virus (29), and recently the backbone structure determination of the GPCR CXCR1 in combination with molecular modeling (30).

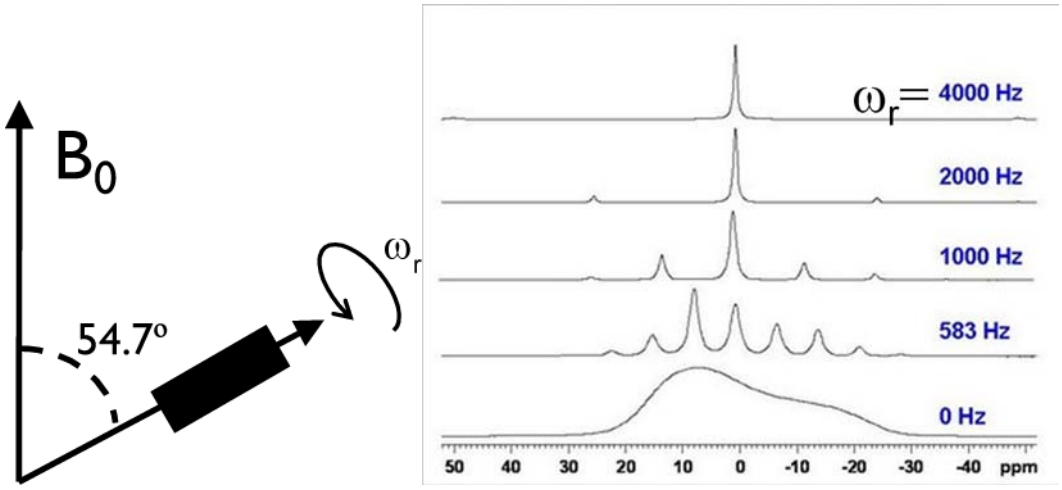

Figure 7. Magic angle spinning. ω_b *refers to the spinning frequency of the MAS rotor.*

1.3.5 Membrane environments

ssNMR experiments can be acquired in a range of different bilayer systems that can be tailored to mimic the lipid composition of native lipid membranes (**Figure 8**). MAS-ssNMR allows for total flexibility in sample lipids and can be performed at a wide range of temperatures. For example, a recent study used lipids that mimic viral membranes to study the M2 channel of influenza virus (31). Similarly, mechanically O-ssNMR experiments can be performed in a range of bilayer conditions. Bicelles, on the other hand, are limited to certain mixtures of long and short-chain lipids. The long-chain lipids need to have predominantly saturated chains and a PC head group even if a portion can be exchanged with a lipid with a different head group and chain saturation. The choice of short-chain lipid is less stringent and several detergents including 1,2-dihexanoyl-glycero-3-phosphocholine (DHPC), dodecylphosphocholine (DPC), Triton X-100 and 3-[(3-Cholamidopropyl)dimethylammonio]-2-hydroxy-1-propanesulfonate (CHAPSO) can be utilized for bicelle formation. In addition, the q value, which is defined as the molar ratio of long chain to short chain lipid, needs to be sufficiently large (usually >3) to achieve alignment. A major advantage of bicelles compared to mechanically aligned bilayers is that the sample conditions (i.e pH, salt concentration) can be easily controlled (32). Bicelles have been successfully utilized to align a number of membrane proteins with as many as seven TM domains (33).

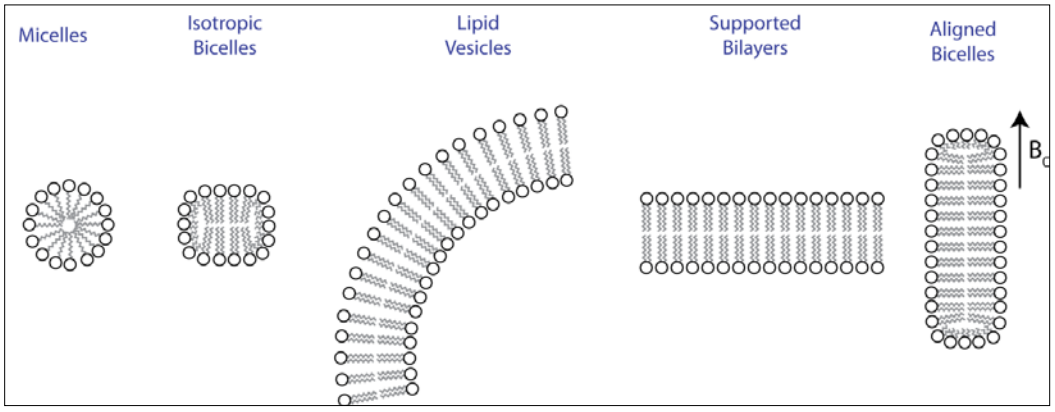

Figure 8. Membrane environments for NMR experiments.

1.4. Cardiac muscle physiology and pathophysiology

Cardiac muscle contraction is initiated by a calcium induced calcium release mechanism where depolarization of the sarcolemma membrane triggers an opening of voltage gated Ca^{2+} channels and a subsequent influx of extra-cellular Ca^{2+} ions into the cytoplasm of the cardiomyocyte (**Figure 9**). Ca^{2+} binds to ryanodine receptors (RyR) in the sarcoplasmic reticulum (SR) membrane causing them to open and release a larger amount of Ca^{2+}. Binding of Ca^{2+} to troponin C causes a conformational rearrangement that allows actin and myosin to interact and produce force. For muscle relaxation the Ca^{2+} levels must be lowered and this is achieved either by transport out of the cell through Ca^{2+}/Na^{+} exchangers (NCX) or by transport into the SR by SR Ca^{2+}-ATPase (SERCA). The latter mechanism is responsible for ~60% of the Ca^{2+} depletion. SERCA is inhibited by PLN, which is present in molar excess of SERCA in the SR membrane (34). Extracellular stimuli of the β-adrenergic receptors leads to raised cAMP levels that triggers protein kinase A (PKA) to phosphorylate PLN and several other proteins that are involved in Ca^{2+} handling (35). Phoshorylation of PLN relieves the inhibition of SERCA and lead to more efficient muscle relaxation (36).

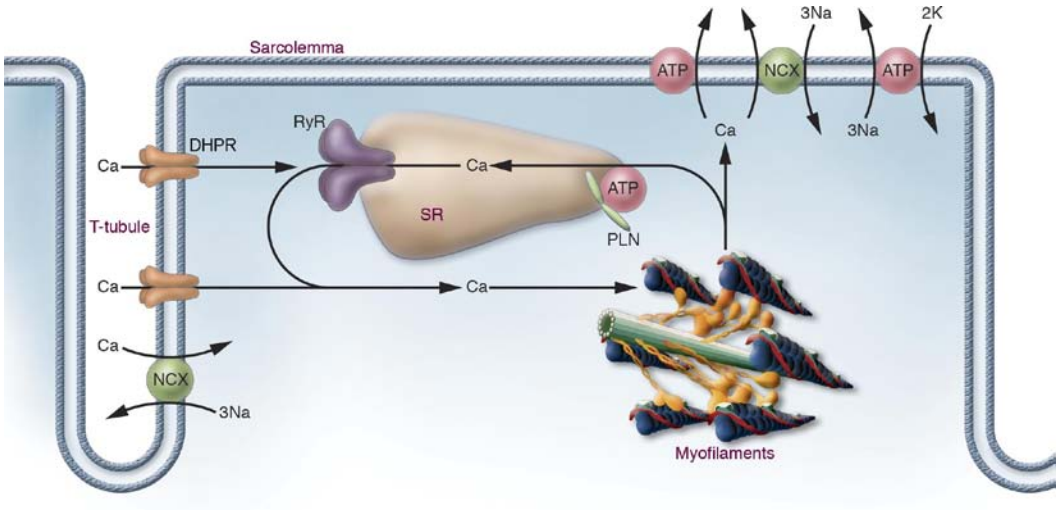

Figure 9. Schematic of a cardiomyocyte, *adapted from Davis et al.* (35) *SERCA is referred to as ATP.*

Defective Ca^{2+} handling in the cardiomyocyte leads to a pathophysiological condition. For example, a reduction of SERCA expression is associated with chronic heart failure, where the heart is unable to pump enough blood to satisfy the demands of the body

(37). Heart failure is one of the leading causes of death in the world and affects more than 2% of the population in the United States (38). Several studies have shown that increasing SERCA activity can restore cardiac muscle function to relieve the effects of heart failure (39). To this end, there are currently three separate clinical trials that utilize adeno-associated virus (AAV) to over-express SERCA and thereby increase the total Ca^{2+} transport into the SR (37). One of the studies reported positive results of phase I trials and also recently of phase II trials (40).

Another approach to increase SERCA activity is by modulation of PLN function. This has been done by decreasing PLN expression using antisense RNA (41) or by delivering a pseudophosphorylated form of PLN where a Ser 16 to Glu (S16E) mutation mimics PKA-mediated phosphorylation. S16E-PLN competes with endogenous PLN for binding to SERCA and this approach has been successfully applied to heart failure animal models (42).

1.5 SERCA and PLN

1.5.1 SERCA

SERCA is a 110 kDa membrane protein that hydrolyses ATP to transport Ca^{2+} ions into the SR against a concentration gradient. SERCA is a P-type ATPase that is present in several isoforms where SERCA1a is the most prevalent in skeletal muscle and SERCA2a in cardiac muscle (43). The enzyme consists of a helical TM and three cytoplasmic domains: actuator (A), nucleotide (N) and phosphorylation (P) domains. ATP binds to the N domain, which results in autophosphorylation of D351 in the P domain, forming a high energy bond that provides the energy to transport two Ca^{2+} ions into the lumen of the SR along with counter-transport of two H^+ ions (44, 45). Several crystal structures have been solved of SERCA, capturing different stages of the enzymatic cycle. Specifically, SERCA populates two major conformational states: the E2 state with low Ca^{2+} affinity (46) and the E1 state with high affinity for Ca^{2+} (47). The structures show that SERCA undergoes major conformational changes in the cytoplasmic domain in the transition between different conformational states (**Figure 10**). However, spectroscopic as well as computational studies have concluded that some crystal structures likely capture extreme conformational states that are not significantly

populated in a membrane environment (48-50). Also, considering the high intracellular nucleotide concentration, the crystal structure of the E1:Ca^{2+} state, which has an open structure with large separation between A and P/N domains, is likely not physiologically relevant (45).

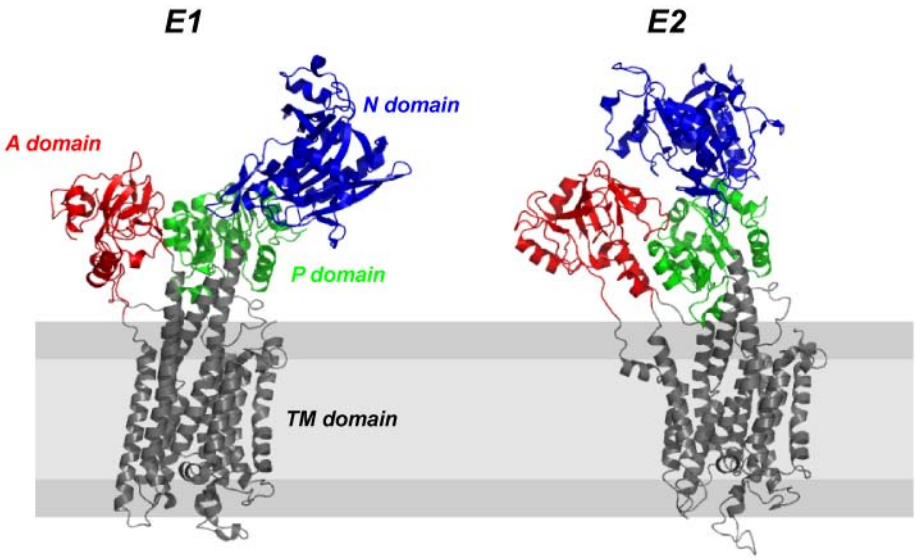

Figure 10. X-ray crystallography structures of SERCA in E1 (induced by high Ca^{2+} concentration) and E2 (induced by presence of the inhibitor thapsigargin) states.

1.5.2 PLN

PLN is a small membrane-spanning protein that is present at a ~5-fold excess to SERCA in the SR membrane of cardiac muscle (34, 51). PLN is present in equilibrium between monomeric and pentameric forms where the monomer binds and regulates SERCA and the pentamer is thought to act as a storage form (52, 53). PLN inhibits SERCA by reducing the Ca^{2+} affinity of the enzyme (Figure 11). The inhibition is relieved by phosphorylation of PLN at S16 by PKA or at T17 by Calmodulin-dependent kinase II (36).

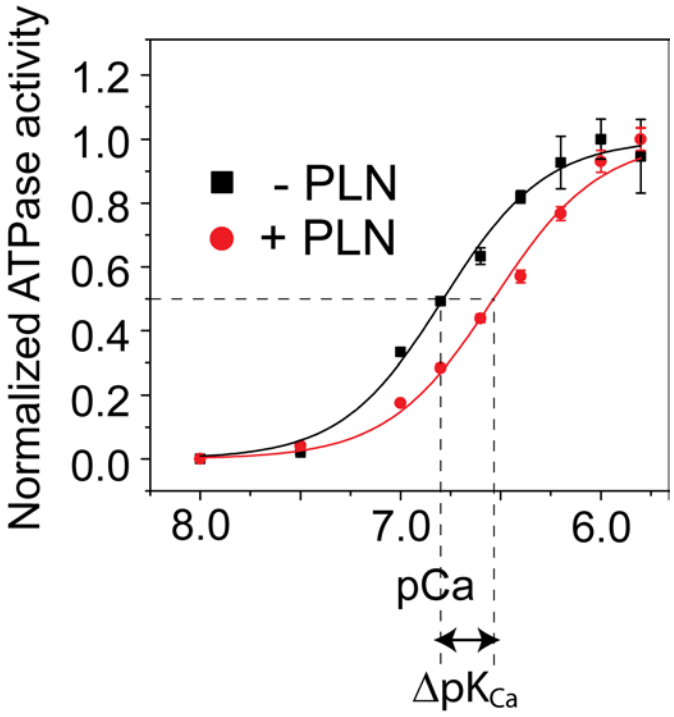

Figure 11. Inhibition of SERCA by PLN. *Normalized ATPase activity of SERCA as a function of Ca^{2+} concentration. Half V_{max} is reached at a higher Ca^{2+} concentration in the presence of PLN and the shift is measured as ΔpK_{Ca}.*

The structure of pentameric as well as monomeric PLN consists of a TM helix connected to a cytosplasmic domain by a short loop (24, 25) (**Figure 12**). The TM domain can be divided into the very hydrophobic domain II (residues 31-52), which resides in the hydrocarbon region of the bilayer and the more hydrophilic domain Ib (residues 23-30), which makes several contacts with the lipid head groups. The cytoplasmic domain, also referred to as domain Ia, contains the two phosphorylation sites, S16 and T17. The structure of domain Ia has been controversial. Initial solution NMR studies in organic solvent and detergent micelles reported an α-helical structure attached to the micelle surface (54, 55) while ssNMR studies in lipid bilayers suggested that domain Ia is unfolded and membrane dissociated (56). Furthermore, a study of pentameric PLN in detergent micelles determined domain Ia to be helical and oriented parallel to the proposed bilayer normal (57). More recently, NMR, electron paramagnetic resonance (EPR) and fluorescence resonance energy transfer (FRET) studies have concluded that in pentameric as well as monomeric PLN domain Ia is in equilibrium between a

membrane-associated, α-helical T state and a membrane-dissociated, unfolded R state, thus resolving the apparent discrepancy from the initial structural studies (58-60) (**Figure 12**). The T state is the dominating conformation in dodecylphosphocholine (DPC) micelles and 1,2-dioleoyl-glycero-3-phosphocholine (DOPC)/ 1,2-dioleoyl-sn-glycero-3-phosphoethanolamine (DOPE) lipid bilayers with the R state populated at <20% (60, 61). Phosphorylation at S16 leads to local unfolding and increased dynamics around the phosphorylation site and a shift in equilibrium towards the R state (58, 62, 63). Similarly, mutations in the loop and domain Ia of PLN can either increase or decrease the dynamics in the cytoplasmic region, which has been shown to correlate with SERCA inhibition (**Figure 13**). For example, a P21G mutation in the loop leads to increased dynamics and lowered inhibition of SERCA making this mutant a possible future candidate in gene therapy applications (64).

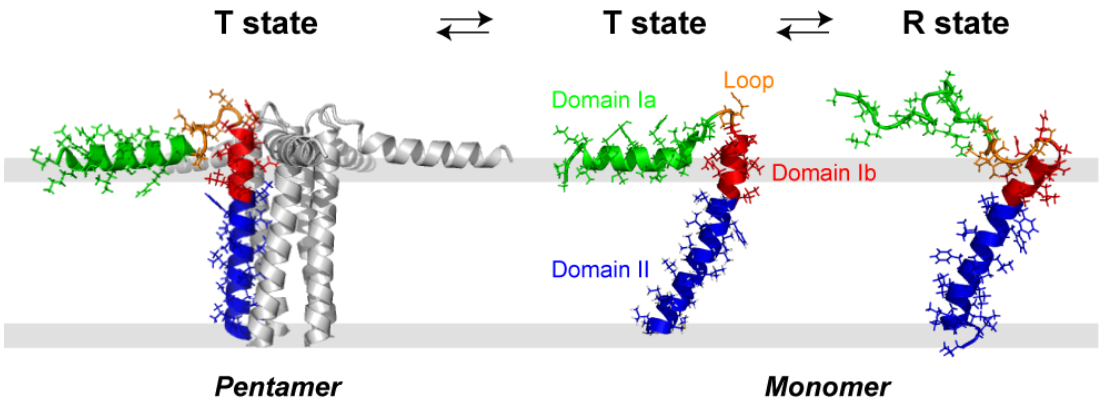

Figure 12. Structures of pentameric PLN (PDB ID 2KYV) and monomeric PLN in T (PDB ID 2KB7) and R states.

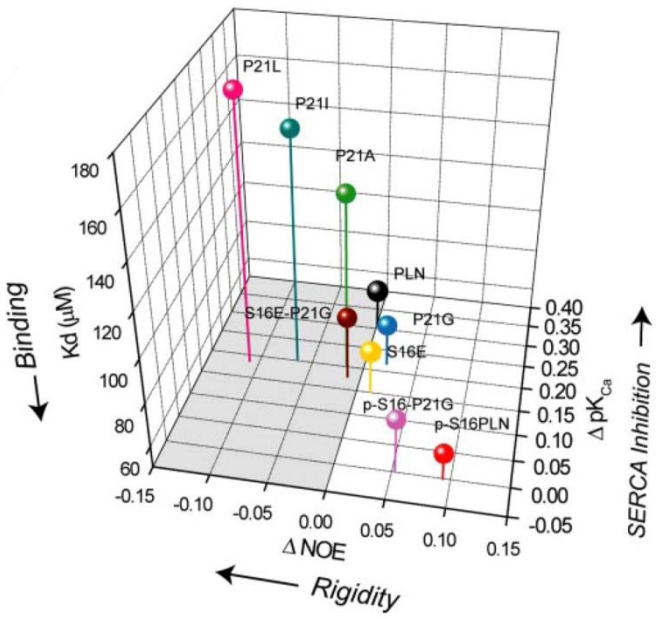

Figure 13. Structure-dynamics-function relationship for PLN mutants. *Adapted from Ha et al.* (64).

1.5.3 The SERCA/PLN complex

Although there are several structures of both SERCA and PLN there is still no high resolution structure of the SERCA/PLN complex. Extensive scanning mutagenesis studies have defined the TM domain of PLN as the primary inhibitory unit while the cytoplasmic region has a regulatory role (65). These studies also defined the side of the TM helix that faces SERCA in the complex and identified a stretch of residues from K397 to K402 in the N domain of SERCA to be crucial for SERCA regulation (66). In agreement with this a bifunctional cross-linker was found to cross-link K3 of PLN to Lys 400 in the N domain of SERCA (67). In addition to this single cytoplasmic cross-link, several cross-links have been formed between the TM domains of SERCA and PLN using different reagents and mutants. Cross-linking is reduced or completely abolished at high Ca^{2+} concentrations or upon phosphorylation of PLN at S16 but increased in the presence of nucleotide (68). This led to the conclusion that PLN inhibits SERCA by interacting with the E2 form of the enzyme and that S16 phosphorylation of PLN relieves the inhibition by dissociation of the complex. However, spectroscopic measurements and immuno-precipitation experiments have shown that neither high Ca^{2+} concentration nor phosphorylation dissociate PLN from SERCA (69, 70). This implies that phosphorylation

relieves the inhibition through a conformational rearrangement of the complex. Based on mutagenesis and cross-linking studies, a solution NMR structure of a monomeric mutant of PLN and the crystal structure of SERCA in the E2 state, a molecular model was proposed of the SERCA/PLN complex (**Figure 14**) (71). In this model, the TM domain of PLN binds in a groove formed by helices M2, M4, M6, and M9 of SERCA. The cytoplasmic domain Ia of PLN is helical and interacts with the N and P domains of SERCA, a position that is heavily biased by the cross-link between K3 and K400 of SERCA. A later study utilized backbone dihedral angle restraints derived from ssNMR experiments to further refine the model of the complex (72). The main difference between the two models is that the latter determined that domain Ib remains helical upon binding to SERCA.

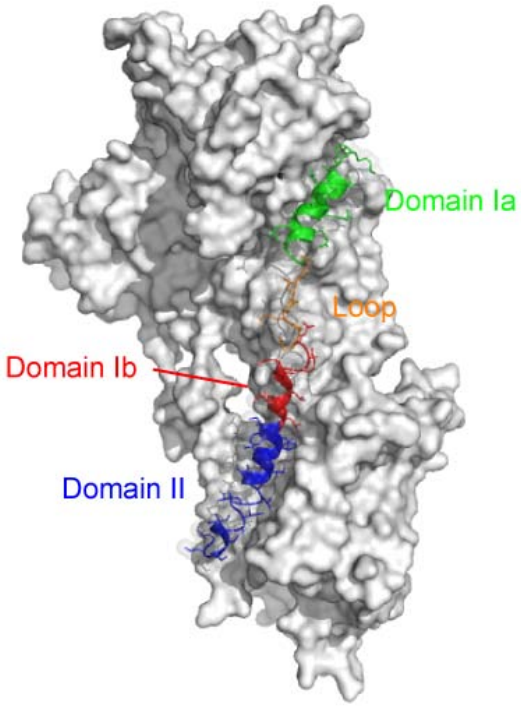

Figure 14. Molecular model of the SERCA/PLN complex. *Structural coordinates were provided by D. H. Maclennan and C. Toyoshima.*

However, a shortcoming of these studies are that they model only one state of PLN bound to SERCA even if both NMR and EPR studies have shown that the T/R state

equilibrium of PLN is retained upon SERCA binding (58, 60). Upon interaction with SERCA, there is a slight shift in the equilibrium in favor of the R state. Also, anchoring of domain Ia to the lipid bilayer using a covalently attached lipid anchor shifts the equilibrium completely to the T state. Phosphorylation of S16 does not relieve the inhibition of lipid-anchored PLN. (58). This implies that the T/R equilibrium is important for PLN function. Still, the functional roles of the T and R states remain elusive.

Additional structural information about the complex has come from cryoelectron microscopy studies of two-dimensional SERCA/PLN co-crystals. These studies produced low resolution images and indicated that PLN binds in between two SERCA monomers, possibly as a pentamer (73, 74). In summary, despite the large number of studies of the SERCA/PLN complex there is a lack of high resolution structural information. A high resolution structure of this membrane protein complex would be a major breakthrough towards the full understanding of SERCA regulation by PLN and a starting point for the development of novel therapies to treat heart failure.

1.6 Objectives

The R and T states of PLN have been detected by several different techniques but the functional relevance of these states has remained unclear. *I hypothesized that the T/R equilibrium is central for PLN function and SERCA regulation.* To test this hypothesis I used NMR spectroscopy in conjunction with other biophysical and biochemical techniques to probe PLN, SERCA and the SERCA/PLN complex. Specifically, I aimed to answer the following questions:

- What are the structures of the T and R state in the absence of SERCA and what are the factors that affect the T/R equilibrium?
- How is SERCA function and PLN regulation affected by the lipid bilayer and how can a SERCA/PLN complex be formed to perform NMR studies under fully functional conditions?
- What is the conformation of PLN in the PLN/SERCA complex and where is the cytoplasmic domain located in the complex?
- What are the other functional roles of the T/R equilibrium?

The answers to these questions could increase the understanding of the molecular basis of regulation of SERCA by PLN and the possible role of the T/R equilibrium in this regulation. This would contribute to the overall goal of the Veglia lab to understand the structural basis of muscle relaxation and could provide important information to target the SERCA/PLN complex in the treatment of heart failure.

1.7 References

1. Singer, S. J. and G.L. Nicolson 1972. The fluid mosaic model of the structure of cell membranes. Science. 175, 720-731.

2. Engelman, D. M. 2005. Membranes are more mosaic than fluid. Nature. 438, 578-580.

3. van Meer, G., D.R. Voelker and G.W. Feigenson 2008. Membrane lipids: Where they are and how they behave. Nat. Rev. Mol. Cell Biol. 9, 112-124.

4. Wallin, E. and G. von Heijne 1998. Genome-wide analysis of integral membrane proteins from eubacterial, archaean, and eukaryotic organisms. Protein Sci. 7, 1029-1038.

5. Bakheet, T. M. and A.J. Doig 2009. Properties and identification of human protein drug targets. Bioinformatics. 25, 451-457.

6. Wimley, W. C. 2003. The versatile beta-barrel membrane protein. Curr. Opin. Struct. Biol. 13, 404-411.

7. von Heijne, G. 2006. Membrane-protein topology. Nat. Rev. Mol. Cell Biol. 7, 909-918.

8. Doyle, D. A., J.M. Cabral, R.A. Pfuetzner, A. Kuo, J.M. Gulbis, S.L. Cohen, B.T. Chait and R. Mackinnon 1998. The structure of the potassium channel : Molecular basis of K+ conduction and selectivity. Science. 280, 69-77.

9. Cherezov, V., D.M. Rosenbaum, M.A. Hanson, S.G. Rasmussen, F.S. Thian, T.S. Kobilka, H.J. Choi, P. Kuhn, W.I. Weis, B.K. Kobilka and R.C. Stevens 2007. High-resolution crystal structure of an engineered human beta2-adrenergic G protein-coupled receptor. Science. 318, 1258-1265.

10. Rasmussen, S. G., H.J. Choi, D.M. Rosenbaum, T.S. Kobilka, F.S. Thian, P.C. Edwards, M. Burghammer, V.R. Ratnala, R. Sanishvili, R.F. Fischetti, G.F. Schertler, W.I. Weis and B.K. Kobilka 2007. Crystal structure of the human beta2 adrenergic G-protein-coupled receptor. Nature. 450, 383-387.

11. Van den Berg, B., W.M. Clemons Jr, I. Collinson, Y. Modis, E. Hartmann, S.C. Harrison and T.A. Rapoport 2004. X-ray structure of a protein-conducting channel. Nature. 427, 36-44.

12. Hiller, S., R.G. Garces, T.J. Malia, V.Y. Orekhov, M. Colombini and G. Wagner 2008. Solution structure of the integral human membrane protein VDAC-1 in detergent micelles. Science. 321, 1206-1210.

13. Berardi, M. J., W.M. Shih, S.C. Harrison and J.J. Chou 2011. Mitochondrial uncoupling protein 2 structure determined by NMR molecular fragment searching. Nature. 476, 109-113.

14. Zhou, Y., T. Cierpicki, R.H. Jimenez, S.M. Lukasik, J.F. Ellena, D.S. Cafiso, H. Kadokura, J. Beckwith and J.H. Bushweller 2008. NMR solution structure of the integral membrane enzyme DsbB: Functional insights into DsbB-catalyzed disulfide bond formation. Mol. Cell. 31, 896-908.

15. Renault, M., R. Tommassen-van Boxtel, M.P. Bos, J.A. Post, J. Tommassen and M. Baldus 2012. Cellular solid-state nuclear magnetic resonance spectroscopy. Proc. Natl. Acad. Sci. U. S. A. 109, 4863-4868.

16. Hong, M., Y. Zhang and F. Hu 2012. Membrane protein structure and dynamics from NMR spectroscopy. Annu. Rev. Phys. Chem. 63, 1-24.

17. McDermott, A. 2009. Structure and dynamics of membrane proteins by magic angle spinning solid-state NMR. Annu. Rev. Biophys. 38, 385-403.

18. Levitt, M. H. 2001. Spin dynamics. John Wiley & sons, New York.

19. Battiste, J. L. and G. Wagner 2000. Utilization of site-directed spin labeling and high-resolution heteronuclear nuclear magnetic resonance for global fold determination of large proteins with limited nuclear overhauser effect data. Biochemistry. 39, 5355-5365.

20. Zhou, Y., T. Cierpicki, R.H. Jimenez, S.M. Lukasik, J.F. Ellena, D.S. Cafiso, H. Kadokura, J. Beckwith and J.H. Bushweller 2008. NMR solution structure of the integral membrane enzyme DsbB: Functional insights into DsbB-catalyzed disulfide bond formation. Mol. Cell. 31, 896-908.

21. Sengupta, I., P.S. Nadaud, J.J. Helmus, C.D. Schwieters and C.P. Jaroniec 2012. Protein fold determined by paramagnetic magic-angle spinning solid-state NMR spectroscopy. Nat. Chem. 4, 410-417.

22. Ketchem, R. R., W. Hu and T.A. Cross 1993. High-resolution conformation of gramicidin A in a lipid bilayer by solid-state NMR. Science. 261, 1457-1460.

23. De Angelis, A. A., S.C. Howell, A.A. Nevzorov and S.J. Opella 2006. Structure determination of a membrane protein with two trans-membrane helices in aligned phospholipid bicelles by solid-state NMR spectroscopy. J. Am. Chem. Soc. 128, 12256-12267.

24. Verardi, R., L. Shi, N.J. Traaseth, N. Walsh and G. Veglia 2011. Structural topology of phospholamban pentamer in lipid bilayers by a hybrid solution and solid-state NMR method. Proc Natl Acad Sci U S A. 108, 9101-9106.

25. Traaseth, N. J., L. Shi, R. Verardi, D.G. Mullen, G. Barany and G. Veglia 2009. Structure and topology of monomeric phospholamban in lipid membranes determined by a hybrid solution and solid-state NMR approach. Proc. Natl. Acad. Sci. U. S. A. 106, 10165-10170.

26. Castellani, F., B. van Rossum, A. Diehl, M. Schubert, K. Rehbein and H. Oschkinat 2002. Structure of a protein determined by solid-state magic-angle-spinning NMR spectroscopy. Nature. 420, 98-102.

27. Zech, S. G., A.J. Wand and A.E. McDermott 2005. Protein structure determination by high-resolution solid-state NMR spectroscopy: Application to microcrystalline ubiquitin. J. Am. Chem. Soc. 127, 8618-8626.

28. Ader, C., R. Schneider, S. Hornig, P. Velisetty, E.M. Wilson, A. Lange, K. Giller, I. Ohmert, M.F. Martin-Eauclaire, D. Trauner, S. Becker, O. Pongs and M. Baldus 2008. A structural link between inactivation and block of a K+ channel. Nat. Struct. Mol. Biol. 15, 605-612.

29. Cady, S. D., K. Schmidt-Rohr, J. Wang, C.S. Soto, W.F. Degrado and M. Hong 2010. Structure of the amantadine binding site of influenza M2 proton channels in lipid bilayers. Nature. 463, 689-692.

30. Park, S. H., B.B. Das, F. Casagrande, Y. Tian, H.J. Nothnagel, M. Chu, H. Kiefer, K. Maier, A.A. De Angelis, F.M. Marassi and S.J. Opella 2012. Structure of the chemokine receptor CXCR1 in phospholipid bilayers. Nature.

31. Luo, W., S.D. Cady and M. Hong 2009. Immobilization of the influenza A M2 transmembrane peptide in virus envelope-mimetic lipid membranes: A solid-state NMR investigation. Biochemistry. 48, 6361-6368.

32. De Angelis, A. A. and S.J. Opella 2007. Bicelle samples for solid-state NMR of membrane proteins. Nat. Protoc. 2, 2332-2338.

33. Park, S. H., S. Prytulla, A.A. De Angelis, J.M. Brown, H. Kiefer and S.J. Opella 2006. High-resolution NMR spectroscopy of a GPCR in aligned bicelles. J. Am. Chem. Soc. 128, 7402-7403.

34. MacLennan, D. H. and E.G. Kranias 2003. Phospholamban: A crucial regulator of cardiac contractility. Nat Rev Mol Cell Biol. 4, 566-77.

35. Davis, J., M.V. Westfall, D. Townsend, M. Blankinship, T.J. Herron, G. Guerrero-Serna, W. Wang, E. Devaney and J.M. Metzger 2008. Designing heart performance by gene transfer. Physiol. Rev. 88, 1567-1651.

36. Wegener, A. D., H.K. Simmerman, J.P. Lindemann and L.R. Jones 1989. Phospholamban phosphorylation in intact ventricles. phosphorylation of serine 16 and threonine 17 in response to beta-adrenergic stimulation. Journal Biological Chemistry. 264, 11468-11474.

37. Hadri, L. and R.J. Hajjar 2011. Calcium cycling proteins and their association with heart failure. Clin. Pharmacol. Ther. 90, 620-624.

38. Roger, V. L., A.S. Go, D.M. Lloyd-Jones, E.J. Benjamin, J.D. Berry, W.B. Borden, D.M. Bravata, S. Dai, E.S. Ford, C.S. Fox, H.J. Fullerton, C. Gillespie, S.M. Hailpern, J.A. Heit, V.J. Howard, B.M. Kissela, S.J. Kittner, D.T. Lackland, J.H. Lichtman, L.D. Lisabeth, D.M. Makuc, G.M. Marcus, A. Marelli, D.B. Matchar, C.S. Moy, D. Mozaffarian, M.E. Mussolino, G. Nichol, N.P. Paynter, E.Z. Soliman, P.D. Sorlie, N. Sotoodehnia, T.N. Turan, S.S. Virani, N.D. Wong, D. Woo, M.B. Turner and American Heart Association Statistics Committee and Stroke Statistics Subcommittee 2012. Executive summary: Heart disease and stroke statistics--2012 update: A report from the american heart association. Circulation. 125, 188-197.

39. Kairouz, V., L. Lipskaia, R.J. Hajjar and E.R. Chemaly 2012. Molecular targets in heart failure gene therapy: Current controversies and translational perspectives. Ann. N. Y. Acad. Sci. 1254, 42-50.

40. Jessup, M., B. Greenberg, D. Mancini, T. Cappola, D.F. Pauly, B. Jaski, A. Yaroshinsky, K.M. Zsebo, H. Dittrich, R.J. Hajjar and Calcium Upregulation by Percutaneous Administration of Gene Therapy in Cardiac Disease (CUPID) Investigators 2011. Calcium upregulation by percutaneous administration of gene therapy in cardiac disease (CUPID): A phase 2 trial of intracoronary gene therapy of sarcoplasmic reticulum Ca2+-ATPase in patients with advanced heart failure. Circulation. 124, 304-313.

41. Zhao, X., S. Hu, J. Li, Y. Mou, K. Bian, J. Sun and Z. Zhu 2008. rAAV-asPLB transfer attenuates abnormal sarcoplasmic reticulum Ca2+-ATPase activity and cardiac dysfunction in rats with myocardial infarction. European Journal of Heart Failure,. 10, 47-54.

42. Hoshijima, M., Y. Ikeda, Y. Iwanaga, S. Minamisawa, M.O. Date, Y. Gu, M. Iwatate, M. Li, L. Wang, J.M. Wilson, Y. Wang, J. Ross Jr and K.R. Chien 2002. Chronic suppression of heart-failure progression by a pseudophosphorylated mutant of phospholamban via in vivo cardiac rAAV gene delivery. Nat. Med. 8, 864-871.

43. Periasamy, M. and A. Kalyanasundaram 2007. SERCA pump isoforms: Their role in calcium transport and disease. Muscle Nerve.

44. Toyoshima, C. and G. Inesi 2004. Structural basis of ion pumping by Ca2+-ATPase of the sarcoplasmic reticulum. Annu. Rev. Biochem. 73, 269-292.

45. Moller, J. V., C. Olesen, A.M. Winther and P. Nissen 2010. The sarcoplasmic Ca2+-ATPase: Design of a perfect chemi-osmotic pump. Q. Rev. Biophys. 43, 501-566.

46. Toyoshima, C. and H. Nomura 2002. Structural changes in the calcium pump accompanying the dissociation of calcium. Nature. 418, 605-11.

47. Toyoshima, C., M. Nakasako, H. Nomura and H. Ogawa 2000. Crystal structure of the calcium pump of sarcoplasmic reticulum at 2.6 A resolution. Nature. 405, 647-55.

48. Winters, D. L., J.M. Autry, B. Svensson and D.D. Thomas 2008. Interdomain fluorescence resonance energy transfer in SERCA probed by cyan-fluorescent protein fused to the actuator domain. Biochemistry. 47, 4246-4256.

49. Espinoza-Fonseca, L. M. and D.D. Thomas 2011. Atomic-level characterization of the activation mechanism of SERCA by calcium. PLoS One. 6, e26936.

50. Hou, Z., Z. Hu, D.J. Blackwell, T.D. Miller, D.D. Thomas and S.L. Robia 2012. 2-color calcium pump reveals closure of the cytoplasmic headpiece with calcium binding. PLoS One. 7, e40369.

51. Simmerman, H. K., J.H. Collins, J.L. Theibert, A.D. Wegener and L.R. Jones 1986. Sequence analysis of phospholamban. identification of phosphorylation sites and two major structural domains. J Biol Chem. 261, 13333-41.

52. Kimura, Y., K. Kurzydlowski, M. Tada and D.H. MacLennan 1997. Phospholamban inhibitory function is activated by depolymerization. J Biol Chem. 272, 15061-4.

53. Becucci, L., A. Cembran, C.B. Karim, D.D. Thomas, R. Guidelli, J. Gao and G. Veglia 2009. On the function of pentameric phospholamban: Ion channel or storage form? Biophys. J. 96, L60-2.

54. Pollesello, P., A. Annila and M. Ovaska 1999. Structure of the 1-36 amino-terminal fragment of human phospholamban by nuclear magnetic resonance and modeling of the phospholamban pentamer. Biophys J. 76, 1784-95.

55. Zamoon, J., A. Mascioni, D.D. Thomas and G. Veglia 2003. NMR solution structure and topological orientation of monomeric phospholamban in dodecylphosphocholine micelles. Biophys. J. 85, 2589-2598.

56. Andronesi, O. C., S. Becker, K. Seidel, H. Heise, H.S. Young and M. Baldus 2005. Determination of membrane protein structure and dynamics by magic-angle-spinning solid-state NMR spectroscopy. J. Am. Chem. Soc. 127, 12965-12974.

57. Oxenoid, K. and J.J. Chou 2005. The structure of phospholamban pentamer reveals a channel-like architecture in membranes. Proc. Natl. Acad. Sci. U. S. A. 102, 10870-10875.

58. Karim, C. B., Z. Zhang, E.C. Howard, K.D. Torgersen and D.D. Thomas 2006. Phosphorylation-dependent conformational switch in spin-labeled phospholamban bound to SERCA. J. Mol. Biol. 358, 1032-1040.

59. Karim, C. B., T.L. Kirby, Z. Zhang, Y. Nesmelov and D.D. Thomas 2004. Phospholamban structural dynamics in lipid bilayers probed by a spin label rigidly coupled to the peptide backbone. Proc Natl Acad Sci U S A. 101, 14437-42.

60. Zamoon, J., F. Nitu, C. Karim, D.D. Thomas and G. Veglia 2005. Mapping the interaction surface of a membrane protein: Unveiling the conformational switch of phospholamban in calcium pump regulation. Proc. Natl. Acad. Sci. U. S. A. 102, 4747-4752.

61. Nesmelov, Y. E., C.B. Karim, L. Song, P.G. Fajer and D.D. Thomas 2007. Rotational dynamics of phospholamban determined by multifrequency electron paramagnetic resonance. Biophys. J. 93, 2805-2812.

62. Metcalfe, E. E., N.J. Traaseth and G. Veglia 2005. Serine 16 phosphorylation induces an order-to-disorder transition in monomeric phospholamban. Biochemistry. 44, 4386-4396.

63. Abu-Baker, S. and G.A. Lorigan 2006. Phospholamban and its phosphorylated form interact differently with lipid bilayers: A 31P, 2H, and 13C solid-state NMR spectroscopic study. Biochemistry. 45, 13312-13322.

64. Ha, K. N., N.J. Traaseth, R. Verardi, J. Zamoon, A. Cembran, C.B. Karim, D.D. Thomas and G. Veglia 2007. Controlling the inhibition of the sarcoplasmic Ca2+-ATPase by tuning phospholamban structural dynamics. J. Biol. Chem. 282, 37205-37214.

65. MacLennan, D. H., Y. Kimura and T. Toyofuku 1998. Sites of regulatory interaction between calcium ATPases and phospholamban. Ann N Y Acad Sci. 853, 31-42.

66. Toyofuku, T., K. Kurzydlowski, M. Tada and D.H. MacLennan 1994. Amino acids lys-asp-asp-lys-pro-val-402 in the Ca2+-ATPase of cardiac sarcoplasmic reticulum are

critical for functional association with phospholamban. Journal Biological Chemistry. 269, 22929-22932.

67. James, P., M. Inui, M. Tada, M. Chiesi and E. Carafoli 1989. Nature and site of phospholamban regulation of the Ca2+ pump of sarcoplasmic reticulum. Nature. 342, 90-2.

68. Chen, Z., B.L. Akin and L.R. Jones 2007. Mechanism of reversal of phospholamban inhibition of the cardiac Ca2+-ATPase by protein kinase A and by anti-phospholamban monoclonal antibody 2D12. J. Biol. Chem. 282, 20968-20976.

69. Asahi, M., E. McKenna, K. Kurzydlowski, M. Tada and D.H. MacLennan 2000. Physical interactions between phospholamban and sarco(endo)plasmic reticulum Ca2+-ATPases are dissociated by elevated Ca2+, but not by phospholamban phosphorylation, vanadate, or thapsigargin, and are enhanced by ATP. J Biol Chem. 275, 15034-8.

70. Mueller, B., C.B. Karim, I.V. Negrashov, H. Kutchai and D.D. Thomas 2004. Direct detection of phospholamban and sarcoplasmic reticulum ca-ATPase interaction in membranes using fluorescence resonance energy transfer. Biochemistry. 43, 8754-65.

71. Toyoshima, C., M. Asahi, Y. Sugita, R. Khanna, T. Tsuda and D.H. MacLennan 2003. Modeling of the inhibitory interaction of phospholamban with the Ca2+ ATPase. Proc Natl Acad Sci U S A. 100, 467-72.

72. Seidel, K., O.C. Andronesi, J. Krebs, C. Griesinger, H.S. Young, S. Becker and M. Baldus 2008. Structural characterization of ca(2+)-ATPase-bound phospholamban in lipid bilayers by solid-state nuclear magnetic resonance (NMR) spectroscopy. Biochemistry. 47, 4369-4376.

73. Stokes, D. L., A.J. Pomfret, W.J. Rice, J.P. Glaves and H.S. Young 2006. Interactions between Ca2+-ATPase and the pentameric form of phospholamban in two-dimensional co-crystals. Biophys. J. 90, 4213-4223.

74. Young, H. S., L.R. Jones and D.L. Stokes 2001. Locating phospholamban in co-crystals with ca(2+)-ATPase by cryoelectron microscopy. Biophys J. 81, 884-94.

Chapter 2 - Lipid-Mediated Folding/Unfolding of Phospholamban Cytoplasmic Domains as a Regulatory Mechanism for the Sarcoplasmic Reticulum Ca2+-ATPase

Reprinted with permission from:

Martin Gustavsson, Nathaniel J. Traaseth, Christine B. Karim, Elizabeth L. Lockamy, David D. Thomas and Gianluigi Veglia. Lipid-Mediated Folding/Unfolding of Phospholamban Cytoplasmic Domains as a Regulatory Mechanism for the Sarcoplasmic Reticulum Ca2+-ATPase. *J Mol Biol.* 2011; 408(4):755-65

The integral membrane protein complex between phospholamban (PLN) and sarcoplasmic reticulum Ca^{2+}-ATPase (SERCA) regulates cardiac contractility. In the unphosphorylated form PLN binds SERCA and inhibits Ca^{2+} flux. Upon phosphorylation of PLN at Ser 16, the inhibitory effect is reversed. Although structural details on both proteins are emerging from X-ray crystallography, cryo-electron microscopy, and NMR studies, the molecular mechanisms of their interactions and regulatory process are still lacking. It has been speculated that SERCA regulation depends on PLN structural transitions (order-to-disorder, i.e. folding-unfolding). Here, we investigated PLN conformational changes upon chemical unfolding by a combination of EPR and NMR spectroscopy, revealing that the conformational transitions involve mostly the cytoplasmic regions, with two concomitant phenomena: 1) membrane binding and folding of the amphipathic domain Ia and 2) the folding/unfolding of the juxtamembrane domain Ib of PLN. Analysis of phosphorylated and unphosphorylated PLN with two phosphomimetic mutants of PLN (S16E and S16D) shows that the population of an unfolded state in domains Ia and Ib (T' state) is linearly correlated to the extent of SERCA inhibition measured by activity assays. Inhibition of SERCA is carried out by the folded ground state (T state) of the protein (PLN), while the relief of inhibition involves promotion of PLN to excited conformational states (Ser 16 phosphorylated PLN). We propose that PLN population shifts (folding/unfolding) are a key regulatory mechanism for SERCA.

2.1 Introduction

Phospholamban (PLN) is a 52-residue integral membrane protein embedded in the sarcoplasmic reticulum (SR) membrane of cardiac muscle (1) that reversibly inhibits the SR Ca^{2+}-ATPase (SERCA), regulating calcium flux and muscle contractility (1-4).

Although several X-ray crystallography and cryo-electron microscopy studies focused on SERCA have revealed important details on calcium translocation (5-9), structural data on the SERCA/PLN complex (10-13) are sparse and do not offer mechanistic details on the regulatory function of PLN.

In the SR membrane, PLN exists as a homopentameric assembly in equilibrium with monomers that bind SERCA (1, 2, 4, 14). Both the monomer and pentamer adopt an L-shaped topology, with a cytoplasmic α-helix (domain Ia, residues 1-16) connected to a membrane-spanning α-helix (residues 23-52) by a short loop (residues 17-22) (15-17). The membrane-spanning helix has two dynamically distinct domains: domain Ib (residues 23-30) that is positioned at the hydrophilic portion of the lipid bilayer and domain II (residues 31-52) that exists in the hydrophobic interior (15, 18, 19).

Previously, using NMR and EPR spectroscopy, we detected a conformational equilibrium between two major states: an ordered T state and a disordered R state (20, 21). According to EPR, the R state population is ~16% (T state ~84%) in the absence of SERCA (22), and becomes slightly more populated in the presence of the enzyme (21). We then speculated that the regulation of SERCA by PLN occurs *via* conformational transitions between the T and R states. This hypothesis was supported by our studies on the structural effects of PLN phosphorylation at Ser 16 (23, 24) and NMR and functional studies of PLN reconstituted in different lipid mimetics (25-27). In fact, phosphorylation of PLN at Ser 16 by protein kinase A relieves SERCA inhibition, allowing for more efficient muscle relaxation (1-3, 28). We found that structurally and dynamically, phosphorylation causes an *order-to-disorder* transition, with an unwinding of domain Ia at residues 14-16 around the phosphorylation site (16, 21, 23, 24). As a result, the phosphoryl transfer shifts the PLN conformational equilibrium, increasing the R state population (21). The latter can be exploited for the design of mutants to control SERCA function (29). It is also possible to rationalize the effects of phosphomimetic mutations (S16E) (29) used in gene

therapy (30). Although we established the foundations for a rational design of mutants and showed that the excited states of PLN are important for SERCA inhibition (29), we did not provide a quantitative interpretation of the conformational transitions of PLN between the ground and excited states or elucidate the structural and dynamic features of the excited conformations.

Here, we used EPR and NMR spectroscopy in conjunction with biological activity assays to define the nature of PLN excited states and at the same time to establish a quantitative correlation between the population of the excited state and the extent of SERCA inhibition. We show that the conformational equilibrium of PLN is more complex than previously anticipated. We present a new model for the PLN conformational pre-equilibrium and show a linear correlation between the loss of function (LOF) of PLN phosphomimetic mutants and their excited state populations.

2.2 Results

2.2.1 A four-state model of PLN conformational equilibrium

Based on our previous studies, we hypothesized that PLN undergoes conformational interconversion between two states: a motionally restricted T state with the cytoplasmic domain absorbed on the membrane surface and a more dynamic R state with domain Ia detached from the membrane and mostly unfolded (20, 21, 29). To test this hypothesis, we monitored the chemical unfolding of PLN upon addition of guanidine hydrochloride (Gdn HCl) using both EPR in 4:1 DOPC:DOPE (1,2-dioleoyl-*sn*-glycero-3-phosphocholine: 1,2-dioleoyl-*sn*-glycero-3-phosphoethanolamine) lipid bilayers and NMR in DPC micelles. We utilized a synthetic (for EPR) or recombinant (for NMR) monomeric variant of PLN (AFA-PLN) that has the same inhibitory power and similar structural topology as wild-type PLN (18, 31).

EPR spectra of TOAC (2,2,6,6-tetramethyl-piperidine-1-oxyl-4-amino-4-carboxylic acid) spin label engineered at position 11 revealed the presence of two resolved peaks: one broad resonance which was assigned to the T state and a sharper peak assigned to the R state (**Figure 1**) (22). The R state is very dynamic, with an order parameter three-fold lower than the corresponding T state (21). To follow the chemical

unfolding of PLN, EPR experiments were carried out by titrating Gdn HCl into the PLN samples and monitoring the spectral changes of TOAC at positions 11 (domain Ia), 24 (domain Ib), and 36 (domain II). In the absence of chemical denaturant, the populations of the R state were 8 and 28% for positions 11 and 24, respectively; while at position 36 only the T state was detected (**Figure 1**). Addition of Gdn HCl to the PLN in vesicles caused the disappearance of the TOAC resonance (position 11) T statecomponent and a concomitant increase of the peak intensity of the R state component. This demonstrates a shift in the PLN conformational equilibrium toward the R state for domain Ia. In contrast, the TOAC spectrum for 36 remained unperturbed upon addition of the denaturant, and showed that while domain Ia unfolded completely, the membrane embedded domain II was still helical in the presence of chemical denaturant. At position 24 (domain Ib), the addition of the Gdn HCl increased the R state population from 28 to 34%.

To analyze the conformational transitions at the atomic level, we monitored the NMR chemical shifts for both the methyl and the amide groups of PLN upon addition of Gdn HCl using 2D heteronuclear single quantum coherence (HSQC) spectra. As a reference for the unfolded R state of PLN, we used a peptide corresponding to the cytoplasmic residues of PLN (PLN_{1-20}). In aqueous solutions, this peptide is soluble and unfolded, while in the presence of DPC (or lipid vesicles) it is helical and associated with the micelle surface (**Figure S1**)(32-35).

Titration of Gdn HCl into a PLN sample in DPC micelles caused gradual changes to the chemical shifts for all of the resonances (methyls and amides) in domain Ia, loop, and domain Ib (**Figures 2 and 3**). Domain II remained mostly unperturbed with the exception of the C-terminal residues, which is in agreement with the results obtained from the EPR experiments at position 36. The chemical shifts for the PLN methyl groups follow trajectories that are close to linear (**Figure 3**), and at a high concentration of denaturant, overlay with those of PLN_{1-20} without DPC (unfolded R state) (**Figure 4A**).

The deviations from linearity, however, are more apparent from the amide chemical shifts. In particular, amide chemical shifts of domain Ia show at least three different states (see triangulation of chemical shifts for I12), while more linear behavior is observed for resonances located in domain Ib (**Figure 3, Figures S3 and S4**). At high

Gdn HCl concentrations, amide chemical shifts in domain Ia overlap with the R state (**Figure 4B**). These results demonstrate that while EPR detects an apparent two-state equilibrium, the conformational states visited by PLN during chemical unfolding are at least three as revealed by NMR spectroscopy. The latter supports the three-state folding model of amphipathic helices proposed by White and co-workers (36, 37). For PLN the unfolding process highlights three major conformational ensembles: 1) a helical T state, 2) a partially unfolded membrane-associated R' state, and 3) a totally unfolded membrane-dissociated R state. Note that while the chemical shifts of the methyl groups are sensitive to environmental changes, like the EPR measurements, they only show an apparent two-state equilibrium. In contrast, the amide groups are more sensitive to secondary structural changes and therefore are able to detect the presence of the R' state more clearly.

Interestingly, the plots of the chemical shift changes as a function of the concentration of Gdn HCl show that residues in domains Ia and Ib have different melting profiles (**Figure 5**). Specifically, unfolding curves for residues in domain Ia have a more cooperative unfolding behavior than residues in domain Ib (larger Hill coefficient; 2.2 ± 0.2 vs. 1.6 ± 0.1 (average ± standard error)) (**Figure S5, Table S1**). Thus, a lower concentration of Gdn HCl is required to induce unfolding for residues in domain Ib. This behavior is typical of less compact states that are likely to interconvert non-cooperatively (38, 39).

Phosphorylation of PLN at Ser 16 causes a complete LOF. This state is responsible for calcium reuptake into the SR membrane and regulates the diastolic phase of the cardiac cycle. Guided by the EPR data (21), we originally interpreted phosphorylation of PLN at Ser 16 as a shift of the conformational equilibrium toward the R state (24). To test this, we compared the chemical shifts of both methyl and amide groups with the unfolding experiments carried out in Gdn HCl. While the methyl group chemical shifts of pS16-AFA-PLN are in line with the trajectories toward the unfolded R state, supporting an apparent two-state equilibrium, the amide group chemical shifts do not overlap with those from the Gdn HCl titration. This distinct state (T' state), which is present in most of the resonances of domain Ia is partially unfolded as revealed by the ^{13}C chemical shift index (**Figure 6**) (23, 24), but primarily membrane attached (23, 27).

Upon titration with Gdn HCl, the T’ state of phosphorylated PLN is perturbed toward the unfolded and membrane detached R state (**Figure 4, Figures S3 and S4**). Note that for most of the resonances the unfolded states of both phosphorylated and unphosphorylated PLN overlap completely. However, slight differences in chemical shifts around the phosphorylation site were observed and are probably due to the charged phosphate group. Also, pS16-AFA-PLN unfolds at significantly lower Gdn HCl concentration than AFA-PLN (average k values of 0.7 ± 0.1 and 1.6 ± 0.1) (**Figure S6**), consistent with the partially unfolded nature of the T' state.

Based on the above results, we can conclude that the conformational interconversions of PLN include at least four major states for domain Ia and two states for domain Ib. The folding-unfolding equilibrium of domain Ia is dictated by its interactions with the lipids and is regulated by phosphorylation (**Figure 7**). The T state can proceed to the R state either through the unfolded and membrane-associated R' state or the T' state. Domain Ib transitions between two states, folded and unfolded, independent of domain Ia.

2.2.2 Pseudo-phosphorylated mutants of PLN and conformational equilibrium.

To further test the presence of the excited T’ state, we monitored the effects of phosphomimetic mutations of PLN (S16D and S16E) by monitoring the chemical shifts of both methyl and amide groups. As with the unfolding studies, the methyl group chemical shifts follow an apparent linear trajectory toward the unfolded R state (**Figure 8**). In contrast, the amide chemical shifts of the mutants do not fall along the unfolding trajectory for pS16-AFA-PLN or AFA-PLN, rather they reside in intermediate positions between the resonances of pS16-AFA-PLN and AFA-PLN. Therefore, it is possible to conclude that pseudo-phosphorylation and phosphorylation promote a gradual shift in population toward the T’ state, consistent with previous reports that pS16 phosphorylation leads to partial unfolding (26).

2.2.3 Quantitative Correlation between the population of excited state and SERCA inhibition

To investigate a relationship between the population of the excited states and the loss of inhibitory power of PLN, we correlated structure (chemical shifts), dynamics (HX-NOEs) (**Figure S9**), and water accessibility (SEA-CLEANEX) (**Figure S10**) with the extent of PLN inhibition on SERCA's calcium affinity (inhibition; ΔpK_{Ca}) induced by the different mutants. Consistent with previous results (29), we found the following overall order of inhibition: AFA-PLN > S16E-AFA-PLN > S16D-AFA-PLN > pS16-AFA-PLN (**Table 1**). In order to link the structure to function, we adopted the approach proposed by Li *et al.* (40), correlating the average chemical shift change (corresponding to T to T') for each mutant with the respective SERCA inhibitory potency. The resonances of AFA-PLN were defined to be 100% T state, while those from pS16-AFA-PLN were set to 100% T' state. The structure-function correlation plot is reported in **Figure 9A**. The linearity of this plot (correlation coefficient = 0.98) indicates a direct correlation between the increase in the population of the T' state and the loss of inhibition. Similar correlations with the inhibitory potency are obtained for both the fast dynamics (ps-ns) and solvent accessibility (**Figures 9B and C**). This is in agreement with the partially unfolded character of the T' state, which makes it more dynamic and solvent accessible than the T state and can exchange directly with the completely unfolded R state (**Figure 7**). *These data suggest that the promotion of PLN from the ground T state to the excited T' state (and likely R state) results in LOF*.

2.3 Discussion

Based on our previous investigations (16), we hypothesized that the conformational equilibrium of PLN is central to SERCA regulation. However, in our original papers both EPR and NMR studies revealed the presence of an apparent two-state equilibrium (T and R states) (20, 21, 41). Here, we provide evidence that PLN exists in a pre-existing equilibrium between several conformational states, exemplified by the folding/unfolding equilibria of both domain Ia and Ib. For domain Ia methyl groups, the chemical shift trajectories for chemical unfolding follow an apparent two-state equilibrium in agreement with EPR data. In contrast, the trajectories for amide group

chemical shifts showed the presence of four conformational states, which is in agreement with the folding model of amphipathic helices proposed by White and co-workers (36, 37). On the other hand, for domain Ib the folding/unfolding process involves a simpler two-state model, as we also found using CPMG relaxation dispersion methods (41). This new, more complex model agrees with recent data from the Lorigan and Middleton groups (25, 26), who proposed an active role of lipids in modulating PLN structural dynamics and SERCA inhibition. At the same time, it explains previous mutagenesis studies, which identified a number of sites in domain Ia of PLN that lead to relief of SERCA inhibition (42). Specifically, residues populating the hydrophobic face of the amphipathic domain Ia (V4, L7, and I12) are among these *hot spots* (42), which in the T state are residues inserted into the lipid bilayer (17). Shortening the side chain of these residues would likely attenuate the interactions of domain Ia with the membrane environment, supporting the hypothesis that lipid bilayers influence the regulatory process in the context of membrane-detachment and helix unfolding. Interestingly, attachment of a lipid anchor to the N-terminus completely shifts PLN to the T state, with Ser 16 phosphorylation of this lipidated PLN failing to relieve SERCA inhibition (21, 33). This result also strongly supports the structure-function relationship reported in **Figure 9**. It is important to stress that the relative population of states can potentially be biased by the choice of membrane mimic. For example, in DPC micelles the T and T' states are primarily detected. However, solid-state NMR experiments in DMPC lipid bilayers found domain Ia to be predominantly unfolded (43). This suggests an important role of lipid charge, head groups and possibly bilayer curvature in influencing the conformational equilibria and extent of aggregation of PLN.

Tuning PLN conformational equilibrium leads to the control of SERCA activity. Recently, we showed that to gain complete control over PLN inhibition, it is necessary to map the transition to the excited states (29). Our new data show that pseudo-phosphorylation and phosphorylation of PLN increase the population of T' state. Since the T' state exchanges more readily with the fully unfolded R state (**Figure 7**), it is likely that the R state also increases in population. The correlation between membrane detachment/unfolding and SERCA inhibition (**Figure 9)** suggests that these states need to be considered in the design of new, more efficient loss-of-function PLN mutants. To this extent, the S16D mutation is more similar in structure and dynamics to pS16-AFA-

PLN than is the S16E mutant. This is supported by SERCA inhibition assays that show a greater LOF character for S16D-AFA-PLN than S16E-AFA-PLN, and would make the S16D mutant a better candidate for positive inotropic therapy (44).

An important corollary of this study is the intrinsic flexibility and versatility of the cytoplasmic domain of PLN that when detached from the membrane surface behaves as an intrinsically disordered domain that can adopt several conformations (45, 46). In the heart muscle, PLN interacts with several different partners to elicit its regulatory function. Specifically, PLN associates with the lipid bilayer, SERCA, PKA, CamKII, AKAP18δ, protein phosphatase 1 (PP1), HAX1, and itself in the form of a pentamer state. How can this protein with such a simple structure and topology bind these diverse biomolecules? We believe the answer is encoded in its flexibility and malleability (i.e. dynamics) that enable PLN to undergo conformational changes and mold into different binding sites.

Finally, it is worth noting that PLN can be divided into two main regions: an inhibitory transmembrane segment and a cytoplasmic regulatory region. The latter is reminiscent of the autoinhibitory elements found in Vav and LOV proteins, where an amphipathic helical switch is activated upon phosphorylation or light (40, 47). In the case of Vav and LOV, this regulatory element is covalently attached to the proteins with the amphipathic helix undergoing folding/unfolding transitions upon interaction with the protein surface. For SERCA, the reversible regulatory element is provided by PLN that is modulated by the folding/unfolding transitions via the lipid bilayer and phosphorylation. Given the high similarity between PLN and other single pass membrane protein subunits such as the FYXD family, it is likely that the mechanism described in this paper is a general one, also found in the regulation of other ion pumps.

2.4 Materials and Methods

2.4.1 Purification of PLN Protein

Recombinant AFA-PLN, S16D-AFA-PLN and S16E-AFA-PLN were grown and purified as described by Buck *et al.* (18). PLN_{1-20} was expressed in *E. coli* and purified as

described by Masterson *et al.* (48). To obtain full phosphorylation at Ser 16, lyophilized AFA-PLN protein was dissolved at a concentration of 0.3 mg/ml in 20 mM MOPS buffer pH 7.0 containing 1%(w/v) *n*-octyl-β-D-glucopyranoside (OG), ATP (1 mM), and $MgCl_2$ (1 mM) (23). Phosphorylation was accomplished by addition of purified recombinant protein kinase A (49, 50) at a 1:2000 PKA:AFA-PLN molar ratio and incubated for ~12 h at 30 ºC. After purification by reversed-phase HPLC, the pS16-AFA-PLN was lyophilized and stored at -20 ºC.

2.4.2 Assay for SERCA Activity

For SERCA activity measurements, AFA-PLN, pS16-AFA-PLN, S16E-AFA-PLN, and S16D-AFA-PLN were reconstituted into 4:1 DOPC:DOPE lipid bilayers. SERCA was purified in octaethylene glycol monododecyl ether ($C_{12}E_8$) (5) and added to the lipid vesicle suspension containing 700:1 lipid:SERCA and 10:1 PLN:SERCA molar ratios. Subsequently, the samples were incubated with Biobeads (30:1 Biobeads:$C_{12}E_8$ by weight) (Bio-Rad Laboratories) to remove excess detergent. A coupled NADH assay was used to measure SERCA activity (hydrolysis of ATP) at 37 ºC as a function of calcium concentration (51). The rate of enzyme activity was measured as a decrease of NADH absorption at 340 nm using a Spectramax plate reader (Molecular Devices). Data were fit using the Hill equation to extract the maximum activity (V_{max}), Hill coefficient (n), and calcium concentration needed to achieve half maximal activity (pK_{Ca}) (51).

2.4.3 EPR spectroscopy

For EPR experiments, AFA-PLN with the TOAC spin label substituted at 11, 24, or 36 was synthesized and reconstituted into lipid vesicles containing DOPC:DOPE (4:1, 200 lipids per PLN) (52). EPR spectra were acquired using a Bruker EleXsys 500 spectrometer with the SHQ cavity. Samples (20 uL in a 0.6 mm i.d. quartz capillary) were maintained at 4 ºC using the Bruker temperature controller with a quartz dewar insert. The field modulation frequency was 100 kHz, with a peak-to-peak amplitude of 2 G. The microwave power was 7.9 mW, producing moderate saturation (so that signal intensity was at least 50% of maximum) without significant effect on the spectral lineshape. EPR spectra were simulated as a sum of one or two components, each component produced by a population having a static random distribution of membrane

orientations and undergoing rotational diffusion in a restricting potential (defined by order parameter S) with a single rotational correlation time (21). Experimental spectra were fit by summing simulated components, yielding mole fractions.

2.4.4 NMR Spectroscopy

To prepare NMR samples of the AFA-PLN variants, lyophilized protein was dissolved in NMR sample buffer containing 20 mM $NaHPO_4$, 120 mM NaCl, 0.01 % NaN_3, 5 % D_2O, 6 M guanidine hydrochloride (Gdn HCl), 300 mM deuterated DPC, and pH 6.0 uncorrected for isotopic effect. Gdn HCl was subsequently dialyzed against 1 L of NMR sample buffer. This procedure gave more homogenous spectral lines and avoided protein aggregation. All of the NMR experiments were performed on Varian VNMRS and Inova spectrometers operating at a ^{1}H frequency of 600 MHz. Data were processed using NMRPipe (53) and viewed and analyzed in Sparky (54). Protein amide fingerprints were analyzed using gradient enhanced [^{1}H,^{15}N]-HSQC experiments (55). The data were acquired at 37 ºC using 1544 complex points in the direct ^{1}H dimension and 50 to 80 increments in the indirect ^{15}N dimension. Gradient enhanced constant-time [^{1}H,^{13}C]-HSQC experiments were utilized to measure methyl group chemical shifts. For PLN_{1-20} and each AFA-PLN mutant, 8 scans were acquired at 37 ºC with 2048 complex points and a spectral width of 12000 Hz in the direct ^{1}H dimension, and 64 points with a spectral width of 3500 Hz in the indirect ^{13}C dimension. After Fourier transformation, the data were zero-filled to a final matrix size of 4096 x 2048.

Heteronuclear [^{1}H-^{15}N] steady-state NOE measurements were acquired using the pulse sequence of Kay and co-workers (56). 2D spectra with and without a 3 s ^{1}H saturation period were acquired at 37 ºC. The ^{1}H-^{15}N steady-state NOE value was obtained as the ratio between peak intensities in the saturated (I_{sat}) and unsaturated (I_{unsat}) spectrum:

$$[\,^{1}H,^{15}N]NOE = I_{sat}/I_{unsat} \qquad (1)$$

The uncertainty of the measurement was estimated for each residue from the relationship (56):

$$\sigma_{[\,^{1}H,^{15}N]NOE}/[\,^{1}H,^{15}N]NOE = \sqrt{((\sigma_{sat}/I_{sat})^2(\sigma_{unsat}/I_{unsat})^2)} \quad (2)$$

Where σ_{sat} and σ_{unsat} is the baseline noise in the saturated and unsaturated spectra and σ_{HNNOE} is the estimated error for the HNNOE values.

To measure the solvent exchange for amide protons, [^{1}H,^{15}N]-SEA-CLEANEX experiments were performed (57). This pulse sequence utilizes a spin-echo filter to select for water magnetization followed by a mixing period to allow for exchange between protein and solvent (58). To eliminate NOE contributions, the CLEANEX-PM mixing scheme was implemented (59). Four different mixing times (30, 60, 120 and 200 ms) were used to follow the build-up of peaks corresponding to solvent exchanging amide protons. A total of 64-96 scans were recorded at 37 ºC with 2048 complex points in the direct ^{1}H dimension and 40 increments in the indirect ^{15}N dimension. Spectral widths were 12000 and 1200 Hz in the direct and indirect dimensions, respectively. A shifted sine bell window function was applied to all data sets, which were zero-filled to 4096 in both dimensions prior to Fourier transformation.

Gdn HCl-induced denaturation was done by titrating Gdn HCl from a 6 M stock solution to AFA-PLN at pH 6.0. Six additions were made to a final Gdn HCl concentration of 2.8 M and [^{1}H,^{15}N]-HSQC and [^{1}H,^{13}C]-HSQC spectra were acquired after each addition as described above. For the analysis of unfolding, spectra were referenced to 10 mM DSS and ^{15}N peak shifts were plotted as a function of Gdn HCl concentration. The data were fit using the Hill equation:

$$\Delta\partial = (\partial_{end} - \partial_{start})\frac{[Gdn\ HCl]^n}{[Gdn\ HCl]^n + k^n}$$

Where n is the Hill coefficient and k is the unfolding half point. Hill coefficients for residues in domain Ib of PLN (22-28) and domain Ia (3-16) were compared using a t-test. Residue 9 was excluded since it could not be assigned and residues 2, 29 and 30 since those fit poorly to the Hill equation. k values for domain Ia and Ib of AFA-PLN and pS16-AFA-PLN (residues 3-16 and 22-28) were compared with a t-test.

2.4.5 Structure, dynamics, function relationship

Chemical shift changes for the different mutants were calculated according to the expression:

$$\Delta\delta_{combined} = \sqrt{(\Delta\delta^{1}H)^{2} + (\Delta\delta^{15}N/5)^{2}} \qquad (6)$$

where $\Delta\delta_{combined}$ is the difference in chemical shift relative to AFA-PLN. Several resonances within the HSQC spectra (**Figure S2**) that have a gradual change in chemical shifts from AFA-PLN → S16E-AFA-PLN → S16D-AFA-PLN → pS16-AFA-PLN (Leu 7, Thr 8, Ala 11, Ile 12, Ala 15, Ile 18, Glu 19, Gln 22, Gln 23, Arg 25, Gln 26, Asn 27, Leu 28, Gln 29, Asn 30) were used in the analysis. Each resonance shift was calculated using the following formula:

$$p = \frac{\omega_{mutant} - \omega_{AFA}}{\omega_{pAFA} - \omega_{AFA}} \qquad (7)$$

where ω is the combined chemical shift and p is the relative peak position for each species. In the formula, the AFA-PLN chemical shifts correspond to 0 and pS16-AFA-PLN corresponds to 1. The heteronuclear NOE value was calculated as an average of HN NOE values for all residues in domains Ia, the loop and domain Ib (residues 2-31). To determine the normalized solvent exchange, peak intensities from [^{1}H,^{15}N]-SEA-CLEANEX spectra were measured using the software Sparky (54). The intensities were corrected for the differences in sensitivity for residues in a [^{1}H-^{15}N]-HSQC spectrum and then normalized among the different PLN species (AFA-PLN, pS16-AFA-PLN, S16D-AFA-PLN, and S16E-AFA-PLN) by assuming Glu 2 to have the same solvent exchange for all mutants. The averaged normalized solvent exchange value included residues in domains Ia, the loop, and domain Ib (2-30). Residues 15-17 were excluded from the analysis due to their proximity to the phosphorylated/mutated Ser 16 and residues 5, 9 and 25 were removed due to spectral overlap.

2.5 References

1. Simmerman, H. K., J.H. Collins, J.L. Theibert, A.D. Wegener and L.R. Jones 1986. Sequence analysis of phospholamban. identification of phosphorylation sites and two major structural domains. J Biol Chem. 261, 13333-41.

2. Reddy, L. G., L.R. Jones and D.D. Thomas 1999. Depolymerization of phospholamban in the presence of calcium pump: A fluorescence energy transfer study. Biochemistry. 38, 3954-62.

3. Tada, M. and M. Kadoma 1989. Regulation of the Ca2+ pump ATPase by cAMP-dependent phosphorylation of phospholamban. Bioessays. 10, 157-63.

4. MacLennan, D. H. and E.G. Kranias 2003. Phospholamban: A crucial regulator of cardiac contractility. Nat Rev Mol Cell Biol. 4, 566-77.

5. Stokes, D. L. and N.M. Green 1990. Three-dimensional crystals of CaATPase from sarcoplasmic reticulum. symmetry and molecular packing. Biophys J. 57, 1-14.

6. Toyoshima, C., M. Nakasako, H. Nomura and H. Ogawa 2000. Crystal structure of the calcium pump of sarcoplasmic reticulum at 2.6 A resolution. Nature. 405, 647-55.

7. Toyoshima, C. and H. Nomura 2002. Structural changes in the calcium pump accompanying the dissociation of calcium. Nature. 418, 605-11.

8. Sorensen, T. L., J.V. Moller and P. Nissen 2004. Phosphoryl transfer and calcium ion occlusion in the calcium pump. Science. 304, 1672-1675.

9. Olesen, C., T.L. Sorensen, R.C. Nielsen, J.V. Moller and P. Nissen 2004. Dephosphorylation of the calcium pump coupled to counterion occlusion. Science. 306, 2251-2255.

10. Stokes, D. L., A.J. Pomfret, W.J. Rice, J.P. Glaves and H.S. Young 2006. Interactions between Ca2+-ATPase and the pentameric form of phospholamban in two-dimensional co-crystals. Biophys. J. 90, 4213-4223.

11. Young, H. S., L.R. Jones and D.L. Stokes 2001. Locating phospholamban in co-crystals with ca(2+)-ATPase by cryoelectron microscopy. Biophys J. 81, 884-94.

12. Seidel, K., O.C. Andronesi, J. Krebs, C. Griesinger, H.S. Young, S. Becker and M. Baldus 2008. Structural characterization of ca(2+)-ATPase-bound phospholamban in lipid bilayers by solid-state nuclear magnetic resonance (NMR) spectroscopy. Biochemistry. 47, 4369-4376.

13. Schmitt, J. P., F. Ahmad, K. Lorenz, L. Hein, S. Schulz, M. Asahi, D.H. Maclennan, C.E. Seidman, J.G. Seidman and M.J. Lohse 2009. Alterations of phospholamban function can exhibit cardiotoxic effects independent of excessive sarcoplasmic reticulum Ca2+-ATPase inhibition. Circulation. 119, 436-444.

14. Cornea, R. L., L.R. Jones, J.M. Autry and D.D. Thomas 1997. Mutation and phosphorylation change the oligomeric structure of phospholamban in lipid bilayers. Biochemistry. 36, 2960-7.

15. Zamoon, J., A. Mascioni, D.D. Thomas and G. Veglia 2003. NMR solution structure and topological orientation of monomeric phospholamban in dodecylphosphocholine micelles. Biophys. J. 85, 2589-2598.

16. Traaseth, N. J., K.N. Ha, R. Verardi, L. Shi, J.J. Buffy, L.R. Masterson and G. Veglia 2008. Structural and dynamic basis of phospholamban and sarcolipin inhibition of ca(2+)-ATPase. Biochemistry. 47, 3-13.

17. Traaseth, N. J., L. Shi, R. Verardi, D.G. Mullen, G. Barany and G. Veglia 2009. Structure and topology of monomeric phospholamban in lipid membranes determined by a hybrid solution and solid-state NMR approach. Proc. Natl. Acad. Sci. U. S. A. 106, 10165-10170.

18. Mascioni, A., C. Karim, J. Zamoon, D.D. Thomas and G. Veglia 2002. Solid-state NMR and rigid body molecular dynamics to determine domain orientations of monomeric phospholamban. J. Am. Chem. Soc. 124, 9392-9393.

19. Metcalfe, E. E., J. Zamoon, D.D. Thomas and G. Veglia 2004. (1)H/(15)N heteronuclear NMR spectroscopy shows four dynamic domains for phospholamban reconstituted in dodecylphosphocholine micelles. Biophys. J. 87, 1205-1214.

20. Zamoon, J., F. Nitu, C. Karim, D.D. Thomas and G. Veglia 2005. Mapping the interaction surface of a membrane protein: Unveiling the conformational switch of phospholamban in calcium pump regulation. Proc. Natl. Acad. Sci. U. S. A. 102, 4747-4752.

21. Karim, C. B., Z. Zhang, E.C. Howard, K.D. Torgersen and D.D. Thomas 2006. Phosphorylation-dependent conformational switch in spin-labeled phospholamban bound to SERCA. J. Mol. Biol. 358, 1032-1040.

22. Nesmelov, Y. E., C.B. Karim, L. Song, P.G. Fajer and D.D. Thomas 2007. Rotational dynamics of phospholamban determined by multifrequency electron paramagnetic resonance. Biophys. J. 93, 2805-2812.

23. Metcalfe, E. E., N.J. Traaseth and G. Veglia 2005. Serine 16 phosphorylation induces an order-to-disorder transition in monomeric phospholamban. Biochemistry. 44, 4386-4396.

24. Traaseth, N. J., D.D. Thomas and G. Veglia 2006. Effects of Ser16 phosphorylation on the allosteric transitions of phospholamban/Ca(2+)-ATPase complex. J. Mol. Biol. 358, 1041-1050.

25. Hughes, E., J.C. Clayton and D.A. Middleton 2009. Cytoplasmic residues of phospholamban interact with membrane surfaces in the presence of SERCA: A new role for phospholipids in the regulation of cardiac calcium cycling? Biochim. Biophys. Acta. 1788, 559-566.

26. Abu-Baker, S. and G.A. Lorigan 2006. Phospholamban and its phosphorylated form interact differently with lipid bilayers: A 31P, 2H, and 13C solid-state NMR spectroscopic study. Biochemistry. 45, 13312-13322.

27. Chu, S., S. Abu-Baker, J. Lu and G.A. Lorigan 2010. (15)N solid-state NMR spectroscopic studies on phospholamban at its phosphorylated form at ser-16 in aligned phospholipid bilayers. Biochim. Biophys. Acta. 1798, 312-317.

28. Wegener, A. D., H.K. Simmerman, J.P. Lindemann and L.R. Jones 1989. Phospholamban phosphorylation in intact ventricles. phosphorylation of serine 16 and threonine 17 in response to beta-adrenergic stimulation. Journal Biological Chemistry. 264, 11468-11474.

29. Ha, K. N., N.J. Traaseth, R. Verardi, J. Zamoon, A. Cembran, C.B. Karim, D.D. Thomas and G. Veglia 2007. Controlling the inhibition of the sarcoplasmic Ca2+-ATPase by tuning phospholamban structural dynamics. J. Biol. Chem. 282, 37205-37214.

30. Hoshijima, M., Y. Ikeda, Y. Iwanaga, S. Minamisawa, M.O. Date, Y. Gu, M. Iwatate, M. Li, L. Wang, J.M. Wilson, Y. Wang, J. Ross Jr and K.R. Chien 2002. Chronic suppression of heart-failure progression by a pseudophosphorylated mutant of phospholamban via in vivo cardiac rAAV gene delivery. Nat. Med. 8, 864-871.

31. Karim, C. B., C.G. Marquardt, J.D. Stamm, G. Barany and D.D. Thomas 2000. Synthetic null-cysteine phospholamban analogue and the corresponding transmembrane domain inhibit the ca-ATPase. Biochemistry. 39, 10892-7.

32. Clayton, J. C., E. Hughes and D.A. Middleton 2005. Spectroscopic studies of phospholamban variants in phospholipid bilayers. Biochem. Soc. Trans. 33, 913-915.

33. Lockwood, N. A., R.S. Tu, Z. Zhang, M.V. Tirrell, D.D. Thomas and C.B. Karim 2003. Structure and function of integral membrane protein domains resolved by peptide-amphiphiles: Application to phospholamban. Biopolymers. 69, 283-92.

34. Hubbard, J. A., L.K. MacLachlan, E. Meenan, C.J. Salter, D.G. Reid, P. Lahouratate, J. Humphries, N. Stevens, D. Bell and W.A. Neville 1994. Conformation of the cytoplasmic domain of phospholamban by NMR and CD. Mol. Membr. Biol. 11, 263-269.

35. Huggins, J. P. and P.J. England 1987. Evidence for a phosphorylation-induced conformational change in phospholamban from the effects of three proteases. FEBS Lett. 217, 32-36.

36. Ladokhin, A. S. and S.H. White 1999. Folding of amphipathic alpha-helices on membranes: Energetics of helix formation by melittin. J. Mol. Biol. 285, 1363-1369.

37. White, S. H. and W.C. Wimley 1999. Membrane protein folding and stability : Physical principles. Annual Review Biophysics Biomolecular Structures. 28, 319-365.

38. Fersht, A. 1999. Structure and Mechanism in Protein Science. W.H. Freeman & Co., New York.

39. D'Onofrio, M., L. Ragona, D. Fessas, M. Signorelli, R. Ugolini, M. Pedo, M. Assfalg and H. Molinari 2009. NMR unfolding studies on a liver bile acid binding protein reveal a global two-state unfolding and localized singular behaviors. Arch. Biochem. Biophys. 481, 21-29.

40. Li, P., I.R. Martins, G.K. Amarasinghe and M.K. Rosen 2008. Internal dynamics control activation and activity of the autoinhibited vav DH domain. Nat. Struct. Mol. Biol. 15, 613-618.

41. Traaseth, N. J. and G. Veglia 2010. Probing excited states and activation energy for the integral membrane protein phospholamban by NMR CPMG relaxation dispersion experiments. Biochim. Biophys. Acta. 1798, 77-81.

42. MacLennan, D. H., Y. Kimura and T. Toyofuku 1998. Sites of regulatory interaction between calcium ATPases and phospholamban. Ann N Y Acad Sci. 853, 31-42.

43. Andronesi, O. C., S. Becker, K. Seidel, H. Heise, H.S. Young and M. Baldus 2005. Determination of membrane protein structure and dynamics by magic-angle-spinning solid-state NMR spectroscopy. J. Am. Chem. Soc. 127, 12965-12974.

44. Stevenson, L. W. 2003. Clinical use of inotropic therapy for heart failure: Looking backward or forward? part II: Chronic inotropic therapy. Circulation., 492-497.

45. Wright, P. E. and H.J. Dyson 2009. Linking folding and binding. Curr. Opin. Struct. Biol. 19, 31-38.

46. Mittag, T., L.E. Kay and J.D. Forman-Kay 2010. Protein dynamics and conformational disorder in molecular recognition. J. Mol. Recognit. 23, 105-116.

47. Yao, X., M.K. Rosen and K.H. Gardner 2008. Estimation of the available free energy in a LOV2-J alpha photoswitch. Nat. Chem. Biol. 4, 491-497.

48. Masterson, L. R., N. Bortone, T. Yu, K.N. Ha, E.C. Gaffarogullari, O. Nguyen and G. Veglia 2009. Expression and purification of isotopically labeled peptide inhibitors and substrates of cAMP-dependant protein kinase A for NMR analysis. Protein Expr. Purif. 64, 231-236.

49. Yonemoto, W. M., M.L. McGlone, L.W. Slice and S.S. Taylor 1991. Prokaryotic expression of catalytic subunit of adenosine cyclic monophosphate-dependent protein kinase. Methods Enzymol. 200, 581-596.

50. Masterson, L. R., A. Mascioni, N.J. Traaseth, S.S. Taylor and G. Veglia 2008. Allosteric cooperativity in protein kinase A. Proc Natl Acad Sci U S A. 105, 506-511.

51. Reddy, L. G., R.L. Cornea, D.L. Winters, E. McKenna and D.D. Thomas 2003. Defining the molecular components of calcium transport regulation in a reconstituted membrane system. Biochemistry. 42, 4585-92.

52. Karim, C. B., T.L. Kirby, Z. Zhang, Y. Nesmelov and D.D. Thomas 2004. Phospholamban structural dynamics in lipid bilayers probed by a spin label rigidly coupled to the peptide backbone. Proc Natl Acad Sci U S A. 101, 14437-42.

53. Delaglio, F., S. Grzesiek, G.W. Vuister, G. Zhu, J. Pfeifer and A. Bax 1995. NMRPipe: A multidimensional spectral processing system based on UNIX pipes. J. Biomol. NMR. 6, 277-293.

54. Goddard, T. D., Kneller,D.G. 1999. SPARKY 3.

55. Kay, L. E., E. Keifer and T. Saarinen 1992. Pure absorption gradient enhanced heteronuclear single quantum correlation spectroscopy with improved sensitivity. J. Am. Chem. Soc. 114, 10663-10665.

56. Farrow, N. A., R. Muhandiram, A.U. Singer, S.M. Pascal, C.M. Kay, G. Gish, S.E. Shoelson, T. Pawson, J.D. Forman-Kay and L.E. Kay 1994. Backbone dynamics of a

free and phosphopeptide-complexed src homology 2 domain studied by 15N NMR relaxation. Biochemistry. 33, 5984-6003.

57. Lin, D., K.H. Sze, Y. Cui and G. Zhu 2002. Clean SEA-HSQC: A method to map solvent exposed amides in large non-deuterated proteins with gradient-enhanced HSQC. J. Biomol. NMR. 23, 317-322.

58. Mori, S., J.M. Berg and P.C. van Zijl 1996. Separation of intramolecular NOE and exchange peaks in water exchange spectroscopy using spin-echo filters. J. Biomol. NMR. 7, 77-82.

59. Hwang, T. L., P.C. van Zijl and S. Mori 1998. Accurate quantitation of water-amide proton exchange rates using the phase-modulated CLEAN chemical EXchange (CLEANEX-PM) approach with a fast-HSQC (FHSQC) detection scheme. J. Biomol. NMR. 11, 221-226.

60. Zhang, H., S. Neal and D.S. Wishart 2003. RefDB: A database of uniformly referenced protein chemical shifts. J. Biomol. NMR. 25, 173-195.

PLN variant	*ΔpKCa*
AFA-PLN	0.20±0.02
S16E-AFA-PLN	0.14±0.04
S16D-AFA-PLN	0.08±0.04
pS16-AFA-PLN	0.02±0.02

Table 1. SERCA inhibition for PLN mutants. *pKCa values were determined from fits to the Hill equation (see material and methods). Inhibition was measured from the difference in pKCa in the absence and presence of a 10-fold excess of PLN (ΔpKCa). Standard errors were calculated from the average of three measurements.*

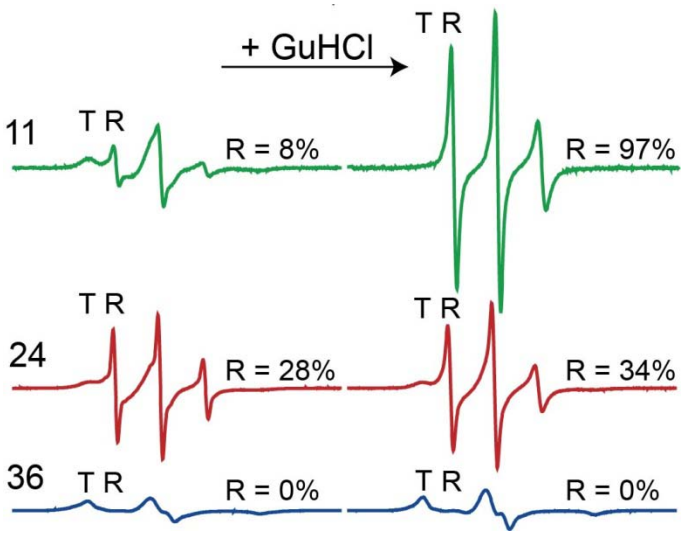

Figure 1. Chemical unfolding of PLN in lipid vesicles. *Continuous wave EPR spectra of TOAC spin label engineered at positions 11 (domain Ia), 24 (domain Ib), and 36 (domain II). Left: EPR spectra in the absence of Gdn HCl. Right: EPR spectra in the presence of 6 M Gdn HCl (right).*

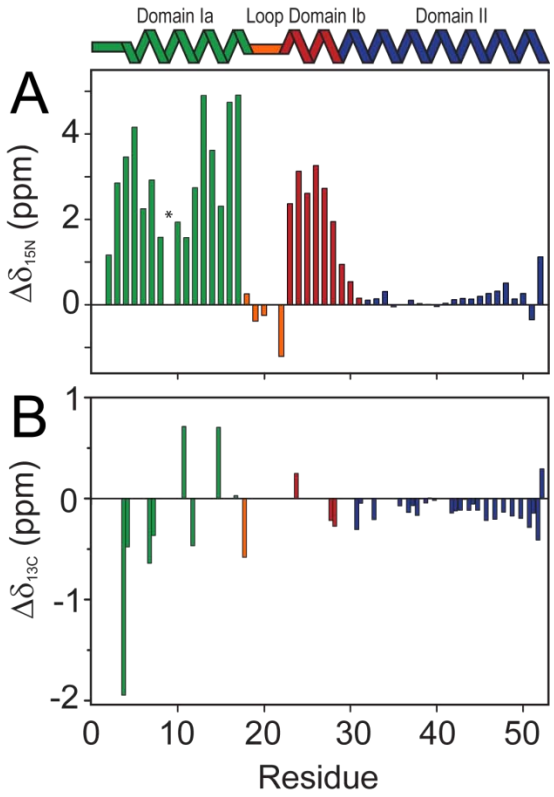

Figure 2. Chemical shift perturbations of AFA-PLN upon unfolding with Gdn HCl. *(A) ^{15}N amide and (B) ^{13}C methyl chemical shift changes as a function of residue. Colors reflect the different structural domains of PLN: domain Ia (green), loop (orange), domain Ib (red), and domain II (blue). The asterisk indicates an overlapped resonance as a result of Gdn HCl unfolding.*

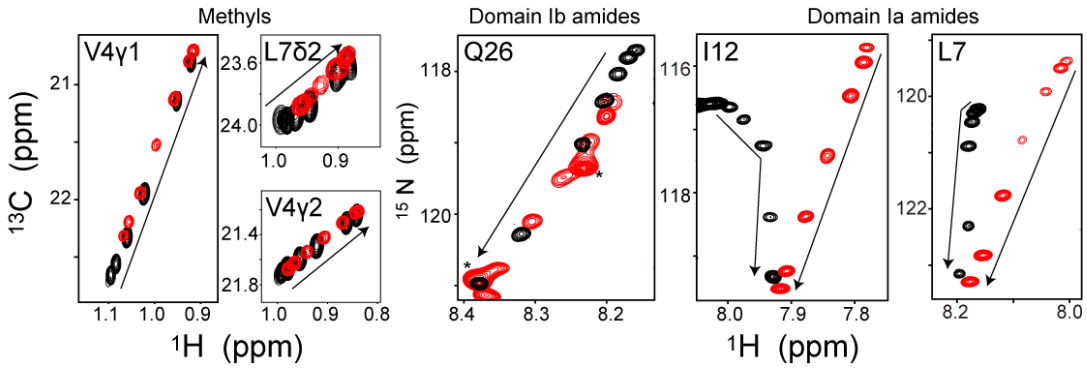

Figure 3. Chemical unfolding of AFA-PLN and pS16-AFA-PLN. *Representative spectra of methyl [^{1}H,^{13}C] and amide [^{1}H,^{15}N]-HSQC experiments for residues in domain Ia (Val 4, Leu 7, and Ile 12) and domain Ib (Gln 26) upon Gdn HCl titration for AFA-PLN (black) and pS16-AFA-PLN (red). AFA-PLN and pS16-AFA-PLN peaks correspond to Gdn HCl concentrations of 0 M, 0.067 M, 0.178 M, 0.48 M, 0.89 M, 1.81 M and 2.79 M. The direction of the arrows represents the increase in Gdn HCl concentration.*

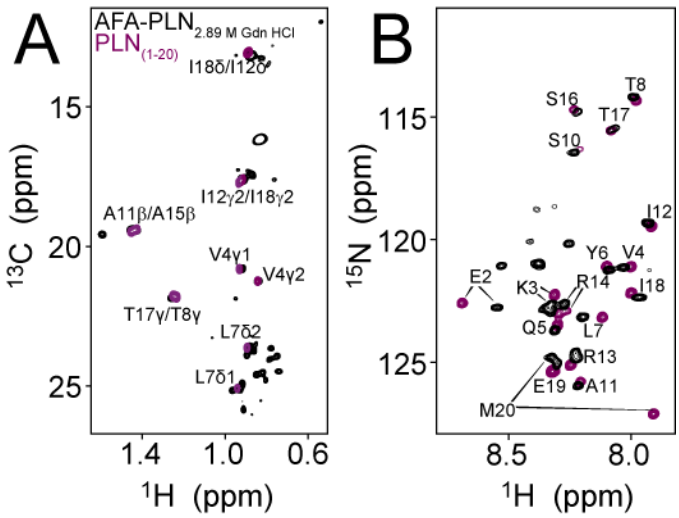

Figure 4. Methyl and amide fingerprint spectra of PLN1-20 and unfolded AFA-PLN. *(A) Overlay of [^{1}H,^{13}C]-HSQC spectra of AFA-PLN in the presence of Gdn HCl (black) and PLN$_{1-20}$ in the absence of DPC (purple). (B) Overlay of the [^{1}H,^{15}N]-HSQC spectra for the species in reported in (A). With the exception of the terminal residues, the chemical shifts of the resonances of the unfolded domain Ia of AFA-PLN and PLN$_{1-20}$ (in the absence of DPC) are very similar, showing that the PLN$_{1-20}$ free peptide is a good mimic of the R state.*

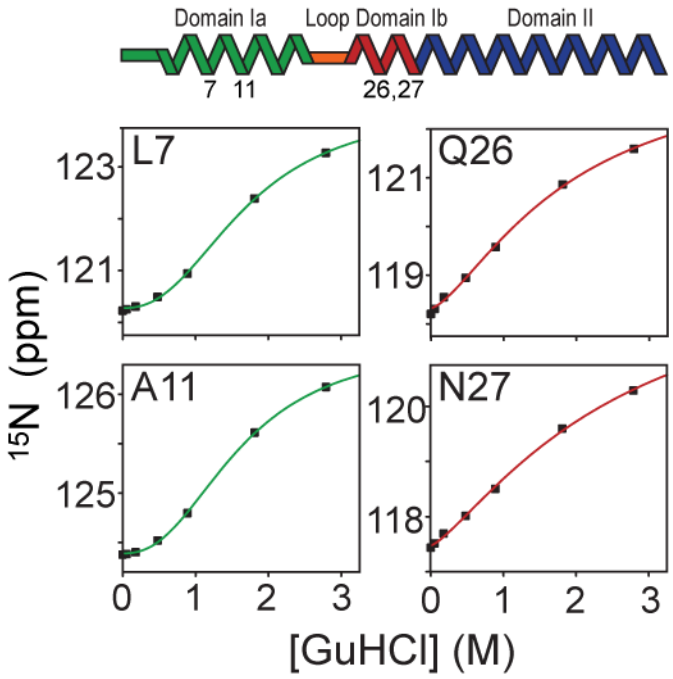

Figure 5. Unfolding of domain Ia and Ib upon titration of Gdn HCl. *Plots of the ^{15}N chemical shifts as a function of Gdn HCl concentration for Leu 7 and Ala 11 in domain Ia (left) and Gln 26 and Asn 27 in domain Ib (right). The unfolding of domain Ia is more cooperative than domain Ib.*

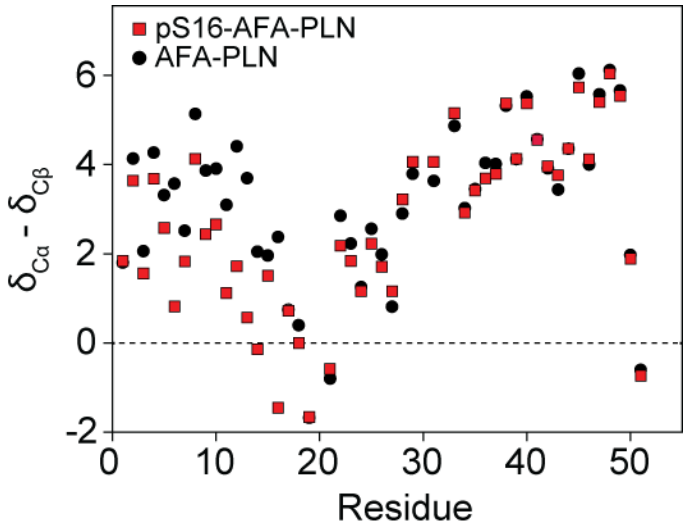

Figure 6. 13C chemical shift index (CSI) for AFA-PLN and pS16-AFA-PLN. *The chemical shift index is calculated as* $^{13}C_{\alpha} - {}^{13}C_{\beta} - ({}^{13}C_{\alpha,RC} - {}^{13}C_{\beta,RC})$*, where RC stands for the random coil chemical shifts reported by Zhang et al* (60)*. Consecutive positive CSI values indicate helix propensity.*

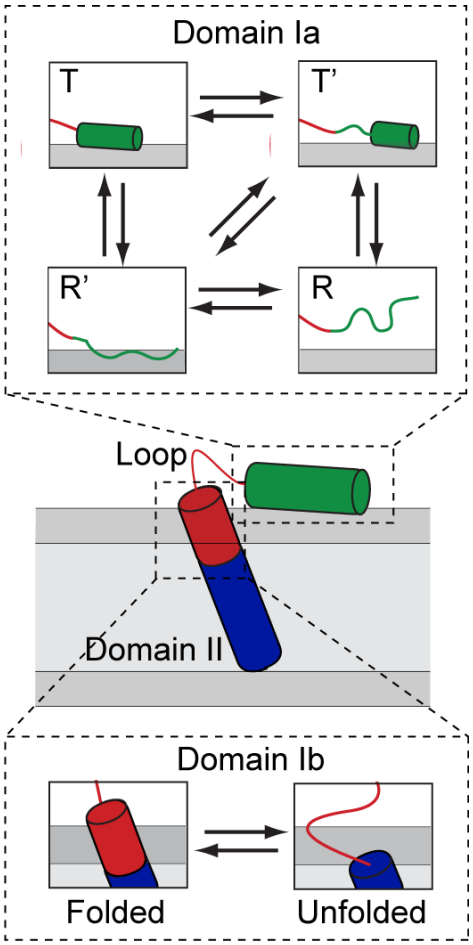

Figure 7. Model of the conformational equilibrium of PLN. *(Top) The T state of domain Ia undergoes unfolding to the R state via an intermediate T' state or R' state. (Bottom) Two-state conformational equilibrium for domain Ib.*

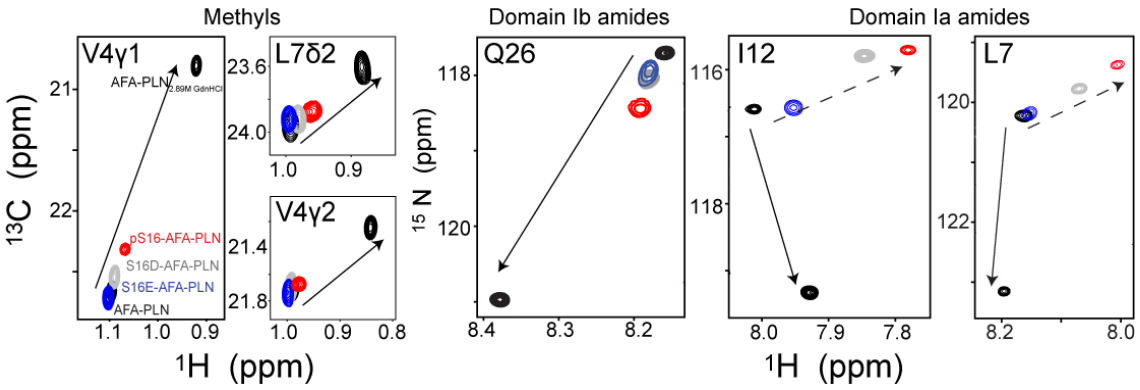

Figure 8. Methyl and amide HSQC spectra for Ser 16 phosphorylated AFA-PLN and the pseudo-phosphorylated variants. *[^{1}H,^{13}C] and [^{1}H,^{15}N]-HSQC spectra AFA-PLN (black), S16E-AFA-PLN (blue), S16D-AFA-PLN (grey), and pS16-AFA-PLN (red). The solid-line arrows point to the AFA-PLN resonance in the presence of Gdn HCl, while the dotted-line arrow visually traces the transition from AFA-PLN (T-state) to pS16-AFA-PLN (T'-state).*

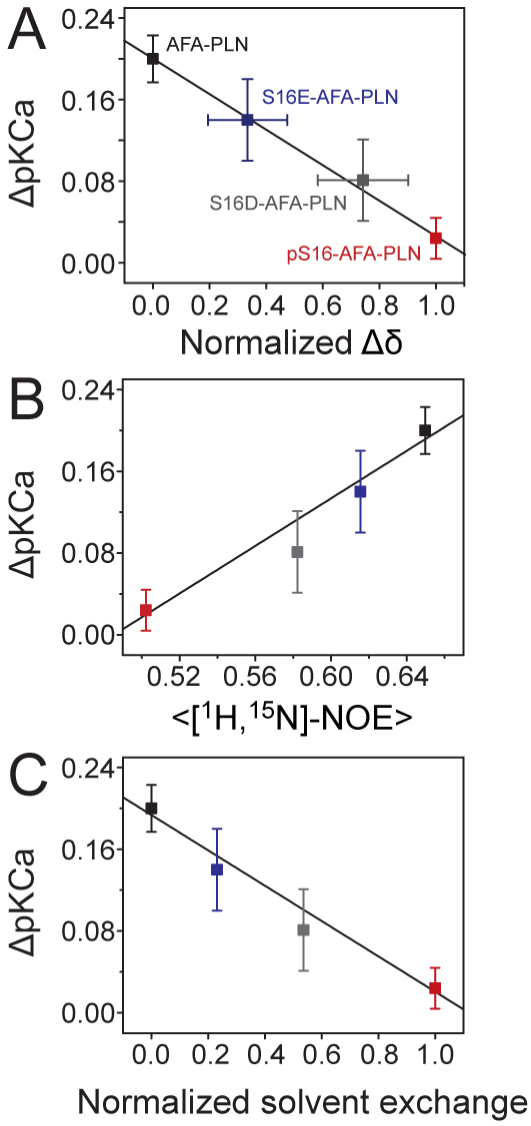

Figure 9. Structure-dynamics-function relationships *for AFA-PLN, Ser 16 phosphorylated AFA-PLN, and pseudo-phosphorylated mutants. (A) Correlation between combined ^{15}N-HSQC chemical shift change (normalized $\Delta\delta$), averaged [^{1}H,^{15}N]-NOE in domain Ia and the loop (B), and normalized solvent exchange from SEA-CLEANEX experiments (C) with SERCA inhibition from ATPase assays (ΔpKCa) for AFA-PLN (black), S16E-AFA-PLN (blue), S16D-AFA-PLN (grey) and pS16-AFA-PLN (red). See materials and methods for calculation of ΔpKCa, normalized $\Delta\delta$, <[^{1}H,^{15}N]-NOE> and normalized solvent exchange.*

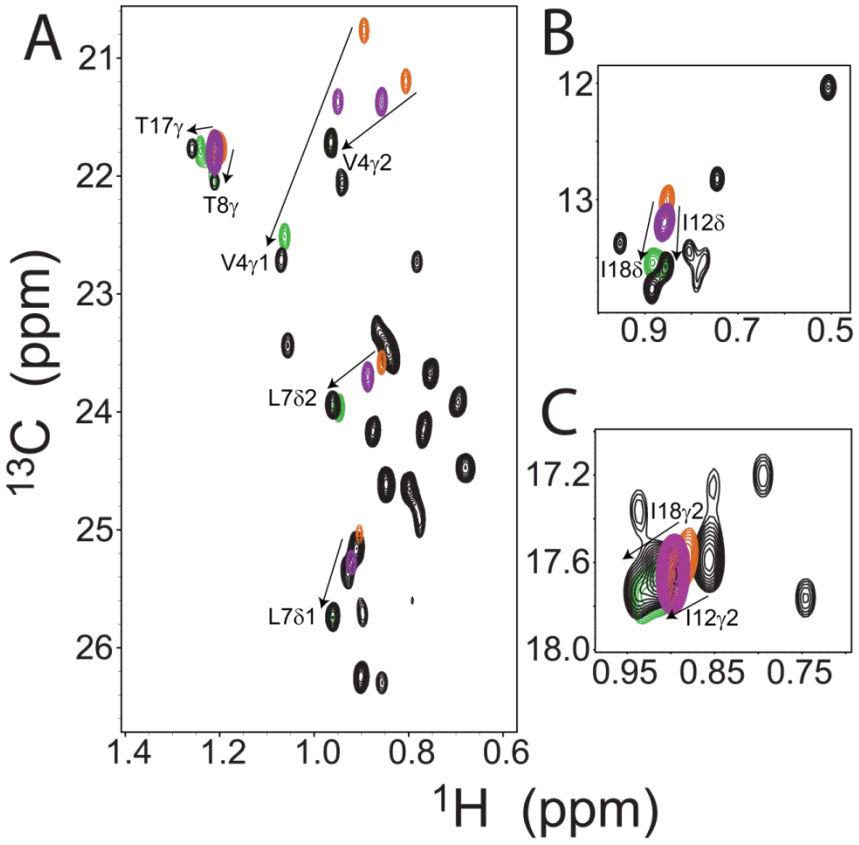

Figure S1. Folding of the PLN1-20 peptide upon titration of DPC. *[^{1}H,^{13}C]-HSQC spectra of PLN_{1-20} without DPC (orange), with 8 mM DPC (purple), and 300mM DPC (green). (A) Leu, Val, Thr, (B) Ile $\delta 1$, and (C) Ile $\gamma 2$ methyl groups. The spectra of PLN_{1-20} are overlaid onto the spectrum of AFA-PLN (black) chosen as a guide for a state that is primarily T state.*

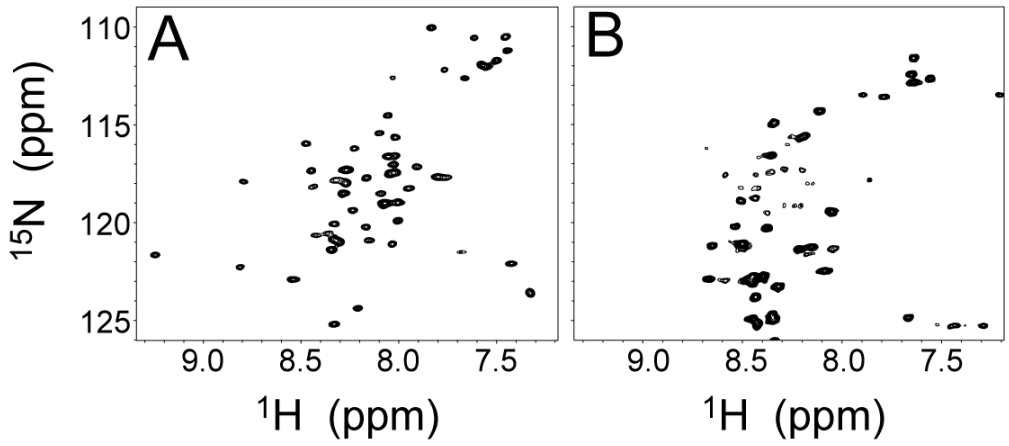

Figure S2. Gdn HCl-induced unfolding of PLN. *[^{1}H,^{15}N]-HSQC spectra of AFA-PLN in the absence (A) and in the presence of 2.79 M Gdn HCl (B).*

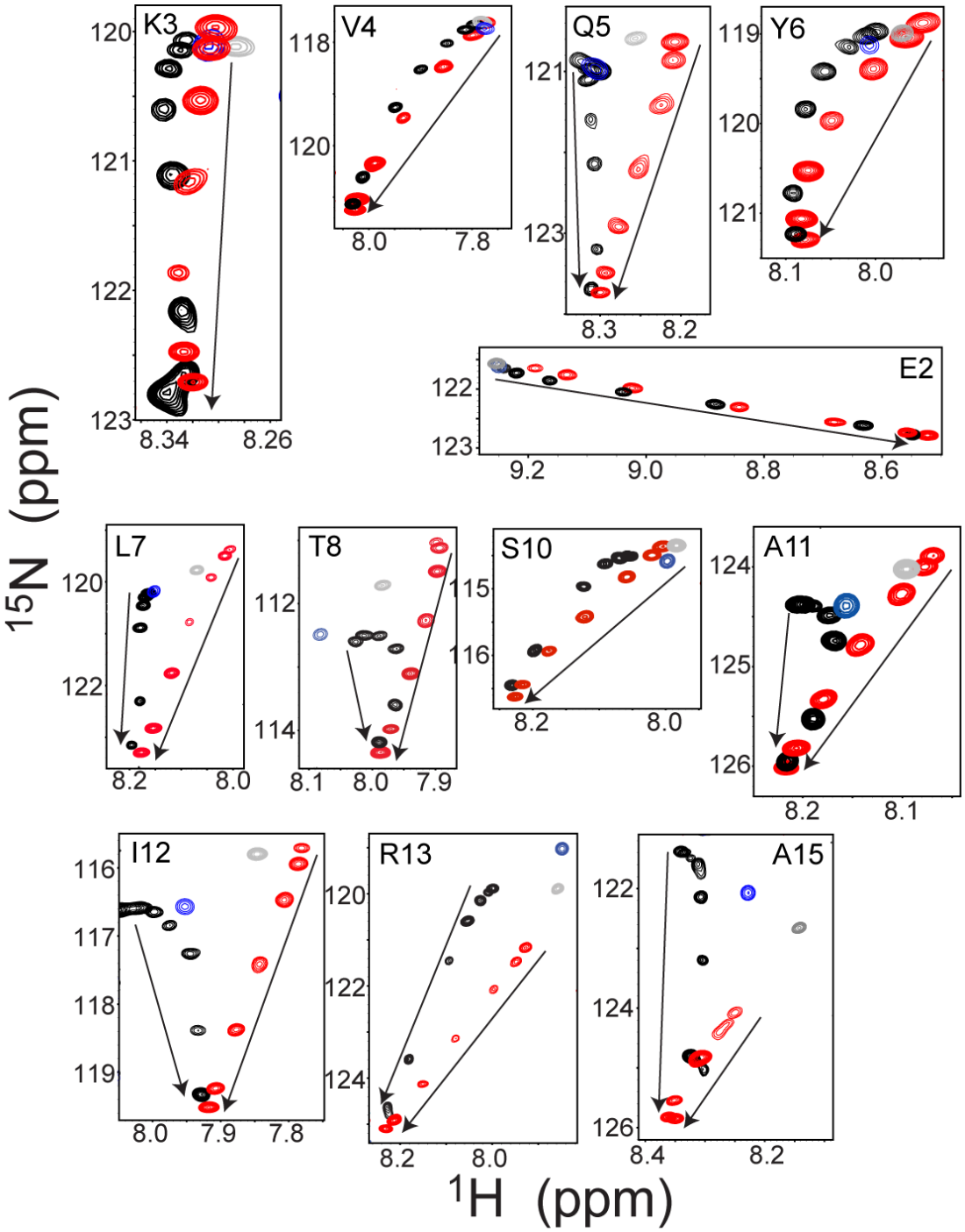
K3
V4
Q5
Y6
E2
L7
T8
S10
A11
I12
R13
A15
15N (ppm)
1H (ppm)

Figure S3. Chemical shift trajectories of residues in domain Ia upon chemical unfolding. *Overlay of [^{1}H,^{15}N]-HSQC spectra of AFA-PLN (black) and pS16-AFA-PLN (red) with increasing amounts of Gdn HCl (the direction of the arrow corresponds with increasing [Gdn HCl]). Peaks corresponding to S16E-AFA-PLN and S16D-AFA-PLN are shown in blue and grey respectively. Note that surrounding and overlapping peaks have been removed for clarity. Residues Q5 and R9 were excluded due to spectral overlap and residue 16 and 17 due to the large effect of mutation or phosphorylation on peak position.*

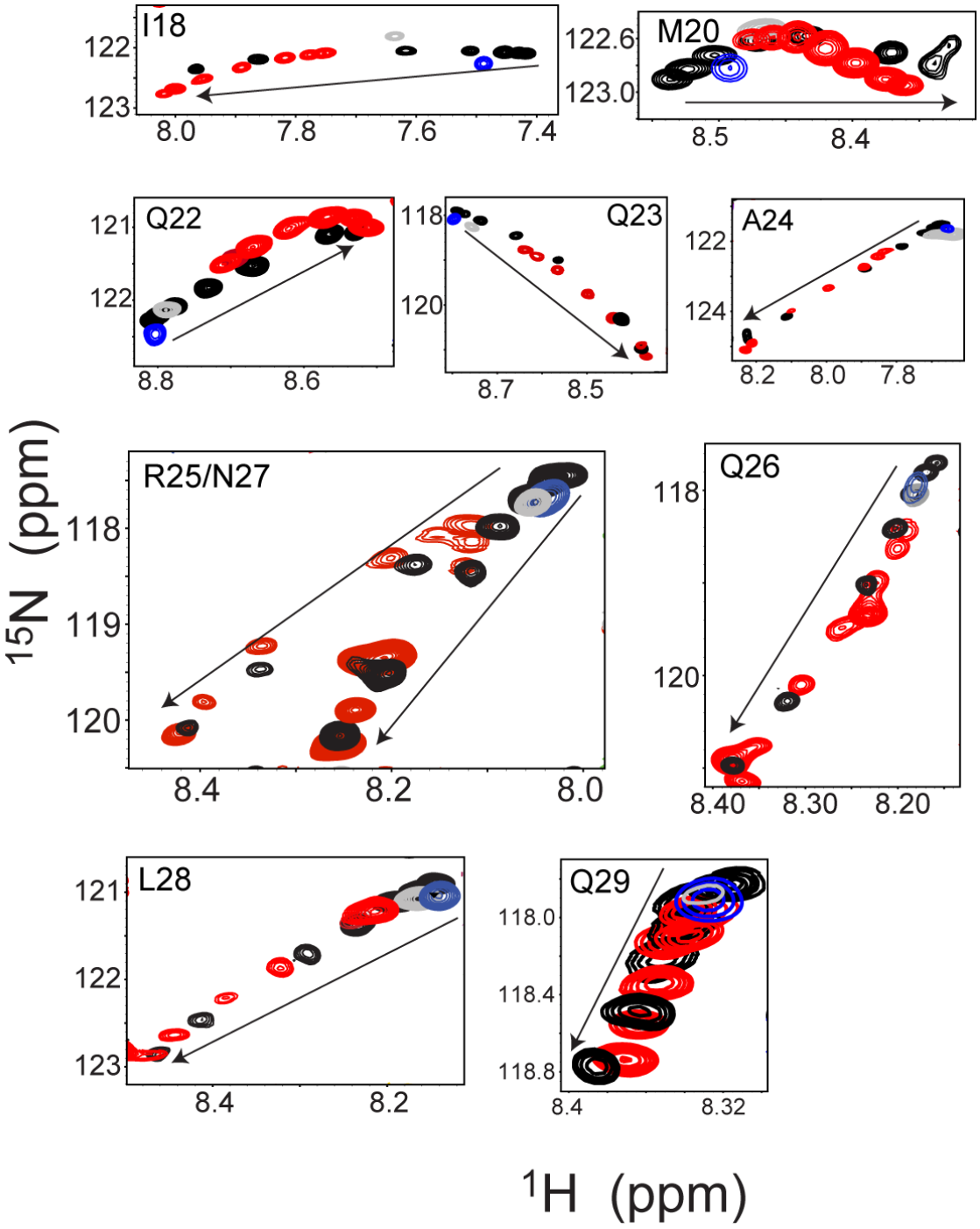
I18
122
123
8.0
7.8
7.6
7.4
M20
122.6
123.0
8.5
8.4
Q22
121
122
8.8
8.6
Q23
118
120
8.7
8.5
A24
122
124
8.2
8.0
7.8
R25/N27
118
119
120
8.4
8.2
8.0
Q26
118
120
8.40
8.30
8.20
L28
121
122
123
8.4
8.2
Q29
118.0
118.4
118.8
8.4
8.32
15N (ppm)
1H (ppm)

Figure S4. Chemical shift trajectories of residues in domain Ib upon chemical unfolding. *Overlay of [^{1}H,^{15}N]-HSQC spectra of AFA-PLN (black) and pS16-AFA-PLN (red) with increasing amounts of Gdn HCl (the direction of the arrow corresponds with increasing [Gdn HCl]). Peaks corresponding to S16E-AFA-PLN and S16D-AFA-PLN are shown in blue and grey, respectively. Surrounding and overlapping peaks have been removed for clarity.*

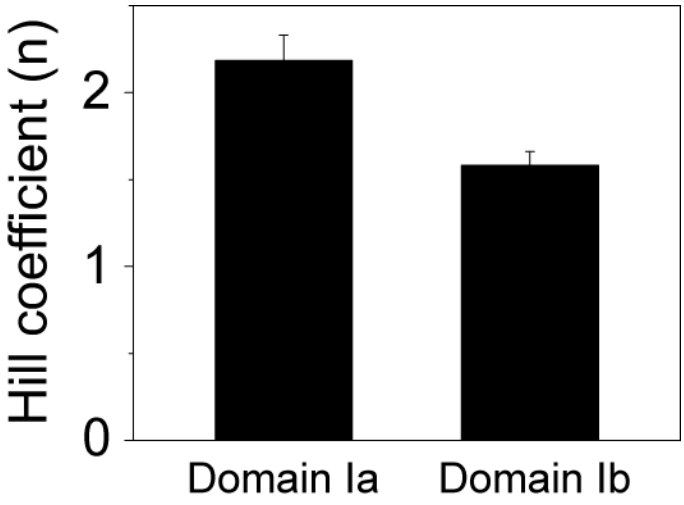

Figure S5. Hill coefficients determined from the hyperbolic fitting of the 15N chemical shift changes upon Gdn HCl unfolding *of AFA-PLN to the Hill equation for domain Ia (residues 3-8 and 10-16) and domain Ib (residues 22-28). Error bars indicate the standard error of the mean. The averages for domains Ia and Ib are significantly different as determined by a student's t-test (p-value of 0.0066).*

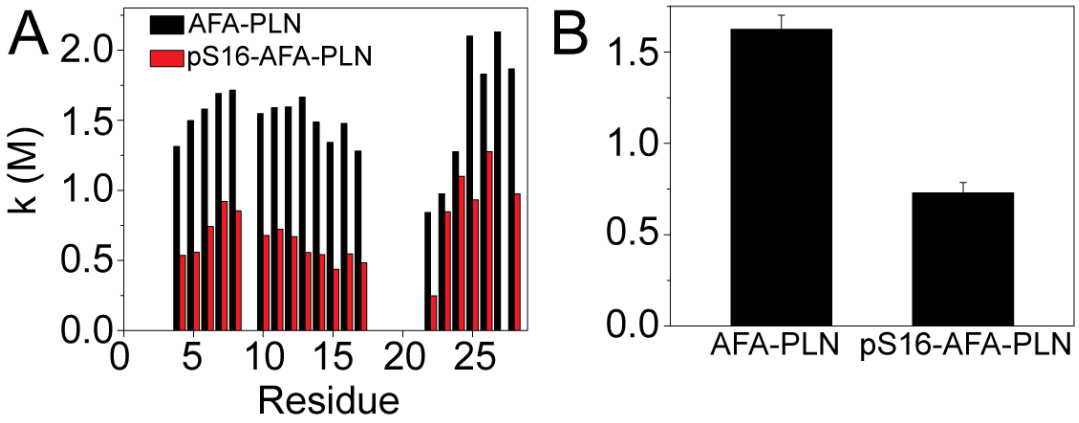

Figure S6. (A.) Unfolding midpoints (k) for residues in domain Ia and Ib of AFA-PLN and pS16-AFA-PLN. (B.) Average unfolding midpoint (k) for residues in domains Ia and Ib (3-17 and 22-28) for AFA-PLN and pS16-AFA-PLN. Error bars indicate the standard error of the mean. The averages for AFA-PLN and pS16-AFA-PLN are significantly different as determined by a t-test (p-value of 0.0042).

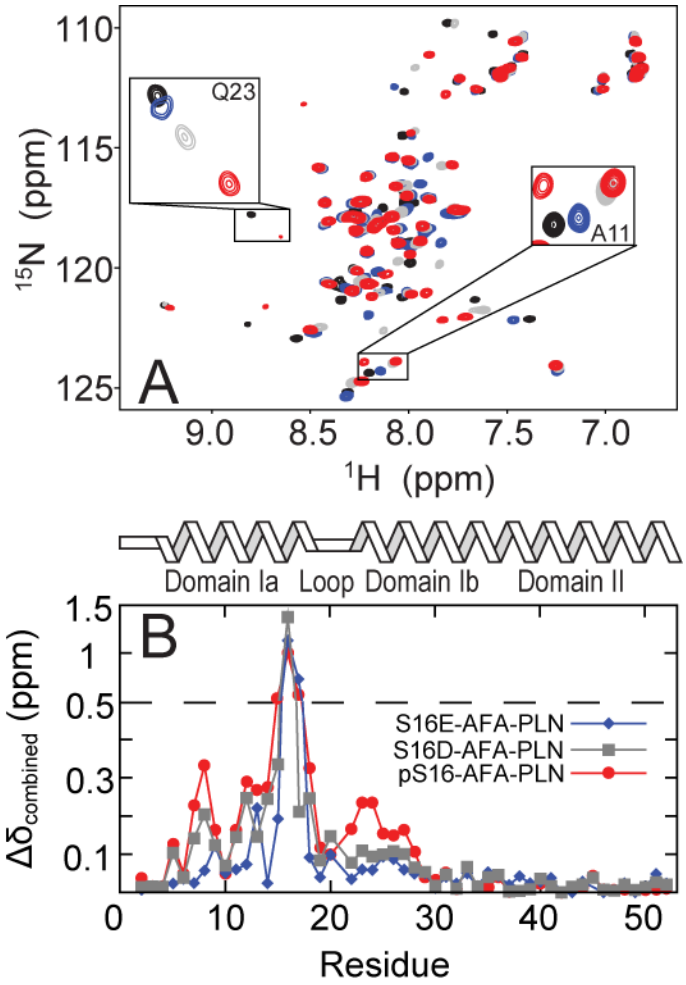

Figure S7. (A) [1H,15N]-HSQC spectra *for AFA-PLN (black), S16E-AFA-PLN (blue), S16D-AFA-PLN (grey), and pS16-AFA-PLN (red). Insets (A): residues showing the gradual change in chemical shifts from AFA-PLN → S16E-AFA-PLN → S16D-AFA-PLN → pS16-AFA-PLN. (B) ^{1}H and ^{15}N combined chemical shift difference ($\Delta\delta_{combined}$, defined in Eq 6) between AFA-PLN and phosphorylated and pseudo-phosphorylated variants (S16E-AFA-PLN, S16D-AFA-PLN and pS16-AFA-PLN).*

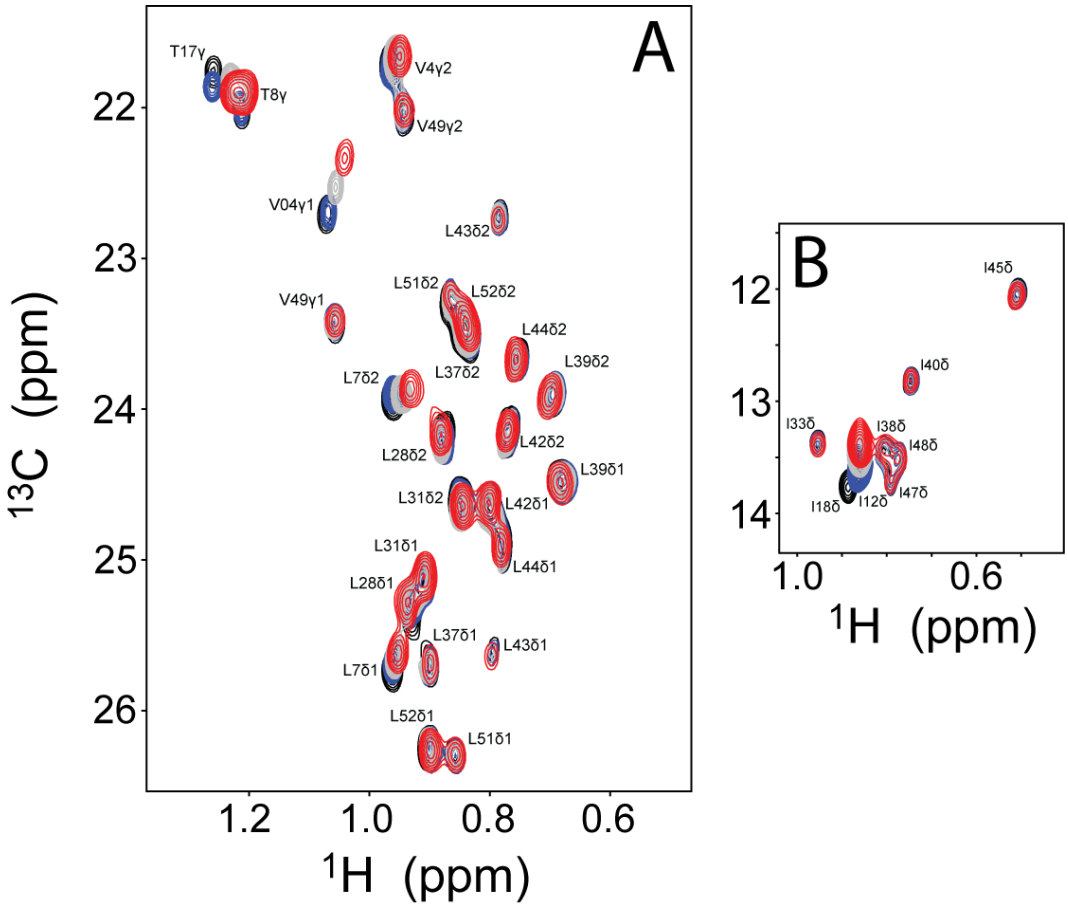

Figure S8. [1H,13C]-HSQC spectra *of (A) Leu, Val, Thr, and (B) Ile methyl groups for AFA-PLN (black), S16E-AFA-PLN (blue), S16D-AFA-PLN (grey) and pS16-AFA-PLN (red).*

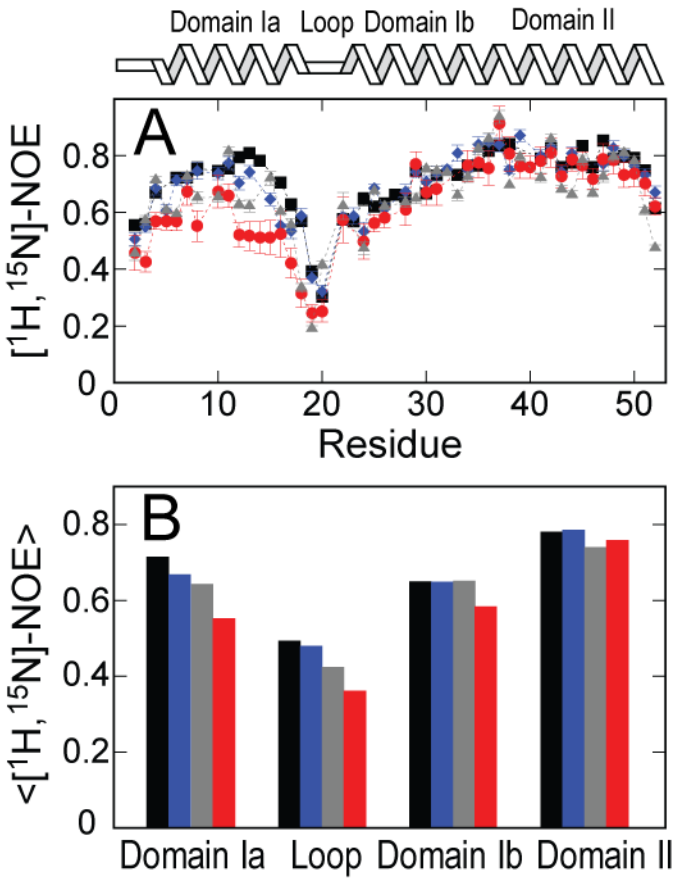

Figure S9. Fast (ps-ns) backbone dynamics *of AFA-PLN and variants. (A) Residue-specific [^{1}H,^{15}N] heteronuclear-NOEs for AFA-PLN (black), S16E-AFA-PLN (blue), S16D-AFA-PLN (grey), and pS16-AFA-PLN (red). (B) Average of [^{1}H,^{15}N] heteronuclear-NOEs for the different dynamic domains.*

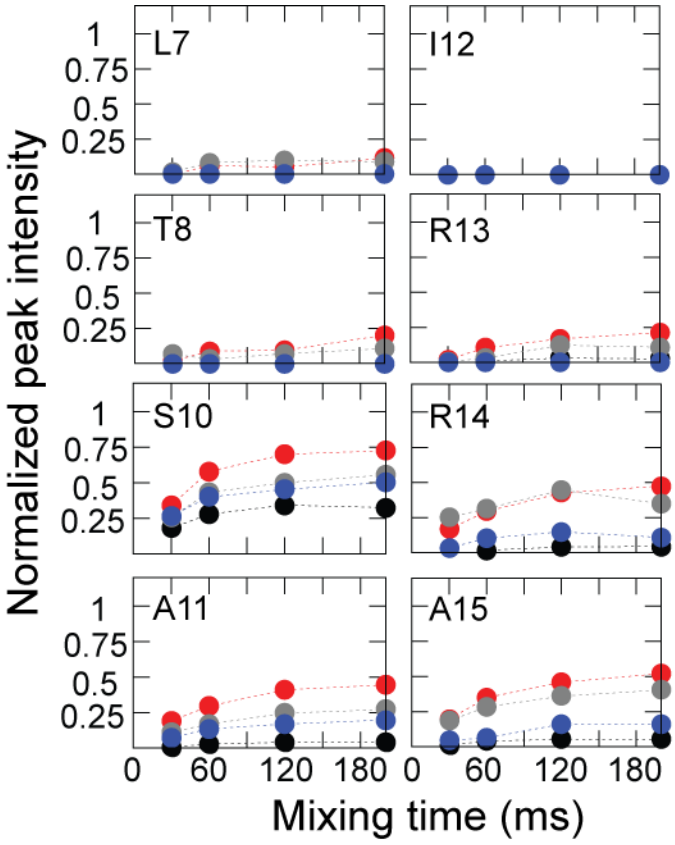

Figure S10. Solvent exchange curves from [1H,15N]-CLEANEX experiments *for residues in domain Ia of AFA-PLN (black), S16E-AFA-PLN (blue), S16D-AFA-PLN (grey), and pS16-AFA-PLN (red). Note for L7, T8, I12, and R13, the black circles are overlapped with the blue points. For I12, all circles are overlapped, indicating very slow amide hydrogen exchange with H_2O.*

Table S1. Amide ^{15}N chemical shift changes upon unfolding, and results from fitting the chemical shift trajectories to the Hill equation for AFA-PLN.

Residue	*START (ppm)*	*END (ppm)*	*k (M)*	*n*
2	121.67	123.86	2.50	0.94
3	120.14	125.41	2.57	1.38
4	117.78	122.19	1.31	1.58
5	120.98	126.48	1.50	1.70
6	119.04	122.10	1.58	1.68
7	120.27	124.01	1.69	2.43
8	112.51	114.51	1.71	3.36
9				
10	114.51	116.88	1.55	2.55
11	124.38	126.35	1.59	2.46
12	116.62	120.05	1.59	2.38
13	120.02	126.57	1.66	1.94
14	119.04	123.49	1.49	2.31
15	121.43	124.07	1.34	2.43
16	110.15	115.94	1.48	2.21
17	110.73	116.55	1.28	1.94
18	122.07	122.40	2.02	5.35
19	125.17	124.76	0.54	2.62
20	122.83	122.64	0.17	5.44
22	122.20	120.88	0.84	1.76
23	118.06	120.51	1.61	1.78
24	121.64	125.30	1.28	1.97
25	117.56	121.76	2.10	1.51
26	117.82	122.69	1.83	1.47
27	117.52	121.97	2.13	1.46
28	120.97	123.95	1.87	1.39
29	117.84	120.55	4.53	1.31

Table S2. Amide ^{15}N chemical shift changes upon unfolding, and results from fitting the chemical shift trajectories to the Hill equation pS16-AFA-PLN

	START (ppm)	END (ppm)	k (M)	n
2	121.65	122.91	0.41	1.24
3	120.07	123.13	0.72	1.39
4	117.64	121.70	0.54	1.31
5	120.70	124.02	0.56	1.49
6	118.87	121.85	0.74	1.13
7	119.37	124.23	0.92	1.31
8	111.00	115.07	0.85	1.32
9				
10	114.39	117.01	0.68	1.28
11	123.91	126.39	0.72	1.31
12	115.79	120.11	0.67	1.33
13	121.30	125.55	0.56	1.40
14	120.28	123.65	0.54	0.97
15	124.22	125.94	0.44	1.74
16	113.35	116.40	0.55	1.31
17	113.10	115.17	0.48	1.40
18	122.10	122.85	0.80	1.57
19	124.79	125.30	4.00	1.30
20	122.58	123.01	0.98	1.75
22	121.46	120.90	0.25	2.44
23	118.75	121.78	0.85	1.13
24	122.30	126.07	1.10	1.16
25	118.12	120.20	0.93	2.54
26	118.45	122.41	1.28	0.98
27				
28	121.23	123.30	0.97	1.24
29	118.00	119.84	4.32	0.93

Chapter 3- cAMP-Dependent Protein Kinase A Selects the Excited State of the Membrane Substrate Phospholamban

Reprinted with permission from:

Masterson, L.R., Yu, T., Shi, L., Wang Y., Gustavsson, M., Mueller, M.M., Veglia, G., cAMP-Dependent Protein Kinase A Selects the Excited State of the Membrane Substrate Phospholamban *J. Mol. Biol.* 2011, 412, 2, 155-164

Phosphorylation of membrane proteins is a central regulatory and signaling mechanism across cell compartments. However, the recognition process and phosphorylation mechanism of membrane-bound substrates by kinases are virtually unknown. cAMP-dependent protein kinase A (PKA) is a ubiquitous enzyme that phosphorylates several soluble and membrane-bound substrates. In cardiomyocytes, PKA targets phospholamban (PLN), a membrane protein that inhibits the sarcoplasmic reticulum Ca^{2+}-ATPase (SERCA). In the unphosphorylated state, PLN binds SERCA, reducing the calcium uptake and generating muscle contraction. PKA phosphorylation of PLN at S16 in the cytoplasmic helix relieves SERCA inhibition, initiating muscle relaxation. Using steady-state kinetic assays, NMR spectroscopy, and molecular modeling, we show that PKA recognizes and phosphorylates the excited, membrane-detached R-state of PLN. By promoting PLN from a ground state to an excited state, we obtained a linear relationship between rate of phosphorylation and population of the excited state of PLN. The conformational equilibrium of PLN is crucial to regulate the extent of PLN phosphorylation and SERCA inhibition.

3.1 Introduction

Protein phosphorylation is a central mechanism in cell signaling and regulation. Inhibitory proteins are reversibly phosphorylated to cycle between active and inactive states. (1) These different states are characterized by conformational and dynamic transitions that are essential for stability and function. (2, 3) Muscle proteins are salient examples of these structure-dynamics-function correlations. The rhythmic contraction and relaxation of the heart muscle, for instance, are orchestrated by protein complexes that regulate calcium homeostasis, and phosphorylation is the driving force to control these cyclic events.(4)

In muscle cell membranes, protein kinases target peripheral or integral membrane proteins involved in regulatory complexes, initiating signaling events that cross the membrane bilayer.(4) This is the case of phospholamban (PLN), a reversible inhibitor of the sarcoplasmic reticulum Ca^{2+}-ATPase (SERCA).(5, 6) SERCA is a 110-kDa membrane-embedded, adenosine 5′-triphosphate (ATP)-driven calcium pump and is regulated by intramembrane interaction with PLN. In its storage form, PLN exists in a pinwheel pentameric assembly that de-oligomerizes upon interaction with SERCA.(5, 7) PLN comprises multiple dynamic domains: the inhibitory domains include the transmembrane segment (domain II) and the juxtamembrane domain Ib, (8-12) while the regulatory elements include a short dynamic loop and an amphipathic helix (domain Ia) that interacts reversibly with the membrane and contains the protein kinase A (PKA) recognition sequence. (13, 14) Domain Ia of PLN exists in at least four conformational states: T-state (membrane attached and helical), T′-state (membrane attached and partially helical), R′-state (membrane attached and unfolded), and R-state (membrane detached and unfolded). (6, 11, 15) PLN phosphorylation at Ser16 by PKA in domain Ia is sufficient to reverse SERCA inhibition and increases the enzyme affinity for calcium that is pumped into the sarcoplasmic reticulum, initiating muscle relaxation. (16) Disruptions in this phosphorylation/dephosphorylation cycle lead to pathologies such as dilated cardiomyopathy. (17)

Once unleashed from its tetrameric assembly by cyclic adenosine monophosphate, (18) the monomeric catalytic subunit of PKA (PKA-C) recognizes, binds, and

phosphorylates PLN. The molecular mechanisms of PLN recognition by PKA are still elusive. Recent NMR and X-ray data on PKA-C in a ternary complex with nucleotide and the cytoplasmic domain of PLN suggest that binding by PKA-C may involve an unfolding of PLN domain Ia (**Figure 1a**). (3) This result is striking given that, in several membrane mimics, the most populated state for the full-length PLN is folded, with the majority of the recognition sequence in close proximity with the lipid membrane. (7-9, 12, 19, 20)

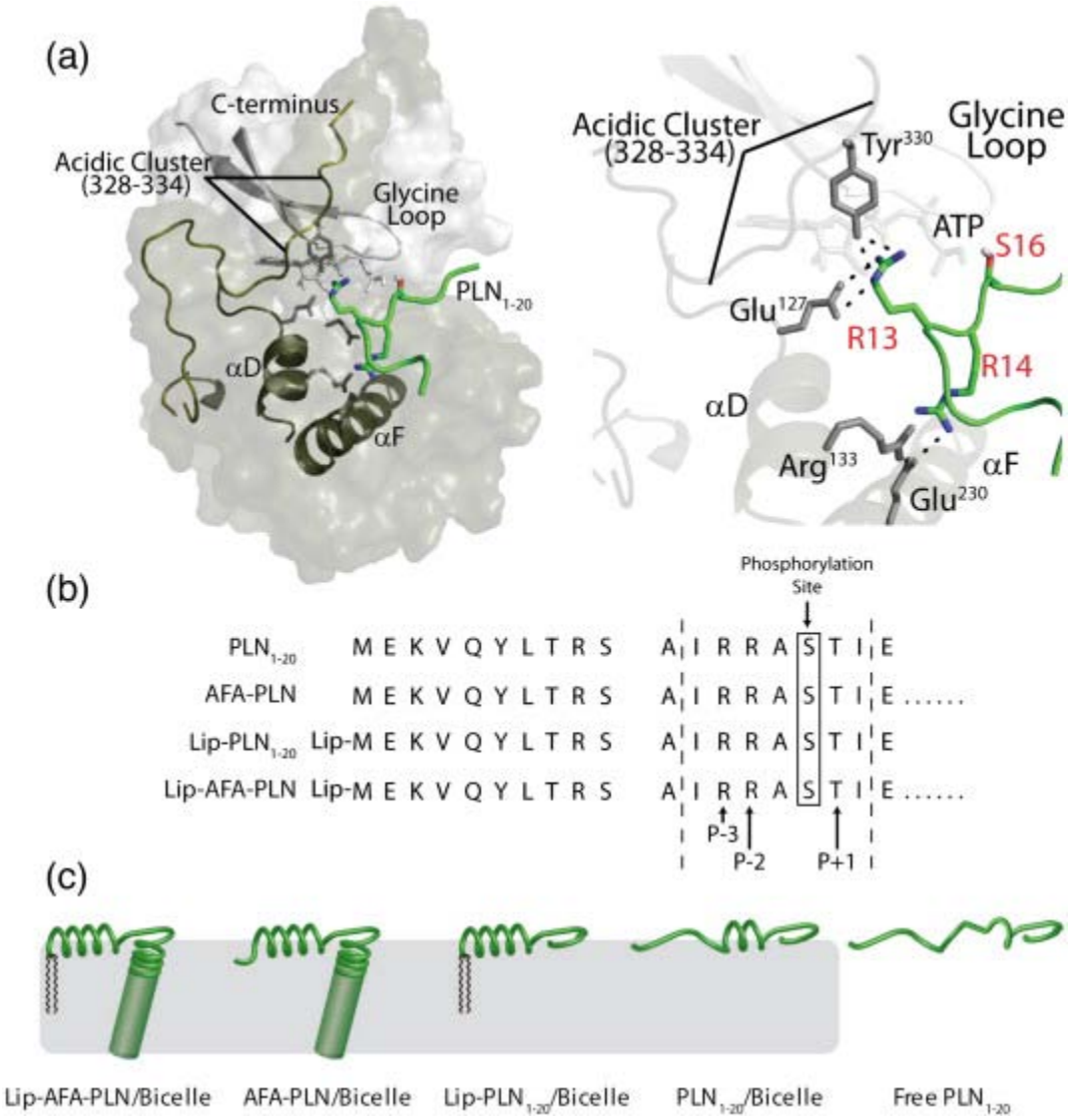

Figure 1. (a) Crystal structure of PKA-C bound to $PLN_{1–20}$ *showing the key contacts between substrate (green) and enzyme (gray) within the binding groove. (b) Primary*

structures and (c) cartoon representations of the different analogs used to mimic the T- and R-states of PLN.

To gain insights into the recognition mechanism of PKA-C for PLN, we used a combination of steady-state kinetic assays, NMR, and molecular modeling. We show that PKA-C preferentially binds and phosphorylates a membrane-detached and unfolded conformation of PLN, corresponding to the excited R-state of this protein. (15) Using a series of PLN variants in different lipid environments, we tuned the extent that domain Ia of PLN interacts with the membrane. We found a linear correlation between the catalytic efficiency of phosphorylation and the population of membrane-detached and unfolded domain Ia of PLN. Molecular modeling from NMR data shows that the kinase binds an extended conformation of PLN in solution. Taken together, these data demonstrate that the conformational equilibrium of PLN is an important requirement for efficient phosphorylation by PKA and activation of SERCA.

3.2 Results

3.2.1 PKA-C selects an extended conformation of PLN

To understand whether PKA-C has a preference for the different conformational states of PLN, we prepared several PLN analogs that mimicked different populations of the ground and excited states of the cytoplasmic domain Ia (**Figure 1b and c**). The first PLN analog was obtained by synthetic incorporation of dialkyl 1′,3′-dioctadecyl-*N*-succinyl-L-glutamate (Lip) to the N-terminus of full-length PLN. This analog has been shown to skew the equilibrium toward the well-folded, membrane-associated T-state, anchoring domain Ia to the lipid membrane. (21) On the other hand, to mimic the membrane-detached, unfolded R-state, we synthesized a peptide corresponding to the cytoplasmic domain Ia (PLN_{1-20}) and studied it in the absence of any membrane-mimicking environment. Under these conditions, PLN_{1-20} is an intrinsically disordered polypeptide as probed by circular dichroism (CD), NMR chemical shifts, and nuclear spin relaxation measurements (3) (**Figure S1**). To mimic the gradual progression from a full T-state to the R-state, we used synthetic and recombinant versions of full-length PLN with no lipidation, as well as a lipidated peptide corresponding to domain Ia of PLN (Lip-PLN_{1-20}).

Finally, since full-length PLN reconstituted in dodecylphosphocholine (DPC) micelles has been well characterized by our laboratory, we also included this form in our studies.

For each of the PLN analogs, PKA-C-catalyzed steady-state phosphorylation assays were performed, and the Michaelis–Menten constants were measured. Although all reactions eventually reached completion and displayed similar values for k_{cat} (Table S1), the K_m values for the reactions differed significantly. Specifically, PLN_{1-20} in the absence of membranes was phosphorylated with a high catalytic efficiency ($k_{cat}/K_m \sim 0.6\ \mu M^{-1}\ s^{-1}$), while full-length PLN in DPC micelles was phosphorylated with a low catalytic efficiency ($k_{cat}/K_m \sim 0.05\ \mu M^{-1}\ s^{-1}$). A variety of intermediate catalytic efficiencies were measured for the phosphorylation of PLN analogs under different conditions, as reported in **Figure 2**. The trend in catalytic efficiencies agrees qualitatively to an increasing population of R-state in PLN.

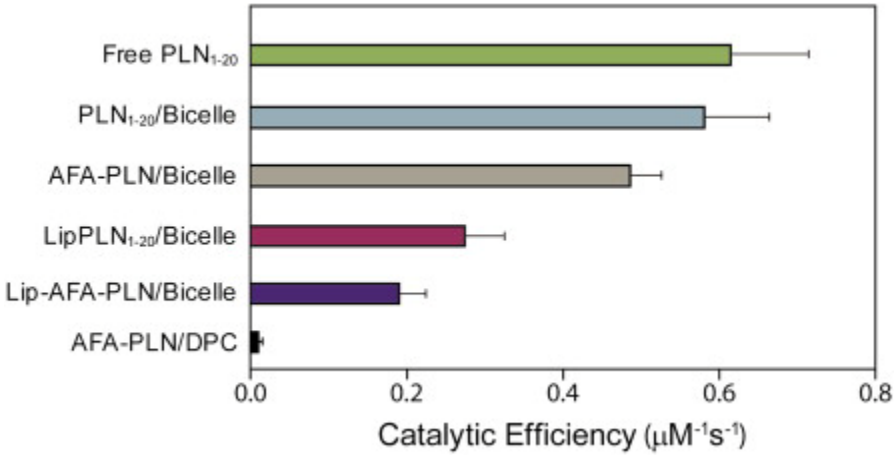

Figure 2. Structure–function correlations for PLN analogs. *The catalytic efficiency of the kinase increases with the increase in the R-state population. The errors were propagated from least-squares fitting analysis. Each data point in the Michaelis–Menten plot represented an average of triplicate measurements.*

To provide a more quantitative analysis for the T-state population of the PLN analogs, we characterized the degree of folding using NMR. As reported previously, (3) the PLN peptide constitutes a good mimic of the cytoplasmic domain of full-length PLN as verified by chemical shift indices (CSIs) and secondary structure propensity scores. The

cytoplasmic domain of PLN is mainly α-helical ($\sim$ 4% R-state) (22) in DPC micelles. (15) CSI and secondary structure propensity scores for PLN_{1-20} in the presence of DPC micelles agreed well with those findings, indicating that the peptide forms a stable α-helix (**Figure S1**). In fact, only small differences were detected between the cytoplasmic regions of both constructs. The latter demonstrates that PLN_{1-20} closely mimics the cytoplasmic region of the full-length protein.

Also, the chemical shifts of methyl-bearing side chains of the PLN cytoplasmic domain provide excellent probes for the T- and R-states of the protein. (15) Therefore, we measured the chemical shift positions of the methyl groups for each of the PLN analogs under conditions similar to the steady-state assays. The methyl groups showed a linear trend between the PLN_{1-20} free in solution (100% R-state (15)) and the PLN in DPC micelles ($\sim$ 4% R-state (22)) (**Figure 3a**). The other analogs represented different intermediates between these two extremes, illustrating that these species gradually shift the population of the R-state toward the T-state (**Figure 3a**). Also, CD spectroscopy measurements on PLN_{1-20} analogs revealed a gradual increase in α-helical content in the presence of bicelles and, in particular, when the analog is lipidated. We therefore used the position of the methyl resonances to estimate the extent of unfolding and quantify the R-state for these analogs (**Figure 3b**). As expected, the comparison of PLN and Lip-PLN in isotropic bicelles showed a decrease in the R-state for Lip-PLN, consistent with the trends observed by CD spectroscopy.

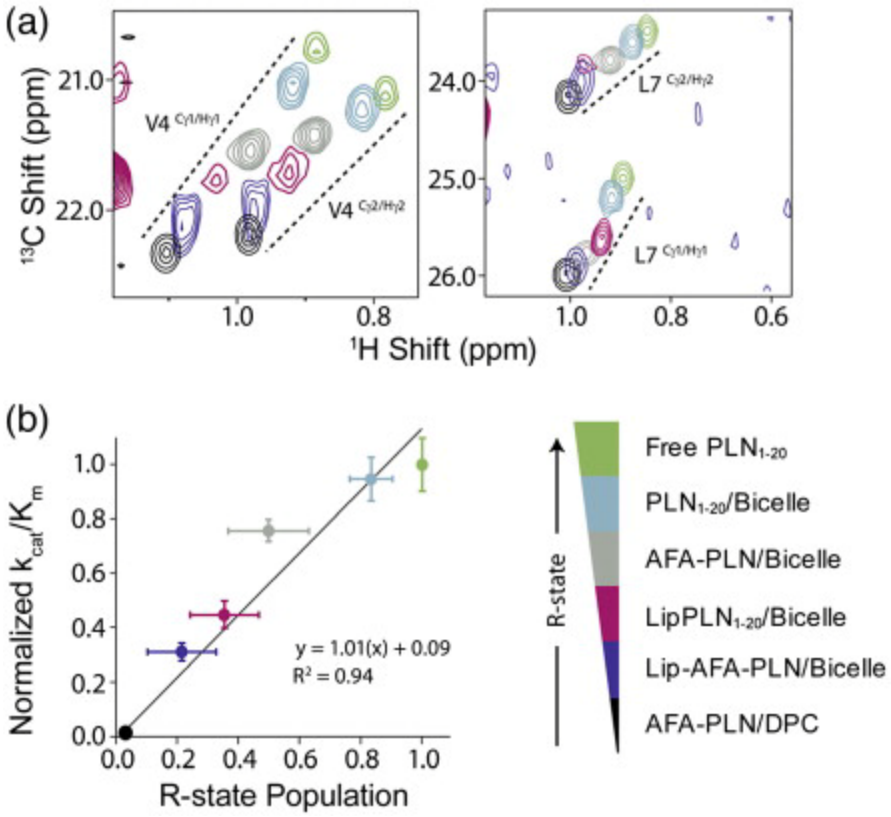

Figure 3. Quantitative relationship between the extent of R-state and phosphorylation efficiency. *(a) Selected regions of the methyl-transverse relaxation optimized spectroscopy NMR spectra for the different PLN analogs display a linear trend in the chemical shifts from the T- to R-state. (b) Linear relationship between the population of R-state of the PLN analogs and their respective phosphorylation kinetics. Errors in % R-state reflect the spread of populations estimated from the position of 12 chemical shifts.* ^{13}C *and* ^{1}H *chemical shifts from residues V4, L7, and I12 were used as probes of the R-state population.*

A quantitative relationship between the efficiency of phosphorylation and the population of the membrane-detached state (full R-state) of PLN was obtained when we plotted kcat/Km against the population of R-state (**Figure 3b**). Notably, the extent of unfolded R-state is linearly correlated with increased phosphorylation efficiency. These results demonstrate that PKA-C preferentially binds and phosphorylates the membrane-detached conformation of PLN.

3.2.2 Molecular modeling of $PLN_{1–20}$ bound to PKA-C

To investigate how PKA-C recognizes and binds PLN and to characterize the protein-protein interface, we used a combination of NMR, mutagenesis, and sequence homology data to model the complex between enzyme and substrate. Chemical shift perturbation profiles in both the substrate and the enzyme were analyzed to provide harmonic distance restraints for the molecular model of the complex. Perturbations in PLN_{1-20} resonances were almost exclusively localized to the recognition region for PKA-C upon titration with the enzyme. These perturbations were used as restraints for modeling the molecular complex. As for our previous titrations with kemptide, (23) residues perturbed in PKA-C upon titration with PLN_{1-20} are located in the immediate vicinity of the substrate binding groove, as well as residues in remote regions of the enzyme. Substantial chemical shift perturbations are observed in the glycine-rich (residues 50-55), Asp184-Phe185-Gly186 (residues 185-187), activation (residues 190-197), and P + 1 (residues 198-205) loops. Distal sites are also affected: residues 30, 31, and 36, which lie toward the N-terminus, and residues 145, 146, 148, and 156 of the E helix. Perturbations are also apparent for residues 163 and 164 of β6, residue 271 in the loop connecting H and I helices, and residue 315 near the C-terminus.

The membrane-free conformation of the PLN_{1-20} peptide is mostly unstructured, with chemical shifts displaying characteristics of an intrinsically disordered polypeptide. (24-26) The negative [^{1}H,^{15}N]heteronuclear nuclear Overhauser effect values and the uniformity of the R_2/R_1 ratios indicate that, in solution, PLN_{1-20} is flexible and monomeric and reorients relatively fast. (27) When bound to PKA-C, the substrate does not show a defined secondary structure (α-helical or β-sheet conformations), as demonstrated by the relatively small changes in the chemical shift perturbation plot, as well as the CSIs for the 13Cα/13Cβ resonances (Fig. S2), supporting the previously published crystallographic structure. (3)

To model the complex, we used the coordinates from the crystal structure of PKA-C in the closed conformation (1ATP). Since PLN_{1-20} has sequence similarity with protein kinase inhibitor (PKI), the endogenous PKA-C inhibitor, we aligned the PLN recognition sequence in the PKA-C binding groove as defined by the crystal structure (

to PKI_{5-24} and ATP. (28) We oriented the side chain of the phosphorylation site (Ser16) of PLN_{1-20} toward the γ-phosphate of the ATP molecule. Chemical shift perturbations for PKA-C indicated that many areas distal to the binding site were perturbed by allosteric effects. Therefore, the crystal structure of PKA-C bound to PKI_{5-24} was used to filter out these long-range effects, considering only those residues in PKA-C with large chemical shifts (greater than the median value) and within 10-Å radius in the binding pocket defined by PKI_{5-24} (**Figure 4b**). The PKA-C crystal structure depleted of $PKI_{5–24}$ (29) was used as the initial structure and held fixed during simulated annealing calculations. The NMR data were implemented as harmonic distance restraints. (30) PLN_{1-20} was modeled starting from a helical conformation(8, 12) and was allowed to be fully flexible during the docking protocol. The final model of the complex is reported in **Figure 4c**. The ensemble of the PLN_{1-20} conformers is in an extended conformation within the enzyme binding pocket. Taken with the kinetic experiments, this model supports the hypothesis that the enzyme selects an extended conformation from the ensemble of states sampled by PLN. This extended conformation has its recognition sequence fully accessible and detached from the membrane surface.

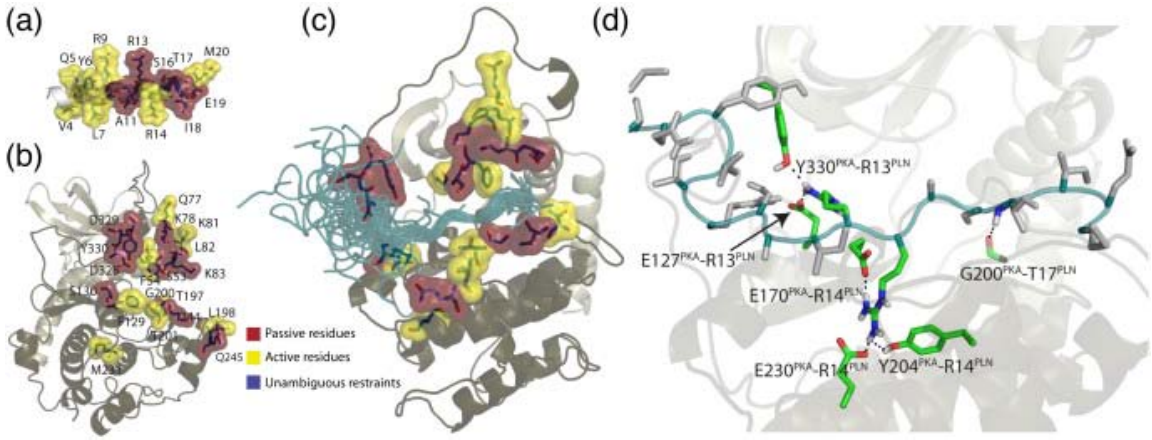

Figure 4. Hybrid X-ray and NMR-based molecular model of the complex between PLN_{1-20} and PKA-C. *Active (red) and passive (yellow) residues are indicated for (a) PLN_{1-20} and (b) PKA-C. (c) Twenty lowest conformers generated with HADDOCK.* (30) *(d) Atomic details of the interactions observed between PKA-C and PLN_{1-20} based on the molecular model.*

3.3 Discussion

Based on phosphorylation kinetic assays, NMR data, and molecular modeling, we propose a recognition model for PLN, as reported in **Figure 5**. Since both PLN and PKA-C undergo conformational equilibria between ground and excited states, (2, 3, 11, 15, 31) the recognition model exemplifies the recently theorized extended conformational selection model, where the two binding partners affect each other, with a mutual adjustment process and changing both energy landscapes. (32) In fact, PLN exists in equilibrium between four major conformational states, driven by the reversible binding of the cytoplasmic domain Ia to the membrane. The T-state (L-shaped configuration) with domain Ia adsorbed on the membrane surface is the most populated and represents the ground state of PLN, while the remaining three states (T′ , partially unfolded in domain Ib; R′ , partially unfolded at the N-terminus and in the C-terminal part of domain Ia; and an R-state, which has domains Ia and Ib unfolded) are less populated and represent the excited states. In the ground state, PLN is less accessible to the protein kinase and is poorly phosphorylated, whereas the excited R-state comprises an ensemble of conformations from which PKA-C selects the extended conformation that molds into the substrate binding site. On the other hand, PLN binding drives the PKA-C conformational equilibrium toward the closed state of the enzyme as probed by both X-ray and NMR spectroscopy. (2, 3)

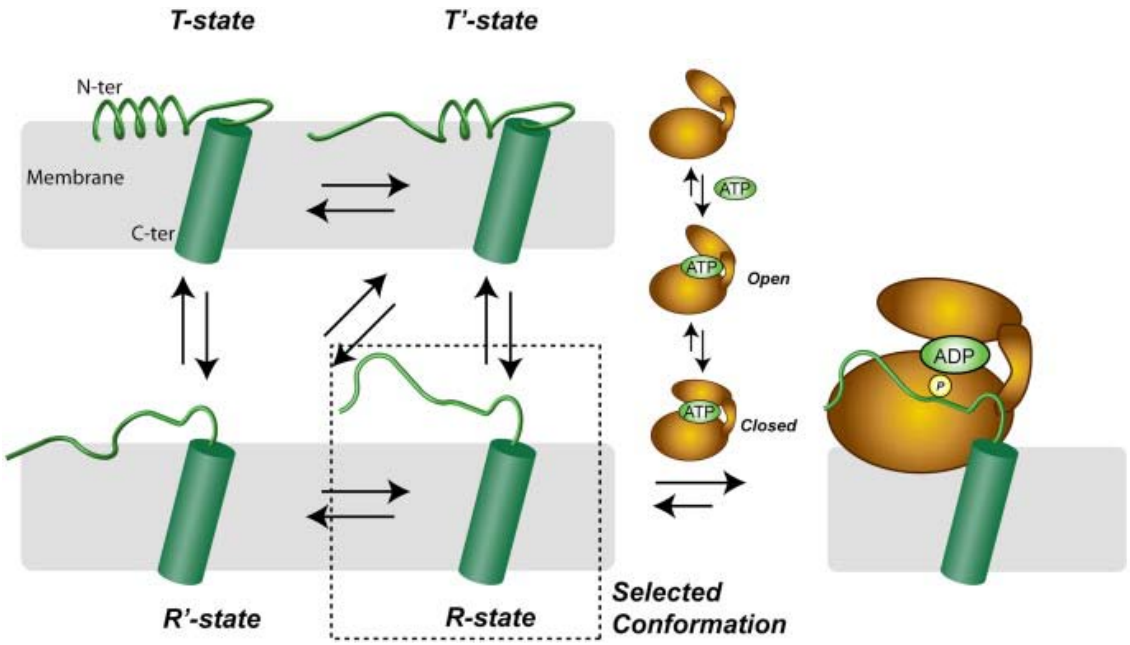

Figure 5. Extended conformational selection model for PLN recognition by PKA-C. *Both PKA-C and PLN have been shown to undergo conformational exchanges. PKA-C undergoes a global change that opens and closes its active site upon interaction with the nucleotide. This likely facilitates efficient binding of PLN, as shown previously.* (3) *PLN also undergoes conformational fluctuations.* (11, 15) *Unfolding of the cytoplasmic portion of PLN and detachment from the membrane facilitate the recognition and subsequent phosphorylation by PKA-C.*

The folding/unfolding transitions of PLN are relatively fast, (11) and the phosphorylation efficiency is proportional to the population of the most excited state (R), in which the helix of domain Ia is melted. In contrast, for the most helical construct studied (PLN in DPC micelles), the conformational equilibrium is skewed toward the full T-state, and the phosphorylation efficiency is much lower.

The overall phosphorylation efficiency trends for both the peptide and the full-length protein mirror one another, demonstrating that the cytoplasmic portion of the protein is a good model for the full protein. This latter result supports the selection of the peptide to model the molecular complex of PKA-C/ATP/PLN_{1-20}. Using chemical shift changes that

occurred upon formation of the Michaelis complex for both PKA-C and PLN_{1-20}, sequence homology with the high-affinity inhibitor peptide of PKA-C, and results from mutagenesis, we modeled the PKA-C/PLN_{1-20} complex. This complex indicates that PKA-C binds an unfolded conformation of PLN. Initial molecular dynamic simulations (data not shown) indicate that this complex is stable, with the recognition sequence of PLN1‑20 confined to the active site of the enzyme and regions outside of this remaining relatively mobile. This matches well with our previous nuclear spin relaxation measurements of the bound peptide, which indicated high mobility across the substrate backbone, with the exception of the recognition sequence, which was more ordered. (3)

The conformational dynamics of the cytoplasmic domain of PLN are reminiscent of the binding-and-folding model proposed for amphipathic helices of membrane proteins. (33, 34) According to this model, interactions with the membrane bilayer surface (likely driven by electrostatic residues) cause the amphipathic peptide to insert and fold onto the membrane with the hydrophobic face pointing toward the hydrocarbon region of the membrane bilayer and the hydrophilic face pointing toward the lipid headgroup/water interface. In addition to regulating the extent of PLN interaction with the membrane bilayer, a similar binding-and-folding mechanism is probably present in the PLN/SERCA inhibitory complex. (8) As suggested by NMR and electron paramagnetic resonance studies, phosphorylation probably shifts the conformational equilibrium toward a non-inhibitory state of PLN, affecting the stability of domains Ia and Ib. We are currently investigating this hypothesis.

The reversible folding of domain Ia is likely part of a more general class of regulation mechanisms that are mediated by amphipathic domains. (35, 36) For instance, a parallel can be made with the autoinhibitory process that takes place in Vav, a multidomain protein that is negatively regulated by its DH domain. (37) In Vav, autoinhibition is reversibly modulated by a folding/unfolding equilibrium of the amphipathic DH helix, which fluctuates between protein-free and bound conformations. This equilibrium is shifted toward the unfolded state upon phosphorylation at Tyr174. Phosphorylation efficiency was correlated with unfolding of this amphipathic domain. Another example is LOV2-Jα. (38, 39) As for Vav, LOV2-Jα also contains a region that can switch between an amphipathic α-helix and an unfolded conformational state. The conformational

equilibrium of this region dictates the inhibitory strength of the protein. These results mirror the current study with PLN, where the catalytic efficiency of the kinase is linearly correlated with the population of the unfolded excited state, which exposes the phosphorylation site to the protein kinase.

This current study demonstrates that the modulation of the cytoplasmic domain to different states affects the ability of PLN to adapt to its binding partner, PKA-C. The ability to interact with other proteins through a population shift highlights the scaffolding capability PLN has for a number of known binding partners: PKA-C, protein phosphatase-1, Ca^{2+}/calmodulin-dependent kinase II, SERCA, HS1-associated protein X-1, and A-kinase anchoring protein 18δ. The coupling of conformational plasticity of the PLN cytoplasmic domain and its interactions with cytosolic proteins (e.g., PKA-C) also demonstrates the importance of dynamics for signaling processes to occur efficiently and transiently to facilitate multiple functional interactions. (40-44) This appears to be particularly important for the case studied here, where a protein links signaling between the cytosolic and the membranous environments of the cell.

Finally, this work underscores the role of the complex conformational fluctuations that PLN undergoes to cater to the phosphorylation process by PKA-C and, ultimately, SERCA regulation. Future studies on the localization of PKA (i.e., role of N-terminal myristoylation and A-kinase anchoring protein binding) will elucidate how regulatory domains, such as domain Ia of PLN, are integrated into macromolecular complexes to achieve signal specificity.

3.4 Materials and Methods

3.4.1 Materials

Lactic dehydrogenase (LDH) from bovine heart and pyruvate kinase (PK) from rabbit muscle were purchased from Sigma (Solon, OH, USA). ATP, phosphoenolpyruvate (PEP), magnesium chloride, and reduced nicotinamide adenine dinucleotide (NADH) were purchased from Sigma-Aldrich (St. Louis, MO, USA).

3.4.2 Expression and purification of PLN and $PLN_{1–20}$

PLN_{1-20} was expressed in *Escherichia coli* cells as a fusion system with maltose binding protein and a 6-histidine tag to facilitate purification. (45, 46) The cells were grown overnight at 30 °C in LB rich media. At OD600 ~ 1.0, cells were transferred into M9 minimum media, containing ^{15}N-labeled NH_4Cl or ^{13}C-labeled glucose for uniformly ^{15}N- or ^{13}C-labeled NMR samples. IPTG (0.5 mM) was added to induce fusion protein expression at 37 ° C for 5 h . The pelleted cells were lysed in phosphate buffer (pH 8.0) in the presence of 6 M guanidine. The cell lysate was separated by centrifugation (18,000 rpm at 4 °C for 40 min). The purification of the fusion protein was carried out using Ni^{2+}-NTA resin. The eluted fusion protein was then dialyzed and cleaved with tobacco etch virus protease, which separated the PLN_{1-20} from maltose binding protein and the 6-His tag. The final purification was achieved by reversed-phase HPLC using a C-18 column (Vydac). After HPLC purification, approximately 2 mg of PLN_{1-20} was obtained from 150 mg of fusion protein. The mass of the purified PLN_{1-20} (2472.8 Da) was confirmed by electrospray ionization time-of-flight mass spectroscopy. The full-length PLN was expressed and purified as reported previously. (46)

3.4.3 Peptide synthesis

Peptide synthesis was performed using standard Fmoc chemistry on an Applied Biosystems Pioneer or a CEM Liberty/Discover microwave synthesizer, starting with Fmoc-Glu(O*t*Bu)-PEG-PS resin (0.4 g, 0.5 mmol/g). The side-chain protecting groups were 2,2,5,78-pentamethylchroman-6-sulfonyl (Pmc) for arginine; N^{ω}-triphenylmethyl (Trt) for asparagine and glutamine; t-butyl ester (O*t*Bu) for glutamic acid; and t-butyl ethers (tBu) for serine, threonine, and tyrosine. Addition of the lipid moiety was performed using standard coupling reagents and dialkyl 1′,3′-dioctadecyl-*N*-succinyl-L-glutamate to the unprotected N-terminal methionine residue. (47) Cleavage of the resin-bound peptide was performed using Reagent K (82.5% trifluoroacetic acid, 5% phenol, 5% thioanisole, 2.5% 1,2-ethandiol, and 5% water) for 3 h at 298 K. The resin mixture was washed three times (2 ml each) using the same cocktail, and filtrate was collected. The peptide was precipitated overnight at 273 K in 80 ml of diethyl ether and then collected by centrifugation and washing the pellet three times with 30 ml of diethyl

ether. The crude peptide was then purified by preparative HPLC using a Waters C18 reversed-phase cartridge (2.5 cm × 10 cm, 15 μm, 300 Å) with 0.1% trifluoroacetic acid and CH_3CN as eluents and detection at 220 nm. A linear gradient of 100:0 to 70:30 over 30 min at 5 ml/min was used. The purity of pooled fractions was > 97% as determined by analytical HPLC using a Vydac C18 column (0.46 cm × 25 cm) and confirmed by electrospray ionization time of flight; for the analog PLN_{1-20}: calculated, 2252.65 *m*/*z*; found, 2252.73 *m*/*z*. Stock solutions were prepared in water/acetonitrile and lyophilized. The concentrations of these solutions were verified by amino acid analysis.

3.4.4 Kinetic assays

The steady-state enzymatic rates of phosphorylation for PLN analogs were measured spectrophotometrically at 299 K following the procedure by Cook *et al*. (48) Briefly, the oxidation of NADH by PK and lactate dehydrogenase is coupled to the production of ADP, which occurs during the PKA-C-catalyzed phosphoryl transfer. The reaction rates were monitored at 340 nm using a Molecular Devices SpectraMax Plus^{384} equipped with a 96-well microplate reader. The reaction solutions contained 50 mM Mops (pH 7.0), 20 mM DTT, 10 mM $MgCl_2$, 5.0 mM ATP, 1.0 mM PEP, 0.2 mM NADH, 12 units of LDH, and 4 units of PK. For the kinetic assays with lipid bicelles, PEP, NADH, LDH, and PK were added after bicelle formation. Stock solutions of 2 mM PLN_{1-20} were prepared fresh and used immediately. For determination of the linear region of PKA-C concentration, PLN_{1-20} was kept at 300 μM, while PKA-C was varied between 2 and 728 nM. The reactions were initiated by the addition of PKA-C, which was equilibrated in a solution containing 50 mM Mops (pH 7.0), 20 mM DTT, and 10 mM $MgCl_2$. No differences in the reaction rates were observed when the substrate was used to initiate these reactions. The measurements were performed in triplicate for each peptide concentration. Rates reflecting the small decrease in absorbance due to intrinsic NADH oxidation were measured and did not exceed ~ 2% of any reaction studied.

The values of k_{cat} and K_m were determined using nonlinear least-squares fitting of the initial velocities versus substrate concentration according to:

$$v = \frac{V_{\max}[\mathrm{S}]}{K_{\mathrm{m}} + [\mathrm{S}]} \qquad (1)$$

where v is the initial velocity, [S] is the concentration of the substrate, V_{max} is the maximum velocity for the reaction, and K_m is the Michaelis–Menten constant. The value of kcat was taken as V_{max} divided by the total PKA-C concentration. Fitting of Eq. (1) to the kinetic data was performed using the software Origin 7.

3.4.5 NMR spectroscopy

NMR experiments were carried out on a Varian Inova operating at 800 MHz equipped with an HCN probe. The temperature of the experiments was held constant at 27 °C. Samples were prepared in 20 mM KH_2PO_4, 180 mM KCl, 1 mM NaN_3, 10 mM DTT, and 5% vol/vol D2O (pH 6.5) at concentrations of ~ 0.3–0.8 mM. Data were processed with the software NMRPipe (49) and visualized and analyzed using SPARKY. (50) Populations of the R-state ($p_{R\text{-}state}$) were quantified using:

$$p_{\mathrm{R-state}} = \frac{\Omega_{\mathrm{x}} - \Omega_{\mathrm{T-state}}}{\Omega_{\mathrm{R-state}} - \Omega_{\mathrm{T-state}}} \qquad (2)$$

where Ω_x, $\Omega_{T\text{-}state}$, and $\Omega_{R\text{-}state}$ are the chemical shifts of sample x, PLN in DPC, and $PLN_{1\text{-}20}$ in aqueous buffer, respectively. The mean of $p_{R\text{-}state}$ was determined from six methyl groups in the protein (originating from V4, L7, and I12) that were observed in [^{1}H/^{13}C]heteronuclear multiple quantum coherence spectra. Due to poor sensitivity for the bicelle-bound states, amide spectra could not be used to estimate the population.

3.4.6 Molecular modeling

The three-dimensional model of the PKA-C/ATP/$PLN_{1\text{-}20}$ complex was generated using HADDOCK 2.0. (30) As an initial configuration, the coordinates from the crystallographic ternary complex of PKA-C/ATP/$PKI_{5\text{-}24}$(1ATP) were used and depleted of $PKI_{5\text{-}24}$. (28) The coordinates of the enzyme were kept fixed during the docking of $PLN_{1\text{-}20}$ using simulated annealing. Restraints based on NMR chemical shift data were implemented as ambiguous interaction restraints. Specifically, active residues were categorized as those that had solvent accessibility > 50% and chemical shift perturbations greater than the median and within 10 Å from the binding pocket of the enzyme. The active residues identified were S53, K78, L82, K83, S130, L198, G200, Q245, D328, D329, and Y330. Solvent-accessible residues within 3 Å of the active residues were categorized

as passive. Active and passive residues were defined for the PLN_{1-20} using the same criteria. An ambiguous interaction restraint was satisfied when any atoms of active residues in one molecule were within 4 Å of an active or a passive residue of the docking partner. Also, the canonical recognition sequence of PLN1–20 (P − 3 to P + 1 site) was aligned to match the corresponding positions of PKI_{5-24} in the binding groove of the 1ATP structure. (28) Based on this alignment, five additional distance restraints were used: three hydrogen bonds from the R14 guanidinium group of PLN_{1-20} to Glu170, Tyr204, and Glu230 of PKA-C; one hydrogen bond from Ser16 of PLN_{1-20} to Ser53 of PKA-C; and one hydrogen bond involving the carboxyl group of Thr17 and the backbone amide of Gly200 in PKA-C. The hydrogen-bond distances (from N or O heteroatoms to hydrogen atoms) were incorporated as nuclear Overhauser enhancement distance restraints using a flat well potential with 1.5 (4) Å as lower (upper)-bound distances. PLN_{1-20} was set to be flexible, with the exception of the residues occupying P − 3 to P + 1 sites of PKA-C, consistent with the results based on NMR dynamic measurements.2 The backbone conformation of PKA-C was kept fixed, while full flexibility was allowed for side chains. The initial structures of PKA-C and peptide were subjected to rigid-body docking and subsequent structure refinement using the docking protocol from HADDOCK with adjusted weighting factors.29 A total of 2000 initial structures of the complex were generated after rigid-body docking, and the 200 lowest energy structures were optimized by simulated annealing, followed by refinement in explicit water using the Tip3 water model. (30) These structures were then clustered according to their pairwise RMSDs with respect to the conformation of PKI in the 1ATP crystal structure. The 20 lowest-energy structures were selected for the final analysis.

4.5 References

1. Johnson, L. N. 2009. The regulation of protein phosphorylation. Biochem. Soc. Trans. 37, 627-641.
2. Masterson, L. R., L. Shi, E. Metcalfe, J. Gao, S.S. Taylor and G. Veglia 2011. Dynamically committed, uncommitted, and quenched states encoded in protein kinase A revealed by NMR spectroscopy. Proc. Natl. Acad. Sci. U. S. A. 108, 6969-6974.
3. Masterson, L. R., C. Cheng, T. Yu, M. Tonelli, A.P. Kornev, S.S. Taylor and G. Veglia 2010. Dynamics connect substrate recognition to catalysis in protein kinase A. Nat Chem Biol. 6, 821-828.

4. Bers, D. M. 2008. Calcium cycling and signaling in cardiac myocytes. Annu. Rev. Physiol. 70, 23-49.

5. MacLennan, D. H. and E.G. Kranias 2003. Phospholamban: A crucial regulator of cardiac contractility. Nat Rev Mol Cell Biol. 4, 566-77.

6. Traaseth, N. J., K.N. Ha, R. Verardi, L. Shi, J.J. Buffy, L.R. Masterson and G. Veglia 2008. Structural and dynamic basis of phospholamban and sarcolipin inhibition of ca(2+)-ATPase. Biochemistry. 47, 3-13.

7. Verardi, R., L. Shi, N.J. Traaseth, N. Walsh and G. Veglia 2011. Structural topology of phospholamban pentamer in lipid bilayers by a hybrid solution and solid-state NMR method. Proc Natl Acad Sci U S A. 108, 9101-9106.

8. Zamoon, J., A. Mascioni, D.D. Thomas and G. Veglia 2003. NMR solution structure and topological orientation of monomeric phospholamban in dodecylphosphocholine micelles. Biophys. J. 85, 2589-2598.

9. Mascioni, A., C. Karim, J. Zamoon, D.D. Thomas and G. Veglia 2002. Solid-state NMR and rigid body molecular dynamics to determine domain orientations of monomeric phospholamban. J. Am. Chem. Soc. 124, 9392-9393.

10. Metcalfe, E. E., J. Zamoon, D.D. Thomas and G. Veglia 2004. (1)H/(15)N heteronuclear NMR spectroscopy shows four dynamic domains for phospholamban reconstituted in dodecylphosphocholine micelles. Biophys. J. 87, 1205-1214.

11. Traaseth, N. J. and G. Veglia 2010. Probing excited states and activation energy for the integral membrane protein phospholamban by NMR CPMG relaxation dispersion experiments. Biochim. Biophys. Acta. 1798, 77-81.

12. Traaseth, N. J., L. Shi, R. Verardi, D.G. Mullen, G. Barany and G. Veglia 2009. Structure and topology of monomeric phospholamban in lipid membranes determined by a hybrid solution and solid-state NMR approach. Proc. Natl. Acad. Sci. U. S. A. 106, 10165-10170.

13. Simmerman, H. K., J.H. Collins, J.L. Theibert, A.D. Wegener and L.R. Jones 1986. Sequence analysis of phospholamban. identification of phosphorylation sites and two major structural domains. J Biol Chem. 261, 13333-41.

14. Simmerman, H. K. and L.R. Jones 1998. Phospholamban: Protein structure, mechanism of action, and role in cardiac function. Physiol Rev. 78, 921-47.

15. Gustavsson, M., N.J. Traaseth, C.B. Karim, E.L. Lockamy, D.D. Thomas and G. Veglia 2011. Lipid-mediated Folding/Unfolding of phospholamban as a regulatory mechanism for the sarcoplasmic reticulum ca(2+)-ATPase. J. Mol. Biol. 408, 755-765.

16. Maclennan, D. H. 2004. Interactions of the calcium ATPase with phospholamban and sarcolipin: Structure, physiology and pathophysiology. J. Muscle Res. Cell. Motil. 25, 600-601.

17. Schmitt, J. P., M. Kamisago, M. Asahi, G.H. Li, F. Ahmad, U. Mende, E.G. Kranias, D.H. MacLennan, J.G. Seidman and C.E. Seidman 2003. Dilated cardiomyopathy and heart failure caused by a mutation in phospholamban. Science. 299, 1410-3.

18. Johnson, D. A., P. Akamine, E. Radzio-Andzelm, M. Madhusudan and S.S. Taylor 2001. Dynamics of cAMP-dependent protein kinase. Chem. Rev. 101, 2243-2270.

19. Traaseth, N. J., J.J. Buffy, J. Zamoon and G. Veglia 2006. Structural dynamics and topology of phospholamban in oriented lipid bilayers using multidimensional solid-state NMR. Biochemistry. 45, 13827-13834.

20. Traaseth, N. J., R. Verardi, K.D. Torgersen, C.B. Karim, D.D. Thomas and G. Veglia 2007. Spectroscopic validation of the pentameric structure of phospholamban. Proc. Natl. Acad. Sci. U. S. A. 104, 14676-14681.

21. Karim, C. B., Z. Zhang, E.C. Howard, K.D. Torgersen and D.D. Thomas 2006. Phosphorylation-dependent conformational switch in spin-labeled phospholamban bound to SERCA. J. Mol. Biol. 358, 1032-1040.

22. Zamoon, J., F. Nitu, C. Karim, D.D. Thomas and G. Veglia 2005. Mapping the interaction surface of a membrane protein: Unveiling the conformational switch of phospholamban in calcium pump regulation. Proc. Natl. Acad. Sci. U. S. A. 102, 4747-4752.

23. Masterson, L. R., A. Mascioni, N.J. Traaseth, S.S. Taylor and G. Veglia 2008. Allosteric cooperativity in protein kinase A. Proc Natl Acad Sci U S A. 105, 506-511.

24. Dyson, H. J. and P.E. Wright 1998. Equilibrium NMR studies of unfolded and partially folded proteins. Nat Struct Biol., 499-503.

25. Dyson, H. J. and P.E. Wright 2001. Nuclear magnetic resonance methods for elucidation of structure and dynamics in disordered states. Methods Enzymol. 339, 258-271.

26. Dyson, H. J. and P.E. Wright 2004. Unfolded proteins and protein folding studied by NMR. Chem. Rev. 104, 3607-3622.

27. Kay, L. E., D.A. Torchia and A. Bax 1989. Backbone dynamics of proteins as studied by 15N inverse detected heteronuclear NMR spectroscopy: Application to staphylococcal nuclease. Biochemistry. 28, 8972-8979.

28. Knighton, D. R., J. Zheng, L.F.T. Eyck, N.H. Xuong, S.S. Taylor and J.M. Sowadski 1991. Structure of a peptide inhibitor bound to the catalytic subunit of cyclic adenosine monophosphate-dependent protein kinase. Science. 253, 414-420.

29. Buechler, J. A., J.A. Toner-Webb and S.S. Taylor 1991. Carbodiimides as probes for protein kinase structure and function. Methods Enzymol. 200, 487-500.

30. Dominguez, C., R. Boelens and A.M. Bonvin 2003. HADDOCK: A protein-protein docking approach based on biochemical or biophysical information. J. Am. Chem. Soc. 125, 1731-1737.

31. Ha, K. N., N.J. Traaseth, R. Verardi, J. Zamoon, A. Cembran, C.B. Karim, D.D. Thomas and G. Veglia 2007. Controlling the inhibition of the sarcoplasmic Ca2+-ATPase by tuning phospholamban structural dynamics. J. Biol. Chem. 282, 37205-37214.

32. Csermely, P., R. Palotai and R. Nussinov 2010. Induced fit, conformational selection and independent dynamic segments: An extended view of binding events. Trends Biochem. Sci. 35, 539-546.

33. White, S. H. and W.C. Wimley 1999. Membrane protein folding and stability : Physical principles. Annual Review Biophysics Biomolecular Structures. 28, 319-365.

34. Engelman, D. M., Y. Chen, C.N. Chin, A.R. Curran, A.M. Dixon, A.D. Dupuy, A.S. Lee, U. Lehnert, E.E. Matthews, Y.K. Reshetnyak, A. Senes and J.L. Popot 2003. Membrane protein folding: Beyond the two stage model. FEBS Lett. 555, 122-125.

35. Johnson, J. E. and R.B. Cornell 1999. Amphitropic proteins: Regulation by reversible membrane interactions (review). Mol. Membr. Biol. 16, 217-235.

36. Cornell, R. B. and S.G. Taneva 2006. Amphipathic helices as mediators of the membrane interaction of amphitropic proteins, and as modulators of bilayer physical properties. Curr. Protein Pept. Sci. 7, 539-552.

37. Li, P., I.R. Martins, G.K. Amarasinghe and M.K. Rosen 2008. Internal dynamics control activation and activity of the autoinhibited vav DH domain. Nat. Struct. Mol. Biol. 15, 613-618.

38. Yao, X., M.K. Rosen and K.H. Gardner 2008. Estimation of the available free energy in a LOV2-J alpha photoswitch. Nat. Chem. Biol. 4, 491-497.

39. Nash, A. I., W.H. Ko, S.M. Harper and K.H. Gardner 2008. A conserved glutamine plays a central role in LOV domain signal transmission and its duration. Biochemistry. 47, 13842-13849.

40. Velyvis, A., Y.R. Yang, H.K. Schachman and L.E. Kay 2007. A solution NMR study showing that active site ligands and nucleotides directly perturb the allosteric equilibrium in aspartate transcarbamoylase. Proc. Natl. Acad. Sci. U. S. A. 104, 8815-8820.

41. Boehr, D. D., R. Nussinov and P.E. Wright 2009. The role of dynamic conformational ensembles in biomolecular recognition. Nat. Chem. Biol. 5, 789-796.

42. Kern, D. and E.R. Zuiderweg 2003. The role of dynamics in allosteric regulation. Curr. Opin. Struct. Biol. 13, 748-757.

43. Selvaratnam, R., S. Chowdhury, B. VanSchouwen and G. Melacini 2011. Mapping allostery through the covariance analysis of NMR chemical shifts. Proc. Natl. Acad. Sci. U. S. A. 108, 6133-6138.

44. Bhabha, G., J. Lee, D.C. Ekiert, J. Gam, I.A. Wilson, H.J. Dyson, S.J. Benkovic and P.E. Wright 2011. A dynamic knockout reveals that conformational fluctuations influence the chemical step of enzyme catalysis. Science. 332, 234-238.

45. Masterson, L. R., N. Bortone, T. Yu, K.N. Ha, E.C. Gaffarogullari, O. Nguyen and G. Veglia 2009. Expression and purification of isotopically labeled peptide inhibitors and substrates of cAMP-dependant protein kinase A for NMR analysis. Protein Expr. Purif. 64, 231-236.

46. Buck, B., J. Zamoon, T.L. Kirby, T.M. DeSilva, C. Karim, D. Thomas and G. Veglia 2003. Overexpression, purification, and characterization of recombinant ca-ATPase

regulators for high-resolution solution and solid-state NMR studies. Protein Expr Purif. 30, 253-61.

47. Lockwood, N. A., R.S. Tu, Z. Zhang, M.V. Tirrell, D.D. Thomas and C.B. Karim 2003. Structure and function of integral membrane protein domains resolved by peptide-amphiphiles: Application to phospholamban. Biopolymers. 69, 283-92.
48. Cook, P. F., M.E. Neville, K.E. Vrana , F.T. Hartl and R. Roskoshi 1982. Adenosine cyclic 3'5'-monophosphate dependent protein kinase: Kinetic mechanism for the bovine skeletal muscle catalytic subunit. Biochemistry. 21, 5794-5799.
49. Delaglio, F., Grzesiek, S., Vuister, G. W., Zhu, G. Pfeifer, J., Bax,A. 1995. NMRPipe: A multidimensional spectral processing system based on UNIX pipes. J. Biomol. NMR. 6, 277-293.
50. Goddard, T. D., Kneller,D.G. 1999. SPARKY 3.

Table S1: Steady-state kinetic parameters for the phosphorylation of PLN analogues.

	k_{cat} (s-1)	K_m (μM)	k_{cat}/K_m (μM^{-1} s^{-1})
PLN_{1-19} (Free)	22.3 ± 1.3	36.4 ± 5.5	0.61 ± 0.10
PLN_{1-19} (Bicelle)	25.0 ± 1.8	43.0 ± 5.2	0.58 ± 0.8
AFA-PLN (Bicelle)	20.2 ± 0.6	47.6 ± 4.3	0.42 ± 0.04
Lip-PLN_{1-19} (Bicelle)	24.7 ± 1.9	90.1 ± 14.9	0.27 ± 0.05
Lip-AFA-PLN (Bicelle)	21.9 ± 1.5	114.8 ± 17.9	0.19 ± 0.03
AFA-PLN (DPC)	13.0 ± 0.8	238.1 ± 21.0	0.05 ± 0.01

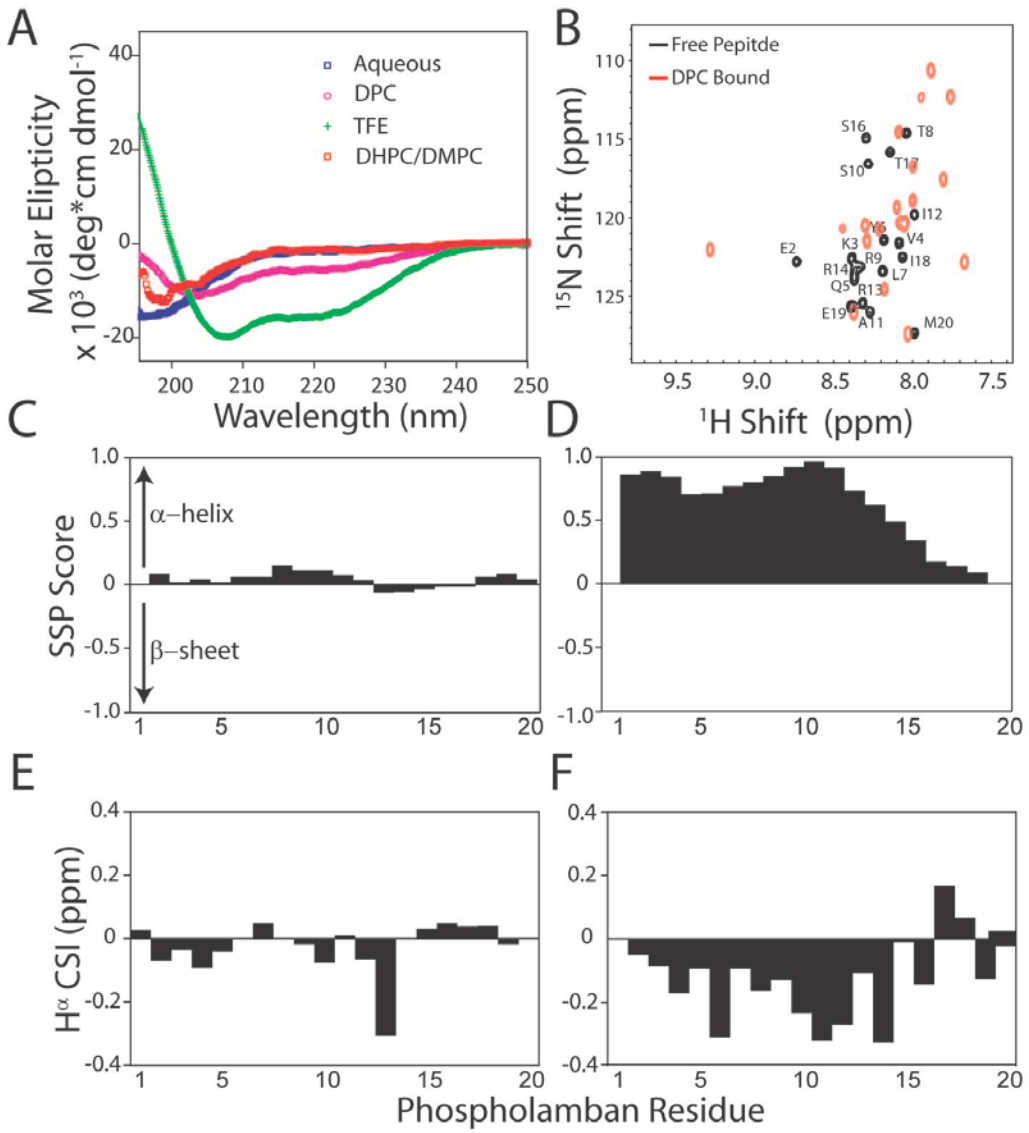

Figure S1: Structural details of PLN_{1-20} in the presence and absence of membrane mimicking environments. *A) CD spectra of PLN_{1-20} in aqueous buffer, TFE, isotropic bicelles, or DPC indicate higher α-helical content in the presence of membrane mimicking environments. B) The amide perturbations from interaction with DPC was followed by recording an $^{1}H/^{15}N$ HSQC NMR spectra of PLN_{1-20} with and without DPC micelles. This supported that drastic changes likely occur in the secondary structure. NMR chemical shifts for $^{13}C^{\alpha}$, $^{13}C^{\beta}$, $^{13}C'$ and $^{15}N^{\alpha}$ resonances were used to determine the secondary structure propensity scores of PLN_{1-20} in C) aqueous solution or with D) DPC micelles. Along with proton H^{α} chemical shift indices (in aqueous solution, E, or DPC micelles, F), the peptide exchanges between a membrane absorbed α-helix and a membrane detached, disordered conformation.*

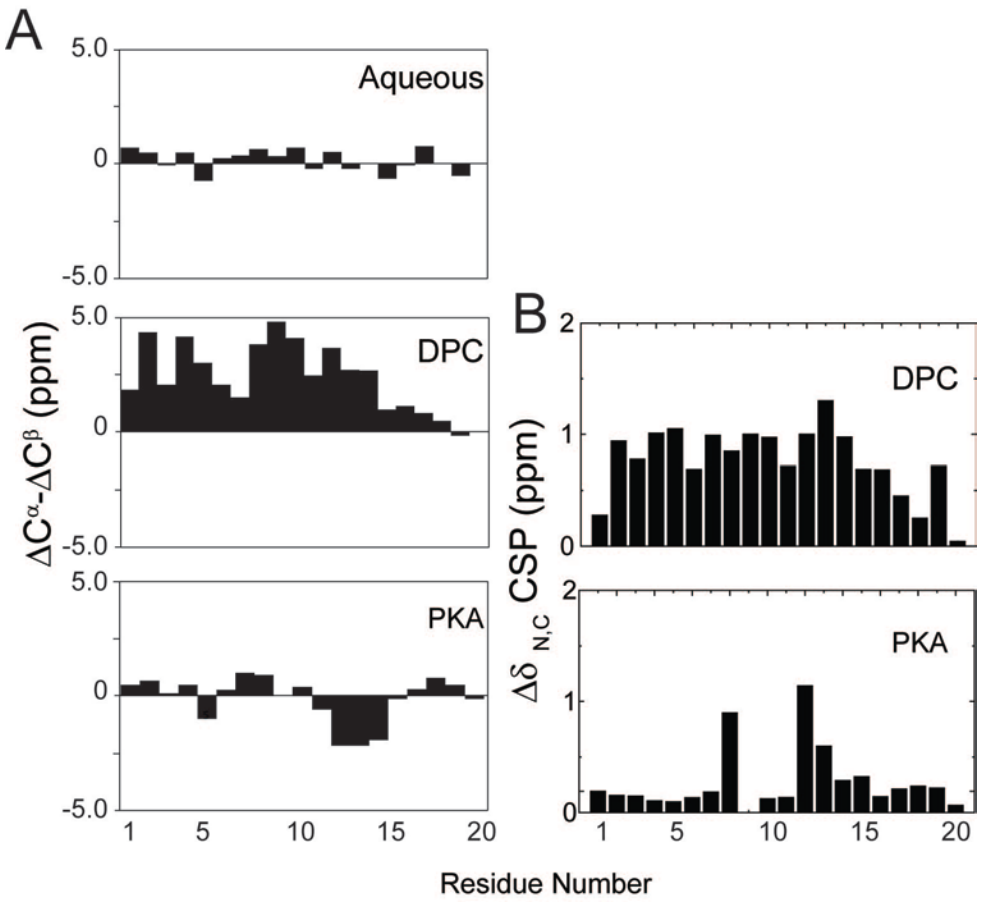

Figure S2: Structural transitions of PLN_{1-20} upon interaction with DPC or PKA-C. *A) Combined chemical shift indices for C^{α} and C^{β} residues indicate the unstructured peptide forms an α-helix upon interaction with DPC micelles, but remains largely unstructured when bound to PKA-C. The changes in secondary structure was also evident from full chemical shift perturbations ($^{13}C^{\alpha}$, $^{13}C^{\beta}$, $^{13}C'$ and $^{15}N^{\alpha}$, panel B) of PLN_{1-20} upon binding DPC or PKA-C.*

Chapter 4 - Paramagnetism-Based NMR Restraints Lift Residual Dipolar Coupling Degeneracy in Multidomain Detergent-Solubilized Membrane Proteins

Reprinted with permission from:

Lei Shi, Nathaniel J. Traaseth, Raffaello Verardi, Martin Gustavsson, Jiali Gao, and Gianluigi Veglia. Paramagnetic-Based NMR Restraints Lift Residual Dipolar Coupling Degeneracy in Multidomain Detergent-Solublized Membrane Proteins *J Am Chem Soc.* 2011; 133(7): 2232–2241.

Residual dipolar couplings (RDCs) give orientational dependent NMR restraints that improve the resolution of NMR conformational ensembles and define the relative orientation of multidomain proteins and protein complexes. The interpretation of RDCs is complicated by protein dynamics and the intrinsic degeneracy of solutions that lead to ill-defined orientations of the structural domains (*ghost orientations*). Here, we illustrate how paramagnetic-based restraints can remove the orientational ambiguity of multidomain membrane proteins solubilized in detergent micelles. We tested this approach for the monomeric form of phospholamban (PLN), a 52-residue membrane protein, which is composed of two helical domains connected by a relatively flexible loop. We show that the combination of classical solution NMR restraints (NOEs and dihedral angles) with RDCs and PREs resolve topological ambiguities, improving the convergence of the PLN structural ensemble and giving the depth of insertion of the protein within the micelle. This combined approach will be necessary for membrane proteins, whose three-dimensional structure is strongly influenced by interactions with the membrane-mimicking environment rather than compact tertiary folds common in soluble proteins.

4.1 Introduction

Residual dipolar couplings (RDCs) constitute an excellent source of structural and dynamic information (1-4). Their use spans from structural refinement (1, 5, 6) to the characterization of unfolded proteins (7-11) and excited states of biomolecules (12, 13). RDCs are also an invaluable NMR parameter to orient multidomain proteins and protein complexes, where the detection of inter-domain or inter-protein nuclear Overhauser effects (NOEs) are very challenging (4, 14, 15). However, the inherent degeneracy of RDCs (ghost orientations) complicates the extraction of orientational information (16). It was originally thought that the RDC equation resulted in eight-fold degeneracy for peptide plane orientations (16), but recently, it was shown that the analytical solution of the RDC equation contains a 16-fold degeneracy (17). This degeneracy is reduced to four if one considers the regular patterns of the dipolar couplings (i.e. dipolar waves) for secondary structure domains (8, 18-22). In favorable cases, this RDC inherent degeneracy is resolved using two or more alignments media (23). Nonetheless, local geometry can still be ill-defined (17) and further confounded by the presence of conformational dynamics (24-27). Therefore, a major issue is to eliminate ghost orientations from the true orientations. Bertini and coworkers have proposed the use of paramagnetism-based NMR restraints (28). These authors have developed a new analysis of the paramagnetic-based restraints to give a comprehensive view of the different conformations and dynamics of calmodulin as well as the calmodulin-α-synuclein complex (28). A similar approach has been utilized for resolving the solution conformation of the ternary complex of the E. coli Hsp70 chaperone (29). Membrane proteins solubilized in detergent micelles are not immune to these challenges. Polytopic (integral and/or peripheral) membrane proteins are often organized in multiple domains (independent or partially independent) that facilitate intra- and inter-cellular communication (30). Flexibility of protein domains can prevent the formation of compact tertiary structures, which results in the structure being defined by domain interactions with the lipid membrane, i.e. topology (31). Several small and medium size membrane proteins involved in regulatory function of ion pumps fall into this category (31). While membrane proteins are amenable to modern solution NMR techniques, it is still a challenging task to obtain long-range distance restraints from nuclear Overhauser effect (NOEs) data (32), especially for helical membrane proteins. Side chain methyl labeling

schemes can help determine the overall fold of membrane proteins, and new protocols have been developed to introduce a variety of different probes on proteins (33-35). RDCs constitute a viable alternative to obtaining long-range distance restraints, and accordingly have been an important source of constraints for membrane proteins. To measure RDCs, membrane proteins need to be aligned in an anisotropic media (36-38) or bound to a lanthanide ion either through adventitious sites (39) or engineered tags (40, 41). In several instances, RDCs were crucial to improving the resolution of the conformational ensemble of membrane proteins solubilized in micelles (32, 42, 43).

In this article, we show that the *ghost orientations* generated after RDC refinement of the detergent solubilized protein phospholamban (PLN) can be eliminated by using paramagnetism-based restraints derived from site-directed spin-labeling using MTSSL (1-oxyl-2,2,5,5-tetramethyl-D3-pyrroline-3-methyl methanethiosulfonate).

4.2 Material and methods

4.4.2 PLN expression, purification, and mutagenesis

The overexpression and purification of AFA-PLN (i.e. cysteine-null monomer, C36A, C41F, C46A) was carried out as described in Buck et al. (44). For the A24C mutant, the plasmid containing fully functional cysteine-null PLN was used as a template to introduce a single point mutation (A24C) by site directed mutagenesis using Quick-change kit (Stratagene, San Diego, CA). PCR was carried out as previously described (44). The primers were designed as follows: forward 5'-GCCGCAGCAGTGCCGCCAGAACCTGC-3′ , reverse 5'- GCAGGTCTGGCGGCACTGCTGCGGC-3' (the mutated codon is underlined). The mutated plasmid was amplified in XL1-blue competent cells (Stratagene, San Diego, CA) and purified using QIAprep Spin kit (Qiagen, Carlsbad, CA). The sequence was confirmed by DNA sequencing (ABI PRISM 3130xl Genetic Analyzer. Biomedical Genomic Center, Minneapolis, MN). BL21(DE3) (Stratagene, San Diego, CA) *E. coli* cells were transformed with 100 ng of purified plasmid and selected on LB agar plates containing ampicillin (100 mg/mL). The L7C mutant was designed in a similar way. Protein expression and purification were carried out using a combination of affinity chromatography and HPLC (44).

4.2.3 A24C-PLN and L7C-PLN spin-labeling with MTSSL

MTSSL (1-oxyl-2,2,5,5-tetramethyl-D3-pyrroline-3-methyl methanethiosulfonate, Toronto Research Chemicals, North York, ON) spin label reacts with the terminal SH of cysteine residue to form a covalent bond. A stock solution of 200 mM MTSSL in DMF was prepared. The labeling reaction protocol was derived from Kirby et al. (45). One mg of lyophilized A24C-PLN (or L7C-PLN) protein was solubilized in 1 mL of spin labeling buffer (60 mM Tris-HCl at pH 7.0 and 0.2% SDS). The final concentration of PLN was ~0.2 mM. A 10-fold molar excess of MTSSL was added to the reaction mix and incubated overnight at 4 °C in the dark. The unreacted spin label was removed by HPLC with the PLN peak collected and lyophilized after removal of organic solvent. Lyophilized MTSSL spin labeled A24C-PLN (or L7C-PLN) was dissolved in 300 mM DPC, 20 mM phosphate buffer (pH = 6.0, 120 mM NaCl, 0.01% NaN_3, and 10% D_2O). The final concentration of A24CPLN was ~0.1 mM.

4.2.4 Sample preparation for RDC measurements

AFA-PLN [U-^{13}C, ^{15}N] was reconstituted into 100 mM deuterated DPC (Cambridge Isotope Laboratories), 25 mM phosphate buffer (pH 6.0), 125 mM NaCl, 10% D_2O, and 0.1% NaN_3 to give a final protein concentration of ~0.8 mM. The stretched gels were polymerized from a 5.7 mm diameter cylinder under the following conditions: 100 mM Tris-HCl (pH 8.0), 5.1% acrylamide, 1.3% bis-acrylamide, 0.1% ammonium persulfate, and 0.33% TEMED. The gels were thoroughly washed twice with 50 mM NaH_2PO_4/Na_2HPO_4 pH 6.5 (8 hr/wash) and then twice with H_2O (8 hr/wash) as described previously (46). The protein/detergent mixture was added to the dried polymerized gel and incubated at 37 °C for ~24 hr. After stretching in a 5 mm Shigemi tube, the length of the gel increased by a factor of ~1.7. The stretching apparatus was purchased from New Era Enterprises, Inc. and has been previously described (46).

4.2.5 NMR Spectroscopy

RDC measurements: Experiments were carried out at 37 °C using a Varian spectrometer operating at a 1H Larmor frequency of 599.54 MHz. 2D TROSY based (1H, 15N) pulse sequences described by Permi and Annila (47) were performed to measure $^{13}C'$-$^{13}C\alpha$ and ^{1}H-^{15}N one-bond couplings. Each 2D experiment was acquired in the presence and absence of the stretched gel where the difference in splitting allowed

for the calculation of the residual dipolar couplings. The total acquisition times in t_1 and t_2 were 62 and 77 ms with spectral widths of 1300 and 6600 Hz in the ^{15}N and ^{1}H dimensions, respectively. In order to measure the 15N-13C' one-bond couplings, we performed a 3D uncoupled HNCO experiment in the presence and absence of stretched gel. Experiments utilized 64 scans, spectral widths of 10000 Hz (^{1}H), 1000 Hz (^{13}C) and 1200 Hz (^{15}N) with total acquisition times of 83.2, 40, and 26.7 ms in the ^{1}H, ^{13}C, and ^{15}N dimensions, respectively. Experiments were acquired at 37 °C with a recycle delay of 1.3 s. All data were processed with NMRPipe (48) and viewed using NMRVIEW (49). The ^{1}H-^{15}N, $^{13}C'$-^{15}N, and $^{13}C'$-$^{13}C\alpha$ RDCs versus residue are shown **Figure 1A**.

PRE measurements: [^{1}H, ^{15}N] heteronuclear single quantum coherence (HSQC) spectra were acquired in the presence of MTSSL (paramagnetic) and the diamagnetic analog at positions 7 and 24 of PLN. The intensity reduction (I_{ox} - diamagnetic, I_{red} - paramagetic) of the amide resonances were converted into R2sp values and then to distance restraints using Eq. 1 (50):

$$\frac{I_{ox}}{I_{red}} = \frac{R_2 e^{-R_2^{sp} t}}{R_2 + R_2^{sp}}$$

$$r = \left[\frac{K}{R_2^{sp}} \left(4\tau_c + \frac{3\tau_c}{1+\omega_H^2 \tau_c^2} \right) \right]^{\frac{1}{6}} \quad [1]$$

where r is the distance between the nuclear spins and the unpaired electron, τ_c is the correlation time for the electron/nuclear spin interaction, ω_h is the proton Larmor frequency, K is a constant that depends on the gyromagnetic ratio, electronic g factor and the Bohr magneton and is set to 1.23×10^{-32} cm^6 s^{-2}. For PLN, we used two different correlation times (τ_c): 8.2 ns for the cytoplasmic domain and 15.4 ns for the transmembrane domain (51). For peaks with intensity retention greater than 90%, no upper limits were used. For the other peaks, the intensity retentions were converted into distances according to equation [1], and implemented with upper and lower bounds of ± 4 Å (50). The PRE quenching data and the converted distance restraints for PLN are shown in **Figure 2**.

Calculation protocol: We used the standard energy target function that has been implemented in XPLOR-NIH (52):

$$E = E_{empirical} + E_{solution} \quad [2]$$

where $E_{empirical}$ is the sum of the energy terms of the covalent geometry (bond stretching, bond bending, improper angle vibration) and short-range repulsion (repulsive VDW interaction):

$$E_{empirical} = w_{bonds}E_{bonds} + w_{angles}E_{angles} + w_{impropers}E_{impropers} + w_{vdw}E_{vdw} \quad [3]$$

$E_{solution}$ includes the penalty functions due to distance restraints from NOEs, dihedral angles, RDCs, and PREs:

$$E_{solution} = w_{NOE}E_{NOE} + w_{CDIH}E_{CDIH} + w_{DB}E_{DB} + w_{RDC}E_{RDC} + w_{PRE}E_{PRE} \quad [4]$$

All of the NOE-derived distance restraints used in the present study are taken from the previously published structure of PLN in DPC micelles (53). A total of 373 distances (142 intra-residue and 231 inter-residue) are included. In addition, 58 hydrogen-bonds derived from H/D exchange measurements are used to constraint the helical amide groups (HN-CO[i, i+4]) of PLN. Finally, we have obtained 38 dihedral angle restraints using the program TALOS (54) based on the chemical shifts of Hα, Cα, Cβ, C′, N, and HN (55). A summary of all of the restraints used in the calculations is listed in **Table S1**. To illustrate the significance of RDC and PRE restraints in the structural refinement of the membrane protein PLN, we used three protocols in the simulated annealing optimization to generate three structural ensembles (56). In the first protocol, we used the restraints derived from typical solution NMR experiments, including NOE-derived distances, dihedral angle restraints generated from chemical shifts (TALOS), and hydrogen-bonding interactions from H/D exchange experiments (53). The second protocol includes the restraints from the first protocol plus RDCs derived from the partial alignment of PLN in stretched gels. Finally, the third protocol was constructed by adding MTSSL distance restraints determined from PRE data to all constraints used in the first two protocols. Details for the calculation are presented in the supporting material.

4.3 Results

4.3.1 Structural refinement with NOE and dihedral angle restraints (protocol one)

To test our approach, we used phospholamban (PLN), a 52-residue integral membrane protein in the sarcoplasmic reticulum (SR) that regulates the SR Ca2+-ATPase (SERCA) (57). PLN exists as an inactive pentamer in the SR and depolymerizes into active monomers upon encountering SERCA (58, 59). To mimic the monomeric state, we mutated the three transmembrane Cys residues (C36A, C41F, C46A) to obtain a stable monomer with activity identical to that of wild type PLN (60). The NMR structure of PLN monomer in dodecylphosphocholine micelles has been solved by our group (53). For the structure determination, we used distance restraints from 15N-edited NOESY spectra, dihedral restraints from chemical shifts (54), and hydrogen bonds derived from exchange factors (61). Based on the results of the calculations and subsequent backbone dynamics studies, we identified four dynamic domains: α-helical domain Ia (residues 1–16), α-helical region spanning domains Ib (residues 23–30) and II (residues 31–52), and a loop connecting the two helical regions (residues 17–22) (51). Given the limited amount of distance and angular restraints found between the loop and its adjacent domains, the final structural ensemble resulted in many different conformers with poor convergence for the overall backbone conformation and topology. In our previous paper, we mapped solvent accessibility using Mn^{2+} ions and the insertion of PLN in the micelles using 5- and 16-DSA, and manually eliminated structures that contradicted the paramagnetic mapping. We concluded that PLN adopts a helical *L*-shaped conformation with the cytoplasmic amphipathic domain Ia adsorbed on the surface of the micelle. These results were also supported by solid-state NMR experiments carried out in the lipid membrane (62). While these studies represent the initial characterization of PLN in membrane mimicking environments, they were limited by two factors: (*a*) the absence of topological restraints with respect to the micelle (the selection was carried out manually), and (*b*) the absence of the relative orientation of the two helical domains.

4.3.2 Structural refinement with RDCs plus NOE (protocol two)

Since the publication of our first paper on PLN, several groups have obtained orientationally dependent information utilizing RDC data for both membrane bound and soluble proteins. Therefore, our first step to improve the solution NMR structural

ensemble of PLN was to introduce restraints from three sets of RDCs obtained from the partial alignment of PLN in a stressed gel system (36, 63). **Figure 1** shows three sets of RDCs versus the PLN residue number: ^{1}H-^{15}N, $^{13}C'$-^{15}N, and $^{13}C'$-$^{13}C\alpha$. As expected from the helical secondary structure of PLN, the values of the RDCs oscillate periodically. There is a significant change in the pattern from residues 20 to 30 for the ^{1}H-^{15}N RDCs. These residues belong to domain Ib, a helical region that is more dynamic and solvent exposed than the transmembrane domain II (51). When fitting these dynamically averaged RDCs to an average structure, a pronounced kink is observed between domain Ib and domain II. In fact, CPMG relaxation dispersion measurements obtained from PLN in DPC indicate the presence of chemical exchange (at least two conformations) for domain Ib (51, 64) and for this reason we excluded RDCs from domain Ib during our structural calculation. Dynamic model or ensemble simulations are needed to explain the discontinuity of RDCs patterns in this domain. One of the difficulties during structural refinement with RDCs is to accurately determine the axial (D_a) and rhombic (R) components of the alignment tensor. Several methods are available to estimate these values such as the maximum likelihood method by Moore and Warren (65) and the histogram method by Bax and co-workers (66). To use these methods, large numbers of RDCs are needed and their reliability is dependent on the accuracy of the experimental measurements. Due to the increased size of the membrane proteins within the detergent micelle, the experimental RDCs have larger errors than their soluble counterparts. Therefore, the errors of heavy atom RDCs such as $^{13}C'$-^{15}N and $^{13}C'$-$^{13}C\alpha$ are much larger after scaling to the ^{15}N-^{1}H RDCs. To overcome this, Da and R were allowed to vary in the simulated annealing procedure (6). This introduced two extra parameters into the structural fitting in addition to the tensor orientations. The refined 400 structures are clustered based on two groups of D_a and R values (**Figure 3**). The solutions with $D_a = -8$ Hz and $R = 0.667$ resulted when RDCs were not properly fitted; these structures were excluded from further analysis. The structures generated from the second group (shown red in **Figure 3**) were used in the following calculation where $D_a = 8.6$ (± 0.3) and R = 0.52 (± 0.04). The high rhombicity R is consistent with the RDC histogram shown in **Figure 1B**. Note that all of the RDCs were implemented in the simulated annealing protocol using a flat-well potential52. The force constants for RDCs during the structure refinement were determined using the R

factor method (R_{RDC}) as described by Clore and co-workers (56). In this method, two factors are monitored as a function of the RDC force constant: (1) the R factor for different sets of RDCs and (2) the energy penalties from energy terms other than RDCs. During the force constant ramping, the tensor values D_a and R were fixed (determined above to be D_a = 8.6 and R = 0.52). We found that the best value for the force constant was 0.5 kcal mol^{-1} Hz^{-2} (see **Figure S1**), which can give reasonable RDC agreement without large penalties from other structural and experimental restraints. After optimizing D_a, R, and the force constants, we generated ~300 structures and selected the lowest 100 structures for further analysis. The resulting structures were clustered into four distinct families (I–IV) when the transmembrane domain II was overlaid. As expected, these structures differ in the relative orientation of the two helical domains giving rise to a four-fold degeneracy (**Figure 5B**). Each structural ensemble shows a backbone RMSD less than 1.6 Å, with good correlations between experimental and calculated RDC values (**Figures S2**). When viewed in the alignment tensor frame (**Figure 3C**), 16 different solutions for two helical domain structures are resolved when only one alignment medium is used. A similar result has been obtained by Bax and co-workers (67) for the monomeric subunit of KcsA solubilized in detergent micelles. For PLN, however, several of these solutions are degenerate, and the reason the structures could be grouped into four unique structural families (I, II, II and IV in **Figure 5B**). The solutions can be distinguished by analyzing the orientation angles (θ,ϕ) for each helical domain in the alignment tensor frame (**Figure 3A**) as well as the inter-helical angle χ (angle between domains Ia and II). For both the transmembrane (blue) and cytoplasmic (red) helices, the orientations correspond to the following angles: (θ, ϕ), (θ, $\pi+\phi$), ($\pi-\theta$, $\pi-\phi$), and ($\pi-\theta$, $2\pi-\phi$) (**Figure 3B**). The same solutions were found using theoretical equations by Wang and co-workers (21). The hydrophobic residues of the cytoplasmic domain Ia are approximately oriented toward the transmembrane domain for families I and II and away from it for families III and IV. As for the interhelical angle, family I has a χ angle of ~90°, while families III and IV display χ angles of ~70°. Family II has a nearly anti-parallel orientation between the two helical domains (χ ~140°). This orientation is similar to the monomer unit obtained using RDCs for the bellflower model of pentameric PLN by Oxenoid and Chou (68).

4.3.3 Structural refinement with RDCs and PREs (protocol three)

To reduce the degeneracy from the RDC solutions and remove the translational degree of freedom between the two domains, we measured PRE distance restraints. Specifically, we implemented PRE distance restraints from MTSSL-PLN constructs. These restraints were included in the calculations using the convention introduced by Battiste and Wagner (50) (see Materials and Methods). To restrict the flexibility of the spin label, we used a dihedral angle potential (sinusoid potential) to restrict the χ_1, χ_2 and χ_3 angles of the spin label, which have been identified to adopt defined values from crystal structures (69). Even with these long-range distances, families I, III and IV remained in the 100 lowest energy structures. However, these three solutions can easily be distinguished based on the PRE energies (E_{PRE}). In protocol two (RDC+NOE refinement), the four families are energetically degenerate (E_{RDC} and E_{NOE}) (**Figure 4A**, B), while in protocol three, each of the three families clearly have different values of E_{PRE} (**Figure 4C,D**). The structures within family I display the lowest PRE and NOE energies, and thus was selected as the final structure ensemble (**Figure 5C**), giving a backbone RMSD of ~ 1.2 Å and good agreement with experimental RDCs (**Figures S4**) and PREs (**Figure S5**). The energy differences between families I, III and IV is very small. In fact, this explains why structures *blindly* selected based on total energy (and not E_{PRE}) cannot adequately decipher between the three families present. PREs were helpful, because the major differences between structural families was in the positioning and facing of the cytoplasmic helix. Only family I had the hydrophobic residues facing toward the transmembrane helix, i.e., facing the micelle interior (**Figure 4C**). As an attempt to further support our justification of using PRE energies to eliminate families III and IV, we tried to label PLN with MTSSL at a different position. When engineered at position 9 (R9C-PLN), however, the spin label inserts into the hydrophobic core of the micelle (**Figure S6C**), while the backbone amide of R9C points toward the solvent (**Figure S6D**, Gd^{3+} quenching pattern). When the MTSSL is engineered, the long chain of MTSSL cross-linked to Cys 9 inserts in the detergent micelle (see quenching of the resonances in the transmembrane domain in **Figure S6C**), resulting in an incorrect positioning of the side chain and faulty interpretation of the structural topology of the protein. Therefore, the flexibility and hydrophobic nature of the MTSSL spin label calls for special care when

engineering site-specific mutants in membrane proteins when those sites are proximal to the membrane (70).

4.3.4 Application to the PLN Pentamer

The structure of the PLN pentamer heavily relied on the use of RDCs in the structure refinement (68). In fact, monomer structures were built prior to assembly in the symmetric pentamer. In the monomer calculation, the alignment tensors (Da=9.00, R=0.33) were determined from singular value decomposition (SVD) (71) using ^{15}N-^{1}H, ^{13}C-^{15}N and ^{13}C'-^{13}Cα RDCs. The alignment tensor was slightly different from the value in our monomer case. A comparison of RDC restraints between the pentamer (Oxenoid and Chou (68)) and monomer (this paper) showed a good correlation (**Figure S7**), especially with the N-H RDCs. We then performed the similar structural calculation using their tensor values and data. Similarly we also obtained four degenerate solutions (**Figure 6A, B**) as in our AFAPLN monomer calculation. Without help from long-range distance PRE restraints, only one of the families was selected to build the high-resolution pentamer. Aside from the degeneracy issue, the choice of the tensor value is also debatable for a symmetric pentamer (or another symmetric oligomeric protein). It is well-known in the literature 15 that the symmetry axis should coincide with the long axes of the alignment tensor, resulting in R=0 (zero rhombicity). It was argued that non-symmetric tensor values could result from protein dynamics (68), however the dynamic averaging of RDCs needs to be interpreted using a dynamic ensemble rather than fitting data to an average structure. We performed structural calculations of the monomer using RDCs measured by Oxenoid and Chou (68) and implemented a symmetric tensor (R=0), as would be expected from a symmetric pentamer. The Da value was determined to be 6.5 using the methods described earlier (**Figure S1**). The structure analysis is shown in **Figure 6C and D**. Note that the φ angle does not have defined minima as in **Figure 6B**. This is also in agreement with a theoretical study, which showed that an infinite number of solutions existed for cases where R=0 17.

4.4 Discussion

To address the challenges of high-resolution structure determination of membrane proteins complexes in micelles, the classical NOE-driven approach has been supplemented with RDCs. However, internal protein dynamics and intrinsic degeneracy

of the RDC solutions complicate the data interpretation, resulting in *ghost orientations*. Here, we show that the degeneracy problem can be addressed by supplementing RDC restraints with PREs from covalent attachment of the MTSSL spin label, which provides a fast and efficient method both for determination of membrane protein structure and its topology. We applied this method to a small multi-domain membrane protein, PLN, which regulates the enzymatic activity of the SR Ca^{2+}-ATPase in cardiac muscle. While structural biologists agree on the secondary structure content of PLN, there is an active debate about the topological arrangement of this protein in the lipid membrane. The structure calculations carried out with NOE based distance restraints do not provide for a high-resolution picture of PLN due to the lack of restraints between the helical domains. The correct orientation of the helical domains of PLN were selected manually based on the PRE data from Mn^{2+} and doxyl stearic acids (53). The introduction of RDCs improves the resolution of the ensemble, but exemplifies four different solutions, with ghost orientations of the cytoplasmic domain Ia. The combination of paramagnetic-based restraints PREs with RDCs and NOEs enabled us to resolve the orientation that agrees best with all available data. This solution (family I) is similar to the recently determined structural ensemble of monomeric PLN in lipids (55, 72). This is not surprising since several recent reports have shown that the structures of membrane proteins in micelles are similar to those determined in lipid bilayers (73). The slight discrepancy in the average rotation angles between the hybrid ensemble and that determined by combining NOEs, RDCs, and PREs (**Figure 7**) has several possible origins. First, there are several approximations used for the determination of the alignment tensor. Second, the cytoplasmic domain of PLN is rather dynamic (51, 64) and our data treatment does not take this into account. Third, the non-planar surface of the micelle can cause bends and curvature to malleable domains of membrane proteins and peptides (46). Last, RDC provides information of bond orientations with respect to three alignment tensor axes in a nonsymmetric tensor. PISEMA only encodes bond orientations with respect to one of the tensor axis (z axis), similar to RDC with a symmetric tensor. Moreover, as with all the NMR parameters, the PREs are affected by protein dynamics (74) and our approach does not take into account these effects. Since the studies of membrane proteins in detergent micelles are likely to continue to offer insightful information, we conclude that for multidomain membrane proteins the use of RDCs is not sufficient to define their

conformational space and topology. Rather, orientational restraints need to be supplemented with long-range paramagnetic restraints from spin labels covalently linked to proteins to uniquely define their topology (32, 75). Finally, we would like to point out that this paper address only the geometric ambiguities derived from RDCs. In fact, intrinsic dynamics complicates the use of both PRE and RDC for structure determination. To overcome these problems, molecular dynamics methods are being developed to for the variability of alignment tensors (76, 77) as well as for the modulations of the PRE effects on long-range interactions (74, 78). A more comprehensive approach for flexible domains of membrane proteins would require the combined use of PRE and RDCs using ensemble molecular dynamics methods (74).

4.5 References

1. Tjandra, N. and A. Bax 1997. Direct measurement of distances and angles in biomolecules by NMR in a dilute liquid crystalline medium. Science. 278, 1111-1114.
2. Bax, A., G. Kontaxis and N. Tjandra 2001. Dipolar coupling in macromolecular structure determination. Methods in Enzymology. 339, 127-174.
3. Prestegard, J. H. 1998. New techniques in structural NMR - anisotropic interactions. Nature Structural Biology., 517.
4. Prestegard, J. H., H.M. Al-Hashimi and J.R. Tolman 2000. NMR structures of biomolecules using field oriented media and residual dipolar couplings. Quarterly Review in Biophysics. 33, 371-424.
5. Tjandra, N., J. Marquardt and Clore M. G. 2000. Direct refinement against proton-proton dipolar coupling in NMR structure of macromolecules. Journal of Magnetic Resonance. 142, 393-396.
6. Clore, M. G., M.A. Gronenborn and N. Tjandra 1998. Direct structure refinement against residual dipolar couplings in the presence of rhombicity of unknown magnitude. Journal of Magnetic Resonance. 131, 159-162.
7. Nodet, G., L. Salmon, V. Ozenne, S. Meier, M.R. Jensen and M. Blackledge 2009. Quantitative description of backbone conformational sampling of unfolded proteins at amino acid resolution from NMR residual dipolar couplings. J. Am. Chem. Soc. 131, 17908-17918.
8. Jensen, M. R. and M. Blackledge 2008. On the origin of NMR dipolar waves in transient helical elements of partially folded proteins. J. Am. Chem. Soc. 130, 11266-11267.
9. Meier, S., M. Blackledge and S. Grzesiek 2008. Conformational distributions of unfolded polypeptides from novel NMR techniques. J. Chem. Phys. 128, 052204.

10. Jha, A. K., A. Colubri, K.F. Freed and T.R. Sosnick 2005. Statistical coil model of the unfolded state: Resolving the reconciliation problem. Proc. Natl. Acad. Sci. U. S. A. 102, 13099-13104.

11. Marsh, J. A. and J.D. Forman-Kay 2009. Structure and disorder in an unfolded state under nondenaturing conditions from ensemble models consistent with a large number of experimental restraints. J. Mol. Biol. 391, 359-374.

12. Vallurupalli, P., D.F. Hansen, E. Stollar, E. Meirovitch and L.E. Kay 2007. Measurement of bond vector orientations in invisible excited states of proteins. Proc. Natl. Acad. Sci. U. S. A. 104, 18473-18477.

13. Baldwin, A. J., D.F. Hansen, P. Vallurupalli and L.E. Kay 2009. Measurement of methyl axis orientations in invisible, excited states of proteins by relaxation dispersion NMR spectroscopy. J. Am. Chem. Soc. 131, 11939-11948.

14. Fischer, M. W. F., J.A. Losonczi, J.L. Weaver and J.H. Prestegard 1999. Domain orientation and dynamics in multidomain proteins from residual dipolar couplings. Biochemistry. 38, 9013-9022.

15. Al-Hashimi, H. M., P.J. Bolon and J.H. Prestegard 2000. Molecular symmetry as an aid to geometry determination in ligand protein complexes. J. Magn. Reson. 142, 153-158.

16. Mueller, G. A., W.Y. Choy, D. Yang, J.D. Forman-Kay, R.A. Venters and L.E. Kay 2000. Global folds of proteins with low densities of NOEs using residual dipolar couplings: Application to the 370-residue maltodextrin-binding protein. J. Mol. Biol. 300, 197-212.

17. Hus, J. C., L. Salmon, G. Bouvignies, J. Lotze, M. Blackledge and R. Bruschweiler 2008. 16-fold degeneracy of peptide plane orientations from residual dipolar couplings: Analytical treatment and implications for protein structure determination. J. Am. Chem. Soc. 130, 15927-15937.

18. Mesleh, M. F., G. Veglia, T.M. DeSilva, F.M. Marassi and S.J. Opella 2002. Dipolar waves as NMR maps of protein structure. J. Am. Chem. Soc. 124, 4206-4207.

19. Mesleh, M. F. and S.J. Opella 2003. Dipolar waves as NMR maps of helices in proteins. J. Magn. Reson. 163, 288-299.

20. Mascioni, A. and G. Veglia 2003. Theoretical analysis of residual dipolar coupling patterns in regular secondary structures of proteins. J. Am. Chem. Soc. 125, 12520-12526.

21. Walsh, J. D. and Y.X. Wang 2005. Periodicity, planarity, residual dipolar coupling, and structures. J. Magn. Reson. 174, 152-162.

22. Mascioni, A., B.L. Eggimann and G. Veglia 2004. Determination of helical membrane protein topology using residual dipolar couplings and exhaustive search algorithm: Application to phospholamban. Chem. Phys. Lipids. 132, 133-144.

23. Al-Hashimi, H. M., H. Valafar, M. Terrell, E.R. Zartler, M.K. Eidsness and J.H. Prestegard 2000. Variation of molecular alignment as a means of resolving orientational ambiguities in protein structures from dipolar couplings. J. Magn. Reson. 143, 402-406.

24. Tolman, J. R., J.M. Flanagan, M.A. Kennedy and J.H. Prestegard 1995. Nuclear magnetic dipole interactions in field-oriented proteins: Information for structure determination in solution. Proceedings Natinal Academy Science U S A. 92, 9279-9283.

25. Tolman, J. R., J.M. Flanagan, M.A. Kennedy and J.H. Prestegard 1997. NMR evidence for slow collective motions in cyanometmyoglobin. Nat Struct Biol. 4, 292-7.

26. Tolman, J. R. and K. Ruan 2006. NMR residual dipolar couplings as probes of biomolecular dynamics. Chem. Rev. 106, 1720-1736.

27. Lakomek, N. A., T. Carlomagno, S. Becker, C. Griesinger and J. Meiler 2006. A thorough dynamic interpretation of residual dipolar couplings in ubiquitin. J. Biomol. NMR. 34, 101-115.

28. Bertini, I., Y.K. Gupta, C. Luchinat, G. Parigi, M. Peana, L. Sgheri and J. Yuan 2007. Paramagnetism-based NMR restraints provide maximum allowed probabilities for the different conformations of partially independent protein domains. J. Am. Chem. Soc. 129, 12786-12794.

29. Bertelsen, E. B., L. Chang, J.E. Gestwicki and E.R. Zuiderweg 2009. Solution conformation of wild-type E. coli Hsp70 (DnaK) chaperone complexed with ADP and substrate. Proc. Natl. Acad. Sci. U. S. A. 106, 8471-8476.

30. White, S. H. and W.C. Wimley 1999. Membrane protein folding and stability : Physical principles. Annual Review Biophysics Biomolecular Structures. 28, 319-365.

31. von Heijne, G. 2006. Membrane-protein topology. Nat. Rev. Mol. Cell Biol. 7, 909-918.

32. Zhou, Y., T. Cierpicki, R.H. Jimenez, S.M. Lukasik, J.F. Ellena, D.S. Cafiso, H. Kadokura, J. Beckwith and J.H. Bushweller 2008. NMR solution structure of the integral membrane enzyme DsbB: Functional insights into DsbB-catalyzed disulfide bond formation. Mol. Cell. 31, 896-908.

33. Traaseth, N. J., R. Verardi and G. Veglia 2008. Asymmetric methyl group labeling as a probe of membrane protein homo-oligomers by NMR spectroscopy. J. Am. Chem. Soc. 130, 2400-2401.

34. Tugarinov, V. and L.E. Kay 2004. An isotope labeling strategy for methyl TROSY spectroscopy. J Biomol NMR. 28, 165-72.

35. Tugarinov, V. and L.E. Kay 2003. Ile, leu, and val methyl assignments of the 723-residue malate synthase G using a new labeling strategy and novel NMR methods. J Am Chem Soc. 125, 13868-78.

36. Tycko, R., F.J. Blanco and Y. Ishii 2000. Alignment of biopolymers in strained gels: A new way to create detectable dipole-dipole couplings in high-resolution biomolecular NMR. Journal of the American Chemical Society. 122, 9340-9341.

37. Douglas, S. M., J.J. Chou and W.M. Shih 2007. DNA-nanotube-induced alignment of membrane proteins for NMR structure determination. Proc. Natl. Acad. Sci. U. S. A. 104, 6644-6648.

38. Lorieau, J., L. Yao and A. Bax 2008. Liquid crystalline phase of G-tetrad DNA for NMR study of detergent-solubilized proteins. J. Am. Chem. Soc. 130, 7536-7537.

39. Veglia, G. and S.J. Opella 2000. Journal of the American Chemical Society., 11733-11734.

40. Ma, C. and S.J. Opella 2000. Lanthanide ions bind specifically to an added "EF-hand" and orient a membrane protein in micelles for solution NMR spectroscopy. J. Magn. Reson. 146, 381-384.

41. Wohnert, J., K.J. Franz, M. Nitz, B. Imperiali and H. Schwalbe 2003. Protein alignment by a coexpressed lanthanide-binding tag for the measurement of residual dipolar couplings. J. Am. Chem. Soc. 125, 13338-13339.

42. Van Horn, W. D., H.J. Kim, C.D. Ellis, A. Hadziselimovic, E.S. Sulistijo, M.D. Karra, C. Tian, F.D. Sonnichsen and C.R. Sanders 2009. Solution nuclear magnetic resonance structure of membrane-integral diacylglycerol kinase. Science. 324, 1726-1729.

43. Cierpicki, T., B. Liang, L.K. Tamm and J.H. Bushweller 2006. Increasing the accuracy of solution NMR structures of membrane proteins by application of residual dipolar couplings. high-resolution structure of outer membrane protein A. J. Am. Chem. Soc. 128, 6947-6951.

44. Buck, B., J. Zamoon, T.L. Kirby, T.M. DeSilva, C. Karim, D. Thomas and G. Veglia 2003. Overexpression, purification, and characterization of recombinant ca-ATPase regulators for high-resolution solution and solid-state NMR studies. Protein Expr Purif. 30, 253-61.

45. Kirby, T. L., C.B. Karim and D.D. Thomas 2004. Electron paramagnetic resonance reveals a large-scale conformational change in the cytoplasmic domain of phospholamban upon binding to the sarcoplasmic reticulum ca-ATPase. Biochemistry. 43, 5842-52.

46. Chou, J. J., J.D. Kaufman, S.J. Stahl, P.T. Wingfield and A. Bax 2002. Micelle-induced curvature in a water-insoluble HIV-1 env peptide revealed by NMR dipolar coupling measurement in stretched polyacrylamide gel. J. Am. Chem. Soc. 124, 2450-2451.

47. Permi, P. and A. Annila 2000. Transverse relaxation optimised spin-state selective NMR experiments for measurement of residual dipolar couplings. J. Biomol. NMR. 16, 221-227.

48. Delaglio, F., Grzesiek, S., Vuister, G. W., Zhu, G. Pfeifer, J., Bax,A. 1995. NMRPipe: A multidimensional spectral processing system based on UNIX pipes. J. Biomol. NMR. 6, 277-293.

49. Johnson, B. A. 2004. Using NMRView to visualize and analyze the NMR spectra of macromolecules. Methods Mol. Biol. 278, 313-352.

50. Battiste, J. L. and G. Wagner 2000. Utilization of site-directed spin labeling and high-resolution heteronuclear nuclear magnetic resonance for global fold determination of large proteins with limited nuclear overhauser effect data. Biochemistry. 39, 5355-5365.

51. Metcalfe, E. E., J. Zamoon, D.D. Thomas and G. Veglia 2004. (1)H/(15)N heteronuclear NMR spectroscopy shows four dynamic domains for phospholamban reconstituted in dodecylphosphocholine micelles. Biophys. J. 87, 1205-1214.

52. Schwieters, C. D., J.J. Kuszewski, N. Tjandra and G.M. Clore 2003. The xplor-NIH NMR molecular structure determination package. J. Magn. Reson. 160, 65-73.

53. Zamoon, J., A. Mascioni, D.D. Thomas and G. Veglia 2003. NMR solution structure and topological orientation of monomeric phospholamban in dodecylphosphocholine micelles. Biophys. J. 85, 2589-2598.

54. Cornilescu, G., F. Delaglio and A. Bax 1999. Protein backbone angle restraints from searching a database for chemical shift and sequence homology. J Biomol NMR. 13, 289-302.

55. Traaseth, N. J., L. Shi, R. Verardi, D.G. Mullen, G. Barany and G. Veglia 2009. Structure and topology of monomeric phospholamban in lipid membranes determined by a hybrid solution and solid-state NMR approach. Proc. Natl. Acad. Sci. U. S. A. 106, 10165-10170.

56. Clore, G. M. and J. Kuszewski 2003. Improving the accuracy of NMR structures of RNA by means of conformational database potentials of mean force as assessed by complete dipolar coupling cross-validation. J. Am. Chem. Soc. 125, 1518-1525.

57. Traaseth, N. J., K.N. Ha, R. Verardi, L. Shi, J.J. Buffy, L.R. Masterson and G. Veglia 2008. Structural and dynamic basis of phospholamban and sarcolipin inhibition of ca(2+)-ATPase. Biochemistry. 47, 3-13.

58. Kimura, Y., K. Kurzydlowski, M. Tada and D.H. MacLennan 1997. Phospholamban inhibitory function is activated by depolymerization. J Biol Chem. 272, 15061-4.

59. Reddy, L. G., L.R. Jones and D.D. Thomas 1999. Depolymerization of phospholamban in the presence of calcium pump: A fluorescence energy transfer study. Biochemistry. 38, 3954-62.

60. Karim, C. B., C.G. Marquardt, J.D. Stamm, G. Barany and D.D. Thomas 2000. Synthetic null-cysteine phospholamban analogue and the corresponding transmembrane domain inhibit the ca-ATPase. Biochemistry. 39, 10892-7.

61. Veglia, G., A.C. Zeri, C. Ma and S.J. Opella 2002. Deuterium/hydrogen exchange factors measured by solution nuclear magnetic resonance spectroscopy as indicators of the structure and topology of membrane proteins. Biophys. J. 82, 2176-2183.

62. Mascioni, A., C. Karim, J. Zamoon, D.D. Thomas and G. Veglia 2002. Solid-state NMR and rigid body molecular dynamics to determine domain orientations of monomeric phospholamban. J. Am. Chem. Soc. 124, 9392-9393.

63. Chou, J. J., S. Gaemers, B. Howder, J.M. Louis and A. Bax 2001. Journal of Molecular Biology. 21, 377-382.

64. Traaseth, N. J. and G. Veglia 2010. Probing excited states and activation energy for the integral membrane protein phospholamban by NMR CPMG relaxation dispersion experiments. Biochim. Biophys. Acta. 1798, 77-81.

65. Warren, J. J. and P.B. Moore 2001. A maximum likelihood method ofr determining da and R for sets of dipolar coupling data. Journal of Magnetic Resonance. 149, 271-275.

66. Clore, M. G., M.A. Gronenborn and A. Bax 1998. A robust method for determining the magnitude of the fully asymmetric alignment tensor of oriented macromolecules in the absence of structural information. Journal of Magnetic Resonance. 133, 216-221.

67. Chill, J. H., J.M. Louis, F. Delaglio and A. Bax 2007. Local and global structure of the monomeric subunit of the potassium channel KcsA probed by NMR. Biochim. Biophys. Acta. 1768, 3260-3270.

68. Oxenoid, K. and J.J. Chou 2005. The structure of phospholamban pentamer reveals a channel-like architecture in membranes. Proc. Natl. Acad. Sci. U. S. A. 102, 10870-10875.

69. Langen, R., K.J. Oh, D. Cascio and W.L. Hubbell 2000. Crystal structures of spin labeled T4 lysozyme mutants: Implications for the interpretation of EPR spectra in terms of structure. Biochemistry. 39, 8396-8405.

70. Sammalkorpi, M. and T. Lazaridis 2007. Modeling a spin-labeled fusion peptide in a membrane: Implications for the interpretation of EPR experiments. Biophys. J. 92, 10-22.

71. Losonczi, J. A., M. Andrec, M.W. Fischer and J.H. Prestegard 1999. Order matrix analysis of residual dipolar coupling using singular value decomposition. Journal of Magnetic Resonance. 138, 334-342.

72. Shi, L., N.J. Traaseth, R. Verardi, A. Cembran, J. Gao and G. Veglia 2009. A refinement protocol to determine structure, topology, and depth of insertion of membrane proteins using hybrid solution and solid-state NMR restraints. J. Biomol. NMR. 44, 195-205.

73. Franzin, C. M., P. Teriete and F.M. Marassi 2007. Structural similarity of a membrane protein in micelles and membranes. J. Am. Chem. Soc. 129, 8078-8079.

74. Dedmon, M. M., K. Lindorff-Larsen, J. Christodoulou, M. Vendruscolo and C.M. Dobson 2005. Mapping long-range interactions in alpha-synuclein using spin-label NMR and ensemble molecular dynamics simulations. J. Am. Chem. Soc. 127, 476-477.

75. Liang, B., J.H. Bushweller and L.K. Tamm 2006. Site-directed parallel spin-labeling and paramagnetic relaxation enhancement in structure determination of membrane proteins by solution NMR spectroscopy. J. Am. Chem. Soc. 128, 4389-4397.

76. Salvatella, X., B. Richter and M. Vendruscolo 2008. Influence of the fluctuations of the alignment tensor on the analysis of the structure and dynamics of proteins using residual dipolar couplings. J. Biomol. NMR. 40, 71-81.

77. De Simone, A., B. Richter, X. Salvatella and M. Vendruscolo 2009. Toward an accurate determination of free energy landscapes in solution states of proteins. J. Am. Chem. Soc. 131, 3810-3811.

78. Salmon, L., G. Nodet, V. Ozenne, G. Yin, M.R. Jensen, M. Zweckstetter and M. Blackledge 2010. NMR characterization of long-range order in intrinsically disordered proteins. J. Am. Chem. Soc. 132, 8407-8418.

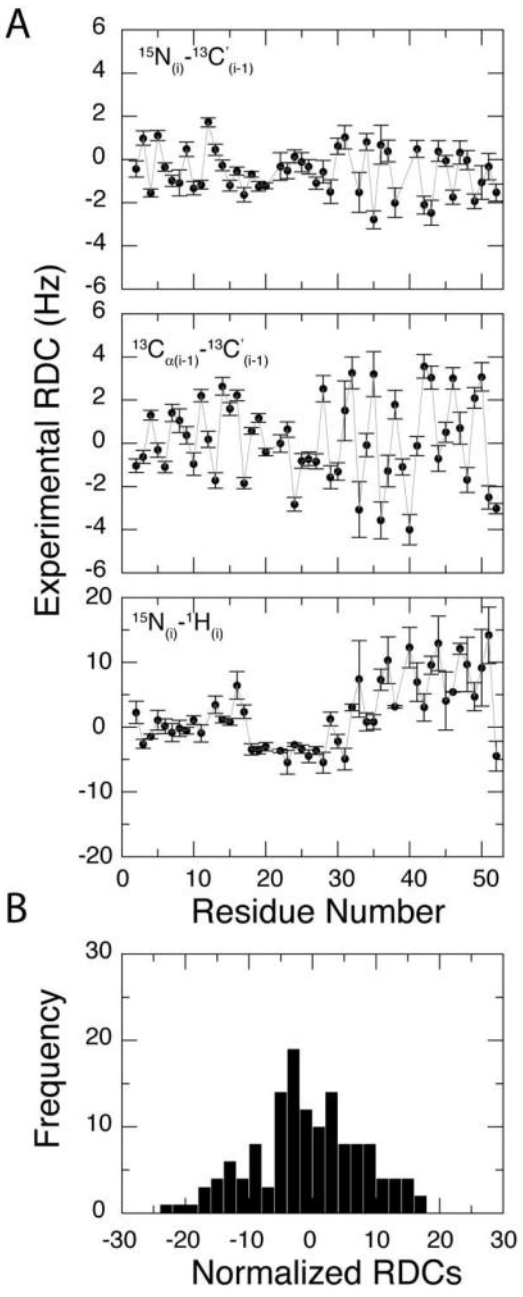

Figure 1. RDC versus residue for PLN weakly oriented in stretched gels. *(A) Top: 13C'-15N RDCs; middle: $^{13}C'$-$^{13}C\alpha$ RDCs; bottom: ^{1}H-^{15}N RDCs. We reported only the RDC values for well resolved peaks. (B) RDC histogram with all the data in (A) scaled to the ^{1}H-^{15}N RDCs.*

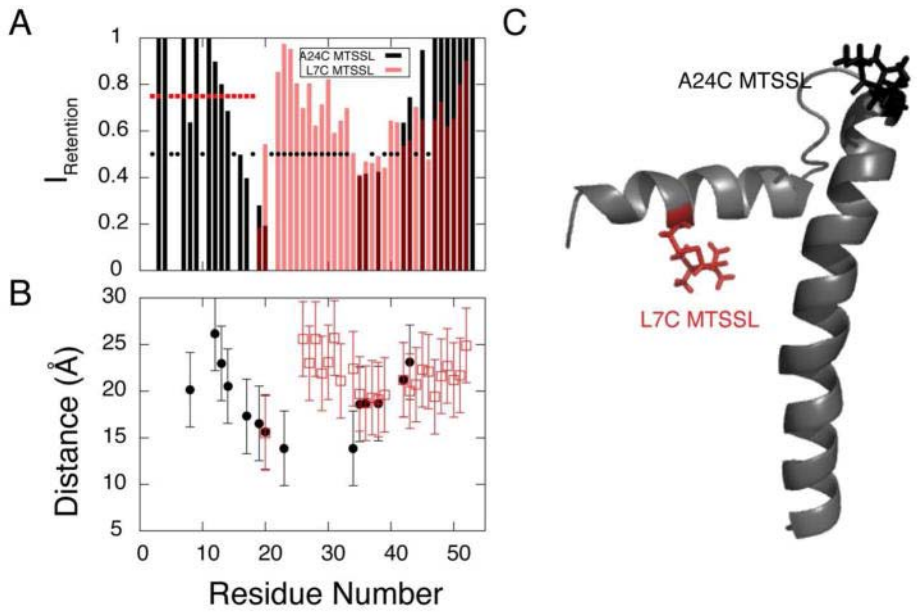

Figure 2. PRE data obtained from A24C-PLN (black) and L7C-PLN (red) cross-linked with MTSSL. *(A) Intensity retention plot for A24C-PLN and L7C-PLN labeled with MTSSL. Unresolved peaks are not reported and are indicated with points. (B) Distances derived from PREs (see materials and methods). Note: only peaks with intensity retention ratio less than 0.95 were used in the calculations. Also some residues lacking R2 values were omitted. (C) Cartoon representation of PLN with MTSSL label at C24 and C7.*

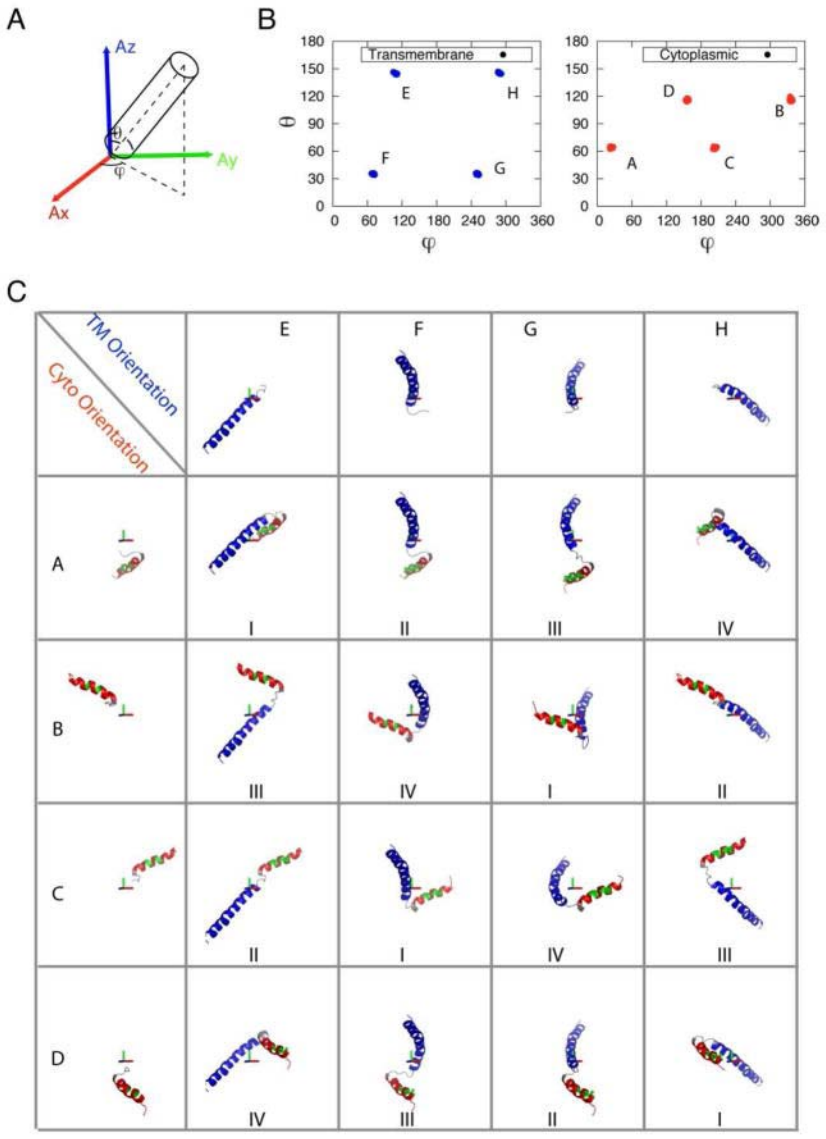

Figure 3. (A) Definition of orientation angles (θ, ϕ) of helical rigid body in the alignment frame. *(B) (θ, ϕ) plot of cytoplasmic (Cyto, red) and transmembrane (TM, blue) domain orientations in the alignment frame. (C) Detailed orientation of TM and Cyto with each letter corresponding to (θ, ϕ) in (B). Different combinations of orientations result in different families (labeled in the bottom).*

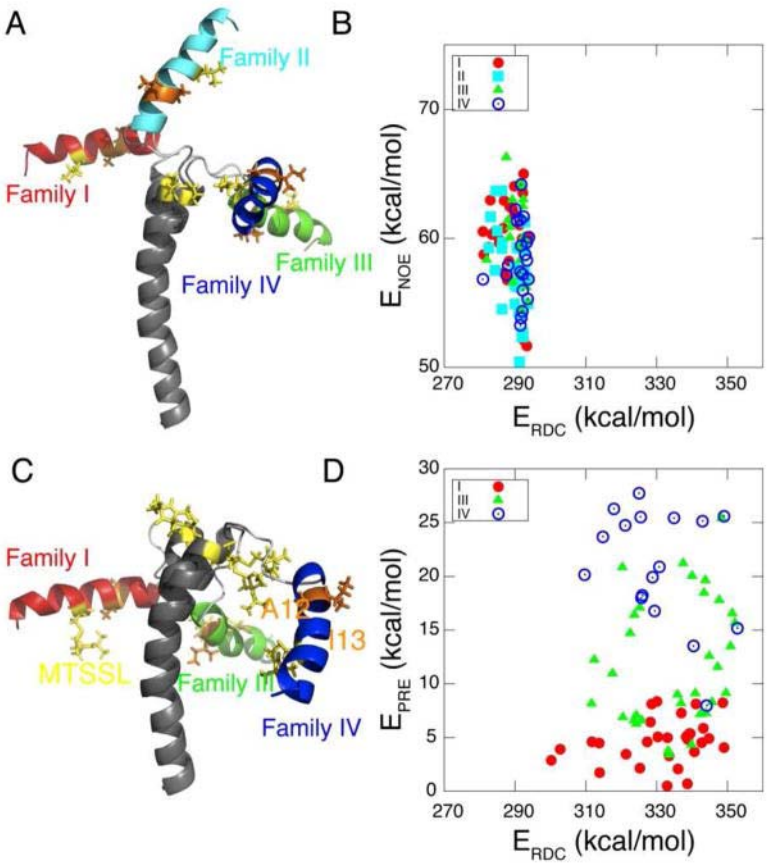

Figure 4. (A) Comparison between representative structures from each family refined from protocol II. *Sidechains of MTSSL label (yellow) and hydrophobic residues (A12 and I13, orange) are shown and labeled. (B) E_{NOE} and E_{RDC} of the four families of structures from protocol II. (C). Similar to (A) except for protocol III. (D) EPRE and ERDC of the three families of structures from protocol III.*

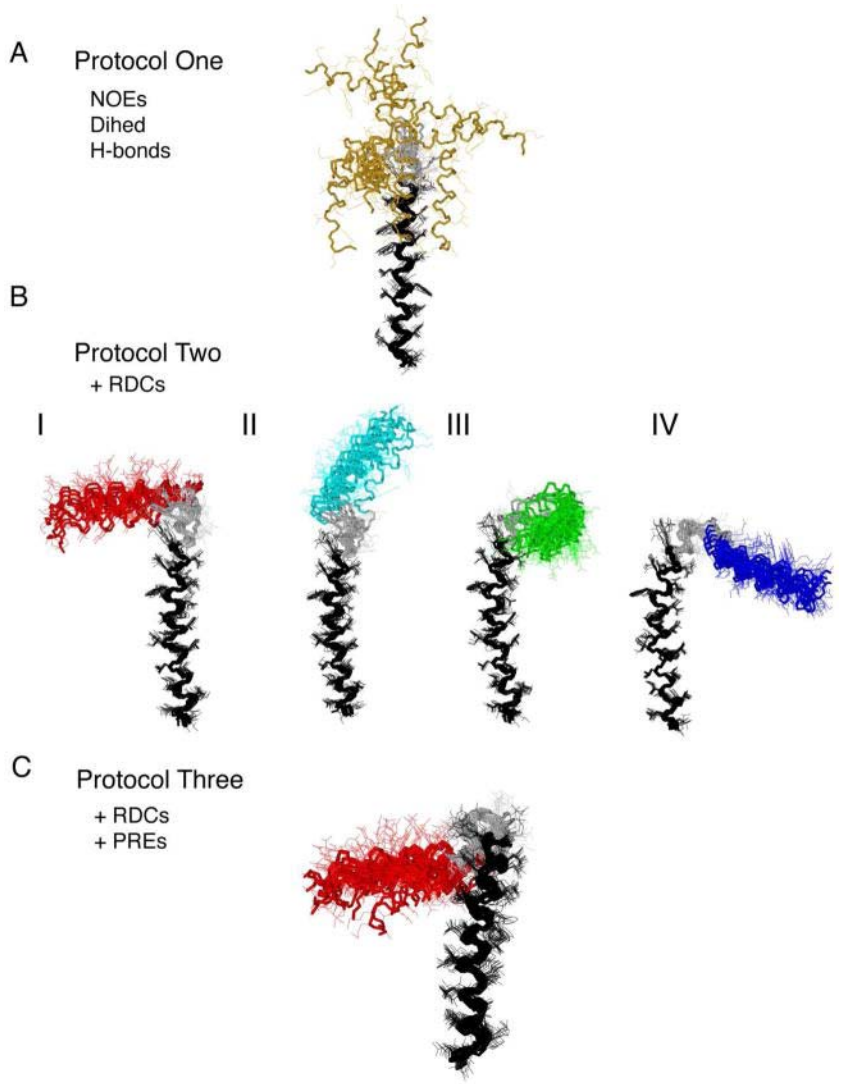

Figure 5. Structure overlay of different ensembles AFA-PLN. *The overlay is done by overlaying backbone atoms from residues 24–50 using MOLMOL. (A) Protocol one: solution-only ensemble (20 monomers) with NOEs, torsion angles and hydrogen bonds. (B) Protocol two: RDC ensemble (15 monomers) with additional* ^{1}H-^{15}N, $^{13}C'$-^{15}N *and* $^{13}C'$-$^{13}C\alpha$ *RDCs. Four families of structures result. (C) Protocol three: PRE ensemble (20 monomers) that utilize RDCs and PREs from MTSSL.*

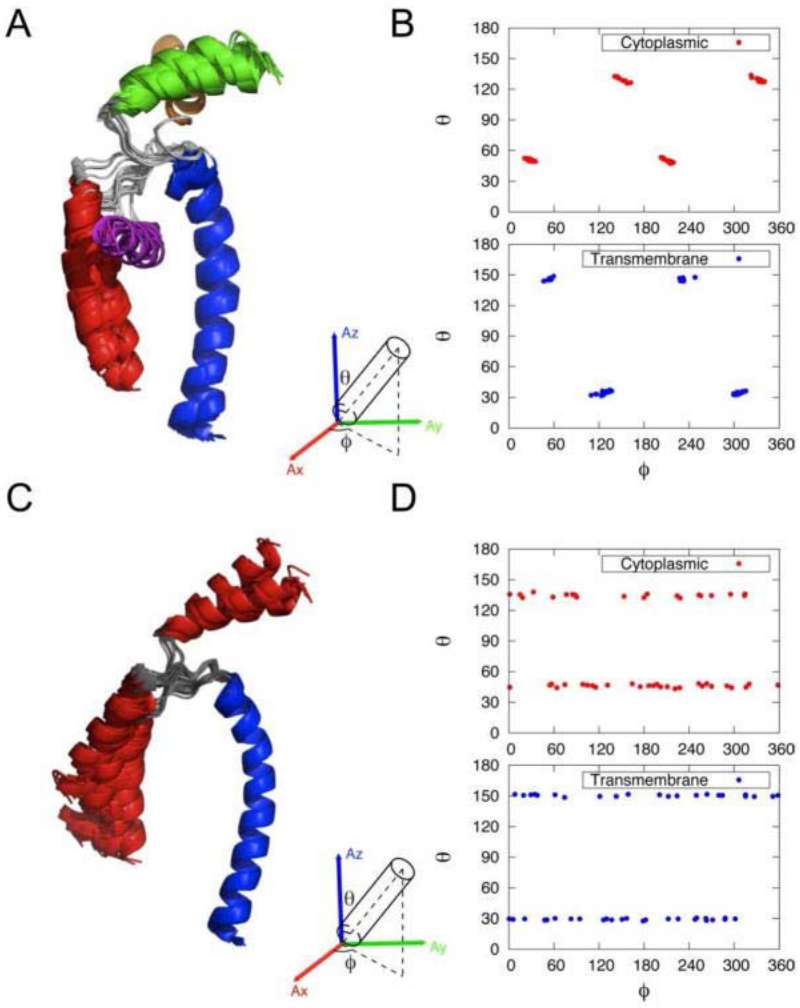

Figure 6. (A) Structure overlay of monomer structures using published RDC data from wt-PLN using non-symmetric tensor. *(B) Orientation angles (θ, ϕ) of helical rigid body in the nonsysmmetric alignment frame. (C) Structure overlay of monomer structures using published RDC data from wt-PLN using symmetric tensor. (D) Orientation angles (θ, ϕ) of helical rigid body in the sysmmetric alignment frame.*

4.6 Supporting information

In the first protocol, we started from a fully extended structure of AFA-PLN and carried out simulated annealing calculations starting at 6000 K and cooled to 0 K in Cartesian and torsion-angle space. The NOEs were modeled using a soft-square potential with a force constant ramping from 2 to 50 kcal $Å^{-2}$, while torsion angles were restrained by a square-well potential with a force constant of 200 kcal rad^{-2}. In addition, the torsion angle database potential 'RAMA' was used to bias the conformational search in the most allowed regions of the Ramachandran plot.

For the protocol two, residual dipolar coupling data were introduced during the lower temperature simulated annealing (3000 K) starting from the folded PLN structures obtained from protocol one. The system was cooled down to 0 K with a cooling rate of 5 K/step using 4000 steps of internal dynamics and 4000 steps of Cartesian dynamics. Only RDCs derived from residues in the helical regions with order parameters $S^2 > 0.6$ were used. The force constants for RDC restraints were ramped from 0.05 to 0.5 kcal Hz^{-2}, which was determined by compromising RDC agreement and geometrical penalties. After obtaining the tensor magnitude, only tensor orientations were allowed to vary during the internal and Cartesian dynamics. For protocol three, additional MTSSL derived distance restraints are added to the restrains used in protocol two. The MTSSL restraints were imposed by a force constant ramped from 2 to 50 kcal $Å^{-2}$. The parameter and topology files for MTSSL were taken from the library available in XPLOR-NIH (52). All calculations were performed on a Linux cluster at the Minnesota Supercomputing Institute.

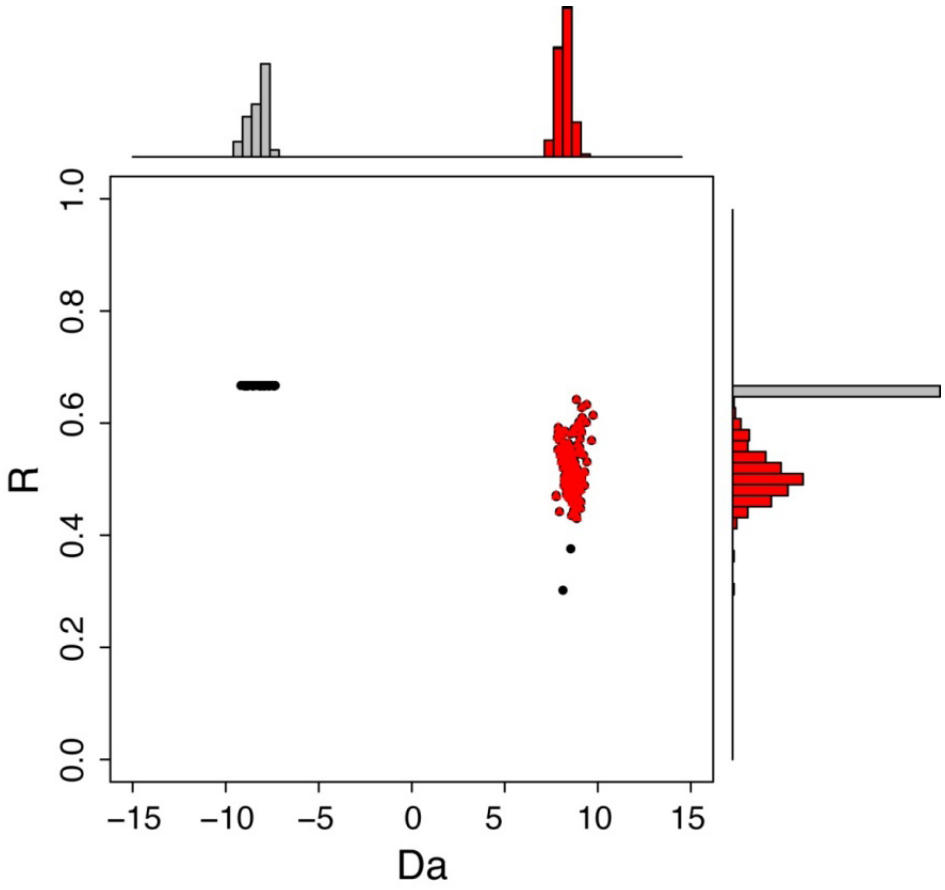

Figure S1. The (Da, R) clustering (black) of structures refined with NOE and RDCs with variable tensor magnitude. *Structures with D_a > 0 and R > 0.4 are selected for further structural calculation and analysis (red).*

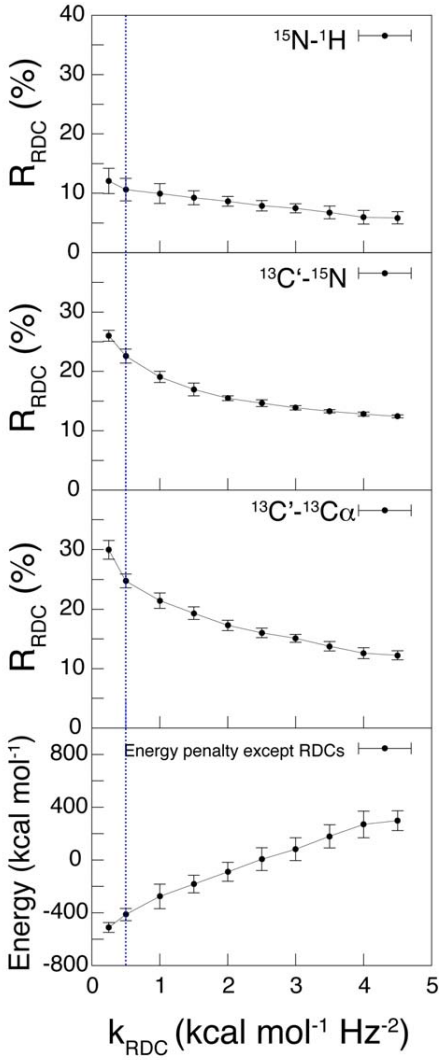

Figure S2. RDC R factors and energy value as functions of force constant used in the simulated annealing. *The force constant for RDC was ramped from 0.25 kcal mol^{-1} Hz^{-2} to 4.5 kcal mol^{-1} Hz^{-2}, while the force constants for other energy terms such as NOEs and torsion angles were fixed. RDCs were modeled using flat-well potentials with the relative weight between ^{15}N-^{1}H, ^{13}C'-^{15}N and ^{13}C'-^{13}Cα was set to be 1:1:1. The energy values are summations from different terms in Equation 1 other than RDCs and the magnitude indicates penalties from other solution NMR data (NOEs and torsion angles) and ideal geometry (bond, angle etc.).*

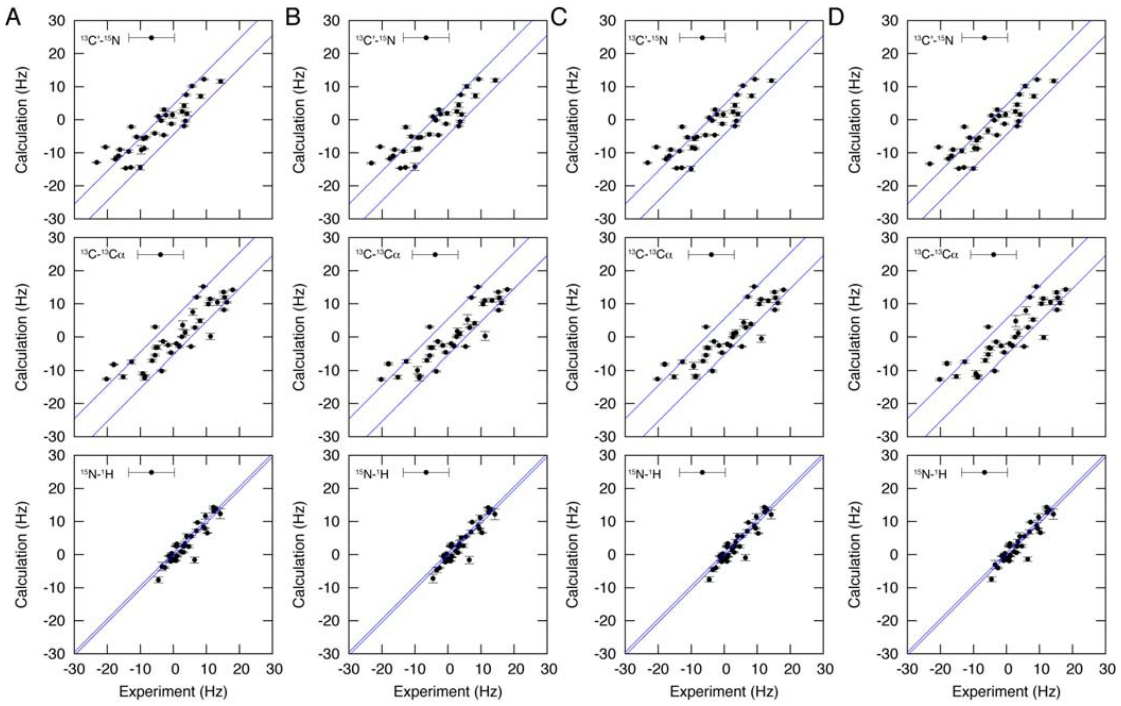

Figure S3. Correlation of experimental versus calculated RDCs of RDC ensemble family I, II, III and IV *(15 monomers). Experimental errors of 3.0 Hz, 4.5 Hz and 0.5 Hz are used for $^{13}C'$-^{15}N (A), $^{13}C'$-$^{13}C\alpha$ (B) and ^{15}N-^{1}H (C) respectively.*

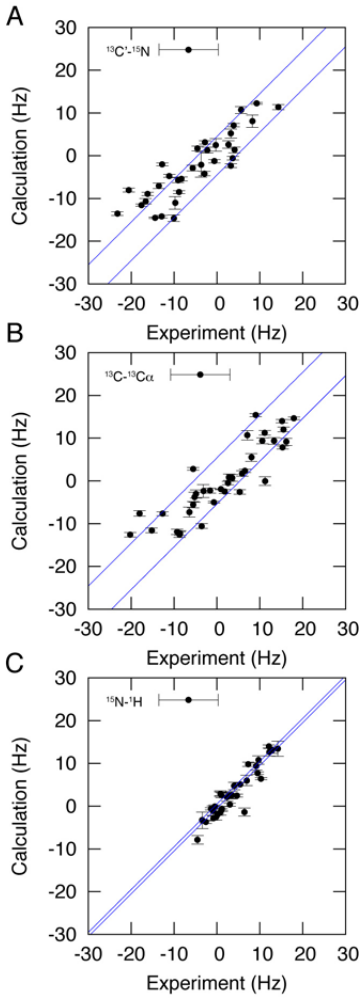

Figure S4. Correlation of experimental versus calculated RDCs from protocol three*, the PRE ensemble (20 monomers). Experimental errors of 3.0 Hz, 4.5 Hz and 0.5 Hz are used for $^{13}C'$-^{15}N (A), $^{13}C'$-$^{13}C\alpha$ (B) and ^{15}N-^{1}H (C) respectively.*

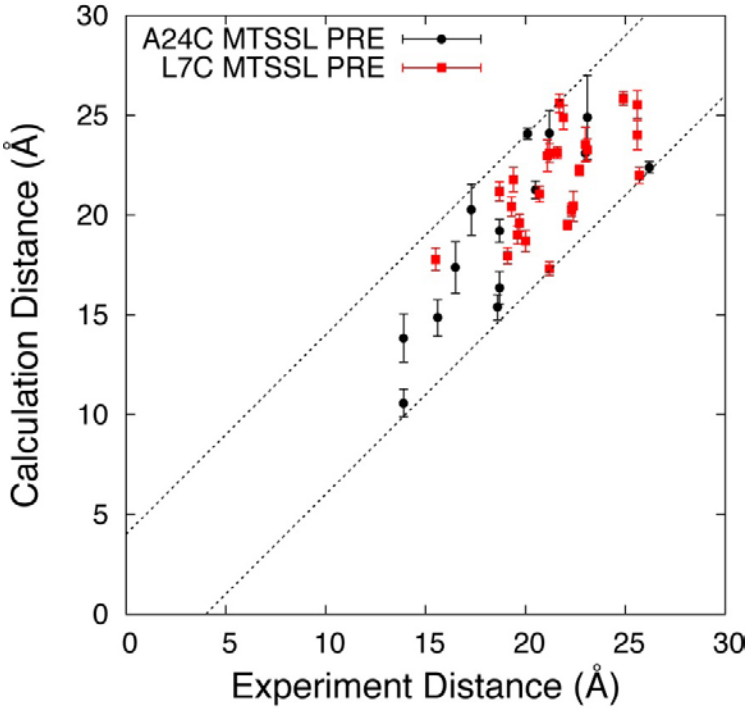

Figure S5. Correlation of experimental distances obtained from PREs (A24C MTSSL in black and L7C MTSSL in red) with calculated distances measured from the PRE ensemble *(20 monomers). Experimental errors of 4 Å are plotted from the correlation line (dotted lines). The calculated distances (and error bars) reflect the average (and standard deviation) from the 20 structures in the PRE ensemble.*

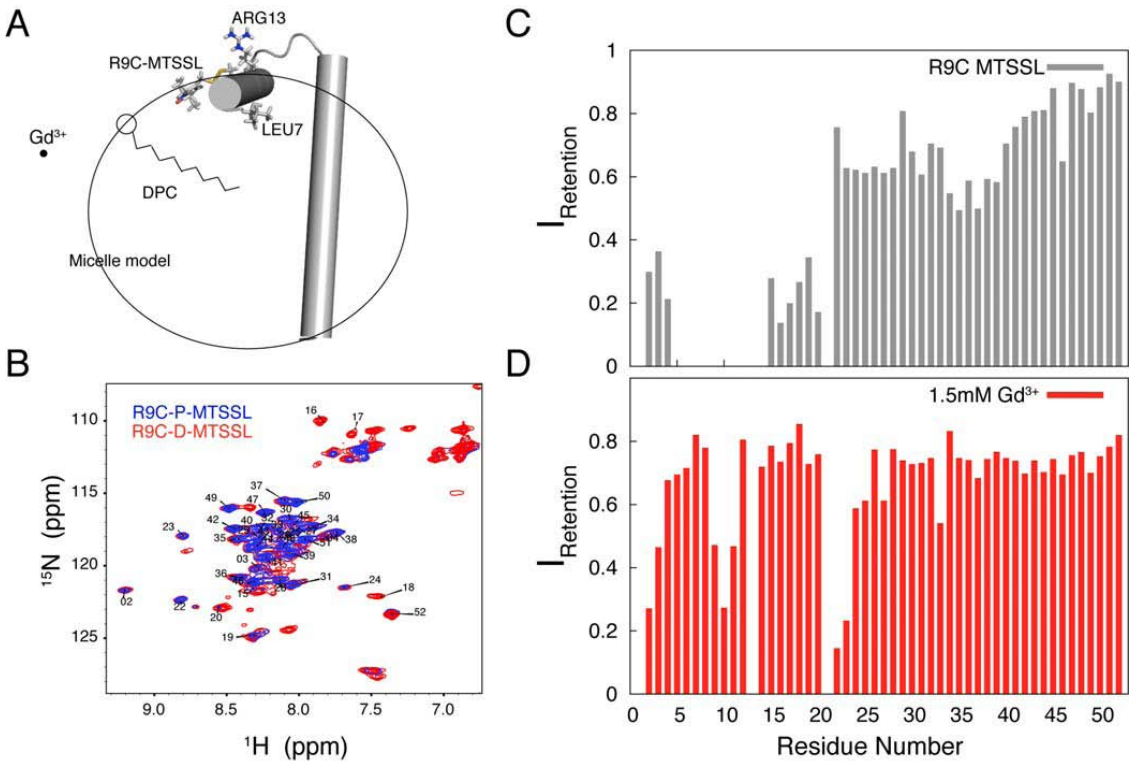

Figure S6. (A) Cartoon representation of R9C-AFA-PLN-MTSSL labeled AFA-PLN in a simplified micelle model. *The model is supported by PRE data obtained from (B) NMR HSQC experiments. (C) Intensity retention from covalent attachment of MTSSL indicates that the hydrophobic spin label prefers to insert into the micelle, significantly quenching inserted residues around 35. (D) Intensity retention from 1.5 mM Gd^{3+} to the HSQC spectrum of R9C-AFA-PLN indicates that the cytoplasmic domain Ia is inserted into the micelle with preferential orientation for hydrophobic (e.g., L7) and hydrophilic residues (e.g., R13).*

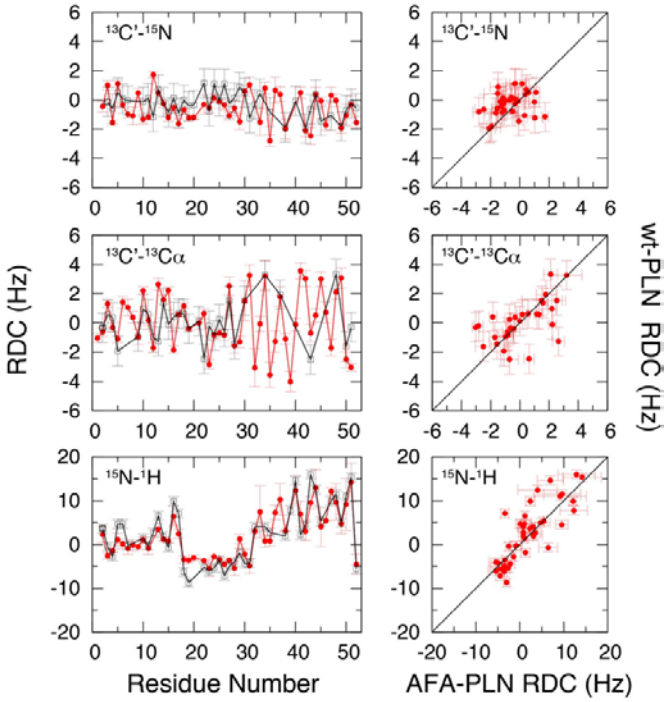

Figure S7. Comparison of 13C'-15N, 13C'-13Cα, and 15N-1H RDCs *of AFA-PLN (monomer, red) and wt-PLN (pentamer, black) by residue number (left column) and as correlation plots (right column).*

	NOE+DIHE	RDC Ensemble				PRE Ensemble
		Family I	Family II	Family III	Family IV	
R.m.s. deviations from experimental restraints						
NOE/H-bond (Å) (431)	0.058	0.043	0.043	0.043	0.043	0.047
Torsion angle (°) (38)	0.072	0.739	0.724	0.746	0.741	1.160
MTSL PRE (Å) (43)	N/A	N/A	N/A	N/A	N/A	0.039
RDC R-factors (%)						
$^1D_{NH}$ (33)	N/A	10.23	10.19	9.20	9.88	10.68
$^1D_{NC'}$ (36)	N/A	22.04	22.16	21.97	22.13	23.55
$^1D_{CCA}$ (33)	N/A	24.75	22.68	25.33	25.09	25.86
R.m.s. deviations from idealized covalent geometry						
Bond (Å)	0.003	0.005	0.005	0.005	0.005	0.005
Angle (°)	0.397	0.655	0.647	0.648	0.650	0.736
Impropers (°)	0.278	0.629	0.612	0.619	0.621	0.684
Measure of structural quality						
% Residues in most favored region	92.5	90.7	91.7	87.1	90.1	85.3
%Residues in additional allowed region	7.5	9.1	7.5	12.3	9.6	10.2
%Residues in generously allowed region	0	0.2	0.8	0.6	0.3	4.5
%Residues in disallowed regions	0	0.0	0.0	0.0	0.0	0.0
Precision of atomic coordinates (Å)						
Backbone all (3-50)	4.402	1.6	1.5	0.9	0.9	1.6
Helix1 (residue 3-18)	0.621	0.2	0.1	0.1	0.1	0.2
Helix 2 (residue 24-50)	0.657	0.5	0.3	0.3	0.3	1.0

All the statistics were carried using Xplor-NIH software package.[1] Ramachandran analysis was carried out using PROCHECK_NMR.[2] Atom superposition was carried out using MOLMOL.[3]

Table S1. NMR and Structural Refinement Statistics

Chapter 5 - Probing Ground and Excited States of Phospholamban in Model and Native Lipid Membranes by Magic Angle Spinning NMR Spectroscopy

Reprinted with permission from:

Martin Gustavsson, Nathaniel J. Traaseth, and Gianluigi Veglia. Probing Ground and Excited States of Phospholamban in Model and Native Lipid Membranes by Magic Angle Spinning NMR Spectroscopy *Biochim Biophys Acta.* 2012;1818(2):146-53

Membrane proteins exist in a Boltzmann distribution of conformational states. Classical structural biology techniques are biased toward the characterization of the average conformations or conformational snapshots along the folding energy landscape. In this paper, we analyzed the ground and excited states of phospholamban (PLN), a membrane protein that regulates sarcoplasmic reticulum calcium ATPase (SERCA), in different membrane mimetic environments. Previously, we proposed that the conformational equilibria of PLN are central to SERCA regulation. Here, we show that these equilibria detected in micelles and bicelles are also present in native sarcoplasmic reticulum lipid membranes as probed by MAS solid-state NMR. Importantly, we found that the kinetics of conformational exchange and the extent of ground and excited states in detergent micelles and lipid bilayers are different, revealing a possible regulatory role of the membrane composition on the allosteric regulation of SERCA. Since the extent of excited states is directly correlated to SERCA inhibition, these findings open up the exciting possibility that calcium transport in the heart can be controlled by the lipid bilayer composition.

5.1 Introduction

Membrane proteins exist as ensembles (Boltzmann distributions) of ground and excited states. These states are accessible by small scale atomic fluctuations around the average structure or large scale reorganizations of entire domains. In addition to intrinsic thermal fluctuations, membrane protein folding energy landscape is shaped by the interactions with the lipid membrane, which have been hypothesized to modulate protein function through allosteric interactions (1). In the past years, the need to obtain high-resolution membrane protein structures for structural genomics initiatives drove researchers toward high-quality views of average conformations or crystallographic snapshots of membrane proteins in non-native detergent micellar environments. This effectively relegated the analysis of conformational fluctuations and protein-lipid interactions to secondary roles. While the structures have given us a vivid view of static membrane proteins, our knowledge on how these biological macromolecules transmit the regulatory effects through the membrane at the atomic level is still primordial. It is clear that a complete description of membrane protein function must include structure, the characterization of their motions (conformational dynamics), and their interactions with lipid membranes. Magic angle spinning (MAS) NMR (2-12) and oriented solid-state (OSS) NMR (13-18) have evolved as powerful methods to study the structure and dynamics of membrane proteins in native-like lipid bilayers. While the development of these solid-state NMR techniques will be instrumental to determine the structure of large membrane proteins, their major advantage with respect to X-ray crystallography will be to describe membrane proteins as ensemble of structures, including ground and excited states.

In the past years, our group has focused attention on the small membrane protein phospholamban (PLN, 52-residue) that regulates the function of sarcoplasmic reticulum (SR) Ca^{2+}-ATPase (SERCA) in cardiac muscle (19, 20). While apparently simple in its secondary structure content, PLN has a complex dynamics when reconstituted both in micelles and synthetic lipid membranes (21-23). In its monomeric and pentameric forms, PLN consists of a membrane spanning helix connected to an amphipathic helix (domain Ia) through a short loop (15, 16, 24) (**Figure 1**). The membrane-spanning helix can be divided into a rigid and hydrophobic domain II and a more dynamic and hydrophilic

domain Ib, which is positioned at the lipid head group and unfolds on a μs time scale (21, 25). Domain Ia of PLN is in a complex conformational equilibrium that involves at least four different states and resembles the folding/unfolding proposed for amphipathic helices: detached/unfolded (R), absorbed/unfolded (R'), absorbed/partially folded (T'), and absorbed/fully folded (T) (26-28). For monomeric and pentameric PLN, the R state has a small population in DPC detergent micelles and mechanically aligned lipid bilayers (< 15%) (28). Although most of the information on the high energy (excited) R, T' and R' states was derived from studies in detergent micelles, we found a direct relationship between the extent (population) of these excited states and PLN effects on SERCA, i.e., the more populated is the R state, the less inhibitory is PLN (26, 29). This structure-function correlation can potentially be used to design loss-of-function PLN analogs to be used in gene therapy (30, 31).

To understand how PLN's conformational equilibria are modulated by lipid membrane composition, we utilized Magic Angle Spinning (MAS) solid-state NMR in conjunction with solution NMR methods. We show that, although the relative populations of the different states can be tuned by the type and charge of lipids, a conformational equilibrium of PLN is present in all of the membrane mimicking systems analyzed, ranging from dodecylphosphocholine (DPC) micelles and 1,2-dimyristoyl-sn-glycero-3-phosphocholine/1,2-dihexanoyl-sn-glycero-3-phosphocholine (DMPC/DHPC) bicelles to native SR lipid bilayers. These results demonstrate the presence and importance of conformational fluctuations in native cellular membranes.

5.2 Materials and methods

5.2.1 Sample preparation

Synthetic lipids and natural egg PC, phosphatidylethanolamine (PE) and phosphatidic acid (PA) lipids were purchased from Avanti polar lipids (Alabaster, AL). Native SR lipids were extracted from rabbit hind leg skeletal muscle using a chloroform:methanol procedure as previously described(32). All experiments utilized a monomeric PLN mutant with Cys36, 41, and 46 mutated to Ala, Phe, and Ala, respectively (AFA-PLN) (33). [U-^{13}C,^{15}N] AFA-PLN was recombinantly expressed and purified according to Buck *et al.* (34) [EQN-^{13}C,^{15}N; A-^{13}C] AFA-PLN was produced by a

reversed labeling method, where unlabeled analogs of all other amino acids were added to the growth medium which also contained ^{13}C-glucose and $^{15}NH_4Cl$ (35). Selectively [^{15}N,^{13}C] labeled AFA-PLN was synthesized using [^{15}N,^{13}C] labeled amino acids (Sigma-Aldrich, Isotec, Miamisburg, OH) on a microwave peptide synthesizer (CEM Corporation, Matthews, NC) essentially as previously described (16, 33). The exceptions were that 1% sodium dodecyl sulfate (SDS) was added during cleavage from the resin and the protein was dissolved in 10% SDS prior to HPLC purification, which utilized a 2-propanol/H_2O gradient from 10% to 90% on a C18 column. To avoid oxidation of Met50, we made a conservative substitution to norleucine in the synthetic samples. This substitution had no effect on the inhibitory effect of AFA-PLN on SERCA. The quality of the final synthetic product was assessed by mass spectrometry and solution NMR in DPC micelles. SERCA activity assays were performed as described previously (29, 36) to confirm that all recombinantly and synthetically produced AFA-PLN proteins inhibited SERCA.

Isotropic bicelle samples for solution NMR were prepared by dissolving 1 mg of [U-^{13}C,^{15}N] AFA-PLN in a 174 mg/mL solution of DHPC containing 20 mM MOPS, 100 mM NaCl, and 5% D_2O. The protein/DHPC solution was added to 21.9 mg of lyophilized DMPC lipids, and was followed by several freeze/thaw cycles to form a clear bicellar solution. The pH was adjusted to 7.0 and the 250 μL sample containing a DHPC:DMPC molar ratio (q) of 0.33 was transferred to a 5 mm Shigemi tube. Negatively charged bicelles were prepared identically with the exception that 33% of the DMPC was replaced by 1,2-dimyristoyl-*sn*-glycero-3-phospho-(1'-rac-glycerol) (DMPG).

Magic angle spinning samples were prepared by dissolving 15 mg of lyophilized lipids in HPLC elution (~70% 2-propanol, ~30% H_2O) containing 1.6 mg AFA-PLN. To this solution, 20 mM MOPS (pH 7.0) and 100 mM NaCl were added based on a final volume of 2 mL. The 2-propanol was then evaporated using nitrogen gas to form AFA-PLN-containing multi-lamellar lipid vesicles (MLVs). The mixture was lyophilized, re-suspended in 2 mL of double distilled H_2O and centrifuged at 200,000×g to yield a hydrated lipid pellet, which was transferred to a 3.2 mm thin wall rotor MAS rotor. The final samples contained ~60% H_2O and had a lipid:AFA-PLN ratio of 80:1. For paramagnetic quenching experiments, gadopentetate dimeglumine (Gd^{3+}) (Magnevist;

Bayer Shering Pharma, Berlin, Germany) was added to the MAS sample and several freeze/thaw cycles were performed (final Gd^{3+} concentration was 20 mM).

5.2.2 NMR experiments

All NMR experiments were performed on a Varian (VNMRS) spectrometer operating at a proton frequency of 600 MHz. Solution NMR chemical shifts of AFA-PLN in isotropic bicelles were assigned using two-dimensional HNCO, HN(CO)Cα, and HNCαCβ experiments and were referenced to 2,2-dimethyl-2-silapentane-5-sulfonate (DSS). Chemical shifts in MLVs were assigned using single quantum double quantum correlation (SQ-DQ), dipolar assisted rotational resonance (DARR) (37), and refocused Insensitive Nuclei Enhanced by Polarization Transfer (38) (rINEPT) experiments acquired using a $^{1}H/^{13}C$ 3.2 mm BioMAS Varian probe. Pulse widths corresponding to a flip angle of $\pi/2$ were typically 5.5 μs (^{13}C, ^{15}N) and 2.5 μs (^{1}H). Proton TPPM decoupling (39) was applied at $\omega_{RF}/(2\pi)$ = 100 kHz. SQ-DQ experiments were acquired at a spinning rate of 8 kHz, a cross-polarization (CP) time of 1 ms and spectral widths of 100 and 16 kHz in the single and double quantum dimensions, respectively. A 500 μs SPC5 element (40) was used for excitation and reconversion. DARR experiments were acquired with a 200 ms mixing time at a spinning speed of 13.3 kHz and a 1 ms cross-polarization (CP) time. 4000 points with a spectral width of 100 kHz and 30 increments with a spectral width of 13.3 kHz were acquired in the direct and indirect ^{13}C dimensions, respectively. rINEPT experiments were acquired at the same spinning rate with the same number of points and spectral width in the direct ^{13}C dimension and 30 increments with a spectral width of 3.33 kHz in the indirect ^{1}H dimension. Chemical shifts were referenced to the CH_2 signal of adamantane (40.48 ppm). Data were processed by NMRPipe (41) and analyzed with Sparky (42).

5.3 Results

5.3.1 Residue-Specific Assignments in Lipid Bilayers

Due to the lack of residue-specific resolution in [U-^{13}C, ^{15}N] MAS spectra, we opted to assign chemical shifts of AFA-PLN from synthetically labeled AFA-PLN reconstituted into egg PC/PE/PA 8/1/1 MLVs (labeling is shown in **Table 1**). Combined with a [QNE-^{13}C, ^{15}N, A-^{13}C]-labeled sample, this allowed for unambiguous backbone

and side chain chemical shifts for domain Ib and II from single-quantum double-quantum (SQ-DQ) correlation spectra (**Figure 2A**). Isotropic backbone and side chain chemical shifts of AFA-PLN were previously reported using solution NMR in DPC micelles (16, 24), which allows for a direct comparison between membrane mimicking systems on AFA-PLN's structure. Importantly, the hydrophobic domain II chemical shifts were markedly similar between micelles and bilayers (**Figure 2B,C**). Given the sensitivity of backbone chemical shifts to secondary structure, this confirms that the structure of domain II is helical in both DPC micelles and lipid bilayers. The ^{13}C chemical shift index (CSI) $(\delta_{C\alpha} - \delta_{C\beta}) - (\delta_{C\alpha,RC} - \delta_{C\beta,RC})$ (43) of domain Ib in lipid bilayers indicates a greater extent of helicity than we observed in DPC micelles. Based on CSI values, we estimated that ~50% was helical in micelles, based on a helicity of ~100% in lipid bilayers. This has important ramifications for SERCA inhibition, since we have previously shown that the hydrophilic domain Ib of AFA-PLN is in equilibrium between folded (helical) and unfolded states (25, 26), which plays a role in inhibiting the ATPase. This difference may be due to the shorter chain length of the micelles (C12 for DPC) compared to the lipids (~C18 for egg lipids) or the intrinsic curvature and more dynamic nature of the micelles.

5.3.2 Domain Ia Conformation in Neutral and Negatively Charged Isotropic Bicelles

In analogy to the classic model of amphipathic helix folding (44, 45), we recently found that domain Ia of AFA-PLN exists in equilibrium between at least four conformational states (26). In micelles, these states are in fast exchange on the NMR timescale with the most populated state possessing helical structure with the hydrophobic face of the helix inserted into the micelle. In contrast, Baldus and co-workers (46) studied AFA-PLN in DMPC vesicles using MAS solid-state NMR and concluded domain Ia was unfolded and membrane detached based on the random coil chemical shifts.

To probe the structure of domain Ia in lipids we reconstituted [U-^{13}C,^{15}N] labeled AFA-PLN into isotropic DMPC/DHPC bicelles with a DMPC:DHPC ratio of 1:3 (q=0.33). The [^{1}H,^{15}N] HSQC spectrum (**Figure 3A**) showed only ~40% of the resonances that were observed in DPC micelles. These resonances were assigned using HN(CO)Cα and HNCαCβ solution NMR experiments, and were confirmed to be residues from domain Ia

and the loop. This suggested that domain Ia was significantly more dynamic than domain Ib or II, and did not assume the overall rotational correlation time of the bicelle. The failure to observe resonances from transmembrane domains in isotropic bicelles has been documented in other membrane protein systems such as those from the small multidrug resistance family, which required high temperatures and deuteration to observe backbone amide signals (47).

In **Figure 3B**, we plot the ^{13}C CSI ($\delta_{C\alpha}$ - $\delta_{C\beta}$) for full-length AFA-PLN obtained in isotropic bicelles and DPC micelles and the values obtained from a cytoplasmic domain peptide (PLN_{1-20}) (48) . The chemical shifts in isotropic bicelles are intermediate between shifts in DPC micelles (AFA-PLN_{DPC}, helical and mostly T state) and the shifts for a peptide corresponding to residues 1-20 of PLN (PLN_{1-20}, unfolded and mostly R state). Thus, in isotropic bicelles the conformational equilibrium is shifted to a more unfolded state than in DPC micelles, but still retains helical character, which is in contrast to the previous results in DMPC bilayers.

Domain Ia has four Arg and Lys residues (K3, R9, R13, R14), which gives PLN a positive charge at physiological pH values. Therefore, the introduction of a negatively charged lipid could potentially increase the association of domain Ia with the bilayer. To test this hypothesis we replaced 33% of the DMPC with DMPG and measured methyl group chemical shifts, since these are the best reporters of the association of domain Ia with lipids (26). **Figure 4** shows spectra for V4, L7, A11, and A15 methyl groups obtained in DPC, DMPC/DHPC, DMPC/DMPG/DHPC, and aqueous PLN_{1-20}. The resonances corresponding to PG-containing bicelles shift toward the AFA-PLN_{DPC} peak, while all peaks are on a linear trajectory spanning from PLN_{1-20} to AFA-PLN_{DPC}. This shows that a) domain Ia is in a fast, apparent two-site exchange between lipid-associated and lipid-dissociated conformations, and b) negatively charged bilayers perturb the conformational equilibrium to favor the membrane-associated conformation. While methyl group chemical shifts are sensitive probes of local environment (i.e., membrane attached or detached) they are less sensitive to secondary structure content. To determine whether the increased affinity of domain Ia for negatively charged lipids was associated with increased helicity, we also measured backbone carbonyl ($^{13}C'$) chemical shifts in isotropic bicelles using an HNCO experiment and compared CSI

values (43) to AFA-PLN_{DPC} (**Figure 4E**). The CSI values in the presence of PG clearly showed a small but significant increase in the helicity of domain Ia. Thus, the presence of negatively charged lipids increased the population of the T state, and also support the unfolding/folding conformational model by which domain Ia exchanges between a helical and membrane embedded conformation and one that is unfolded and detached from the surface.

5.3.3 MAS in DMPC Lipids

To validate our results in detergent micelles and isotropic bicelles, we also used MAS experiments with AFA-PLN reconstituted into MLVs. It is well-known that INEPT based transfers filter out immobile domains due to short transverse relaxation times (46). Using refocused INEPT and CP-based experiments of [U-^{13}C,^{15}N] AFA-PLN we detected chemical shifts of AFA-PLN at 30°C in DMPC vesicles that were in excellent agreement with previously published results in the same lipid bilayers and temperature (46). However, due to the abundance of transmembrane domain residues (~60% of the protein), CP-based spectra were significantly overlapped, which necessitated the use of selectively labeled samples in domain Ia. We synthesized AFA-PLN with Val4, Leu7, Ala11, Ile12, Ala15 and Ile18 [U-^{13}C,^{15}N] labeled (AFA-PLN_{6cyt}) and acquired 2D DARR spectra at 30°C. From these experiments we were able to detect intense peaks that corresponded to these six labels. Some of the observed chemical shifts were identical to the random coil values measured from refocused INEPT experiments (**Figure 5**). However, we also detected several peaks in the DARR spectrum that were absent from the rINEPT experiment. Specifically, we detected a second population of peaks that had ^{13}C chemical shifts consistent with helical structure. Interestingly, in contrast to DPC micelles and isotropic bicelles the two states observed in the DARR experiments were in slow exchange on the NMR time scale (two peaks are observed in the spectrum).

5.3.4 Effect of Temperature on the Conformational Equilibria of Domain Ia

To determine the effect of temperature on the conformational equilibrium of AFA-PLN we acquired an additional DARR experiment at -25°C. At this temperature the helical chemical shifts dominated the spectrum showing that the conformational equilibrium has shifted to favor the T state. With the exception of Ala15 at the C-terminal end of the domain Ia helix, there is excellent agreement between the T state chemical

shifts and the shifts of AFA-PLN_{DPC} (**Figure 6**). This shows that the domain Ia helix (T state) may be slightly shorter in lipid bilayers than in DPC micelles. Importantly, this also implies that AFA-PLN samples similar conformational space regardless of the membrane mimicking system (detergent micelle, isotropic bicelle, lipid bilayer, *etc*), but that the populations of the conformational states are very sensitive to the choice of membrane mimic.

It is important to note that solution NMR data in DPC micelles show at least four resolved conformational states (T, T', R, and R'). However, it is possible that the T' and R' states have chemical shifts very similar to the T and R states and, therefore, are indistinguishable in the MAS spectra (i.e., broader lines than the detergent micelle spectra). Alternatively, the T' and R' states may be scarcely populated in lipids and therefore not detectable.

5.3.5 MAS in Native SR Lipids

While DMPC vesicles are a well-characterized model membrane system, they lack several characteristics of a native lipid bilayer of the SR. For example, the SR membrane, where PLN is embedded, contains a significant portion of PE and PS head groups and has an average lipid chain length of 18 carbons compared to the 14 carbons of DMPC (32). To support our conclusions in synthetic lipid membranes, we reconstituted AFA-PLN_{6cyt} into lipids extracted from the SR of rabbit skeletal muscle. In these lipids, DARR spectra acquired at -25°C and 20°C were in good agreement with spectra obtained using DMPC lipids (**Figure 7**). Spectra acquired at -25°C and 20°C show multiple peaks with a shift in equilibrium toward the T state component at the lower temperature. Taken together, these data confirmed that the conformational equilibrium of AFA-PLN is also present in native lipids.

5.3.6 Solvent accessibility of T and R states

To further support our assignment of two populations (T and R states), we used paramagnetic relaxation enhancement (PRE) by acquiring DARR experiments in SR lipids in the presence and absence of 20 mM water-soluble Gd^{3+}. These experiments were performed at 4°C to have approximately equal intensities of R and T state peaks. **Figure 8** shows that the R state (36% signal retained on average) is quenched more

than the T state (63% signal retained on average) for residues Val4, Leu7, Ala11, and Ile12. Ala15 and Ile18 were excluded from the analysis since they have similar chemical shifts in the T and R states. These results confirmed that the T state is membrane-associated and solvent-protected while the R state is exposed to solvent, and are thus in strong agreement with our conformational model of AFA-PLN(26).

5.4 Discussion

The secondary structure content of the transmembrane domain II of PLN is preserved in all membrane mimicking systems, spanning from organic solvents (49) and detergent micelles (24) to lipid bilayers of different compositions(15, 16). In particular, the chemical shifts obtained in DPC micelles and lipid bilayers are in remarkable agreement (**Figure 2**). This suggests that while detergent micelles have limitations, they can still offer structural insights on rigid, membrane-spanning portions of membrane proteins. On the other hand, DPC micelles altered the conformational equilibria for domains Ia and Ib of AFA-PLN that were more malleable and solvent exposed (21, 50). For instance, the chemical shifts for domain Ib in lipids have a greater extent of helicity than those obtained in DPC micelles, although in both membrane mimics the predominant conformation was helical. In contrast, the amphipathic domain Ia is significantly more helical in DPC micelles that in lipids, revealing an almost complete shift towards the T state in this detergent. The latter is in agreement with the topology of AFA-PLN determined in mechanically aligned DOPC/DOPE bilayers (16). Interestingly, in lipid vesicles and native SR lipids, the R and T states exchange on a slow time scale. Thus, the dynamic nature of the detergent and the isotropic bicelle may act to lower the activation energy barrier between the states, which would alter the exchange rates. The multiple populations observed in lipids allowed us to analyze the chemical shifts and exposure to water separately. Our PRE measurements show that the R state is unfolded and solvent-exposed, as proposed previously (26). Also, the excellent overlay between spectra acquired in SR lipids and DMPC suggests that the conformations of AFA-PLN are conserved between the different lipid systems.

It is important to stress that neither the unfolded R state nor the folded T state is analogous to the architecture of the pentameric PLN solved in DPC micelles with domain Ia in a helical, membrane-dissociated conformation (51). However, our data help explain

the results reported by Baldus and co-workers (46) from MAS experiments in DMPC lipid vesicles. Using INEPT-based transfer experiments, the flexible R state of AFA-PLN was detected, filtering out the resonances of the T state. We showed that by using both CP- and INEPT-based transfers it is possible to detect both conformational states of AFA-PLN (T and R states). One possibility why Baldus and co-workers did not observe the T state of domain Ia could be the low lipid/protein ratio, which would promote the R state, since a smaller amount of lipid surface area would be present. In addition to observing both T and R states, we also found the AFA-PLN conformational equilibrium to have strong temperature dependence, with the T state favored at lower temperature and the R state at higher temperature. This behavior is similar to that observed for the membrane-active peptide Tat, which is in a random coil conformation at high temperature but forms a β-sheet at lower temperatures (52). The dependence of AFA-PLN domain Ia on temperature as well as the choice of membrane mimic shows that caution must be taken when comparing experiments acquired at different temperatures and in different membrane-environments.

At temperatures above 20°C the R state dominates over the T state (**Figure 6**). In this regard domain Ia of PLN resembles an intrinsically disordered protein, which folds into a helix upon interaction with the lipid bilayer (53, 54). In addition to the bilayer interactions, PLN binds a number of different proteins. We have recently shown that protein kinase A (PKA) preferentially binds an extended conformation of domain Ia (48, 55). Thus, the malleability of PLN allows for recognition by different binding partners. Further research is needed to determine what conformation(s) of PLN is recognized by other proteins. Nevertheless, since promotion of the R state relieves the inhibitory effect of SERCA by PLN, perturbations that alter the T/R equilibrium directly affect the regulation of SERCA. One example of this is the introduction of negatively charged PG lipids, which promotes the T state conformation (**Figure 4**). This observation suggests that lipid-PLN interactions may regulate SERCA function.

In our first characterization of the calcium regulatory cycle, we defined PLN as an allosteric modulator of SERCA, without specifying its role in the *allosteric* phenomenon (19, 28, 29, 56). In the light of our recent results, we propose that the allosteric regulation of SERCA by PLN has two aspects: a) a more classical aspect (57-60),

where PLN controls SERCA function via intramembrane, long-range interactions, *i.e.,* without direct interference with the chemistry of the enzyme (hydrolysis of ATP) or calcium translocation, and b) a more modern aspect (59-63), with PLN interconverting between ground and excited states, with the latter representing the inactive conformational state. These phenomena are interconnected and constitute part of the complex mechanism for allosteric signal transduction in the heart muscle. Based on the data presented here, it is becoming clear that by fine-tuning PLN conformational equilibria, lipid membranes represent a third element for allosteric control of SERCA. Through the alteration of the lipid composition from diet or pathophysiology (64-66), it is possible that lipid membranes *shape* both the conformation and function of the SERCA/PLN complex, affecting muscle contractility.

From a more biophysical point of view, these studies revive an old concept of the allosteric regulation of lipid membranes (1). Furthermore, the possibility of using solid-state NMR to study membrane proteins under native lipid compositions allows for the characterization of lipid-protein interactions at the atomic level to reveal the role of lipids in activation and deactivation of protein function.

5.5 References

1. Farias, R. N., B. Bloj, R.D. Morero, F. Sineriz and R.E. Trucco 1975. Regulation of allosteric membrane-bound enzymes through changes in membrane lipid compostition. Biochim. Biophys. Acta. 415, 231-251.
2. McDermott, A. and T. Polenova 2007. Solid state NMR: New tools for insight into enzyme function. Curr. Opin. Struct. Biol. 17, 617-622.
3. Lange, V., J. Becker-Baldus, B. Kunert, B.J. van Rossum, F. Casagrande, A. Engel, Y. Roske, F.M. Scheffel, E. Schneider and H. Oschkinat 2010. A MAS NMR study of the bacterial ABC transporter ArtMP. Chembiochem. 11, 547-555.
4. Tang, M., L.J. Sperling, D.A. Berthold, A.E. Nesbitt, R.B. Gennis and C.M. Rienstra 2011. Solid-state NMR study of the charge-transfer complex between ubiquinone-8 and disulfide bond generating membrane protein DsbB. J. Am. Chem. Soc. 133, 4359-4366.
5. Cady, S. D., K. Schmidt-Rohr, J. Wang, C.S. Soto, W.F. Degrado and M. Hong 2010. Structure of the amantadine binding site of influenza M2 proton channels in lipid bilayers. Nature. 463, 689-692.

6. Shi, L., I. Kawamura, K.H. Jung, L.S. Brown and V. Ladizhansky 2011. Conformation of a seven-helical transmembrane photosensor in the lipid environment. Angew. Chem. Int. Ed Engl. 50, 1302-1305.

7. Mills, F. D., V.C. Antharam, O.K. Ganesh, D.W. Elliott, S.A. McNeill and J.R. Long 2008. The helical structure of surfactant peptide KL4 when bound to POPC: POPG lipid vesicles. Biochemistry. 47, 8292-8300.

8. Linser, R., M. Dasari, M. Hiller, V. Higman, U. Fink, J.M. Lopez Del Amo, S. Markovic, L. Handel, B. Kessler, P. Schmieder, D. Oesterhelt, H. Oschkinat and B. Reif 2011. Proton-detected solid-state NMR spectroscopy of fibrillar and membrane proteins. Angew. Chem. Int. Ed Engl. 50, 4508-4512.

9. Qiang, W., Y. Sun and D.P. Weliky 2009. A strong correlation between fusogenicity and membrane insertion depth of the HIV fusion peptide. Proc. Natl. Acad. Sci. U. S. A. 106, 15314-15319.

10. Saito, H. and A. Naito 2007. NMR studies on fully hydrated membrane proteins, with emphasis on bacteriorhodopsin as a typical and prototype membrane protein. Biochim. Biophys. Acta. 1768, 3145-3161.

11. Bajaj, V. S., M.L. Mak-Jurkauskas, M. Belenky, J. Herzfeld and R.G. Griffin 2009. Functional and shunt states of bacteriorhodopsin resolved by 250 GHz dynamic nuclear polarization-enhanced solid-state NMR. Proc. Natl. Acad. Sci. U. S. A. 106, 9244-9249.

12. de Planque, M. R., D.T. Rijkers, J.I. Fletcher, R.M. Liskamp and F. Separovic 2004. The alphaM1 segment of the nicotinic acetylcholine receptor exhibits conformational flexibility in a membrane environment. Biochim. Biophys. Acta. 1665, 40-47.

13. De Angelis, A. A., D.H. Jones, C.V. Grant, S.H. Park, M.F. Mesleh and S.J. Opella 2005. NMR experiments on aligned samples of membrane proteins. Methods Enzymol. 394, 350-82.

14. Sharma, M., M. Yi, H. Dong, H. Qin, E. Peterson, D.D. Busath, H.X. Zhou and T.A. Cross 2010. Insight into the mechanism of the influenza A proton channel from a structure in a lipid bilayer. Science. 330, 509-512.

15. Verardi, R., L. Shi, N.J. Traaseth, N. Walsh and G. Veglia 2011. Structural topology of phospholamban pentamer in lipid bilayers by a hybrid solution and solid-state NMR method. Proc Natl Acad Sci U S A. 108, 9101-9106.

16. Traaseth, N. J., L. Shi, R. Verardi, D.G. Mullen, G. Barany and G. Veglia 2009. Structure and topology of monomeric phospholamban in lipid membranes determined by a hybrid solution and solid-state NMR approach. Proc. Natl. Acad. Sci. U. S. A. 106, 10165-10170.

17. Buffy, J. J., N.J. Traaseth, A. Mascioni, P.L. Gor'kov, E.Y. Chekmenev, W.W. Brey and G. Veglia 2006. Two-dimensional solid-state NMR reveals two topologies of sarcolipin in oriented lipid bilayers. Biochemistry. 45, 10939-10946.

18. Traaseth, N. J., J.J. Buffy, J. Zamoon and G. Veglia 2006. Structural dynamics and topology of phospholamban in oriented lipid bilayers using multidimensional solid-state NMR. Biochemistry. 45, 13827-13834.

19. Traaseth, N. J., K.N. Ha, R. Verardi, L. Shi, J.J. Buffy, L.R. Masterson and G. Veglia 2008. Structural and dynamic basis of phospholamban and sarcolipin inhibition of ca(2+)-ATPase. Biochemistry. 47, 3-13.

20. MacLennan, D. H. and E.G. Kranias 2003. Phospholamban: A crucial regulator of cardiac contractility. Nat Rev Mol Cell Biol. 4, 566-77.

21. Metcalfe, E. E., J. Zamoon, D.D. Thomas and G. Veglia 2004. (1)H/(15)N heteronuclear NMR spectroscopy shows four dynamic domains for phospholamban reconstituted in dodecylphosphocholine micelles. Biophys. J. 87, 1205-1214.

22. Karim, C. B., T.L. Kirby, Z. Zhang, Y. Nesmelov and D.D. Thomas 2004. Phospholamban structural dynamics in lipid bilayers probed by a spin label rigidly coupled to the peptide backbone. Proc Natl Acad Sci U S A. 101, 14437-42.

23. Abu-Baker, S., J.X. Lu, S. Chu, C.C. Brinn, C.A. Makaroff and G.A. Lorigan 2007. Side chain and backbone dynamics of phospholamban in phospholipid bilayers utilizing (2)h and (15)n solid-state NMR spectroscopy. Biochemistry. 46, 11695-11706.

24. Zamoon, J., A. Mascioni, D.D. Thomas and G. Veglia 2003. NMR solution structure and topological orientation of monomeric phospholamban in dodecylphosphocholine micelles. Biophys. J. 85, 2589-2598.

25. Traaseth, N. J. and G. Veglia 2010. Probing excited states and activation energy for the integral membrane protein phospholamban by NMR CPMG relaxation dispersion experiments. Biochim. Biophys. Acta. 1798, 77-81.

26. Gustavsson, M., N.J. Traaseth, C.B. Karim, E.L. Lockamy, D.D. Thomas and G. Veglia 2011. Lipid-mediated Folding/Unfolding of phospholamban as a regulatory mechanism for the sarcoplasmic reticulum ca(2+)-ATPase. J. Mol. Biol. 408, 755-765.

27. Karim, C. B., Z. Zhang, E.C. Howard, K.D. Torgersen and D.D. Thomas 2006. Phosphorylation-dependent conformational switch in spin-labeled phospholamban bound to SERCA. J. Mol. Biol. 358, 1032-1040.

28. Zamoon, J., F. Nitu, C. Karim, D.D. Thomas and G. Veglia 2005. Mapping the interaction surface of a membrane protein: Unveiling the conformational switch of phospholamban in calcium pump regulation. Proc. Natl. Acad. Sci. U. S. A. 102, 4747-4752.

29. Ha, K. N., N.J. Traaseth, R. Verardi, J. Zamoon, A. Cembran, C.B. Karim, D.D. Thomas and G. Veglia 2007. Controlling the inhibition of the sarcoplasmic Ca2+-ATPase by tuning phospholamban structural dynamics. J. Biol. Chem. 282, 37205-37214.

30. Kaye, D. M., M. Hoshijima and K.R. Chien 2008. Reversing advanced heart failure by targeting Ca2+ cycling. Annu. Rev. Med. 59, 13-28.

31. del Monte, F., S.E. Harding, G.W. Dec, J.K. Gwathmey and R.J. Hajjar 2002. Targeting phospholamban by gene transfer in human heart failure. Circulation. 105, 904-907.

32. Bick, R. J., L.M. Buja, W.B. Van Winkle and G.E. Taffet 1998. Membrane asymmetry in isolated canine cardiac sarcoplasmic reticulum: Comparison with skeletal muscle sarcoplasmic reticulum. J. Membr. Biol. 164, 169-175.

33. Karim, C. B., C.G. Marquardt, J.D. Stamm, G. Barany and D.D. Thomas 2000. Synthetic null-cysteine phospholamban analogue and the corresponding transmembrane domain inhibit the ca-ATPase. Biochemistry. 39, 10892-7.

34. Buck, B., J. Zamoon, T.L. Kirby, T.M. DeSilva, C. Karim, D. Thomas and G. Veglia 2003. Overexpression, purification, and characterization of recombinant ca-ATPase regulators for high-resolution solution and solid-state NMR studies. Protein Expr Purif. 30, 253-61.

35. Tong, K. I., M. Yamamoto and T. Tanaka 2008. A simple method for amino acid selective isotope labeling of recombinant proteins in E. coli. J Biomol NMR. 42, 59-67.

36. Reddy, L. G., R.L. Cornea, D.L. Winters, E. McKenna and D.D. Thomas 2003. Defining the molecular components of calcium transport regulation in a reconstituted membrane system. Biochemistry. 42, 4585-92.

37. Takegoshi, K., S. Nakamura and T. Terao 2001. 13C–1H dipolar-assisted rotational resonance in magic-angle spinning NMR. Chem. Phys. Lett. 344, 631.

38. Morris, G. A. and R.J. Freeman 1979. Enhancement of nuclear magnetic resonance signals by polarization transfer. J. Am. Chem. Soc. 101, 760-762.

39. Bennett, A. E., C.M. Rienstra, M. Auger, K.V. Lakshmi and R.G. Griffin 1995. Heteronuclear decoupling in rotating solids. J Chem Phys. 103, 6951-8.

40. Hohwy, M., C.M. Rienstra, C.P. Jaroniec and R.G. Griffin 1999. Fivefold symmetric homonuclear dipolar recoupling in rotating solids: Application to double quantum spectroscopy. J Chem Phys. 110, 7983-7992.

41. Delaglio, F., S. Grzesiek, G.W. Vuister, G. Zhu, J. Pfeifer and A. Bax 1995. NMRPipe: A multidimensional spectral processing system based on UNIX pipes. J. Biomol. NMR. 6, 277-293.

42. Goddard, T. D. and D.G. Kneller SPARKY 3. University of California, San Francisco.

43. Zhang, H., S. Neal and D.S. Wishart 2003. RefDB: A database of uniformly referenced protein chemical shifts. J. Biomol. NMR. 25, 173-195.

44. White, S. H. and W.C. Wimley 1999. Membrane protein folding and stability : Physical principles. Annual Review Biophysics Biomolecular Structures. 28, 319-365.

45. Engelman, D. M., Y. Chen, C.N. Chin, A.R. Curran, A.M. Dixon, A.D. Dupuy, A.S. Lee, U. Lehnert, E.E. Matthews, Y.K. Reshetnyak, A. Senes and J.L. Popot 2003. Membrane protein folding: Beyond the two stage model. FEBS Lett. 555, 122-125.

46. Andronesi, O. C., S. Becker, K. Seidel, H. Heise, H.S. Young and M. Baldus 2005. Determination of membrane protein structure and dynamics by magic-angle-spinning solid-state NMR spectroscopy. J. Am. Chem. Soc. 127, 12965-12974.

47. Poget, S. F., S.M. Cahill and M.E. Girvin 2007. Isotropic bicelles stabilize the functional form of a small multidrug-resistance pump for NMR structural studies. J. Am. Chem. Soc. 129, 2432-2433.

48. Masterson, L. R., T. Yu, L. Shi, Y. Wang, M. Gustavsson, M.M. Mueller and G. Veglia 2011. cAMP-dependent protein kinase A selects the excited state of the membrane substrate phospholamban. J. Mol. Biol. 412, 155-164.

49. Lamberth, S., H. Schmid, M. Muenchbach, T. Vorherr, J. Krebs, E. Carafoli and C. Griesinger 2000. NMR solution structure of phospholamban. Helvetica Chimica Acta. 83, 2141-2151.

50. Traaseth, N. J. and G. Veglia 2009. Probing excited states and activation energy for the integral membrane protein phospholamban by NMR CPMG relaxation dispersion experiments. Biochim. Biophys. Acta.

51. Oxenoid, K. and J.J. Chou 2005. The structure of phospholamban pentamer reveals a channel-like architecture in membranes. Proc. Natl. Acad. Sci. U. S. A. 102, 10870-10875.

52. Su, Y., A.J. Waring, P. Ruchala and M. Hong 2010. Membrane-bound dynamic structure of an arginine-rich cell-penetrating peptide, the protein transduction domain of HIV TAT, from solid-state NMR. Biochemistry. 49, 6009-6020.

53. Mittag, T., L.E. Kay and J.D. Forman-Kay 2010. Protein dynamics and conformational disorder in molecular recognition. J. Mol. Recognit. 23, 105-116.

54. Wright, P. E. and H.J. Dyson 2009. Linking folding and binding. Curr. Opin. Struct. Biol. 19, 31-38.

55. Masterson, L. R., C. Cheng, T. Yu, M. Tonelli, A.P. Kornev, S.S. Taylor and G. Veglia 2010. Dynamics connect substrate recognition to catalysis in protein kinase A. Nat Chem Biol. 6, 821-828.

56. Traaseth, N. J., D.D. Thomas and G. Veglia 2006. Effects of Ser16 phosphorylation on the allosteric transitions of phospholamban/Ca(2+)-ATPase complex. J. Mol. Biol. 358, 1041-1050.

57. Monod, J., J. Wyman and J.P. Changeux 1965. On the nature of allosteric transitions: A plausible model. J Mol Biol. 12, 88-118.

58. Koshland, D. E.,Jr, G. Nemethy and D. Filmer 1966. Comparison of experimental binding data and theoretical models in proteins containing subunits. Biochemistry. 5, 365-385.

59. Tsai, C. J., A. Del Sol and R. Nussinov 2009. Protein allostery, signal transmission and dynamics: A classification scheme of allosteric mechanisms. Mol. Biosyst. 5, 207-216.

60. Cui, Q. and M. Karplus 2008. Allostery and cooperativity revisited. Protein Sci. 17, 1295-1307.

61. Smock, R. G. and L.M. Gierasch 2009. Sending signals dynamically. Science. 324, 198-203.

62. Ma, B. and R. Nussinov 2010. Enzyme dynamics point to stepwise conformational selection in catalysis. Curr. Opin. Chem. Biol. 14, 652-659.

63. Tzeng, S. R. and C.G. Kalodimos 2009. Dynamic activation of an allosteric regulatory protein. Nature. 462, 368-372.

64. Taffet, G. E., T.T. Pham, D.L. Bick, M.L. Entman, H.J. Pownall and R.J. Bick 1993. The calcium uptake of the rat heart sarcoplasmic reticulum is altered by dietary lipid. J. Membr. Biol. 131, 35-42.

65. Mrak, R. E. and S. Fleischer 1982. Lipid composition of sarcoplasmic reticulum from mice with muscular dystrophy. Muscle Nerve. 5, 439-446.

66. Krainev, A. G., D.A. Ferrington, T.D. Williams, T.C. Squier and D.J. Bigelow 1995. Adaptive changes in lipid composition of skeletal sarcoplasmic reticulum membranes associated with aging. Biochim. Biophys. Acta. 1235, 406-418.

Table 1. Synthetically labeled AFA-PLN samples

Sample	[^{13}C,^{15}N] Residues
1	V4, L7, A11, I12, A15, I18
2	N30, L31, F32, I33
3	N34, F35, A36, L37, I38
4	L39, I40, F41, L42
5	L44, I45, A46, I47
6	A24, I48, V49, L51

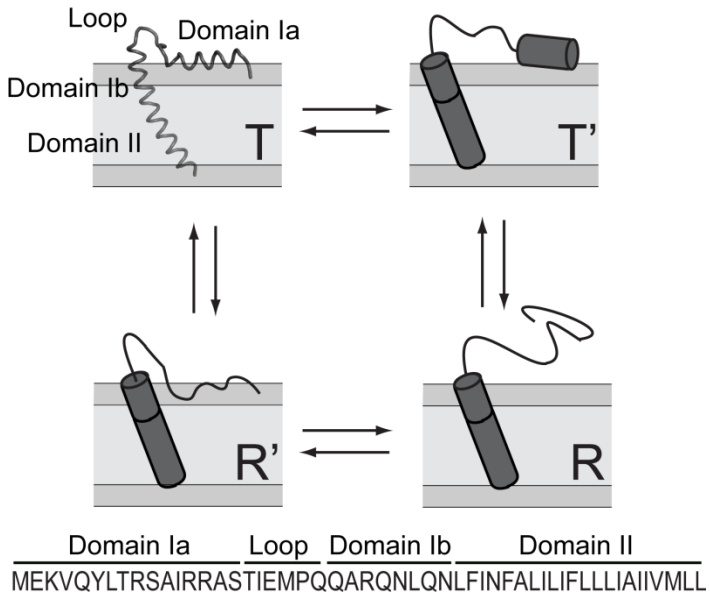

Figure 1. Conformational equilibria and primary sequence. *A.) Conformational equilibria of monomeric PLN. The T state is represented by its high resolution structure (PDB ID: 1N7L)* (16)*. B.) Primary sequence of AFA-PLN.*

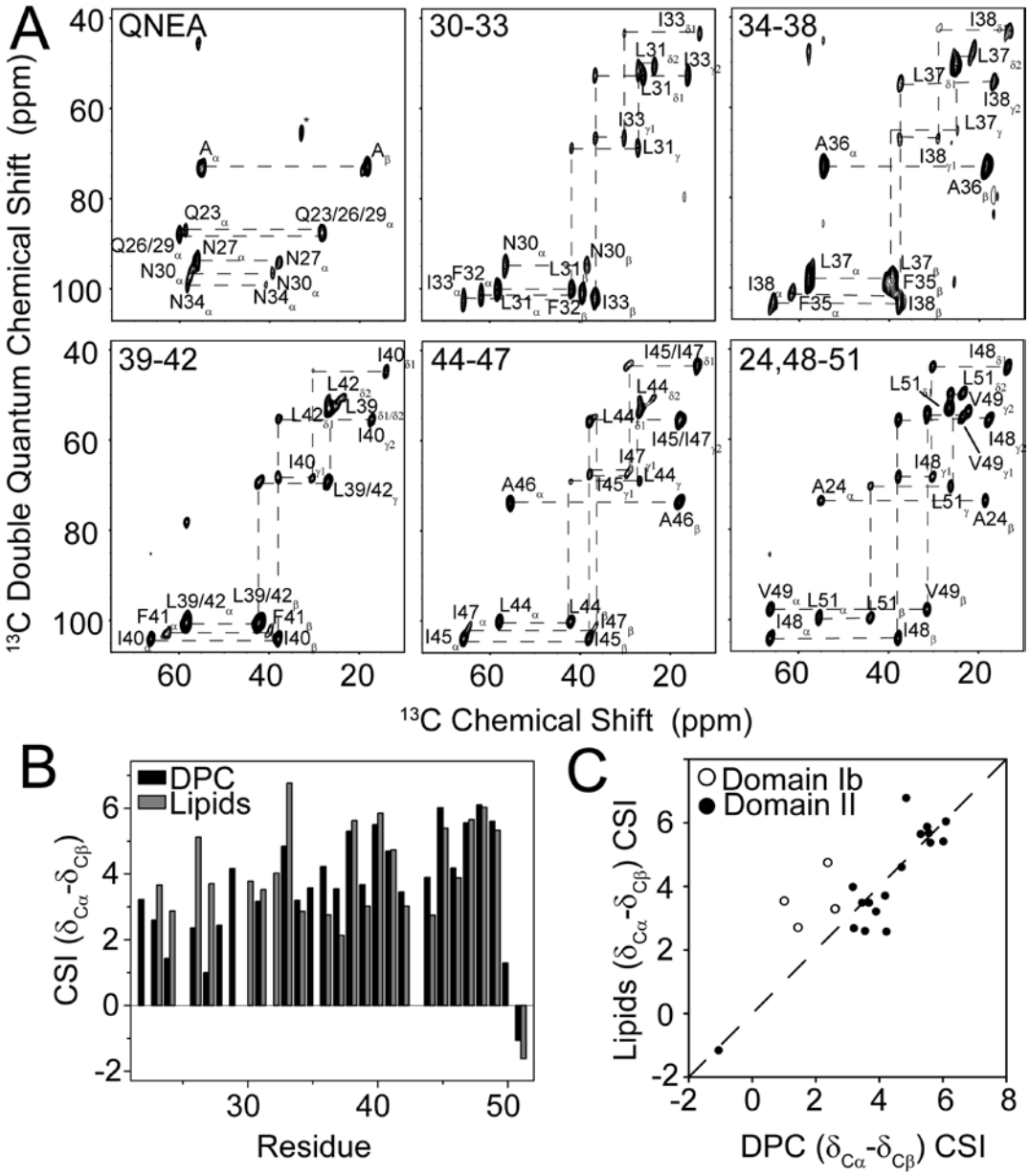

Figure 2. Assignment of domain Ib and II in lipids and comparison with DPC micelles. A.) SQ-DQ correlation experiments of AFA-PLN reconstituted into egg PC/PE/PA 8/1/1. B.) 13Cα-13Cβ CSI for residues in domain Ib and II of AFA-PLN in DPC micelles and EY lipids. CSI was calculated as δ13Cα – δ13Cβ – ($\delta^{13}C_{\alpha,RC}$ – $\delta^{13}C_{\beta,RC}$), where RC stands for the random coil chemical shifts (43). C.) Correlation between CSI values in DPC micelles and egg lipids. Residues in domain Ib are shown as open circles and residues in domain II as filled circles.

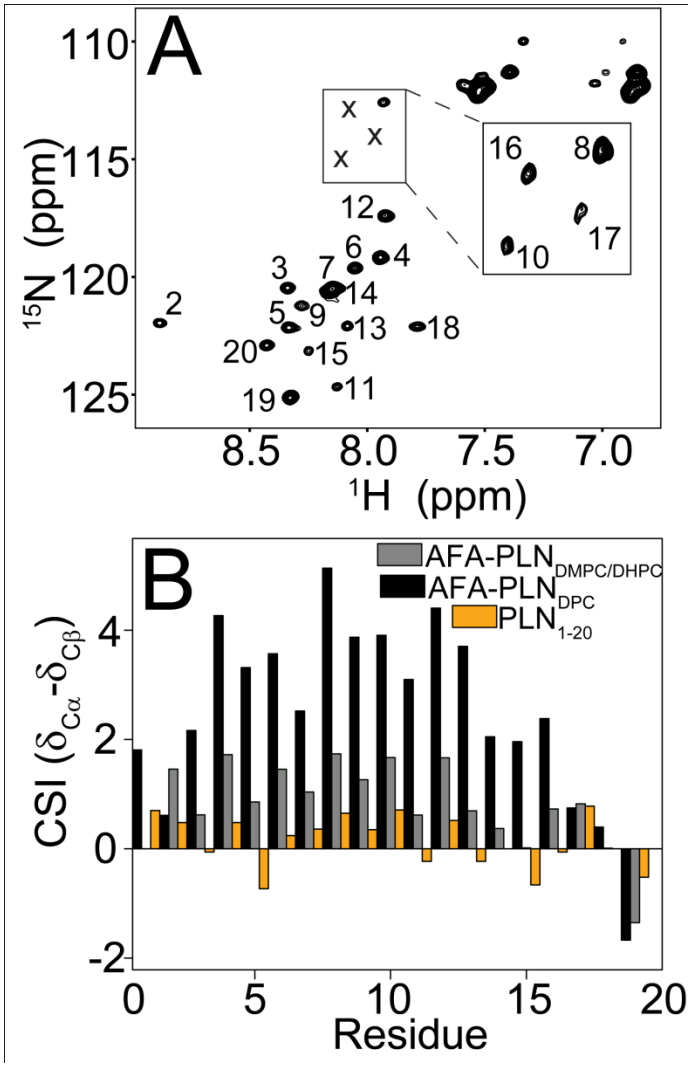

Figure 3. PLN in isotropic bicelles. *A.) [^{15}N]-HSQC of AFA-PLN in DMPC/DHPC isotropic bicelles with q=0.33. Peak corresponding to residues S10, S16 and T17 (marked with x) were detected at a lower noise level as shown in the inset. B.) Helicity of domain Ia in different membrane mimics. $^{13}C_{\alpha}$ – $^{13}C_{\beta}$ CSI for domain Ia of AFA-PLN in DPC micelles (black), DMPC/DHPC isotropic bicelles (red) and a peptide corresponding to residues 1-20 of PLN*(48) *(PLN$_{1-20}$, orange).*

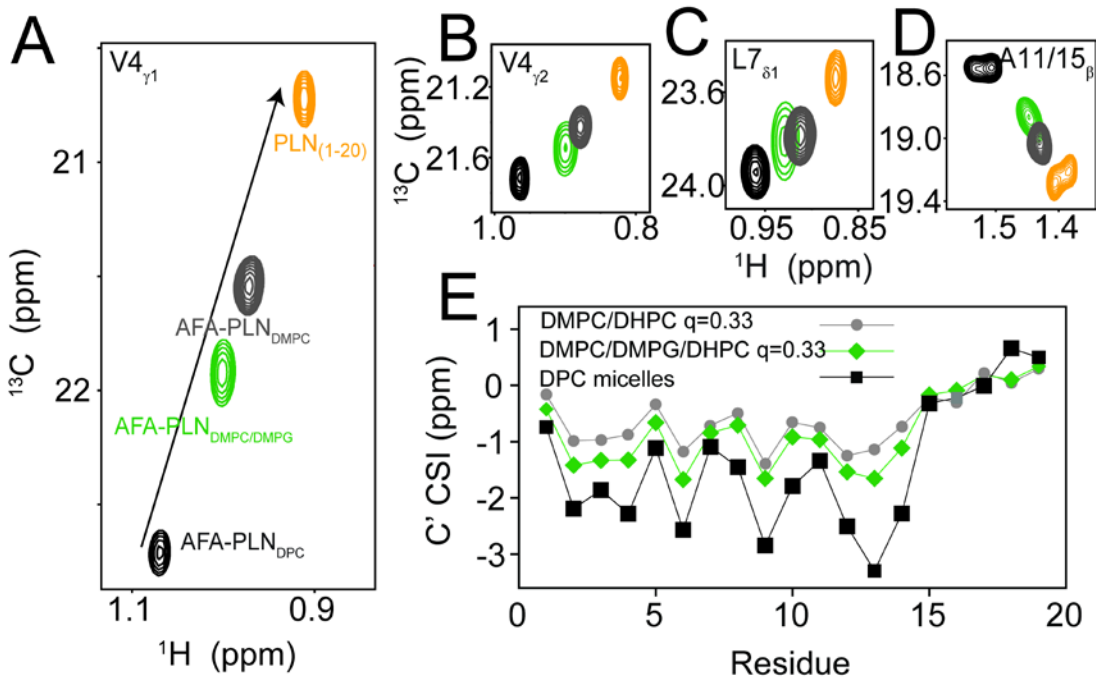

Figure 4. Negatively charged lipids shifts the equilibrium towards the T state. *A-D.) ^{13}C HSQC experiments of AFA-PLN in DPC micelles (black, T state), DMPC/DHPC, q=0.33, isotropic bicelles (grey) DMPC/DMPG/DHPC (4:1 DMPC:DMPG) isotropic bicelles (green) and PLN_{1-20} (orange, R state). E.) CO CSI for AFA-PLN in different membrane mimics.*

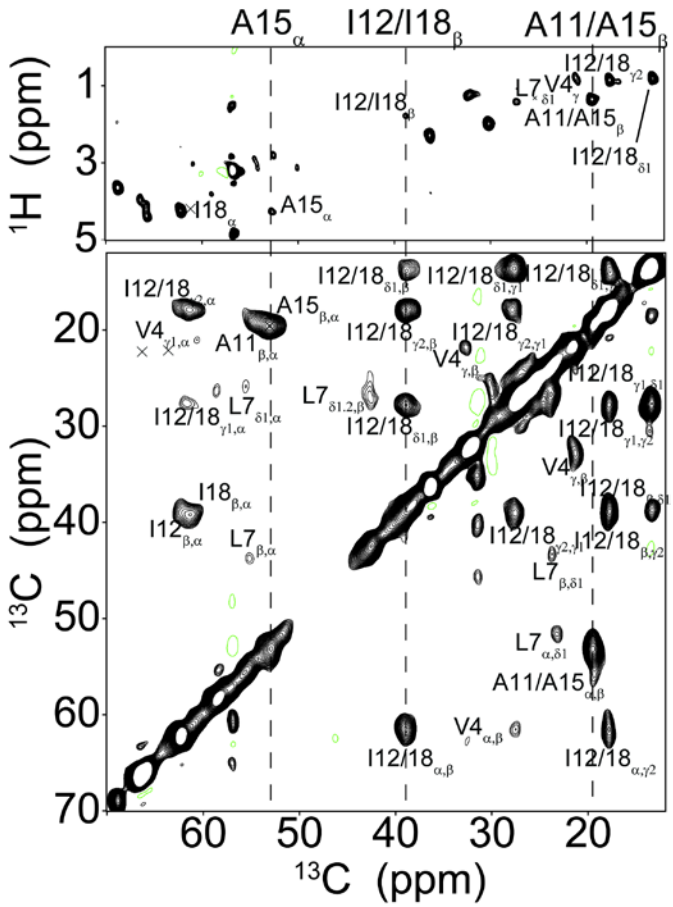

Figure 5. CP-transfers detect chemical shifts that are absent from INEPT-based experiments. *Comparison of rINEPT (top) and DARR (bottom, 200ms mixing time) experiments of AFA-PLN$_{6cyt}$ reconstituted into d$_{54}$-DMPC MLVs at 30°C. Dashed lines highlight examples of peaks that are detected in both experiments.*

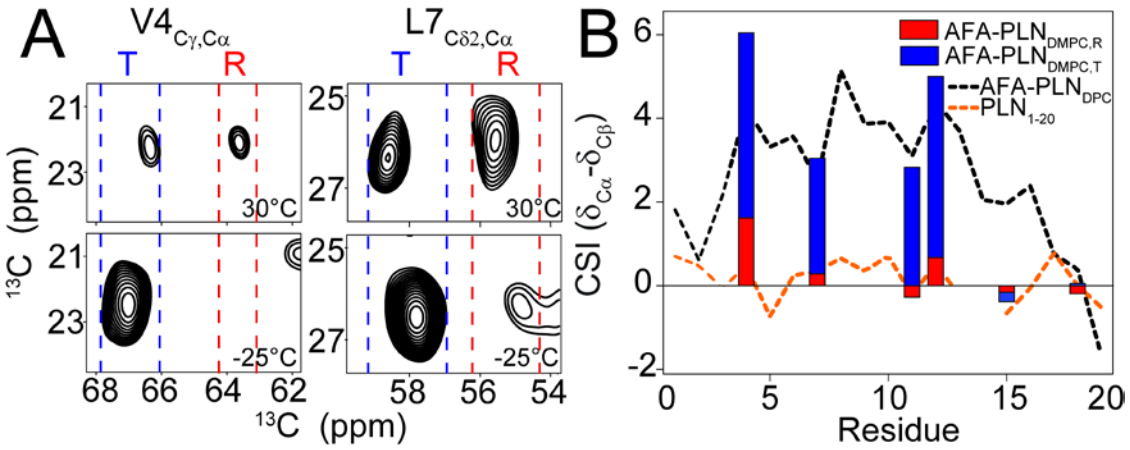

Figure 6. Conformational equilibrium of AFA-PLN in DMPC at different temperatures. *A.) Cross-peaks from DARR spectra corresponding to a C_α-C_γ correlation for Val4 (left) and C_α-$C_{\delta 2}$ correlation for Leu7 (right) at 30°C (top) and -25°C (bottom). Blue and red dashed lines highlight the chemical shift regions of the folded T state and unfolded R state respectively. B) $C\alpha$-$C\beta$ CSI of the folded T state (measured from experiments at -25°C, blue bars) and unfolded R state (measured from experiments at 30°C, red bars) compared to DPC micelles (black dotted lines, predominantly T state) and PLN_{1-20} (orange dotted line, predominantly R state).*

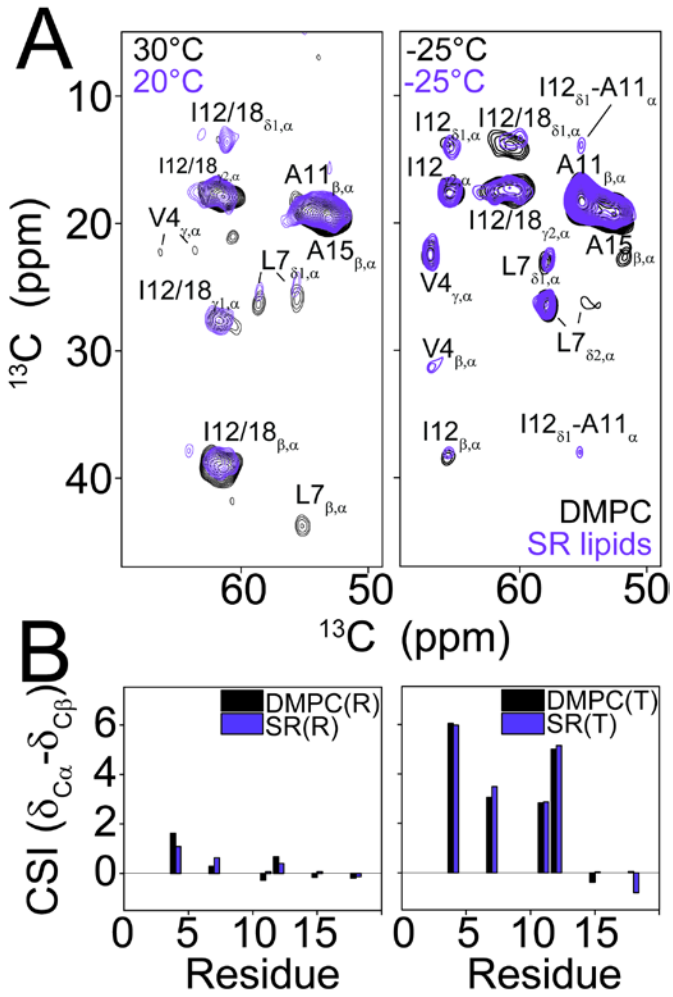

Figure 7. The conformational equilibrium of AFA-PLN is conserved in native SR lipids. *A.) Overlay of DARR experiments of AFA-PLN$_{6cyt}$ reconstituted into DMPC (black) or extracted SR lipids (purple). Experiments in SR lipids were acquired at -25°C and 20°C and experiments DMPC were acquired at -25°C and 30°C. All experiments utilized a 200ms mixing time. B.) $^{13}C_\alpha$ – $^{13}C_\beta$ CSI of the R and T state components in DMPC (black) and SR lipids (purple).*

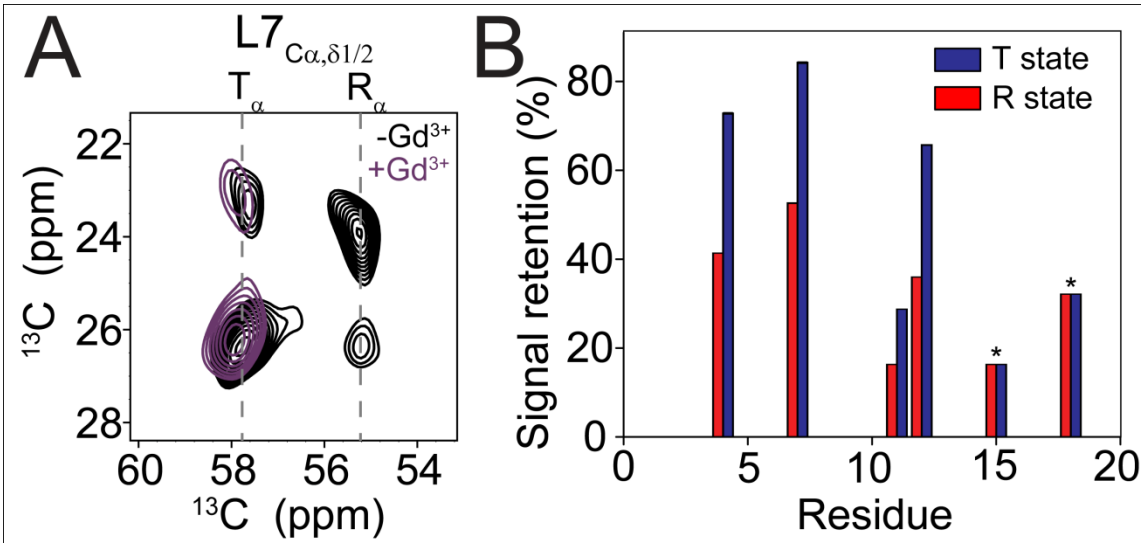

Figure 8. The T state is inserted into the lipid bilayer. *A.) Region from DARR spectra of AFA-PLN$_{6cyt}$ in SR lipids acquired in the presence (turquoise) and absence (black) of 20 mM Gd^{3+}. B.) Signal retention of peaks corresponding to the T and R states quantified from DARR spectra acquired in the presence and absence of 20 mM Gd^{3+}. Signal retention was calculated as I_{Gd3+}/I_0. in DARR spectra quenching of T and R states of AFA-PLN. For Ala15 and Ile18 the T and R state peaks are overlapped and therefore the signal retention reports on a combination of T and R states.*

Chapter 6 - Activating and Deactivating roles of lipid bilayers on the Ca^{2+}-ATPase/Phospholamban Complex

Reprinted with permission from:

Martin Gustavsson, Nathaniel J. Traaseth, and Gianluigi Veglia. Activating and Deactivating roles of lipid bilayers on The Ca^{2+}-ATPase/Phospholamban Complex *Biochemistry*. 2011;50(47):10367-74

The physicochemical properties of the lipid bilayer shape the structure and topology of membrane proteins and regulate their biological function. Here, we investigated the functional effects of various lipid bilayer compositions on the sarcoplasmic reticulum (SR) Ca^{2+}-ATPase (SERCA) in the presence and absence of its endogenous regulator, phospholamban (PLN). In the cardiac muscle, SERCA hydrolyzes one ATP molecule to translocate two Ca^{2+} ions into the SR membrane per enzymatic cycle. Unphosphorylated PLN reduces SERCA's affinity for Ca^{2+} and affects the enzymatic turnover. We varied bilayer thickness, head group, fluidity, and found that both the maximal velocity (V_{max}) of the enzyme and its apparent affinity for Ca2+ (KCa) are strongly affected. Our results show that a) SERCA Vmax has a biphasic dependence on bilayer thickness, reaching its maximum with 22-carbon lipid chain length, b) phosphatidylethanolamine (PE) and phosphatidylserine (PS) decrease KCa, and c) monounsaturated lipids afford higher SERCA Vmax and Ca2+-affinity than diunsaturated lipids. The presence of PLN removes the activating effect of PE and shifts SERCA's activity profile, with a maximal activity reached in bilayers with 20-carbon lipid chain length. Our results in synthetic lipid systems compare well with those carried out in native SR lipids. Importantly, we found that specific membrane compositions closely reproduce PLN effects (V_{max} and K_{Ca}) found in living cells, reconciling an ongoing controversy regarding the regulatory role of PLN on SERCA function. Taken with the physiological changes occurring in the SR membrane composition, these studies underscore a possible allosteric role of the lipid bilayers on the SERCA/PLN complex.

6.1 Introduction

Sarcoplasmic reticulum (SR) Ca^{2+}-ATPase (SERCA) is a multi-domain membrane-spanning enzyme that regulates muscle relaxation by Ca^{2+} translocation from the cytosol into the SR lumen (1, 2). SERCA is a P-type ATPase and transports two Ca^{2+} ions per hydrolyzed ATP (3). Phospholamban (PLN) is the main endogenous inhibitor of SERCA activity in cardiomyocytes and its inhibition is relieved upon phosphorylation at Ser 16 or Thr 17 of PLN (4-7). Since SERCA and PLN are the main regulators of the cardiac output, they are targets for treatment of cardiac disease (8, 9).

SERCA function has been measured in several different systems including mammalian cell lines (10), insect cell microsomes (11), and reconstituted lipid vesicles (12). In a reconstituted system, the bilayer lipid composition can be tightly controlled, making it ideal for studying the effects of lipids on SERCA function. Specifically, the effects of bilayer thickness, head group, and membrane fluidity have all been previously investigated. SERCA activity directly depends on bilayer thickness, with a maximum activity found for a lipid chain length of 18 carbons and a gradual decrease in activity for either thicker or thinner bilayers (13, 14). Later data from Cornea and Thomas support these results and, more importantly, showed that the effect of bilayer thickness is correlated to the degree of SERCA oligomerization (15). The biochemical results were supported by molecular dynamics simulations, which show that SERCA can adapt to the thickness of the bilayer through small conformational changes but that this adaptation is not efficient in thin (14-carbon) bilayers (16). Moreover, Squier and co-workers showed that the zwitterionic phosphatidylethanolamine (PE), which represents 16% and 27% of the skeletal and cardiac SR membrane lipid, respectively (17), increases SERCA's maximal activity (Vmax) (18). A similar activating effect was seen for the anionic lipids phosphatidylserine (PS) and phosphatidylinositol (PI) phosphate which are present at lower concentrations in the SR membrane (19). In addition, SERCA requires fluid, liquid crystalline bilayers to function properly (i.e., more active in 18:1 phosphocholine (PC) than 18:0 PC) (20). All of these SERCA activity studies based their conclusions on the maximum ATPase activity or the activity at a single Ca2+ concentration. Also, the functional effects of lipids on the SERCA/PLN complex are currently unknown.

Here, we analyzed the effects of bilayer thickness, head group composition and fluidity for SERCA and the SERCA/PLN complex in reconstituted lipid vesicles, monitoring the ATPase activity using enzyme-coupled assays. We show how apparent Ca^{2+} affinity (K_{Ca}) and V_{max} are strongly dependent on the nature of the lipid bilayer. Importantly, our data reveal how the lipid bilayer composition influences the regulation of SERCA by PLN. Our conclusions on model membranes are supported by activity measurements in lipid membranes extracted from rabbit skeletal muscle.

6.2 Experimental procedures

All synthetic lipids (**Table 1**) were purchased form Avanti Polar Lipids (Alabaster, AL). Skeletal SR lipids were extracted using an acidified solution of 2:1 chloroform:methanol (17).

SERCA1a was purified from rabbit skeletal muscle using a reactive red affinity column (21) and was reconstituted for functional assays according to a well established protocol (12, 22-28). Briefly, the lipids solubilized in chloroform were dried under N_2(g), desiccated for several hours, and resuspended in a buffer containing 20 mM Imidazole, 0.1 M KCl, 5 mM $MgCl_2$, 10% (v/v) Glycerol and octaethylene glycol monododecyl ether ($C_{12}E_8$) at 4:1 (w/w) $C_{12}E_8$:lipid ratio. SERCA (~1 mg/mL in 0.1% w/v $C_{12}E_8$) was added to the suspension to a final lipid:SERCA (mol/mol) ratio of 700:1. To remove the detergent, the samples were incubated with Biobeads SM2 (75:1 (w/w) Biobeads:$C_{12}E_8$) for three hours at 30°C (for experiments where the bilayer thickness or lipid chain saturation was varied) or 20°C (for all other experiments). A temperature of 30°C was chosen to ensure that lipids with relatively high gel-liquid crystal transition temperature (Tm) (i.e. 24:1 PC) were in the liquid crystalline phase during the incubation period. A coupled enzyme assay was used to monitor SERCA activity (hydrolysis of ATP) at 37 ºC as a function of calcium concentration (12). The rate of enzyme activity was measured as a decrease of NADH absorption at 340 nm using a Spectramax plate reader (Molecular Devices). Data were fit using the Hill equation:

$$V = V_{max} \frac{[Ca^{2+}]^n}{[Ca^{2+}]^n + {K_{Ca}}^n}$$

to extract the maximum activity (V_{max}), Hill coefficient (n), and calcium concentration needed to achieve half maximal activity (K_{Ca}).

To monitor the inhibition of SERCA by PLN, we chose a monomeric mutant of PLN (AFA-PLN^{N27A}) that induces a larger shift in SERCA's apparent Ca^{2+} affinity than wild-type PLN (PLN^{wt}). Recombinant AFA-PLN^{N27A} and PLN^{wt} were expressed and purified as described previously (29). The co-reconstitution of SERCA and PLN was identical to the free SERCA samples with the exception that PLN (AFA-PLN^{N27A} or PLN^{wt}) dissolved in a 4:1 (v/v) mixture of trifluoroethanol/cholorform was dried together with the lipids at a molar ratio of 10:1 or 5:1 PLN:SERCA.

6.3 Results

6.3.1 Effects of lipid chain structure on SERCA activity

The lipid chain structure is the main determinant of the fluidity as well as the thickness of the lipid bilayer. To evaluate the effects of bilayer thickness on SERCA activity, we conducted ATPase assays in *cis*-mono unsaturated PC bilayers of varied lipid chain length. PC lipids were utilized since they constitute the major lipid of the SR membrane (17). In our experience, SERCA V_{max} varies between different rabbits and preparations (2.9 ± 1.4 I.U, average ± standard deviation for four preparations in 4:1 (w/w) $18:1^{\Delta 9\text{-Cis}}$ PC (DOPC)/$18:1^{\Delta 9\text{-Cis}}$ PE (DOPE) bilayers), while K_{Ca} is highly reproducible (0.47 ± 0.01 μM). Thus, we express SERCA V_{max} as a relative value to our standard bilayers (DOPC or 4:1 (w/w) DOPC/DOPE) while K_{Ca} is reported as raw values. In **Figure 1A and B**, we show that SERCA activity is highest in bilayers with a chain length of 22 carbons (22:1 bilayers) with a V_{max} value ~40-fold higher than in 14:1 bilayers, which had the lowest V_{max}. Previous studies, however, found that 18:1 bilayers support the highest SERCA activity. (13, 15). The discrepancy with our results might be due to the higher Ca^{2+}-concentration used in the previous studies (10-fold excess relative to this study), which relied on measuring SERCA activity at only one Ca^{2+} concentration. Since our activity assays were measured for several Ca^{2+} concentrations (complete Ca^{2+} dependence curves), their fits provide an accurate estimate of V_{max}. From the fitting of the activity curves, we also measured the SERCA K_{Ca} for each lipid

length. **Figure 1C and D** show that SERCA affinity for Ca^{2+} is biphasic, with the minimum K_{Ca} (highest apparent Ca^{2+} affinity) in 20:1 bilayers. Taken together, these data indicate that SERCA has the highest V_{max} in relatively thick bilayers (22:1), while bilayers with a thickness similar to the native SR membrane (average chain length of 18.1 carbons in cardiac SR and 17.8 carbons in skeletal SR) (17) give the highest affinity for Ca^{2+}. Therefore, the native SR lipid composition seems tuned to maximize the apparent Ca^{2+} affinity of SERCA.

Bilayer fluidity is another important physical property of the lipid bilayer and SERCA requires a fluid bilayer to function (20). To test the dependence of SERCA on bilayer fluidity, we reconstituted SERCA into $18:1^{\Delta 9\text{-Trans}}$ PC (similar bilayer thickness but less fluid than DOPC as determined by fluorescence polarization of 1,6-diphenyl-1,3,5-hexatriene (DPH)) (14, 30) and $18:2^{\Delta 9,\Delta 12\text{-Cis}}$ PC (similar bilayer thickness but more fluid than DOPC) (14, 30). In $18:1^{\Delta 9\text{-Trans}}$ PC, SERCA V_{max} is slightly higher than in DOPC, while in $18:2^{\Delta 9,\Delta 12\text{-Cis}}$ PC V_{max} is significantly lower (**Figure 2A**). However, in both $18:2^{\Delta 9,\Delta 12\text{-Cis}}$ PC and $18:1^{\Delta 9\text{-Trans}}$ PC bilayers K_{Ca} is significantly higher than in DOPC (**Figure 2B**). In the cardiac SR, the average number of unsaturated (*cis*) bonds per lipid chain is 1.6 (17), which is intermediate between that of DOPC and $18:2^{\Delta 9,\Delta 12\text{-Cis}}$ PC. Thus, both the thickness and fluidity of the SR bilayer are probably optimized for K_{Ca} rather than V_{max}.

An inherent shortcoming of our studies is that bilayer thickness and fluidity cannot be varied independently (i.e $18:1^{\Delta 9\text{-Trans}}$ PC bilayers are thicker than DOPC bilayers). Therefore it is important to emphasize that a change in SERCA activity cannot be explained by one single characteristic of the lipid bilayer. Nevertheless, the difference in bilayer thickness between DOPC and $18:1^{\Delta 9\text{-Trans}}$ PC is only ~1 Å (14) compared to the difference between for example 20:1 PC and 18:1 PC (~3Å) ((14). Thus, the difference in SERCA V_{max} and K_{Ca} between $18:1^{\Delta 9\text{-Trans}}$ PC and DOPC can be mainly attributed to the difference in fluidity between the two bilayers.

6.3.2 Effects of phosphoethanolamine (PE) on the activity of the SERCA/PLN complex

Since the two major components of the native SR membrane are PC and PE lipids (17), 4:1 (w/w) DOPC/DOPE lipid bilayers preparations have been used to study SERCA activity (12, 31). To determine the effects of PE on SERCA function, we carried out functional assays at different molar ratios of DOPC:DOPE. Since pure PE membranes form hexagonal phases and inhibit SERCA activity (32), we limited the PE content to 60% (w/w) of the total lipid bilayer composition to retain the liquid crystalline phase.

When SERCA was reconstituted in the absence of PLN, we found that increased PE content steadily increases V_{max} at PE ratios greater than 20% (w/w), with no significant effects observed at PE content <20% (w/w) (**Figure 3A and B**), in agreement with previous studies (18, 32). Also, we found that the DOPC:DOPE bilayers have a significantly lower K_{Ca} compared to pure DOPC bilayers (**Figure 3D, E**). Thus, PE has an activating role on SERCA function, increasing both the apparent Ca^{2+} affinity and V_{max}.

PE is a curvature-forming non-bilayer lipid (33), which can affect membrane protein function by inducing curvature and changing the lateral pressure in the membrane (34, 35). To test if this change in bilayer property could explain the effects of PE on SERCA function we measured SERCA activity in the presence of phosphoserine (PS) lipids, which make up ~10% of the total SR membrane lipid content (17) and does not induce membrane curvature. In this case, we found that the 4:1 (w/w) PC:PS bilayers decreased SERCA V_{max} relative to both PC and 4:1 (w/w) PC:PE bilayers (**Figure 3C**). However, K_{Ca} values were slightly lower than those obtained in PC:PE (**Figure 3F**). The effects on K_{Ca} and V_{max} are present also at a physiological 9:1 (w/w) PC:PS ratio. These data show that PS increases the apparent Ca^{2+} affinity of SERCA and reveal a possible activating role of PS similar to PE lipids. This also suggests that the activation of SERCA by PE is not due to increased bilayer curvature.

In situ and *in vitro* experiments have shown that SERCA's apparent Ca^{2+} affinity is lowered in the presence of PLN (11, 12, 23). To determine the effects of bilayer composition on SERCA inhibition by PLN, we co-reconstituted a monomeric,

superinhibitory mutant of PLN (AFA-PLN^{N27A}) (12, 36) with SERCA into lipid vesicles composed of DOPC or DOPC/DOPE mixtures. We found that AFA-PLN^{N27A}'s effects on SERCA are the same either in the absence or presence of 20% PE (w/w). In both cases AFA-PLN^{N27A} increases both V_{max} and K_{Ca} (**Figure 4**). Note that in the presence of AFA-PLN^{N27A}, SERCA activity is insensitive to a change in PE content. Therefore, the presence of PLN removes the activating effects of PE on SERCA Ca^{2+} affinity.

6.3.3 PLN regulation of SERCA and bilayer thickness

To analyze how PLN regulation of SERCA depends on the bilayer thickness, we co-reconstituted SERCA and AFA-PLN^{N27A} into bilayers of varied chain length and with 20% (w/w) DOPE to maximize the effects on SERCA activity. From the data in **Figure 5** it is clear that the effects of AFA-PLN^{N27A} on SERCA function are dependent on the bilayer composition. In 18:1 bilayers, AFA-PLN^{N27A} binding increases SERCA V_{max} and decreases its Ca^{2+} affinity, as previously noted (12, 23). However, in 22:1 bilayers AFA-PLN^{N27A} does not alter the enzyme's V_{max} but lowers its Ca^{2+} affinity in a manner that is strikingly similar to the behavior of the SERCA/PLN complex in co-expression systems (11). These results imply that differences in bilayer composition may account for some of the discrepancies seen between *in vitro* and *in vivo* studies. In addition, AFA-PLN^{N27A} shifts the highest V_{max} of SERCA to thinner bilayers (from 24:1 to 20:1). The slight difference in maximum V_{max} in the absence of SERCA from that measured in pure PC bilayers (**Figure 1**) is probably attributable to the DOPE (18:1) lipids, which may reduce the thickness of 20:1, 22:1 and 24:1 bilayers. As shown in **Figure 4**, AFA-PLN^{N27A} removes the activating effects of PE on SERCA. Also, AFA-PLN^{N27A} attenuates the differences in K_{Ca} found for bilayers of different chain length (*i.e.*, 5-fold vs 1.5-fold difference between 20:1 and 24:1 in the absence and presence of AFA-PLN^{N27A}, respectively). Thus, PLN binding alters the effects of head group composition and chain length on SERCA activity.

6.3.4 Lipid effects on the SERCA/PLN complex at physiological protein to lipid ratios

A lipid-to-protein ratio of 700:1 is typically used in the current literature for the ATPase assays (12, 31). To determine if the effects of lipids is preserved under more physiological lipid-to-protein ratios, we measured SERCA activity using 150:1

lipid:SERCA molar ratio. We found that under these conditions both V_{max} (35% increase) and K_{Ca} (0.63 ± 0.02 μM vs 0.47 ± 0.01 μM) are slightly higher than in 700:1 bilayers. **Figure 6A** shows that incorporation of 20% (w/w) PE leads to an increase of V_{max}, which is also seen in 700:1 bilayers but at slightly higher PE concentrations. Also, 20% (w/w) PE leads to lower K_{Ca} (**Figure 6B**) and thus a higher apparent Ca^{2+} affinity in agreement with the data obtained with 700:1 lipid-to-protein ratio (**Figure 3**). Therefore, the conclusions obtained in bilayers with a 700:1 lipid:SERCA molar ratio are also valid for 150:1 bilayers, which mimic the SR composition.

In the cardiac SR membrane, SERCA is surrounded by a ~5-fold molar excess of PLN (37). Wild type PLN (PLN^{wt}) forms a pentamer (38, 39), but de-oligomerizes into monomers to form a 1:1 complex with SERCA (40, 41). To supplement the results with the superinhibitory, monomeric AFA-PLN^{N27A} mutant we co-reconstituted PLN^{wt} with SERCA at a 5:1 PLN^{wt}:SERCA molar ratio into bilayers containing 150 lipid molecules per SERCA, mimicking the conditions of the native SR membrane. As for the superinhibitory monomeric PLN, addition of PLN^{wt} increases K_{Ca} and raises V_{max} of SERCA (**Figure 6**). Importantly, in the presence of PLN^{wt}, PE head groups do not have an effect on the K_{Ca} or V_{max} of SERCA in analogy to the results with AFA-PLN^{N27A} at a 700:1 lipid:SERCA molar ratio (**Figure 4**). Thus, we conclude that the effects of lipids are similar for pentameric and monomeric PLN and that our results with AFA-PLN^{N27A} are representative also for other PLN variants.

6.3.5 SERCA function and regulation by PLN in native lipids

Previous studies have shown discrepancies in SERCA function and PLN regulation (V_{max}) between different membrane mimicking systems (11, 12, 23). To confirm that our conclusions in model membranes apply to native SR lipids, we reconstituted SERCA and AFA-PLN^{N27A} into lipids extracted from rabbit hind-leg skeletal muscle. While these extracted lipids cannot fully mimic all properties of the SR membrane (i.e., asymmetric distribution of lipids between bilayer leaflets or presence of lipid rafts) they allowed us to test SERCA activity and PLN regulation in a fully physiological bilayer composition. In SR lipids, SERCA V_{max} ($V_{max,SR}/V_{maxDOPC}$ = 1.3) and K_{Ca} (0.81 μM) are slightly higher than in the 4:1 (w/w) DOPC:DOPE bilayers used to mimic the SR composition (**Figure 7**). Addition of AFA-PLN^{N27A} leads to an increase in

V_{max} ($V_{max,+PLN}/V_{max-PLN}$ = 2.6) and a shift in K_{Ca} (to 2.0 μM). These effects are similar to those obtained in synthetic lipid preparations (**Figure 4**). Interestingly, addition of AFA-PLN^{N27A} increases the degree of Ca^{2+} binding cooperativity (Hill coefficient). This effect has been seen in SR vesicles (42) and reconstituted lipid bilayers consisting of a mixture of natural egg yolk PC and PA (phosphatidic acid) lipids(23) but was not detected in synthetic model membranes (**Figure 4**). Nevertheless, the differences between the native lipids and the DOPC:DOPE bilayers are relatively minor considering the sensitivity of SERCA to the bilayer thickness and the nature of the lipid head group.

6.4 Discussion

The importance of lipid bilayer composition for protein function is well established for SERCA (43, 44) as well as for other membrane bound enzymes (45). In the present study, we show that SERCA V_{max} and K_{Ca} are significantly affected by the lipid bilayer composition. Thus, lipids with different chain length and head groups have activating or inhibitory effects on the enzyme. Since PE and PS lipids increase the apparent Ca^{2+} affinity of SERCA (**Figure 3**), we believe these to be *activating* with respect to PC lipids. This activation could be a result either of specific protein-lipid interactions (46) or non-specific effects on bilayer properties (47). Previously, it has been shown that addition of PE to PC bilayers does not alter lipid chain dynamics or the overall SERCA rotational correlation time (18), and that change in lipid head group composition has marginal effect on bilayer thickness (48). Thus, the SERCA activation by PE head groups is likely due to specific protein-lipid interactions rather than macroscopic changes of the lipid bilayer properties. A possible explanation for such interactions is that in contrast to PC, PE and PS can function as hydrogen bond donors and potentially form hydrogen bonds with sites on SERCA in agreement with other membrane proteins (46). In fact, lipid molecules have been detected in SERCA crystal structures (3) with the bound lipids modeled as PE and located in the groove between helices M2, M4 and M6. These lipids could possibly be responsible for the activating effects of PE on SERCA. Interestingly, this lipid binding site overlaps with the proposed binding site for PLN (49). Here, we showed that in the presence of PLN, SERCA activity is independent of PE (**Figure 4**).

Therefore, the inhibitory PLN and the activating PE lipids might compete for the same binding site, which could explain part of the inhibitory effect that PLN has on SERCA.

It is widely accepted that PLN inhibits SERCA by lowering its apparent Ca^{2+} affinity. However, contrasting studies have reported that PLN increases (12, 23) or does not affect V_{max} (11). The increase of V_{max} has mainly been observed in reconstituted systems, but vanishes at high lipid:SERCA ratios (12). Based on our results in model membranes, PLN increases (16:1, 18:1, 20:1), does not change (22:1), or decreases (24:1) the enzyme's V_{max} in bilayers of different thickness (**Figure 5**). In 22:1 bilayers AFA-PLN^{N27A} lowers the Ca^{2+} affinity of SERCA without affecting V_{max}. The similarity of these data with those from co-expression systems (11) raises the question whether SERCA and PLN preferentially localize to thicker regions of the bilayer *in vivo*. Another possibility is that PLN changes the thickness of the lipid bilayers, affecting V_{max}. In the absence of PLN (and in the presence of 20% (w/w) DOPE), SERCA reaches its maximum activity in 24:1 lipid bilayers (**Figure 5A**). In contrast, when co-reconstituted with AFA-PLN^{N27A}, SERCA reaches its maximum activity in 20:1 lipid bilayers (**Figure 5A**). This result may be rationalized by a thickening of the bilayer caused by PLN. Under diluted conditions (high lipid:AFA-PLN^{N27A} molar ratios), the effects of AFA-PLN^{N27A} on V_{max} vanishes (12). It is possible that under these conditions AFA-PLN^{N27A} concentration is too low to affect the thickness of the bilayer, thus losing its ability to increase V_{max}. In fact, depleting membrane proteins from bilayers can change the thickness by ~5 Å (50), which corresponds to a difference in chain length of ~3 carbons. In the native SR membrane, the lipid:SERCA molar ratio is ~100:1 (51), and thus significantly lower than the 700:1 ratio used in our measurements. Even if additional proteins, lipids, and other biomolecules are present *in vivo*, PLN-induced changes to the lipid bilayer could be important for regulation of SERCA in the muscle cell. Previous studies have shown that the effect of bilayer thickness on SERCA V_{max} is correlated to reversible aggregation (15). In light of those results, SERCA aggregation is another possible mechanism for regulation of the enzyme by PLN. Also, PLN is in conformational equilibria between different conformational states (31, 52, 53), which are sensitive to the composition of the lipid bilayer (54, 55). Furthermore, negatively charged lipids influence the ability of a soluble peptide corresponding to residues 1-23 of PLN to regulate SERCA activity (56).

Further studies are needed to determine if a shift in the conformational equilibrium of PLN is responsible for the effects of lipid composition on the SERCA/PLN complex.

Cardiac and skeletal SR membranes have an average lipid chain length of ~18, and an average of 1.6 unsaturated bonds per lipid chain. They are mainly composed of lipids with PC head groups (~53% (cardiac), ~68% (skeletal)) with smaller amounts of PE (~27%, ~16%), PS (~10%, 10%), and PI (~1%, ~2%) lipids (17). Our data show that in bilayers with this chain length (**Figure 1**), fluidity (**Figure 2**) and head group content (**Figure 3**) SERCA's apparent apparent Ca^{2+} affinity is optimal in while V_{max}, is higher in thicker, less fluid bilayers. Thus, the SR membrane appears to be tuned to maximize the apparent Ca^{2+} affinity of SERCA. Our data also show that a PE concentration $\geq$ 20% (w/w) raises SERCA Vmax and KCa is significantly lowered at PE concentrations of less than 20% (**Figure 3**). Therefore, at physiological PE concentrations, small changes in the PE head group content of the SR could significantly alter intracellular calcium cycling. The same is true for changes in bilayer thickness or lipid saturation.

Changes to the bilayer composition in mice have been shown to occur with muscular dystrophy (57) and aging (58). In addition, diet can also alter the distribution of lipids, as shown in another mouse study where increased levels of unsaturated lipids occurred from *exclusive* fish intake. These mice had lower Ca^{2+} uptake into the SR (59). In agreement with this finding, our activity assays using model membranes show that SERCA V_{max} is significantly lower in polyunsaturated $18{:}2^{\Delta 9,\Delta 12\text{-Cis}}$ PC than in monounsaturated DOPC (**Figure 2**). This implies that differences in SERCA function between bilayers with different lipid chain structure could be explained by differences in lipid bilayer thickness. Also, a recent study showed that obesity-induced ER stress can significantly raise the PC:PE ratio of the ER (60). Interestingly, this change in head group composition was correlated to a decreased SERCA activity which is in excellent agreement with our *in vitro* studies.

In the cardiac SR, PLN is present at a five-fold excess molar concentration with respect to SERCA (37). Our data show that SERCA activity is significantly less sensitive to alterations of the lipid thickness of the PC:PE bilayer in the presence of AFA-PLN^{N27A}.

Thus, PLN may have a *buffering effect* for SERCA in response to any changes in membrane structure due to pathology or diet.

In summary, we have shown that SERCA activity and its regulation by PLN are sensitive to bilayer thickness, fluidity and head group content with maximum activity in bilayers that are slightly thicker than the native SR membrane. SERCA's apparent Ca^{2+} affinity, however, is optimized in bilayers mimicking the native SR membrane. The presence of PLN decreases the calcium affinity, removes the activating effects of PE and attenuates the effects on SERCA activity in lipids of varying chain length. These new findings for Ca^{2+} translocation underline the importance of lipids for SERCA function and its regulation by PLN and could reconcile discrepancies between reconstituted and co-expression systems.

6.5 References

1. Bers, D. M. 2002. Cardiac excitation-contraction coupling. Nature. 415, 198-205.
2. Brini, M. and E. Carafoli 2009. Calcium pumps in health and disease. Physiol. Rev. 89, 1341-1378.
3. Obara, K., N. Miyashita, C. Xu, I. Toyoshima, Y. Sugita, G. Inesi and C. Toyoshima 2005. Structural role of countertransport revealed in ca(2+) pump crystal structure in the absence of ca(2+). Proc. Natl. Acad. Sci. U. S. A. 102, 14489-14496.
4. Simmerman, H. K., J.H. Collins, J.L. Theibert, A.D. Wegener and L.R. Jones 1986. Sequence analysis of phospholamban. identification of phosphorylation sites and two major structural domains. J Biol Chem. 261, 13333-41.
5. Wegener, A. D., H.K. Simmerman, J.P. Lindemann and L.R. Jones 1989. Phospholamban phosphorylation in intact ventricles. phosphorylation of serine 16 and threonine 17 in response to beta-adrenergic stimulation. Journal Biological Chemistry. 264, 11468-11474.
6. MacLennan, D. H. and E.G. Kranias 2003. Phospholamban: A crucial regulator of cardiac contractility. Nat Rev Mol Cell Biol. 4, 566-77.
7. Traaseth, N. J., K.N. Ha, R. Verardi, L. Shi, J.J. Buffy, L.R. Masterson and G. Veglia 2008. Structural and dynamic basis of phospholamban and sarcolipin inhibition of ca(2+)-ATPase. Biochemistry. 47, 3-13.
8. Kaye, D. M., M. Hoshijima and K.R. Chien 2008. Reversing advanced heart failure by targeting Ca2+ cycling. Annu. Rev. Med. 59, 13-28.

9. Inesi, G., A.M. Prasad and R. Pilankatta 2008. The Ca2+ ATPase of cardiac sarcoplasmic reticulum: Physiological role and relevance to diseases. Biochem. Biophys. Res. Commun. 369, 182-187.

10. Vandecaetsbeek, I., M. Trekels, M. De Maeyer, H. Ceulemans, E. Lescrinier, L. Raeymaekers, F. Wuytack and P. Vangheluwe 2009. Structural basis for the high Ca2+ affinity of the ubiquitous SERCA2b Ca2+ pump. Proc. Natl. Acad. Sci. U. S. A. 106, 18533-18538.

11. Mahaney, J. E., J.M. Autry and L.R. Jones 2000. Kinetics studies of the cardiac ca-ATPase expressed in Sf21 cells: New insights on ca-ATPase regulation by phospholamban. Biophys. J. 78, 1306-1323.

12. Reddy, L. G., R.L. Cornea, D.L. Winters, E. McKenna and D.D. Thomas 2003. Defining the molecular components of calcium transport regulation in a reconstituted membrane system. Biochemistry. 42, 4585-92.

13. Froud, R. J., C.R. Earl, J.M. East and A.G. Lee 1986. Effects of lipid fatty acyl chain structure on the activity of the (Ca2+ + Mg2+)-ATPase. Biochim. Biophys. Acta. 860, 354-360.

14. Caffrey, M. and G.W. Feigenson 1981. Fluorescence quenching in model membranes. 3. relationship between calcium adenosinetriphosphatase enzyme activity and the affinity of the protein for phosphatidylcholines with different acyl chain characteristics. Biochemistry. 20, 1949-1961.

15. Cornea, R. L. and D.D. Thomas 1994. Effects of membrane thickness on the molecular dynamics and enzymatic activity of reconstituted ca-ATPase. Biochemistry. 33, 2912-2920.

16. Sonntag, Y., M. Musgaard, C. Olesen, B. Schiott, J.V. Moller, P. Nissen and L. Thogersen 2011. Mutual adaptation of a membrane protein and its lipid bilayer during conformational changes. Nat. Commun. 2, 304.

17. Bick, R. J., L.M. Buja, W.B. Van Winkle and G.E. Taffet 1998. Membrane asymmetry in isolated canine cardiac sarcoplasmic reticulum: Comparison with skeletal muscle sarcoplasmic reticulum. J. Membr. Biol. 164, 169-175.

18. Hunter, G. W., S. Negash and T.C. Squier 1999. Phosphatidylethanolamine modulates ca-ATPase function and dynamics. Biochemistry. 38, 1356-1364.

19. Szymanska, G., H.W. Kim and E.G. Kranias 1991. Reconstitution of the skeletal sarcoplasmic reticulum Ca2(+)-pump: Influence of negatively charged phospholipids. Biochim. Biophys. Acta. 1091, 127-134.

20. Lee, A. G. 2003. Lipid-protein interactions in biological membranes: A structural perspective. Biochim. Biophys. Acta. 1612, 1-40.

21. Stokes, D. L. and N.M. Green 1990. Three-dimensional crystals of CaATPase from sarcoplasmic reticulum. symmetry and molecular packing. Biophys J. 57, 1-14.

22. Afara, M. R., C.A. Trieber, J.P. Glaves and H.S. Young 2006. Rational design of peptide inhibitors of the sarcoplasmic reticulum calcium pump. Biochemistry. 45, 8617-8627.

23. Trieber, C. A., M. Afara and H.S. Young 2009. Effects of phospholamban transmembrane mutants on the calcium affinity, maximal activity, and cooperativity of the sarcoplasmic reticulum calcium pump. Biochemistry. 48, 9287-9296.

24. Trieber, C. A., J.L. Douglas, M. Afara and H.S. Young 2005. The effects of mutation on the regulatory properties of phospholamban in co-reconstituted membranes. Biochemistry. 44, 3289-3297.

25. Levy, D., A. Gulik, A. Bluzat and J.L. Rigaud 1992. Reconstitution of the sarcoplasmic reticulum ca(2+)-ATPase: Mechanisms of membrane protein insertion into liposomes during reconstitution procedures involving the use of detergents. Biochim. Biophys. Acta. 1107, 283-298.

26. Young, H. S., L.G. Reddy, L.R. Jones and D.L. Stokes 1998. Co-reconstitution and co-crystallization of phospholamban and ca(2+)-ATPase. Ann. N. Y. Acad. Sci. 853, 103-115.

27. Reddy, L. G., L.R. Jones, S.E. Cala, J.J. O'Brian, S.A. Tatulian and D.L. Stokes 1995. Functional reconstitution of recombinant phospholamban with rabbit skeletal ca(2+)-ATPase. J Biol Chem. 270, 9390-7.

28. Young, H. S., J.L. Rigaud, J.J. Lacapere, L.G. Reddy and D.L. Stokes 1997. How to make tubular crystals by reconstitution of detergent-solubilized Ca2(+)-ATPase. Biophys. J. 72, 2545-2558.

29. Buck, B., J. Zamoon, T.L. Kirby, T.M. DeSilva, C. Karim, D. Thomas and G. Veglia 2003. Overexpression, purification, and characterization of recombinant ca-ATPase regulators for high-resolution solution and solid-state NMR studies. Protein Expr Purif. 30, 253-61.

30. Roach, C., S.E. Feller, J.A. Ward, S.R. Shaikh, M. Zerouga and W. Stillwell 2004. Comparison of cis and trans fatty acid containing phosphatidylcholines on membrane properties. Biochemistry. 43, 6344-6351.

31. Ha, K. N., N.J. Traaseth, R. Verardi, J. Zamoon, A. Cembran, C.B. Karim, D.D. Thomas and G. Veglia 2007. Controlling the inhibition of the sarcoplasmic Ca2+-ATPase by tuning phospholamban structural dynamics. J. Biol. Chem. 282, 37205-37214.

32. Starling, A. P., K.A. Dalton, J.M. East, S. Oliver and A.G. Lee 1996. Effects of phosphatidylethanolamines on the activity of the ca(2+)-ATPase of sarcoplasmic reticulum. Biochem. J. 320 (Pt 1), 309-314.

33. Dowhan, W. and M. Bogdanov 2011. Lipid-protein interactions as determinants of membrane protein structure and function. Biochem. Soc. Trans. 39, 767-774.

34. Moe, P. and P. Blount 2005. Assessment of potential stimuli for mechano-dependent gating of MscL: Effects of pressure, tension, and lipid headgroups. Biochemistry. 44, 12239-12244.

35. Scarlata, S. and S.M. Gruner 1997. Role of phosphatidylethanolamine lipids in the stabilization of protein-lipid contacts. Biophys. Chem. 67, 269-279.

36. Kimura, Y., M. Asahi, K. Kurzydlowski, M. Tada and D.H. MacLennan 1998. Phospholamban domain ib mutations influence functional interactions with the Ca2+-ATPase isoform of cardiac sarcoplasmic reticulum. J Biol Chem. 273, 14238-41.

37. Ferrington, D. A., Q. Yao, T.C. Squier and D.J. Bigelow 2002. Comparable levels of ca-ATPase inhibition by phospholamban in slow-twitch skeletal and cardiac sarcoplasmic reticulum. Biochemistry. 41, 13289-13296.

38. Cornea, R. L., L.R. Jones, J.M. Autry and D.D. Thomas 1997. Mutation and phosphorylation change the oligomeric structure of phospholamban in lipid bilayers. Biochemistry. 36, 2960-7.

39. Verardi, R., L. Shi, N.J. Traaseth, N. Walsh and G. Veglia 2011. Structural topology of phospholamban pentamer in lipid bilayers by a hybrid solution and solid-state NMR method. Proc Natl Acad Sci U S A. 108, 9101-9106.

40. Robia, S. L., K.S. Campbell, E.M. Kelly, Z. Hou, D.L. Winters and D.D. Thomas 2007. Forster transfer recovery reveals that phospholamban exchanges slowly from pentamers but rapidly from the SERCA regulatory complex. Circ. Res. 101, 1123-1129.

41. Kimura, Y., K. Kurzydlowski, M. Tada and D.H. MacLennan 1997. Phospholamban inhibitory function is activated by depolymerization. J Biol Chem. 272, 15061-4.

42. Hicks, M. J., M. Shigekawa and A.M. Katz 1979. Mechanism by which cyclic adenosine 3':5'-monophosphate-dependent protein kinase stimulates calcium transport in cardiac sarcoplasmic reticulum. Circ Res. 44, 384-91.

43. Lee, A. G. 1998. How lipids interact with an intrinsic membrane protein: The case of the calcium pump. Biochim. Biophys. Acta. 1376, 381-390.

44. Lee, A. G. and J.M. East 1998. The effects of phospholipid structure on the function of a calcium pump. Biochem. Soc. Trans. 26, 359-365.

45. Farias, R. N., B. Bloj, R.D. Morero, F. Sineriz and R.E. Trucco 1975. Regulation of allosteric membrane-bound enzymes through changes in membrane lipid compostition. Biochim. Biophys. Acta. 415, 231-251.

46. Hakizimana, P., M. Masureel, B. Gbaguidi, J.M. Ruysschaert and C. Govaerts 2008. Interactions between phosphatidylethanolamine headgroup and LmrP, a multidrug transporter: A conserved mechanism for proton gradient sensing? J. Biol. Chem. 283, 9369-9376.

47. Bogdanov, M., P. Heacock, Z. Guan and W. Dowhan 2010. Plasticity of lipid-protein interactions in the function and topogenesis of the membrane protein lactose permease from escherichia coli. Proc. Natl. Acad. Sci. U. S. A. 107, 15057-15062.

48. Rand, R. P., N. Fuller, V.A. Parsegian and D.C. Rau 1988. Variation in hydration forces between neutral phospholipid bilayers: Evidence for hydration attraction. Biochemistry. 27, 7711-7722.

49. Toyoshima, C., M. Asahi, Y. Sugita, R. Khanna, T. Tsuda and D.H. MacLennan 2003. Modeling of the inhibitory interaction of phospholamban with the Ca2+ ATPase. Proc Natl Acad Sci U S A. 100, 467-72.

50. Juretic, D., R.W. Hendler, F. Kamp, W.S. Caughey, M. Zasloff and H.V. Westerhoff 1994. Magainin oligomers reversibly dissipate delta microH+ in cytochrome oxidase liposomes. Biochemistry. 33, 4562-4570.

51. Tada, M., T. Yamamoto and Y. Tonomura 1978. Molecular mechanism of active calcium transport by sarcoplasmic reticulum. Physiol. Rev. 58, 1-79.

52. Gustavsson, M., N.J. Traaseth, C.B. Karim, E.L. Lockamy, D.D. Thomas and G. Veglia 2011. Lipid-mediated Folding/Unfolding of phospholamban as a regulatory mechanism for the sarcoplasmic reticulum ca(2+)-ATPase. J. Mol. Biol. 408, 755-765.

53. Karim, C. B., Z. Zhang, E.C. Howard, K.D. Torgersen and D.D. Thomas 2006. Phosphorylation-dependent conformational switch in spin-labeled phospholamban bound to SERCA. J. Mol. Biol. 358, 1032-1040.

54. Gustavsson, M., N.T. Traaseth and G. Veglia 2011. Probing ground and excited states of phospholamban in model and native lipid membranes by magic angle spinning NMR spectroscopy. Biochim. Biophys. Acta. 1818.

55. Matsuzaki, K. 1999. Why and how are peptide-lipid interactions utilized for self-defense? magainins and tachyplesins as archetypes. Biochim. Biophys. Acta. 1462, 1-10.

56. Hughes, E., J.C. Clayton and D.A. Middleton 2009. Cytoplasmic residues of phospholamban interact with membrane surfaces in the presence of SERCA: A new role for phospholipids in the regulation of cardiac calcium cycling? Biochim. Biophys. Acta. 1788, 559-566.

57. Mrak, R. E. and S. Fleischer 1982. Lipid composition of sarcoplasmic reticulum from mice with muscular dystrophy. Muscle Nerve. 5, 439-446.

58. Krainev, A. G., D.A. Ferrington, T.D. Williams, T.C. Squier and D.J. Bigelow 1995. Adaptive changes in lipid composition of skeletal sarcoplasmic reticulum membranes associated with aging. Biochim. Biophys. Acta. 1235, 406-418.

59. Taffet, G. E., T.T. Pham, D.L. Bick, M.L. Entman, H.J. Pownall and R.J. Bick 1993. The calcium uptake of the rat heart sarcoplasmic reticulum is altered by dietary lipid. J. Membr. Biol. 131, 35-42.

60. Fu, S., L. Yang, P. Li, O. Hofmann, L. Dicker, W. Hide, X. Lin, S.M. Watkins, A.R. Ivanov and G.S. Hotamisligil 2011. Aberrant lipid metabolism disrupts calcium homeostasis causing liver endoplasmic reticulum stress in obesity. Nature. 473, 528-531.

Lipid	Chemical name
$14:1^{\Delta 9\text{-Cis}}$ PC	1,2-di-(9Z-tetradecenoyl)-sn-glycero-3-phosphocholine
$16:1^{\Delta 9\text{-Cis}}$ PC	1,2-di-(9Z-hexadecenoyl)-sn-glycero-3-phosphocholine
$18:1^{\Delta 9\text{-Cis}}$ PC (DOPC)	1,2-di-(9Z-octadecenoyl)-sn-glycero-3-phosphocholine
$18:1^{\Delta 9\text{-Trans}}$ PC	1,2-di-(9E-octadecenoyl)-sn-glycero-3-phosphocholine
$18:2^{\Delta 9,\Delta 12\text{-Cis}}$ PC	1,2-di-(9Z,12Z-octadecadienoyl)-sn-glycero-3-phosphocholine
$20:1^{\Delta 11\text{-Cis}}$ PC	1,2-di-(11Z-eicosenoyl)-sn-glycero-3-phosphocholine
$22:1^{\Delta 13\text{-Cis}}$ PC	1,2-di-(13Z-docosenoyl)-sn-glycero-3-phosphocholine
$24:1^{\Delta 15\text{-Cis}}$ PC	1,2-di-(15Z-tetracosenoyl)-sn-glycero-3-phosphocholine
$18:1^{\Delta 9\text{-Cis}}$ PE (DOPE)	1,2-di-(9Z-octadecenoyl)-sn-glycero-3-phosphoethanolamine
$18:1^{\Delta 9\text{-Cis}}$ PS (DOPS)	1,2-di-(9Z-octadecenoyl)-sn-glycero-3-phospho-L-serine

Table 1. Synthetic lipids used for reconstitutions.

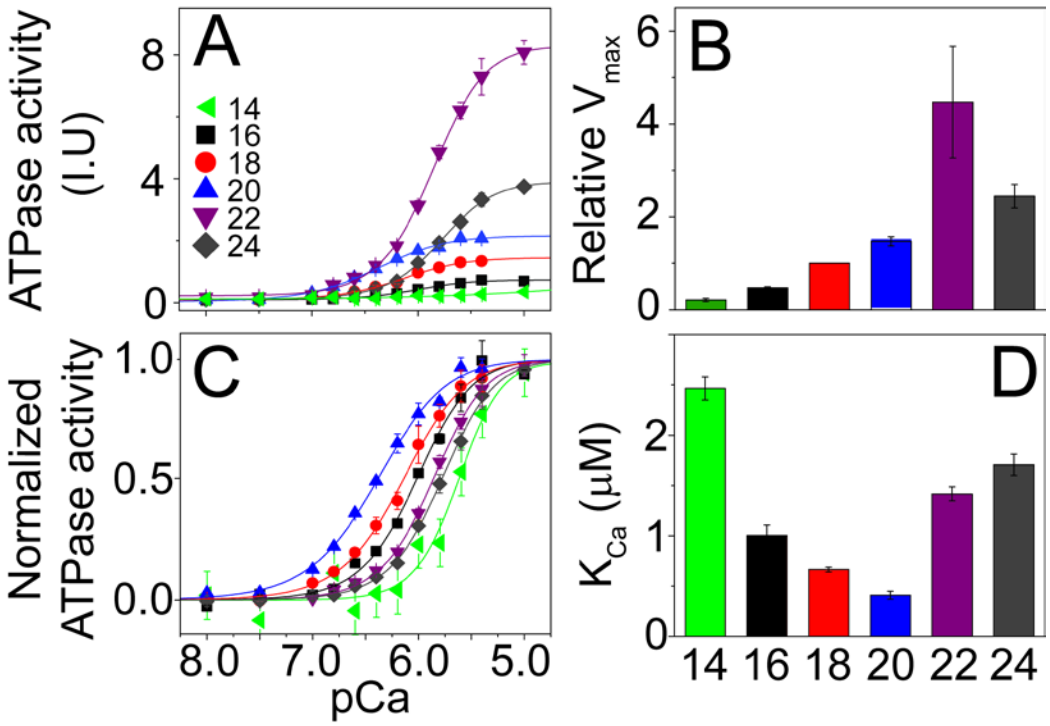

Figure 1. SERCA activity in bilayers of varying thickness. *A, C.) Representative curves of raw and normalized ATPase activity as a function of calcium concentration in 14:1$^{\Delta 9\text{-}Cis}$, 16:1$^{\Delta 9\text{-}Cis}$, DOPC, 20:1$^{\Delta 11\text{-}Cis}$, 22:1$^{\Delta 13\text{-}Cis}$ and 24:1$^{\Delta 15\text{-}Cis}$ PC bilayers. Each point represents the average and standard error from three measurements. B.) V_{max} of SERCA relative to DOPC ($V_{max}/V_{max,DOPC}$) as a function of bilayer chain length. Error bars represent the standard error from at least three separate reconstitutions D.) K_{Ca} in bilayers of varying thickness. Each bar was determined from the average of ≥ 3 reconstitutions and error bars show the standard error of the mean.*

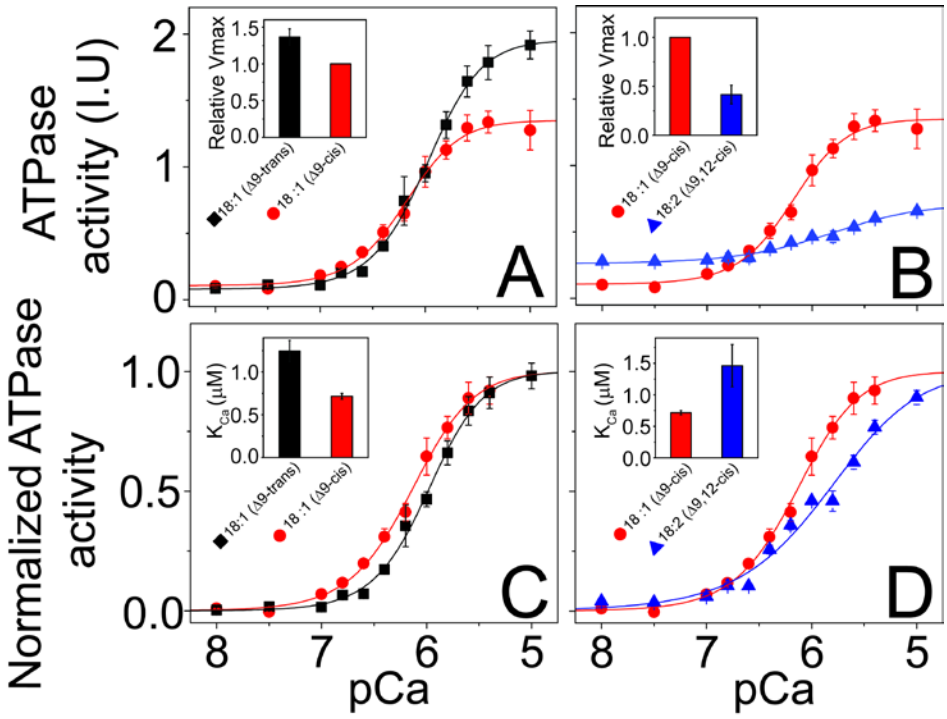

Figure 2. SERCA activity in C18 bilayers with different fluidity. *A, C.) Raw and normalized ATPase activity in PC bilayers with differences in geometry around the unsaturated bond (18:1$^{\Delta 9\text{-trans}}$ PC vs DOPC (18:1$^{\Delta 9\text{-cis}}$ PC)) but identical length of the aliphatic chains. B, D.) ATPase activity in PC bilayers with differences in chain saturation (DOPC vs 18:2$^{\Delta 9,\ \Delta 12\text{-cis}}$ PC) but identical length of the aliphatic chains. Error bars correspond to the standard error of three measurements. Averaged K_{Ca} and relative V_{max} are shown as insets, with the error bars representing the standard error of three or more separate reconstitutions.*

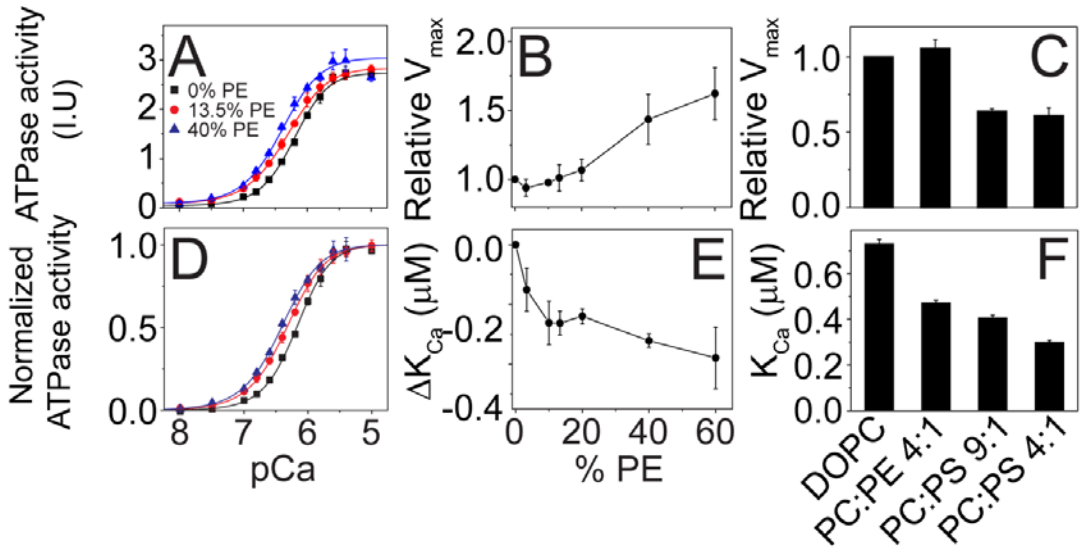

Figure 3. Effects of PE and PS head groups on SERCA activity. *A,D.) Representative curves of raw and normalized SERCA activity in bilayers composed of DOPC and different mole fractions of 18:1 DOPE as indicated in figure. Error bars represent an average of triplicate measurements and are for some points smaller than the symbol. B.)* V_{max} *of SERCA in bilayer with varied amount of PE head group.* V_{max} *values are shown relative to the* V_{max} *in 0% PE (DOPC). C.)* V_{max} *relative to* $V_{max,DOPC}$ *in 4:1 (w/w) DOPC:DOPE and 4:1 or 9:1 (w/w) DOPC:DOPS. E.)* K_{Ca} *of SERCA in different amounts of PE.* ΔK_{Ca} *corresponds to* $K_{Ca,X\%\ PE}$ *-* $K_{Ca,0\%\ PE}$ *where X is the mole fraction of PE in the bilayer. F.)* K_{Ca} *in DOPC, 4:1 (w/w) DOPC:DOPE and 4:1 or 9:1 (w/w) DOPC:DOPS. Error bars in B,C,E and F represent the standard error of three or more separate reconstitutions. For points where error bars are not visible they are smaller than the symbol.*

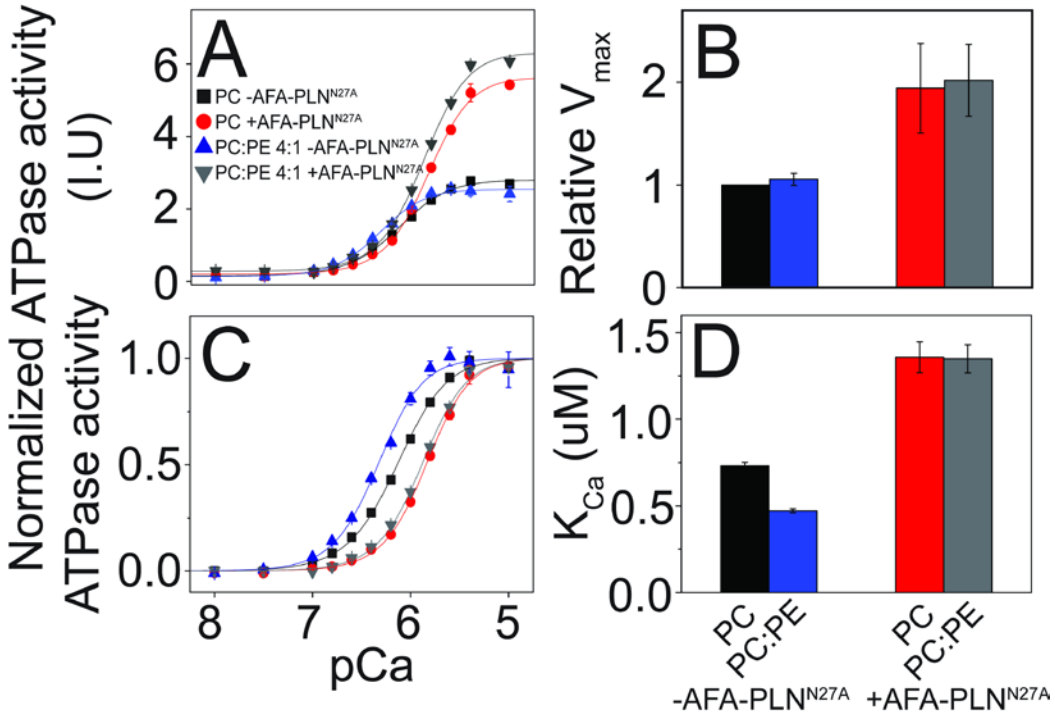

Figure 4. Inhibition of SERCA by AFA-PLNN27A in bilayers with different head group composition. *A,C.) Representative curves of raw and normalized SERCA activity in DOPC and 4:1 (w/w) DOPC:DOPE in the absence and presence of a 10-fold molar excess of AFA-PLN^{N27A}. Each point shows the average and standard error of three measurements, for some points the error bar is smaller than the symbol. B.) Average V_{max} in DOPC and 4:1 (w/w) DOPC:DOPE in the presence and absence of AFA-PLN^{N27A} Values are reported relative to the value in DOPC. D.) Averaged K_{Ca} values. Error bars in B.) and D.) represent the standard error of three or more separate reconstitutions.*

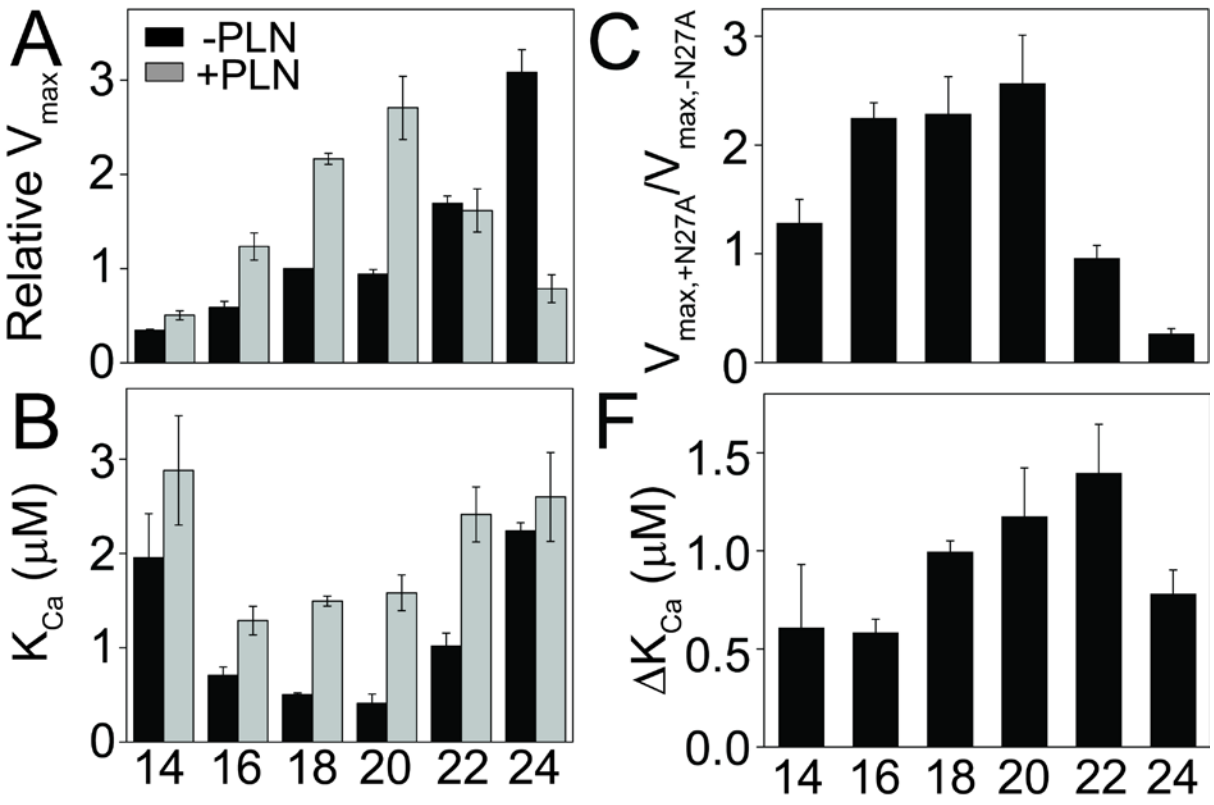

Figure 5. Effects of AFA-PLNN27A on SERCA Vmax and KCa in bilayers of varying thickness composed of 4:1 *(w/w) 14:1 - 20:1$^{\Delta 9\text{-}Cis}$ PC:DOPE. A, B.) V_{max} values relative to 4:1 (w/w) DOPC:DOPE in the absence and presence of AFA-PLN$_{N27A}$. C.) SERCA Vmax change caused by AFA-PLN$_{N27A}$ measured as $V_{max,+AFA\text{-}PLNN27A}$ / $V_{max,-AFA\text{-}PLNN27A}$, D, E.) K_{Ca} values in the absence and presence of AFA-PLN^{N27A}. F.) K_{Ca} change due caused by AFA-PLN^{N27A} and measured as $\Delta K_{Ca} = K_{Ca,+AFA\text{-}PLNN27A} - K_{Ca,-AFA\text{-}PLNN27A}$. The error bars represent standard error for ≥3 separate reconstitutions.*

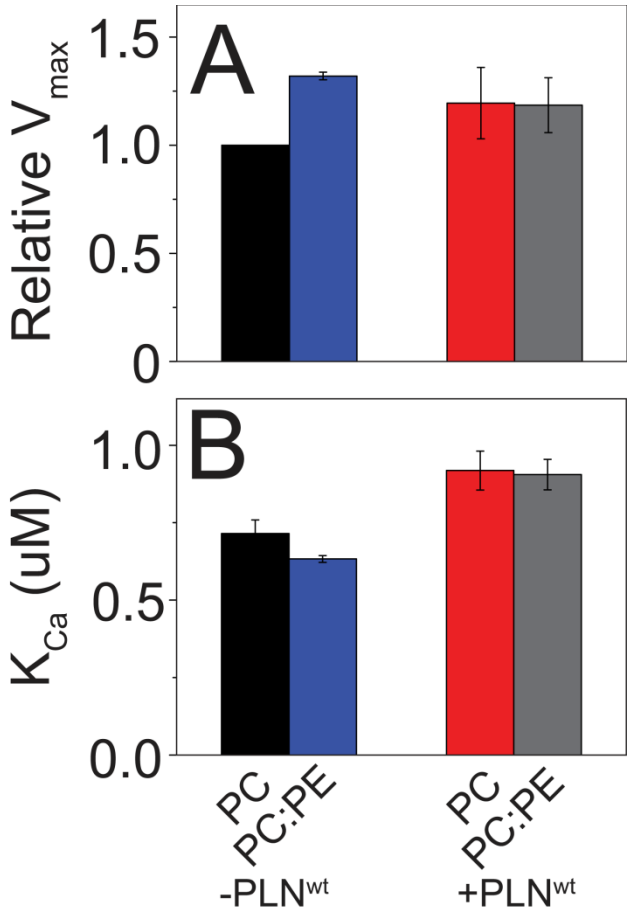

Figure 6. Lipid effects on SERCA and PLNwt at a physiological lipid concentration. *SERCA activity in samples reconstituted with a lipid:PLN^{wt}:SERCA molar ratio of 150:5:1. A.) Average V_{max} in the presence and absence of PLN^{wt} in DOPC and 4:1 (w/w) DOPC:DOPE. V_{max} is relative to the value in DOPC. B.) Averaged K_{Ca} values. All error bars represent the standard error of three separate reconstitutions.*

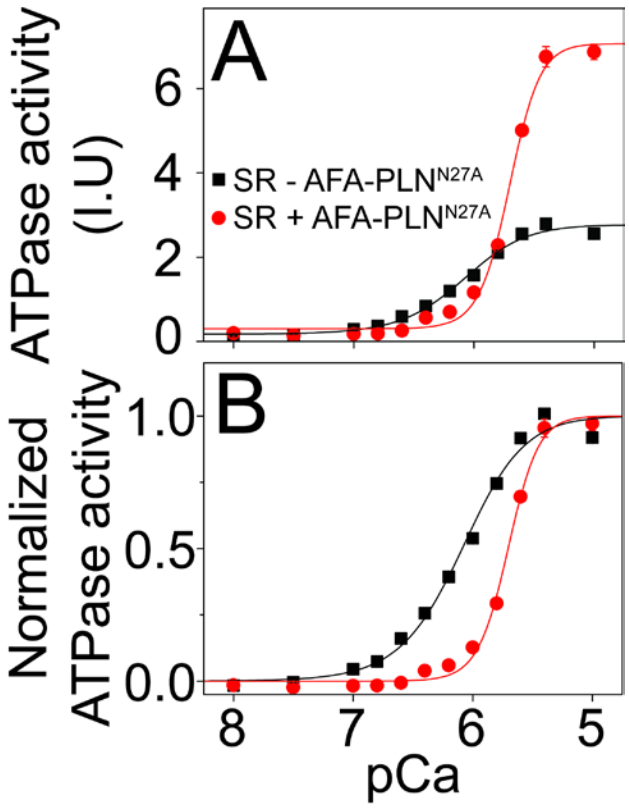

Figure 7. SERCA and PLN in native lipids. *SERCA ATPase activity and AFA-PLN^{N27A} regulation with proteins reconstituted into lipids extracted from rabbit skeletal muscle SR. A.) Raw activity. B.) Normalized values. Error bars display the standard error of three measurements and are smaller than the symbol for several of the data points.*

Chapter 7- Phospholamban Excited State Control of SERCA Revealed by Paramagnetic Relaxation Enhancements and Solid-State NMR

The membrane protein complex between the sarcoplasmic reticulum (SR) Ca^{2+}-ATPase (SERCA) and phospholamban (PLN) regulates Ca^{2+} transport in the SR, thereby controlling cardiac contractility. Using a combination of asymmetric isotopic and spin labeling techniques in concert with magic angle spinning NMR spectroscopy, we mapped the physical interactions between PLN and SERCA in membrane bilayers and revealed the molecular mechanisms of the regulatory cycle. When bound to SERCA, the PLN transmembrane domain remains anchored to the ATPase, while the cytoplasmic domain populates a helical T state and an unfolded R state. The T state remains embedded onto the bilayer surface, whereas the R state interacts transiently with the enzyme's nucleotide binding and phosphorylation domains, forming a *fuzzy complex*. We conclude that conformational equilibrium of PLN is central to SERCA regulation and maintains Ca^{2+} concentration within a physiological range. These results reveal that SERCA function is controlled by conformationally excited state of PLN and explain why biasing the population of the excited state generates loss-of-function mutants of PLN. The methodological advances described here further open the landscape to conducting structural studies of membrane protein complexes of molecular weights beyond 100 kDa.

7.1 Introduction

The SERCA/PLN complex regulates Ca^{2+} translocation into the sarcoplasmic reticulum (SR) of cardiomyocytes and constitutes the main mechanism of cardiac relaxation (diastole). (1-4) SERCA is a P-type ATPase that translocates 2 Ca^{2+} ions per ATP molecule hydrolyzed in exchange of 3 H^+.(5) The enzyme is organized into a multi-span transmembrane (TM) ion channel, comprising ten helical segments and a large cytoplasmic region with three structural domains: nucleotide binding domain (N), actuator domain (A), and phosphorylation domain (P). (5, 6) PLN is the endogenous inhibitor of the ATPase, with a helical TM region (divided into a hydrophilic domain Ib and hydrophobic domain II) anchored to SERCA's TM domain, and an amphipathic region (domain Ia), harboring the recognition sequence for cAMP-dependent protein

kinase A (PKA). (3, 7, 8) Upon β-adrenergic stimulation, PKA phosphorylates PLN at Ser 16, reversing its inhibitory action and augmenting Ca^{2+} transport into the SR. Phosphorylation is reversed by protein phosphatase 1, which reinitiates the cycle (8). Disruptions in SERCA regulation by PLN degenerate into Ca^{2+} mishandling and lead to heart failure. (3)

Although several X-ray structures of SERCA have been determined along the enzymatic coordinates (5, 6, 9, 10), the high-resolution structure of the SERCA/PLN complex is still missing, and more importantly, the atomic details of the regulatory process remain unknown. Although informative, cryo-EM studies have offered low-resolution images of PLN within the complex (11, 12). Mutagenesis and cross-linking data suggest that PLN inhibitory region is positioned into a binding groove located between the TM helices M2, M4, M6 and M9 of SERCA. (13-16) These studies also suggested that PLN domain Ia binds SERCA's N-domain in a α-helical conformation, supporting a 'folding upon binding' mechanism. (13)

In the absence of SERCA, PLN undergoes a conformational equilibrium. The α–helical domain II of PLN is relatively rigid and membrane-embedded, while the cytoplasmic domains Ia, Ib, and the intervening loop are dynamic and more solvent exposed. (17, 18) Importantly, the amphipathic domain Ia is metamorphic, adopting a helical structure when in contact with membrane (T or ground state) and becoming unfolded when detached (R or excited state). (19-24) These ground and excited states have been detected both in synthetic and natural SR lipid membranes. (21, 23) On average, the *L-shaped* T state is the most populated in either monomeric or pentameric PLN. (25, 26), with the R state accounting for 16-20% of the overall population. (27) To date, however, the significance of PLN conformational equilibrium and the role of the excited state in the context of enzymatic regulation have remained elusive.

Here, we used a combination of asymmetric isotopic and spin-labeling schemes to characterize the conformational equilibrium for the SERCA/PLN complex and elucidate the role of the R state in the regulatory mechanism. We found that upon complex formation, the T state of PLN remains embedded on the surface of the lipid membrane, while the R state transiently interacts with the cytoplasmic domain of the enzyme,

reversing the inhibition. PLN domain Ia binds SERCA in an unfolded and dynamic conformation, which reverses the inhibitory action. Taken with our biological assays, these results show that PLN conformational equilibrium plays a central role in SERCA regulation and Ca^{2+} homeostasis, and at the same time, explain why shifting PLN conformational equilibrium (*i.e.*, promoting the excited R state) via site specific mutagenesis reverses SERCA inhibition. (21, 28) Biasing the conformational equilibrium of PLN toward the excited state represents a new paradigm for rational design of inotropic gene therapies with PLN loss-of-function mutants to ameliorate heart muscle disease (29).

7.2 Results and discussion

7.2.1 SERCA selects the R state conformation of PLN domain Ia

Unfolding studies show that the cytoplasmic domain of PLN can occupy at least four different conformational states: a T state, membrane-associated and helical; a T' state, membrane-associated and partially helical, an R' state, membrane-associated and unfolded; and an R state, solvent exposed and completely unfolded. While the T' and R' states are detectable for PLN reconstituted in dodecylphosphocholine micelles, the T and R are the most populated states both in synthetic and SR lipid membranes (23). Importantly, the conformational equilibrium of PLN persists in the presence of SERCA (19, 22), which upon binding modulates the relative populations of the T and R states. To map the conformational equilibrium in lipid membranes at the atomic level and understand the role of the excited R state, we used magic angle spinning (MAS) NMR spectroscopy. We co-reconstituted SERCA with isotopically labeled, monomeric PLN (PLN^{AFA} carrying C36A, F41F, and C46A mutations) into egg yolk phosphatidylcholine/phosphatidylethanolamine/phosphatidic acid (PC/PE/PA) lipid vesicles (8:1:1 molar ratio) at a 150:1:1 lipid:SERCA:PLN^{AFA} molar ratio. This lipid composition closely mimics the head group and lipid chain composition of the SR (30) and fully preserves SERCA's function as well as its native interactions with PLN as confirmed by enzyme coupled assays and fluorescence resonance energy transfer (FRET) (**Figure S1**). Using MAS dipolar assisted rotational resonance (DARR)

experiments (31), we found that, with the exception of Asn 34, which consistently showed a > 1 ppm perturbation in both synthetic and recombinant samples, the Cα resonances corresponding to the TM domain II and domain Ib remain mostly unperturbed when bound to the enzyme (**Figure S2,S3**). In contrast, the methyl resonances of the TM domains show significant chemical shift perturbations. In particular, Ile 38 and Leu 42, which were predicted to be cofacial to the TM residues of the ATPase, change chemical shift in the presence of the ATPase (**Figure 1**). (13) For several residues belonging to PLN cytoplasmic domain Ia, we observed two distinct populations, corresponding to chemical shifts for helical and unfolded conformations, which we assigned to the T and R states, respectively (**Figure 2**). The relative intensity (population) of the resonances corresponding to the two states changes as a function of the temperature, demonstrating the presence of a conformational exchange in the slow regime of the NMR time scale (**Figure S4**). The chemical shifts of PLN's T state are similar both in the free and SERCA-bound forms (**Figure S3**). In contrast, the presence of the ATPase causes large chemical shift perturbations for residues in the R state (**Figure S3**). In particular, SERCA binding shifts the resonance corresponding to the C_α chemical shift of Leu 7 by approximately 1 ppm (**Figure 2B**). Remarkably, the chemical shifts of the bound R state are indicative of a random coil conformation, showing that the interaction with SERCA does not induce the previously proposed helical conformation of domain Ia (13, 24). The latter excludes the previously proposed mechanism of 'folding upon binding' suggested on the basis of molecular modeling and NMR spectroscopy (13, 24) Based on these results, we conclude that a) SERCA binds PLN with the inhibitory TM domain II and domain Ib in a helical conformation, b) the T state of the cytoplasmic domain does not interact with the enzyme, and c) the R state of domain Ia binds SERCA in an unfolded and dynamic conformation.

7.2.2 Mapping of SERCA/PLN interactions by PREs

To map the physical interactions between PLN^{AFA} and SERCA, we utilized paramagnetic relaxation enhancements (PREs) measured by MAS NMR spectroscopy. For our studies, we used a combination of asymmetric isotopic and spin-labeling schemes which are summarized in **Figure S5**. First, we engineered a TEMPO spin label on SERCA at

Cys 674 ($SERCA^{C674SL}$). This residue is situated in the P-domain of the enzyme and is an ideal reporter for SERCA/PLN interactions.(32). Next, we reconstituted $SERCA^{C674\text{-}sl}$ with uniformly or selectively ^{13}C-labeled PLN^{AFA} (33). Using ^{13}C-^{13}C DARR experiments, we mapped the PRE effects on PLN by monitoring the intensities of the ^{13}C resonances of PLN^{AFA}. Since the T to R conformational equilibrium is slow, we monitored the PRE effects on the two peak populations, simultaneously. The spin-label positioned in the cytoplasmic P-domain of SERCA did not affect the PLN^{AFA} residues in the TM domains Ib and II (**Figure S6**). In contrast, several resonances of domain Ia in the R state were selectively quenched relative to the T state (**Figure 3**). Since the R state is more dynamic, it can be detected using refocused INEPT (Insensitive Nuclei Enhanced by Polarization Transfer, rINEPT) experiments (34). The rINEPT experiment filters out the resonances associated with the rigid T state as well as residues in domain Ib and II, and detects only the most mobile residues of PLN (23, 35). Remarkably, the intensities of several resonances in domain Ia are significantly reduced upon formation of the $SERCA^{C674sl}$/PLN^{AFA} complex (**Figures 4 and S7**). The most affected residues are located in the middle of domain Ia, with Tyr 6 and Leu 7 almost completely quenched. The latter demonstrates that these residues in the complex are near SERCA's P domain. In contrast, residues located at both the C- and N-terminal regions of domain Ia (Ala 0, Met 1, Met 20, and Pro 21) remain largely unperturbed (**Figure 4C**). A different quenching pattern is observed when PLN^{AFA} is bound to SERCA labeled with 4-maleimido-TEMPO at both Cys 344 (P domain) and Cys 364 (N domain) ($SERCA^{C344C364\text{-}sl}$) (36) (**Figure 4**). Upon $SERCA^{C344C364\text{-}sl}$/$PLN^{AFA}$ complex formation, several resonances spanning the central region of domain Ia are quenched, with the exception of residues located at both N- and C-terminal ends of domain Ia. The most prominent PRE effect was registered for the C_γ resonance of Lys 3 ($I/I_0 \sim 0.45$). This PRE pattern is consistent with the effects observed for $SERCA^{C674\text{-}sl}$, supporting that the R state is located near the P and N domains of SERCA. Interestingly, the proximity of Cys 364 to Lys 397 and the strong reduction of Lys 3 peak intensity agrees with previous reports of a crosslink formation between Lys 397/400 of SERCA and Lys 3 of PLN^{AFA} .(37)

7.2.3 PRE effects of PLN^{-sl} on methyl-labeled SERCA

To monitor the PRE effects of PLN on SERCA, we engineered an MTSSL spin label at residue 7 of PLN^{AFA} (PLN^{AFA-sl}) and labeled SERCA extracted from mammalian tissues with ^{13}C- methyl methanethiosulfonate (MMTS) (38). This reagent reacts with SERCA native cysteines, forming methyl thiocysteines (MTC). MTC-labeled SERCA (MTC-SERCA) retains ~80% ATPase activity as determined by coupled enzyme activity assays (**Figure S8**) (39). To assess the MTC labeling of the SERCA cysteines, we reconstituted MTC-SERCA in DPC detergent micelles and acquired a [^{1}H,^{13}C]-HSQC spectrum. The spectrum shows six resolved resonances, corresponding to six of the most accessible cysteines of SERCA (**Figure 5A,B**). We co-reconstituted the MTC-SERCA with PLN^{AFA-sl} in 1,2-dimyristoyl-sn-glycero-3-phosphocholine (DMPC) lipid vesicles. The methyl group signals from MTC-SERCA, were detected using conventional and water-edited cross-polarization (CP) experiments (40) in the presence of reduced and oxidized PLN^{AFA-sl}. A single unresolved peak for all of the 6 labeled sites is observed at approximately 25 ppm (**Figure 5C**). The water-edited CP eliminates most of the lipid background and enhances the peak envelope corresponding to the MTC groups. Upon binding, PLN^{AFA-sl} significantly reduces the intensity of the methyl peaks of MTC-SERCA in both types of experiments and reduction of the spin label reverses this effect, demonstrating that upon interaction with SERCA, the cytoplasmic region of PLN reaches up to the N- and P domains of SERCA. Although at this stage we cannot resolve the methyl group resonances of MTC-SERCA in the NMR spectra, these data confirm and complement the mapping of PRE on the PLN backbone.

7.2.4 Mapping Lipid Association of the SERCA/PLN complex

Since no PRE effects were detected for the T state resonances, we deduced that the amphipathic T state helix is bilayer associated in the SERCA/PLN complex. To substantiate this conclusion, we used rINEPT experiments to measure PRE effects from the SERCA/PLN^{AFA-sl} complex to the ^{13}C resonances of the lipid bilayer. The plot of the ^{13}C resonance intensities show a bimodal distribution, with a significant reduction of the ^{13}C resonances for the lipid chain and head groups, with the glycerol region of the lipids virtually unaffected by PLN^{AFA-sl} (**Figure 6A**). These data show that the nitroxide spin

label in the T state must be deeply embedded into the membrane to quench the hydrocarbon resonances of the lipids. On the other hand, the reduction of the peak intensities corresponding to the head groups can be explained by transient interactions of the nitroxide in the R state with the surface of the lipid bilayer. To further support lipid association of the T state of PLN, we engineered a PE head group with a nitroxide spin-label (PE^{sl}, 1,2-dioleoyl-sn-glycero-3-phosphoethanolamine-N-amido-TEMPO, **Figure S9**) and measured PRE from PE^{sl} to selectively ^{13}C-labeled PLN^{AFA} in complex with SERCA. The nitroxide spin label of PE^{sl} is localized in the glycerol region of the lipid bilayer, as shown in **Figure S10**. We found that PE^{sl} quenches the T state resonances of domain Ia (**Figure 6B**), further validating that these residues must be embedded on the surface of the lipid membrane.

7.2.5 SERCA/PLN complex and conformational equilibrium

Trapping the SERCA/PLN complex in a defined, crystallizable state has been challenging. Although cryo-EM data provided critical information on the SERCA/PLN complex (11, 12) they offer low resolution images and do not make it possible to distinguish secondary structure and membrane architecture within the complex. A more defined model was provided by mutagenesis, biochemical, computational, as well as solid-state NMR data (24). The resulting overall architecture of the complex is very similar to previous molecular modeling studies carried out by Toyoshima and co-workers (13). The helical domains Ib and II were docked to the putative PLN binding groove defined by mutagenesis. The loop bridging the TM and cytoplasmic domain were modeled in an unfolded configuration, stretching toward the N-domain of SERCA to satisfy the cross-linking data from Lys 3 of PLN to Lys 397 of SERCA.(37). PLN domain Ia was modeled in a α-helical conformation docked into SERCA's N domain. For both models, SERCA/PLN contacts were based only on co-immunoprecipitation and cross-linking assays. In contrast, the combination of PRE effects and MAS NMR spectroscopy on asymmetrically labeled proteins presented here enable us to map the transient interactions between these two membrane proteins. Importantly, all the spectroscopic measurements were carried out in lipid membranes that accurately mimic the natural bilayer. We found that PLN conformational equilibrium persists in the presence of

SERCA, which upon binding shifts the pre-existing conformational equilibrium towards the excited state of PLN. The positioning of domain Ia differs from the predicted models (13, 24), with the unfolded domain Ia reaching out and binding the cytoplasmic region of SERCA close to Cys 674 and Cys 344 as well as Cys 364 (**Figure 4**). In the Toyoshima model, Tyr6 and Leu7 residues are approximately 31 and 29 Å away from Cys 674.(13) In contrast, the PRE data show that the Tyr6$_{\varepsilon 1}$ and Leu7$_{\delta 2}$ resonances are almost completely quenched by the spin-label at Cys 674 of SERCA (**Figure 4B**), probing significantly shorter distances. Importantly, domain Ia does not 'fold upon binding', as previously reported; rather, it remains in an unfolded and dynamic conformation in the bound form, as demonstrated by the ^{13}C chemical shift index probed by rINEPT experiments. In contrast, the T state of domain Ia remains largely unperturbed by SERCA, but interacts strongly with the membrane bilayer (**Figure 6**). The SERCA/PLN complex exemplifies transient, low-affinity encounter complexes ('fuzzy complexes') (41, 42) that been found in several signaling membrane protein complexes. (43) *For the SERCA/PLN complex, we can speculate that the presence of the conformational equilibrium explain the reversibility of the inhibitory action to enable cyclic translocation of Ca^{2+} ions, contributing to the coupled cardiac contraction and relaxation processes.*

The presence of PLN conformational equilibrium within the SERCA/PLN complex was not apparent in the previous solid-state NMR studies, which were performed in a temperature range of 235-270K.(24) Under these conditions, PLN populates predominantly the helical T state and the R state is virtually invisible. (23) In this study, we covered a range of temperatures close to the physiological conditions for SERCA function (277-293K), where NMR and EPR spectroscopy detect both the T and R states (22, 23).

7.2.6 Excited state control and physiological window of SERCA regulation

Based on our findings and previous studies, we propose that the equilibrium between the T and R state corresponds to the *inhibitory* and *non-inhibitory* states of PLN that determine SERCA's physiological window of inhibition (**Figure 7A**) (44). In the T state, PLN interacts with SERCA only via the TM domain with domain Ia laying on the surface

of the lipid bilayer. In the R state, the TM domain of PLN is still bound to SERCA (as supported by methyl chemical shifts (**Figure 1**) and fluorescence studies (45)), and domain Ia interacts with the P and N domains of SERCA. According to this model, the cytoplasmic domain Ia would reduce the inhibitory potency of PLN, which is further reduced upon phosphorylation. To support our conclusions, we co-reconstituted SERCA with a truncated version of PLN^{AFA}, corresponding to domains Ib and II (PLN^{AFA}_{23-52}) and analyzed its function using coupled enzyme assays. As predicted by our model, the deletion of the regulatory domain Ia resulted in a more inhibitory species than full length PLN^{AFA}. (**Figure 7B,C**). Furthermore, phosphorylation of PLN^{AFA} at Ser 16 ($PLN^{pS16AFA}$) completely reverses inhibition of SERCA (22, 23, 28).

From the physiological window model, it emerges that PLN does not work as a simple on/off switch for Ca^{2+} translocation; rather its conformational equilibrium exerts a gradual control ('physiological rheostat') on SERCA activity. If SERCA's apparent Ca^{2+} affinity exceeds the physiological window, the heart muscle enters a pathological state, leading to cardiomyopathy. (46) An analogous situation occurs if SERCA's apparent Ca^{2+} affinity is drastically reduced. In this scenario, the correct balance between T and R state ensures that SERCA inhibition occurs within the physiological window. PLN phosphorylation at Ser16 by protein kinase A skews the conformational ensemble toward the excited state, increasing SERCA's apparent Ca^{2+} affinity, and augmenting the contractility within the physiological window. In contrast, aberrant or lack of PLN phosphorylation causes SERCA's activity to be outside the physiological window, degenerating Ca^{2+} handling (47, 48). The conformational ensemble model of SERCA regulation by PLN fully explains our recent structural-dynamic-function correlations. In fact, we found that by promoting PLN R state, it is possible to augment SERCA function. (21, 28). Specifically, we reported that PLN point mutations inducing membrane detachment or unfolding of domain Ia decrease SERCA inhibition, with an effect similar to phosphorylation. Controlling Ca^{2+} trafficking in cardiomyocytes is emerging as a new possible avenue to treat heart failure (3, 49-52). In addition to SERCA overexpression (51), Ca^{2+} transport can be augmented by engineering loss-of-function (*i.e.*, dominant-negative) mutants of PLN (49). The rational design of dominant-negative mutants of PLN

will be possible by engineering mutations that bias PLN conformational equilibrium toward the excited state.

In conclusion, we used MAS NMR and PRE effects to map the interactions between SERCA and PLN in a dynamic complex. We found that the ensemble of conformations (ground and excited states), rather than one unique state of PLN, contributes to SERCA regulation. Unlike previously proposed models, we found that PLN cytoplasmic domain binds SERCA in an unfolded conformation, which forms transient interactions with both P and N domains of the ATPase. The presence of PLN conformational equilibrium between a fully inhibitory T state and a non-inhibitory R state underscores an excited state control of PLN over SERCA function. At the same time, these results explain why the promotion of the R state via point mutations generates loss-of-function variants of PLN. These mutants are ideal candidates for modulating SERCA function and represent a possible new avenue for protein therapy to reverse heart failure by fine tuning Ca^{2+} transport. Finally, we point out that the analysis of membrane protein-protein complexes is particularly challenging for the current approaches of structural biology (53, 54). Our approach involving multiple PRE mapping (enzyme-inhibitor, inhibitor-enzyme, inhibitor-lipid, lipid-inhibitor) used for SERCA/PLN^{AFA} complex is a powerful method to define the topology and map the interactions and conformational equilibrium of membrane protein complexes in their native lipid environment.

7.3 Experimental details

All unlabeled lipids were purchased from Avanti Polar Lipids (Alabaster, AL). Spin labeled sl-PE lipid was synthesized by attaching a TEMPO spin label to the head groups of PE lipids (see Supplementary Information). SERCA Ia was purified from hind-leg rabbit skeletal muscle as previously described, eluting the protein either in $C_{12}E_8$ (55) or DPC (19). Recombinant PLN^{AFA} was expressed and purified according to Buck et al. (33) with uniform ^{13}C,^{15}N labeling or with amino acid specific labeling achieved by utilizing reverse labeling schemes (23, 56). Synthesis of PLN^{AFA} and PLN^{AFA}_{23-52} was done using a microwave synthesizer (CEM) as described elsewhere (22, 23, 25). sl-PLN^{AFA} was produced as previously described (57). All PLN^{AFA} preparations were tested for inhibitory

activity on SERCA using a coupled-enzyme assay as described previously (28, 39). MAS samples were prepared by reconsitituting SERCA and PLN^{AFA} in lipid vesicles (see Supplementary Information for details). The final sample contained >60% bulk water with a lipid:SERCA:PLN molar ratio of 150:1:1. MAS NMR experiments were performed on Varian (VNMRS) spectrometers operating at proton frequencies of 600 and 700 MHz and equipped with $^{1}H/^{13}C$ 3.2 mm BioMAS Varian probes.

7.4 References

1. Bers, D. M. 2002. Cardiac excitation-contraction coupling. Nature. 415, 198-205.

2. Brini, M. and E. Carafoli 2009. Calcium pumps in health and disease. Physiol. Rev. 89, 1341-1378.

3. MacLennan, D. H. and E.G. Kranias 2003. Phospholamban: A crucial regulator of cardiac contractility. Nat Rev Mol Cell Biol. 4, 566-77.

4. Simmerman, H. K. and L.R. Jones 1998. Phospholamban: Protein structure, mechanism of action, and role in cardiac function. Physiol Rev. 78, 921-47.

5. Moller, J. V., C. Olesen, A.M. Winther and P. Nissen 2010. The sarcoplasmic Ca2+-ATPase: Design of a perfect chemi-osmotic pump. Q. Rev. Biophys. 43, 501-566.

6. Toyoshima, C., M. Nakasako, H. Nomura and H. Ogawa 2000. Crystal structure of the calcium pump of sarcoplasmic reticulum at 2.6 A resolution. Nature. 405, 647-55.

7. Simmerman, H. K., J.H. Collins, J.L. Theibert, A.D. Wegener and L.R. Jones 1986. Sequence analysis of phospholamban. identification of phosphorylation sites and two major structural domains. J Biol Chem. 261, 13333-41.

8. Wegener, A. D., H.K. Simmerman, J.P. Lindemann and L.R. Jones 1989. Phospholamban phosphorylation in intact ventricles. phosphorylation of serine 16 and threonine 17 in response to beta-adrenergic stimulation. Journal Biological Chemistry. 264, 11468-11474.

9. Toyoshima, C. and H. Nomura 2002. Structural changes in the calcium pump accompanying the dissociation of calcium. Nature. 418, 605-11.

10. Olesen, C., T.L. Sorensen, R.C. Nielsen, J.V. Moller and P. Nissen 2004. Dephosphorylation of the calcium pump coupled to counterion occlusion. Science. 306, 2251-2255.

11. Stokes, D. L., A.J. Pomfret, W.J. Rice, J.P. Glaves and H.S. Young 2006. Interactions between Ca2+-ATPase and the pentameric form of phospholamban in two-dimensional co-crystals. Biophys. J. 90, 4213-4223.

12. Young, H. S., L.R. Jones and D.L. Stokes 2001. Locating phospholamban in co-crystals with ca(2+)-ATPase by cryoelectron microscopy. Biophys J. 81, 884-94.

13. Toyoshima, C., M. Asahi, Y. Sugita, R. Khanna, T. Tsuda and D.H. MacLennan 2003. Modeling of the inhibitory interaction of phospholamban with the Ca2+ ATPase. Proc Natl Acad Sci U S A. 100, 467-72.

14. Asahi, M., N.M. Green, K. Kurzydlowski, M. Tada and D.H. MacLennan 2001. Phospholamban domain IB forms an interaction site with the loop between transmembrane helices M6 and M7 of sarco(endo)plasmic reticulum Ca2+ ATPases. Proc Natl Acad Sci U S A. 98, 10061-6.

15. MacLennan, D. H., Y. Kimura and T. Toyofuku 1998. Sites of regulatory interaction between calcium ATPases and phospholamban. Ann N Y Acad Sci. 853, 31-42.

16. Jones, L. R., R.L. Cornea and Z. Chen 2002. Close proximity between residue 30 of phospholamban and cysteine 318 of the cardiac Ca2+ pump revealed by intermolecular thiol cross-linking. J Biol Chem. 277, 28319-29.

17. Traaseth, N. J. and G. Veglia 2010. Probing excited states and activation energy for the integral membrane protein phospholamban by NMR CPMG relaxation dispersion experiments. Biochim. Biophys. Acta. 1798, 77-81.

18. Metcalfe, E. E., J. Zamoon, D.D. Thomas and G. Veglia 2004. (1)H/(15)N heteronuclear NMR spectroscopy shows four dynamic domains for phospholamban reconstituted in dodecylphosphocholine micelles. Biophys. J. 87, 1205-1214.

19. Zamoon, J., F. Nitu, C. Karim, D.D. Thomas and G. Veglia 2005. Mapping the interaction surface of a membrane protein: Unveiling the conformational switch of phospholamban in calcium pump regulation. Proc. Natl. Acad. Sci. U. S. A. 102, 4747-4752.

20. Karim, C. B., T.L. Kirby, Z. Zhang, Y. Nesmelov and D.D. Thomas 2004. Phospholamban structural dynamics in lipid bilayers probed by a spin label rigidly coupled to the peptide backbone. Proc Natl Acad Sci U S A. 101, 14437-42.

21. Gustavsson, M., N.J. Traaseth, C.B. Karim, E.L. Lockamy, D.D. Thomas and G. Veglia 2011. Lipid-mediated Folding/Unfolding of phospholamban as a regulatory mechanism for the sarcoplasmic reticulum ca(2+)-ATPase. J. Mol. Biol. 408, 755-765.

22. Karim, C. B., Z. Zhang, E.C. Howard, K.D. Torgersen and D.D. Thomas 2006. Phosphorylation-dependent conformational switch in spin-labeled phospholamban bound to SERCA. J. Mol. Biol. 358, 1032-1040.

23. Gustavsson, M., N.T. Traaseth and G. Veglia 2011. Probing ground and excited states of phospholamban in model and native lipid membranes by magic angle spinning NMR spectroscopy. Biochim. Biophys. Acta. 1818.

24. Seidel, K., O.C. Andronesi, J. Krebs, C. Griesinger, H.S. Young, S. Becker and M. Baldus 2008. Structural characterization of ca(2+)-ATPase-bound phospholamban in lipid bilayers by solid-state nuclear magnetic resonance (NMR) spectroscopy. Biochemistry. 47, 4369-4376.

25. Traaseth, N. J., L. Shi, R. Verardi, D.G. Mullen, G. Barany and G. Veglia 2009. Structure and topology of monomeric phospholamban in lipid membranes determined by a hybrid solution and solid-state NMR approach. Proc. Natl. Acad. Sci. U. S. A. 106, 10165-10170.

26. Verardi, R., L. Shi, N.J. Traaseth, N. Walsh and G. Veglia 2011. Structural topology of phospholamban pentamer in lipid bilayers by a hybrid solution and solid-state NMR method. Proc Natl Acad Sci U S A. 108, 9101-9106.

27. Nesmelov, Y. E., C.B. Karim, L. Song, P.G. Fajer and D.D. Thomas 2007. Rotational dynamics of phospholamban determined by multifrequency electron paramagnetic resonance. Biophys. J. 93, 2805-2812.

28. Ha, K. N., N.J. Traaseth, R. Verardi, J. Zamoon, A. Cembran, C.B. Karim, D.D. Thomas and G. Veglia 2007. Controlling the inhibition of the sarcoplasmic Ca2+-ATPase by tuning phospholamban structural dynamics. J. Biol. Chem. 282, 37205-37214.

29. Kairouz, V., L. Lipskaia, R.J. Hajjar and E.R. Chemaly 2012. Molecular targets in heart failure gene therapy: Current controversies and translational perspectives. Ann. N. Y. Acad. Sci. 1254, 42-50.

30. Bick, R. J., L.M. Buja, W.B. Van Winkle and G.E. Taffet 1998. Membrane asymmetry in isolated canine cardiac sarcoplasmic reticulum: Comparison with skeletal muscle sarcoplasmic reticulum. J. Membr. Biol. 164, 169-175.

31. Takegoshi, K., S. Nakamura and T. Terao 2001. 13C–1H dipolar-assisted rotational resonance in magic-angle spinning NMR. Chem. Phys. Lett. 344, 631.

32. Mueller, B., C.B. Karim, I.V. Negrashov, H. Kutchai and D.D. Thomas 2004. Direct detection of phospholamban and sarcoplasmic reticulum ca-ATPase interaction in membranes using fluorescence resonance energy transfer. Biochemistry. 43, 8754-65.

33. Buck, B., J. Zamoon, T.L. Kirby, T.M. DeSilva, C. Karim, D. Thomas and G. Veglia 2003. Overexpression, purification, and characterization of recombinant ca-ATPase regulators for high-resolution solution and solid-state NMR studies. Protein Expr Purif. 30, 253-61.

34. Morris, G. A. and R.J. Freeman 1979. Enhancement of nuclear magnetic resonance signals by polarization transfer. J. Am. Chem. Soc. 101, 760-762.

35. Andronesi, O. C., S. Becker, K. Seidel, H. Heise, H.S. Young and M. Baldus 2005. Determination of membrane protein structure and dynamics by magic-angle-spinning solid-state NMR spectroscopy. J. Am. Chem. Soc. 127, 12965-12974.

36. Saito-Nakatsuka, K., T. Yamashita, I. Kubota and M. Kawakita 1987. Reactive sulfhydryl groups of sarcoplasmic reticulum ATPase. I. location of a group which is most reactive with N-ethylmaleimide. J. Biochem. 101, 365-376.

37. James, P., M. Inui, M. Tada, M. Chiesi and E. Carafoli 1989. Nature and site of phospholamban regulation of the Ca2+ pump of sarcoplasmic reticulum. Nature. 342, 90-2.

38. Religa, T. L., A.M. Ruschak, R. Rosenzweig and L.E. Kay 2011. Site-directed methyl group labeling as an NMR probe of structure and dynamics in supramolecular protein systems: Applications to the proteasome and to the ClpP protease. J. Am. Chem. Soc. 133, 9063-9068.

39. Reddy, L. G., R.L. Cornea, D.L. Winters, E. McKenna and D.D. Thomas 2003. Defining the molecular components of calcium transport regulation in a reconstituted membrane system. Biochemistry. 42, 4585-92.

40. Ader, C., R. Schneider, K. Seidel, M. Etzkorn, S. Becker and M. Baldus 2009. Structural rearrangements of membrane proteins probed by water-edited solid-state NMR spectroscopy. J. Am. Chem. Soc. 131, 170-176.

41. Tang, C., J. Iwahara and G.M. Clore 2006. Visualization of transient encounter complexes in protein-protein association. Nature. 444, 383-386.

42. Volkov, A. N., J.A. Worrall, E. Holtzmann and M. Ubbink 2006. Solution structure and dynamics of the complex between cytochrome c and cytochrome c peroxidase determined by paramagnetic NMR. Proc. Natl. Acad. Sci. U. S. A. 103, 18945-18950.

43. Sigalov, A. B. 2011. Uncoupled binding and folding of immune signaling-related intrinsically disordered proteins. Prog. Biophys. Mol. Biol. 106, 525-536.

44. Vangheluwe, P., K.R. Sipido, L. Raeymaekers and F. Wuytack 2006. New perspectives on the role of SERCA2's Ca2+ affinity in cardiac function. Biochim. Biophys. Acta. 1763, 1216-1228.

45. Li, J., Z.M. James, X. Dong, C.B. Karim and D.D. Thomas 2012. Structural and functional dynamics of an integral membrane protein complex modulated by lipid headgroup charge. J. Mol. Biol. 418, 379-389.

46. Haghighi, K., F. Kolokathis, L. Pater, R.A. Lynch, M. Asahi, A.O. Garmolini, G. Fan, D. Tsiapras, H.S. Hahn, S. Adamopoulos, S.B. Liggett, G.W.I. Dorn, D.H. Mac Lennan, D.T. Kremastinos and E.G. Kranias 2003. Human phospholamban null results in lethal dilated cardiomyopathy revealing a critical difference between mouse and human. J Clin Invest. 111, 869-876.

47. Schmidt, A. G., J. Zhai, A.N. Carr, M.J. Gerst, J.N. Lorenz, P. Pollesello, A. Annila, B.D. Hoit and E.G. Kranias 2002. Structural and functional implications of the phospholamban hinge domain: Impaired SR Ca2+ uptake as a primary cause of heart failure. Cardiovasc Res. 56, 248-59.

48. Haghighi, K., A.G. Schmidt, B.D. Hoit, A.G. Brittsan, A. Yatani, J.W. Lester, J. Zhai, Y. Kimura, G.W. Dorn 2nd, D.H. MacLennan and E.G. Kranias 2001. Superinhibition of sarcoplasmic reticulum function by phospholamban induces cardiac contractile failure. J. Biol. Chem. 276, 24145-24152.

49. Hoshijima, M., Y. Ikeda, Y. Iwanaga, S. Minamisawa, M.O. Date, Y. Gu, M. Iwatate, M. Li, L. Wang, J.M. Wilson, Y. Wang, J. Ross Jr and K.R. Chien 2002. Chronic suppression of heart-failure progression by a pseudophosphorylated mutant of phospholamban via in vivo cardiac rAAV gene delivery. Nat. Med. 8, 864-871.

50. del Monte, F., S.E. Harding, G.W. Dec, J.K. Gwathmey and R.J. Hajjar 2002. Targeting phospholamban by gene transfer in human heart failure. Circulation. 105, 904-907.

51. Kawase, Y., D. Ladage and R.J. Hajjar 2011. Rescuing the failing heart by targeted gene transfer. J. Am. Coll. Cardiol. 57, 1169-1180.

52. Schmidt, A. G., I. Edes and E.G. Kranias 2001. Phospholamban: A promising therapeutic target in heart failure? Cardiovasc Drugs Ther. 15, 387-96.

53. von Heijne, G. 2011. Introduction to theme "membrane protein folding and insertion". Annu. Rev. Biochem. 80, 157-160.

54. McDermott, A. 2009. Structure and dynamics of membrane proteins by magic angle spinning solid-state NMR. Annu. Rev. Biophys. 38, 385-403.

55. Stokes, D. L. and N.M. Green 1990. Three-dimensional crystals of CaATPase from sarcoplasmic reticulum. symmetry and molecular packing. Biophys J. 57, 1-14.

56. Tong, K. I., M. Yamamoto and T. Tanaka 2008. A simple method for amino acid selective isotope labeling of recombinant proteins in E. coli. J Biomol NMR. 42, 59-67.

57. Shi, L., N.J. Traaseth, R. Verardi, M. Gustavsson, J. Gao and G. Veglia 2011. Paramagnetic-based NMR restraints lift residual dipolar coupling degeneracy in multidomain detergent-solubilized membrane proteins. J Am Chem Soc. 133, 2232-2241.

58. Zhang, H., S. Neal and D.S. Wishart 2003. RefDB: A database of uniformly referenced protein chemical shifts. J. Biomol. NMR. 25, 173-195.

59. Birmachu, W., F.L. Nisswandt and D.D. Thomas 1989. Conformational transitions in the calcium adenosinetriphosphatase studied by time-resolved fluorescence resonance energy transfer. Biochemistry. 28, 3940-3947.

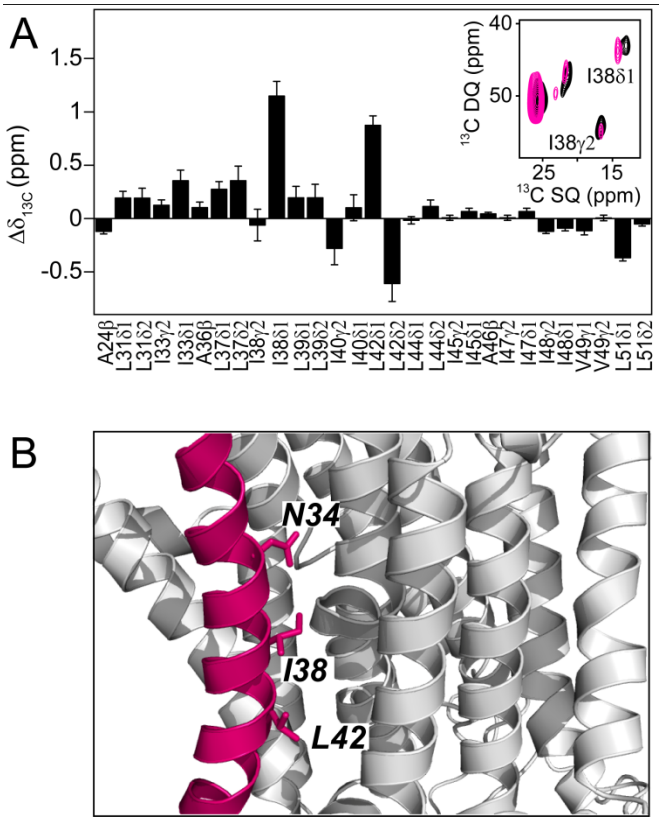

Figure 1. Intramembrane interactions between PLN and SERCA. A) Methyl group chemical shift perturbations in the PLN TM domain measured as $\Delta\delta_{13C} = \delta_{13C+SERCA} - \delta_{13C-SERCA}$*. The inset shows the methyl region of a single quantum double quantum correlation spectrum of* ^{13}*C N34,F35,A36,L37,I38 PLN*^{AFA} *free (black) and in complex with SERCA (pink). B) Transmembrane region of the previously proposed model for the SERCA/PLN interaction.* (13) *PLN residues with large chemical shift perturbations are indicated in the figure. Coordinates of the complex were generously provided by D. H. Maclennan and C. Toyoshima.*

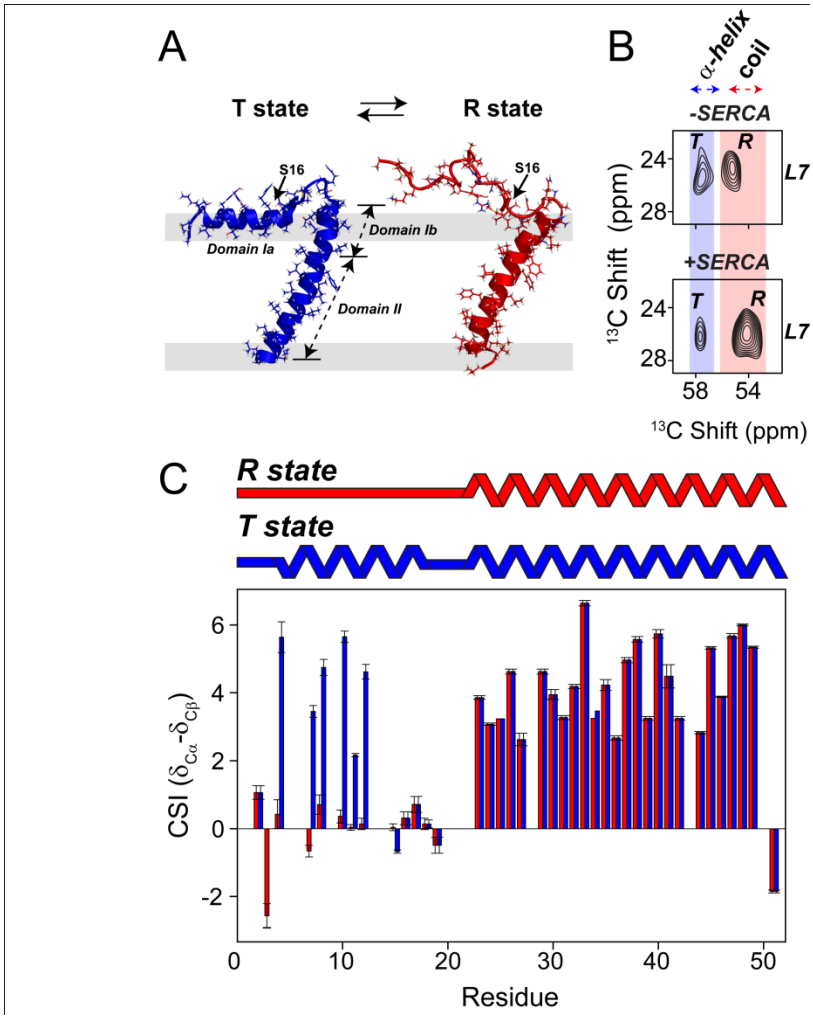

Figure 2. T and R states of PLN in the presence of SERCA. A.) Structures of T and R states of PLN^{AFA}, respectively. B.) Portion of the [^{13}C,^{13}C]-DARR spectrum showing Leu7 C_α-C_δ correlations in the absence (top) and presence (bottom) of SERCA. Blue and red shaded regions indicate helical and coil regions of Leu C_α. C.) Histograms showing C_α-C_β chemical shift index (CSI) for R and T states of PLN in complex with SERCA. The CSI was calculated as $\delta_{13C\alpha}-\delta_{13C\beta}-(\delta_{13C\alpha,RC}-\delta_{13C\beta,RC})$, where RC refers to the random coil chemical shifts. (58) *For residues in domain Ib and II and residues E2, S16, T17, I18 and E19 in domain Ia the peaks corresponding to R and T states are not resolved.*

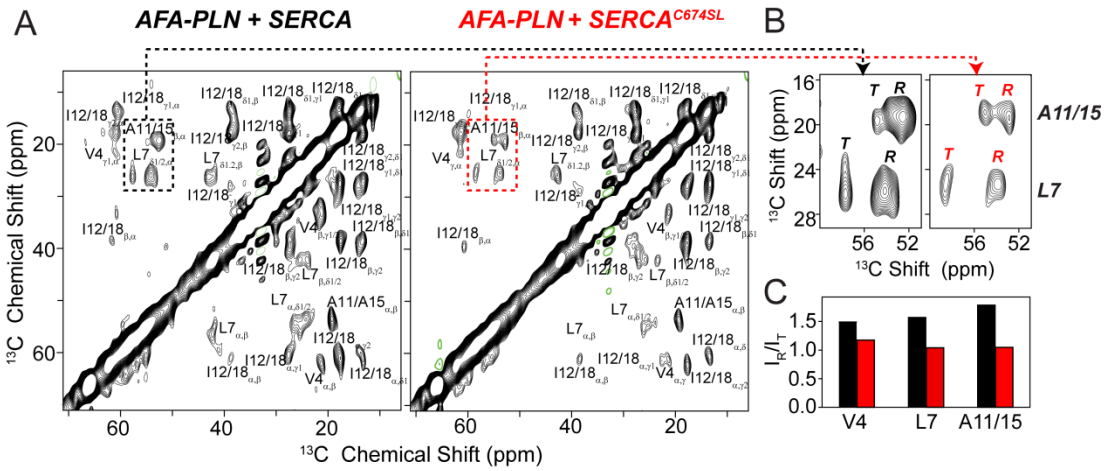

Figure 3. PREs effects from SERCA$^{C674\text{-}sl}$ to PLN^{AFA} A.) [^{13}C,^{13}C]-DARR spectra of ^{13}C and ^{15}N selectively labeled PLN^{AFA} at Val4, Leu7, Ala11, Ile12, Ala15, Ile18, (PLN^{AFA6cyt}) in complex with SERCA in the absence and presence of TEMPO spin label at Cys 674. B) Zoom-in of the [^{13}C,^{13}C]-DARR spectra showing C_α-C_β and C_α-C_δ correlations for Ala 11 and Leu 7 corresponding to the T and R states. C) Plot of the relative peak intensities (I_R/I_T) for T and R state resonances for selected residues obtained in the presence and absence of the spin label on SERCA.

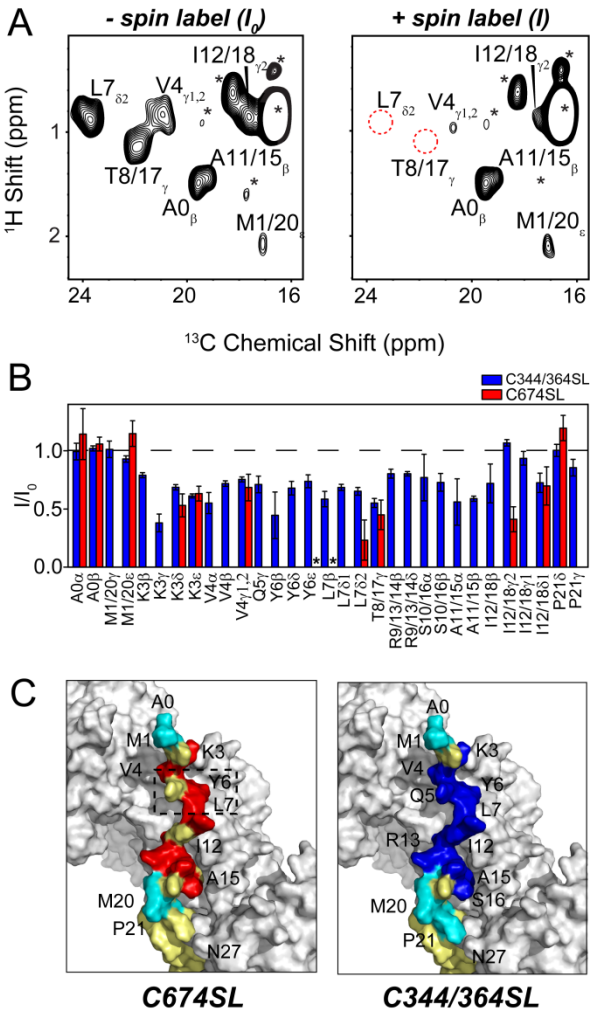

Figure 4. PRE effects on domain Ia of PLN. A) Methyl region of ^{13}C-^{1}H rINEPT spectra in the presence and absence of TEMPO at Cys674 of SERCA. Lipid peaks are marked with asterisks. B) Intensity retention plot for residues in domain Ia probed by rINEPT experiments. I and I_o are the peak intensities in the presence and absence of the spin label, respectively. Error bars reflect the signal-to-noise in the spectra. Resonances broadened beyond detection are marked with asterisks. C) Mapping of the PRE onto PLN structure in the R state. PREs from C674SL and C344/364SL are colored in red and blue, respectively; while resonances unaffected are colored in yellow. The dashed box highlights resonances that are broadened out beyond detection.

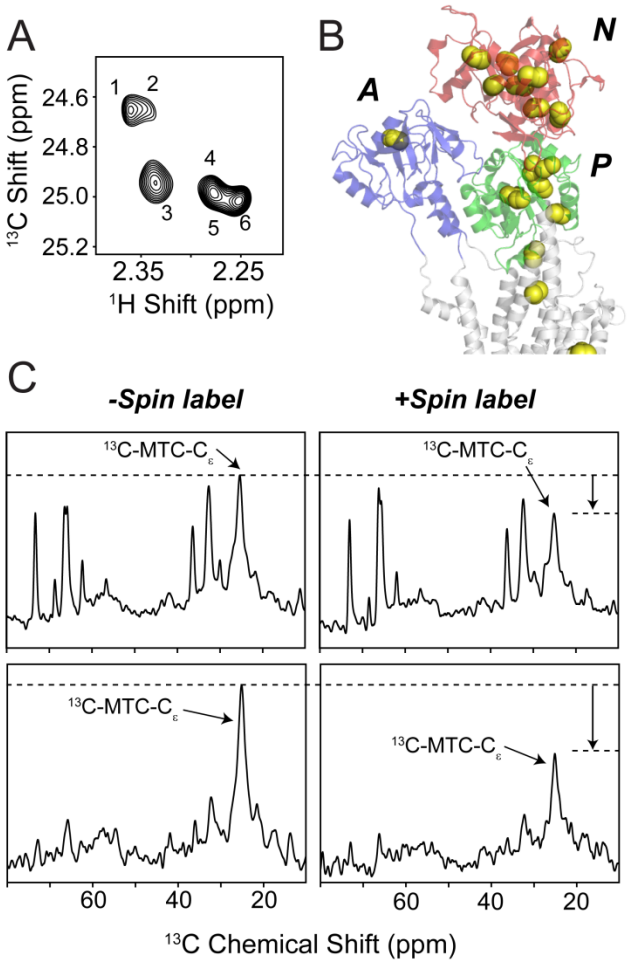

Figure 5. PRE effects from spin labeled PLN on methyl-labeled SERCA. A) [^{1}H,^{13}C]-HSQC spectrum of ^{13}C-MTC-SERCA in DPC micelles. B) Location of the cysteine residues in the cytoplasmic domain of SERCA (PDB ID: 1IWO). C) CP spectra (top) and water-edited CP spectra (bottom) of ^{13}C-MTC-SERCA in the presence of PLN$^{AFA\text{-}sl}$ acquired before and after addition of ascorbate. The additional peaks in the spectra correspond to the natural abundance ^{13}C resonances of lipids and proteins.

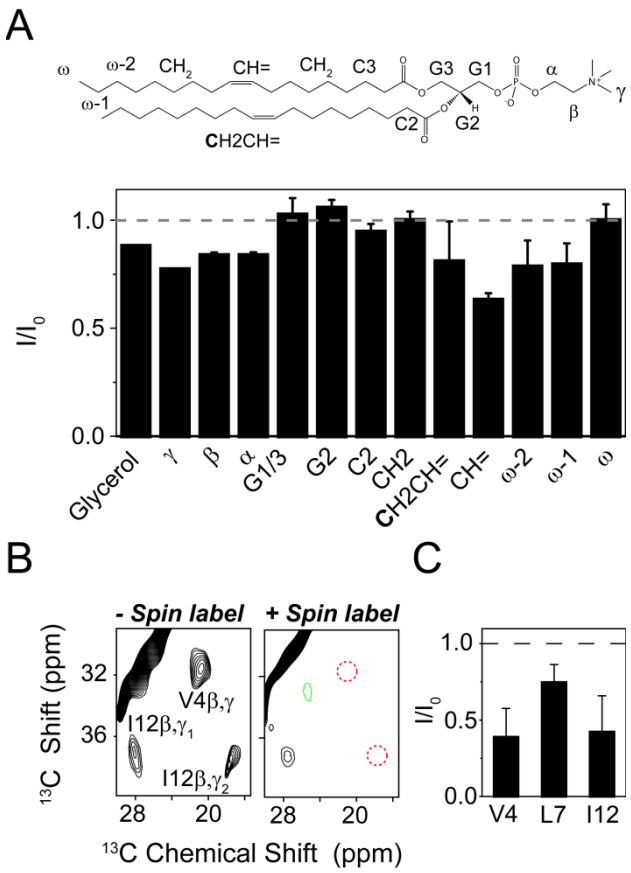

Figure 6. Lipid association of PLN domain Ia determined by PRE effect. A) Top: chemical structure and nomenclature of DOPC; bottom: PRE effects on PC/PE/PA lipid resonances from PLN$^{AFA\text{-}sl}$ in complex with SERCA. The bar labeled "Glycerol" corresponds to the PRE effect of PLN$^{AFA\text{-}sl}$ on the free glycerol present in the buffer (NMR buffer contains 2.5% glycerol to prevent loss of SERCA activity) I and I_0 correspond to the peak intensities before and after addition of 10 mM ascorbate, respectively. B) Chemical structure of the synthesized PE^{sl}. C.) Representative regions of [^{13}C, ^{13}C]-DARR spectra of ^{13}C,^{15}N Val4, Leu7, Ile12 labeled PLN^{AFA} in complex with SERCA before and after addition of 10 mM DTT. E.) Average PRE values for V4, L7 and I12 in domain Ia. Error bars show the standard error of three resonances from each indicated residue.

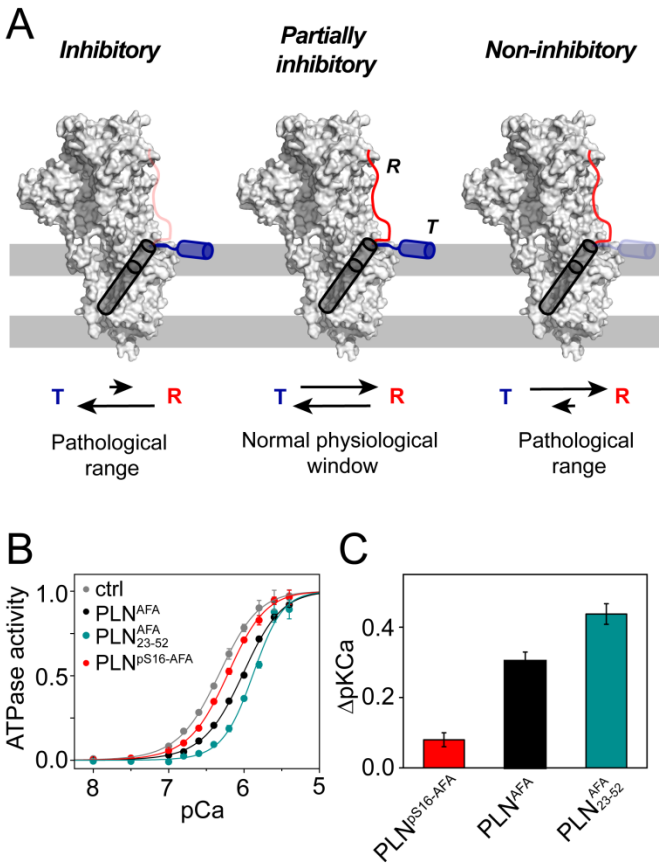

Figure 7. Functional effect of domain Ia interaction with SERCA. A.) Correlation between the conformational equilibrium of PLN and the inhibitory state of SERCA B.) Representative SERCA activity curves in the absence of regulator (ctrl) and in the presence of a 5-fold molar excess of PLN^{AFA}, $PLN^{pS16AFA}$ and PLN_{23-52}^{AFA}. C.) Averaged inhibitory activity for PLN variants. ΔpKCa was calculated as $pK_{Ca,SERCA}$- $pK_{Ca,PLN}$, error bars represent the standard errors of four independent reconstitutions.

7.5 Supporting information

7.5.1 Synthesis of spin-labeled lipid (PE^{sl})

1,2-dioleoyl-sn-glycero-3-phosphoethanolamine (DOPE) (8.2 mL, of a 2 % w/v solution in $CHCl_3$) (0.22 mmol, 164 mg) was placed in a 25 mL round bottom flask and the $CHCl_3$ was removed under a stream of N_2. Dichloromethane (10 mL) was added and removed *in vacuo* to remove possible traces of ethanol. A solution of EDC (0.22 mmol, 38.4 mg) with 4-carboxy-TEMPO (0.22 mmol, 40.0 mg) in dichloromethane (1.0 mL) was added to DOPE lipids dissolved in dichloromethane (9 mL). DIEA (0.22 mmol, 39.0 uL) was added to the mixture and the reaction was stirred for ~48 h. The dichloromethane was removed *in vacuo* and the residue was taken up in ethyl acetate (25 mL) and transferred to a separatory funnel. The solution was washed with 1N HCl (3 x 15 mL). An emulsion formed that was partially broken by addition of small amounts of MeOH and saturated NaCl solution. The emulsion was mainly found in the aqueous phase and could be extracted without loss of product. The organic phase was dried over $MgSO_4$ and concentrated using a vacuum pump. The crude product was analyzed by TLC (R_f = 0.71, $CHCl_3$/MeOH/H_2O, 65:31:4). The final yield was 118 mg, 58 %. Deconvoluted ESI-MS, calc.: 925.7, found: 925.7.

7.5.2 FRET experiments

SERCA was incubated for 30 min by a 20-fold excess of 5-((((1-iodoacetyl)amino)ethyl)amino)naphthalene-1-sulfonic acid (IAEDANS) (Invitrogen) to attach the fluorescent AEDANS group to Cys 674 (32). The label-ing extent was determined by absorbance at 334 nm (εAEDANS= 6100 M-1 cm-1) (59). To introduce an acceptor for energy transfer, AFA-PLN was incubated in 1% SDS, 100 mM $NaHCO_3$ at pH 9 for 16 h with a 20-fold excess of 4-((4-(dimethylamino)phenyl)azo)benzoic acid, succinimidyl ester (dabcyl-SE), and free label was removed using reverse-phase HPLC. Labeling efficiency was determined by electrospray ionization mass spectrometry (ESI-MS). $SERCA^{AEDANS}$ was co-reconstituted with PLN^{Dab} at molar ratios of 1:0, 1:1 and 1:2 at a 700:1 lipid:$SERCA^{AEDANS}$ ratio. Steady-state fluorescence was measured with a Varian Eclipse Fluorimeter, using an excitation wavelength of 351 nm (20 nm bandwidth) and emission wavelengths between 400 and 600 nm.

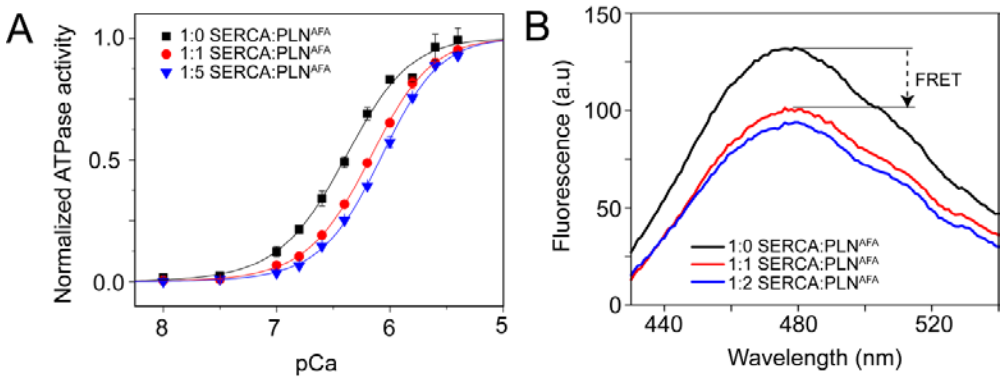

Figure S1. A.) Ca^{2+}-dependent ATPase activity of SERCA/PLN complex in Egg PC/PE/PA lipid vesicles measured using a coupled enzyme assay. B.) FRET between $SERCA^{AEDANS}$ and $PLN^{Dab\text{-}AFA}$. FRET was measured as a decreased in $SERCA^{AEDANS}$ (donor) steady state fluoresence due to the presence of $PLN^{Dab\text{-}AFA}$ (acceptor).

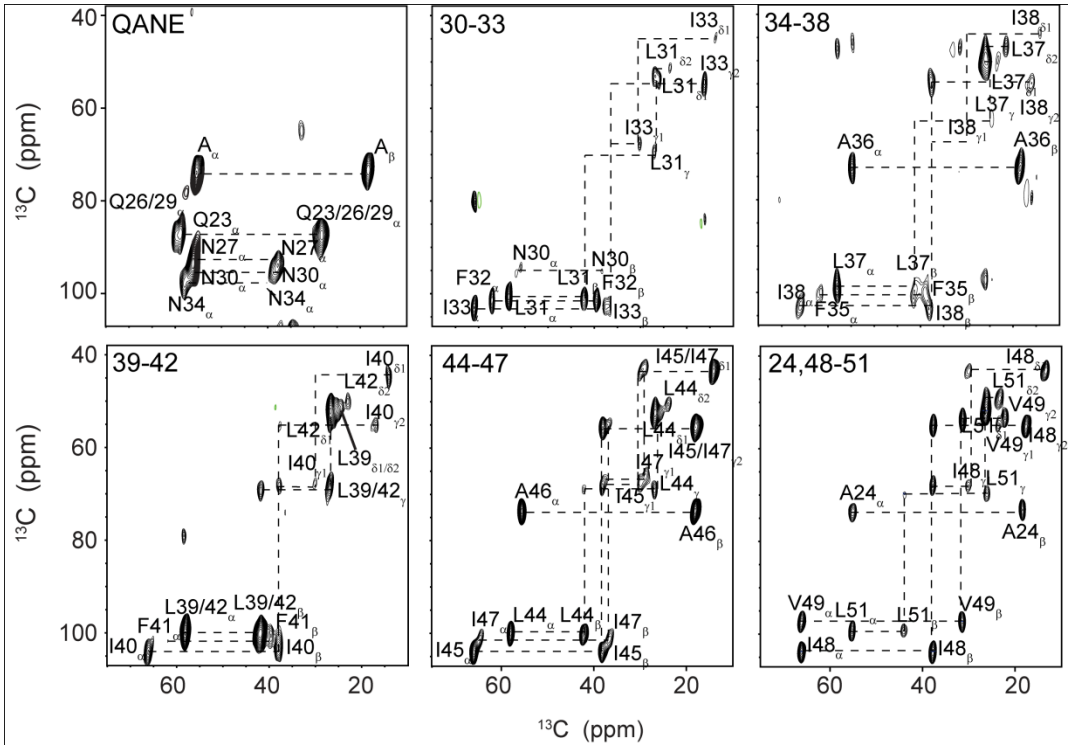

Figure S2. Representative spectra for assignment of PLN^{AFA} in complex with SERCA from synthetically and recombinantly labeled samples. ^{13}C-labeled residues are indicated in the spectra.

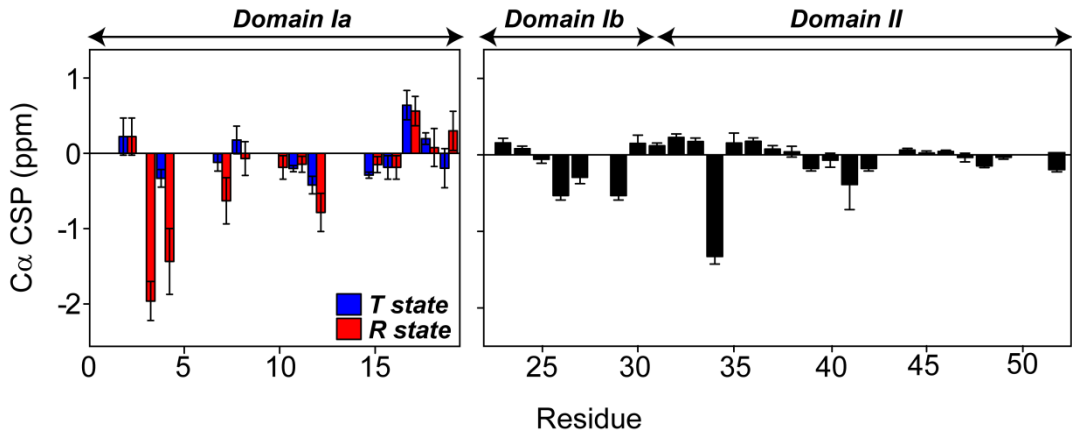

Figure S3. Effects of SERCA binding on PLN resonances for domain Ia and the loop. The Cα chemical shifts were obtained from [^{13}C,^{13}C]-DARR experiments in egg PC/PE/PA bilayers in a 8:1:1 molar ratio. The chemical shift perturbations (CSP) are differences between the chemical shifts in the presence and absence of SERCA (δ_{+SERCA} - δ_{-SERCA}).

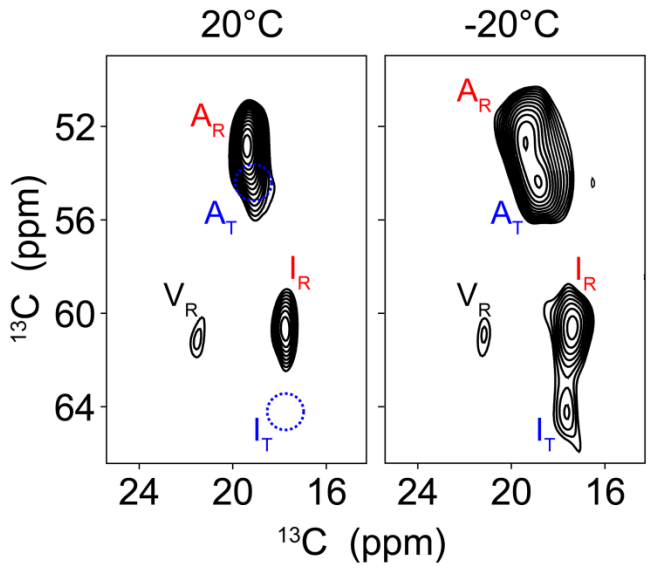

Figure S4. Regions of the [^{13}C,^{13}C]-DARR spectra of the SERCA/PLNAFA complex at 20 and -20 oC. Dotted circles highlight the position of Ile and Ala T state peaks, which are not detectable or significantly attenuated at 20°C.

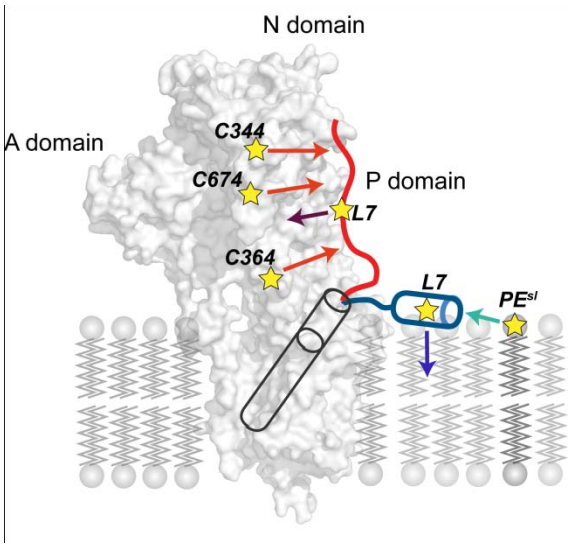

Figure S5. Schematic of the spin labeling schemes used to probe the topology and the conformational equilibrium of the SERCA/PLN complex. PREs measured by NMR experiments included SERCA$^{C674\text{-}sl}$ and SERCA$^{C344/364\text{-}sl}$ to ^{13}C labeled PLN (orange arrows), PLN$^{L7\text{-}sl}$ to ^{13}C MTC-SERCA (purple arrow), PLN$^{L7\text{-}sl}$ to lipid (^{13}C natural abundance) (blue arrow), and PE^{sl} to ^{15}N, ^{13}C labeled PLN (cyan arrow).

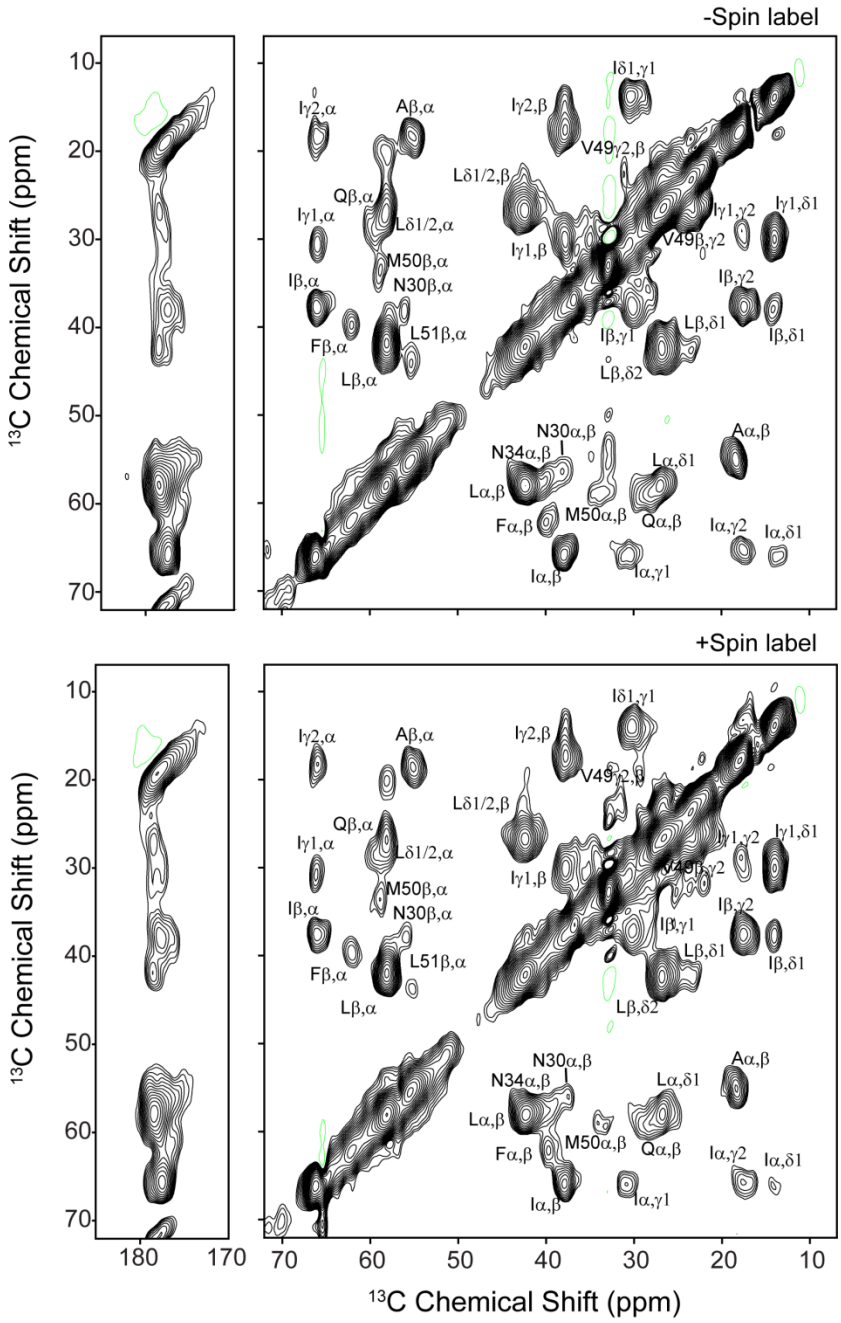

Figure S6. [^{13}C,^{13}C]-DARR spectra of u^{13}C-PLN in complex with SERCA$^{C344C364\text{-}sl}$ before (top) and after (bottom) addition of 10 mM DTT. Experiments were acquired with a 6 ms DARR mixing time.

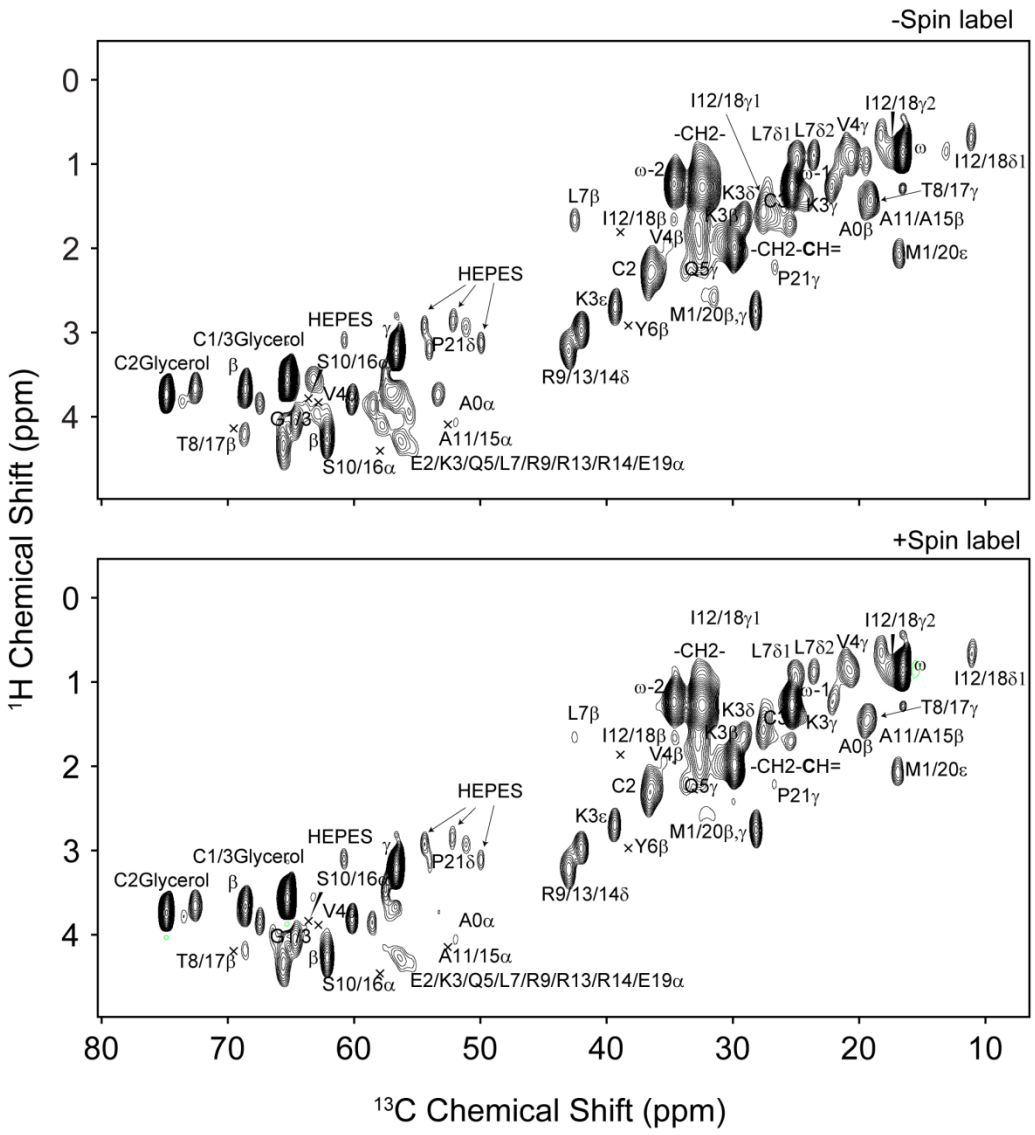

Figure S7. [^{1}H,^{13}C]-rINEPT spectra of PLN in complex with SERCAC$^{344C364\text{-}sl}$ before (bottom) and after (top) addition of 10 mM DTT.

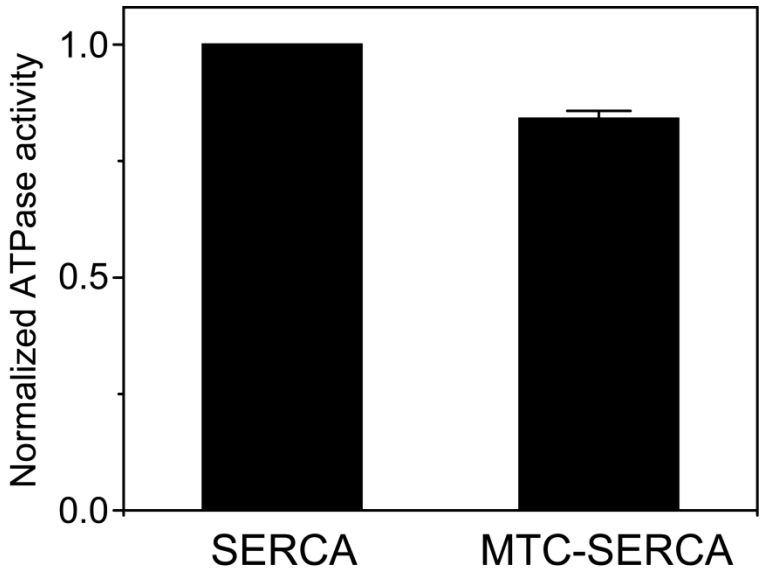

Figure S8. Comparison of SERCA activity before and after methylation at the cysteine residues. The activity was normalized to an unlabeled control. Error bars represent the standard deviation of three independent measurements.

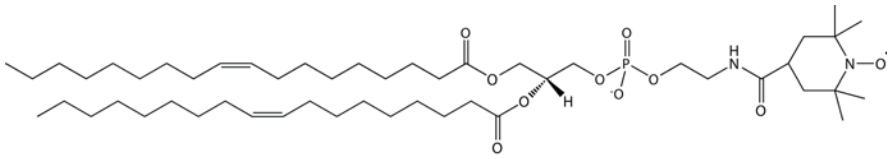

Figure S9. Spin labeled PE^{-sl} lipid.

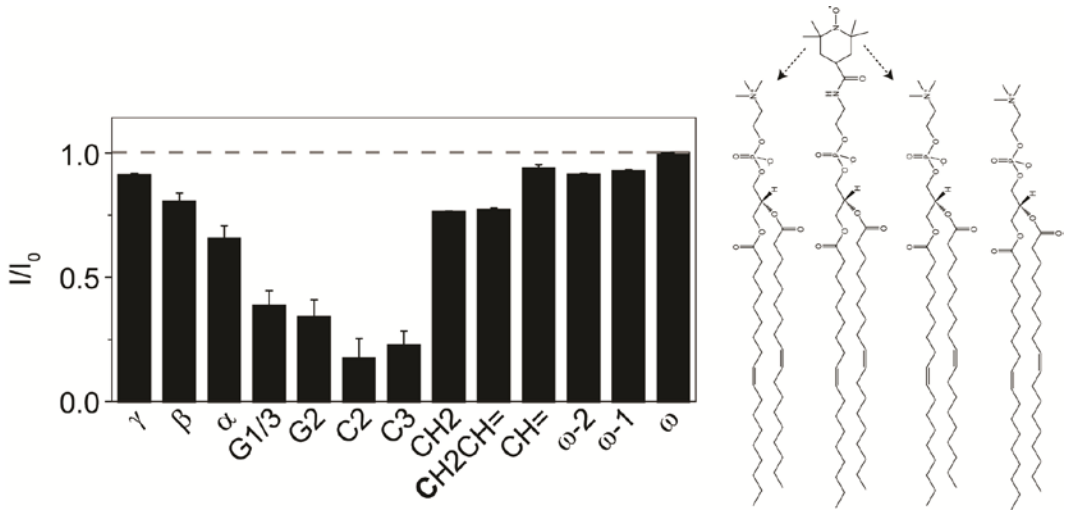

Figure S10. Intensity retention of the ^{13}C resonances of PC/PE/PA lipid bilayers (8:1:1 molar ratio) doped with PE_{sl} (2% w/w) obtained from [^{13}C,^{13}C]-rINEPT experiments at 20°C before (I) and after (I_0) addition of 10 mM DTT.

Chapter 8 - Tuning the structural coupling between the transmembrane and cytoplasmic domains of phospholamban to control sarcoplasmic reticulum Ca(2+)-ATPase (SERCA) function

Reprinted with permission from:

Ha KN, Gustavsson M, Veglia G *Tuning the structural coupling between the transmembrane and cytoplasmic domains of phospholamban to control sarcoplasmic reticulum Ca(2+)-ATPase (SERCA) function* J Muscle Res Cell Motil. 2012 In press

Ca^{2+} ions signal muscle contraction and relaxation, coupling the membrane action potential and the mechanical contraction of muscle (1, 2). The interplay between the sarcoplasmic reticulum ATPase (SERCA) and phospholamban (PLN) is crucial to intracellular Ca^{2+} cycling and proper cardiac muscle contraction and relaxation, and dysfunction in their protein–protein interactions have been implicated in cardiac disease (3). SERCA is a 110 kDa integral membrane P-type ATPase which utilizes ATP hydrolysis to transport Ca^{2+} into the SR (4). SERCA is responsible for 70 % of the calcium reuptake during diastole in human cardiomyocytes (4). SERCA comprises a large cytoplasmic domain that includes the actuator domain, the phosphorylation domain, and a nucleotide binding domain, along with ten transmembrane helices constituting the Ca^{2+} transport pathway (5). The cardiac isoform of SERCA (SERCA2a) is regulated by PLN, a single-pass membrane protein that binds the enzyme via intramembrane interactions, reducing its apparent Ca^{2+} affinity (6-8). β-Adrenergic stimulation unleashes protein kinase A (PKA) that phosphorylates PLN at Ser16, reversing its inhibition of SERCA and augmenting the diastolic phase (9).

8.1 Introduction

PLN is a 52-amino acid integral membrane protein which is comprised of three structural domains (10-12) that are further subdivided into four dynamic domains (cytoplasm: domain Ia (residues 1–16), loop (residues 17–22), domain Ib (residues 23–30); transmembrane: domain II (residues 31–52)) (10, 11, 13) (**Figure 1**). The transmembrane helix of PLN is the principle structural domain that inhibits SERCA (14, 15), while the regulatory phosphorylation Ser16 site, which determines the inhibitory or non-inhibitory state, lies in the cytoplasmic helix (16). PLN can populate several conformational states, and domain Ia and Ib participate in folding/unfolding equilibria, which are important for SERCA inhibition as well as recognition by PKA (17-20). The loop connecting these two domains also has functional relevance, in particular the Pro21 residue that lies in the center of the loop. Squier and co-workers reported that mutation of Pro21 to Ala in a monomeric cysteine-null background led to partial inhibition of SERCA, increase in overall helicity, decreased dynamics at the C-terminus, and local structural changes at the loop leading to diminished solvent accessibility (21). Additionally, our group found that the SERCA inhibition and binding could be tuned modulating the conformational dynamics of the loop through mutation in the Pro21 site, via a so-called *dynamic rheostat* (22). Our studies identified the mutant species AFA-PLN^{P21G} to be a possible candidate for treatment of heart failure by delivery via rAAV gene therapy. AFA-PLN^{P21G} was found to have the same structural dynamics and functional characteristics as PLN^{S16E}, a PLN pseudo-phosphorylated mutant already proven to be successful in reversing heart failure in large and small animal models by Chien and coworkers ((23, 24).

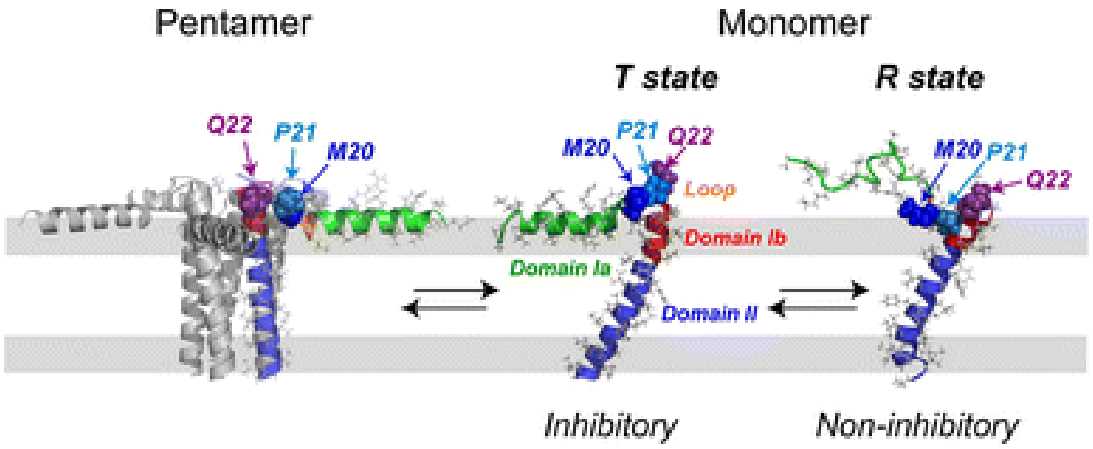

Figure. 1 Hybrid solution and solid state NMR structures for pentameric wt-PLN (PDB 2KYV, left) and monomeric AFA-PLN (PDB 2KB7, center) and structure of the R state of PLN *determined from solution NMR and molecular dynamics simulations. The four dynamic domains of PLN are color-coded: green domain Ia, orange loop, red domain Ib, blue domain II. Sites of loop mutations are rendered in the space-filling motif.*

Naturally occurring mutations in PLN have also been linked to familial forms of cardiomyopathy: R9C (25), R9L and R9H (26), R14del (27), and L39stop (28). PLN has also become a target for gene therapy (23, 24, 29), namely by delivering PLN mutants which decrease SERCA inhibition. The challenge remains in how to rationally design PLN mutants with tunable effects on SERCA to account for the diversity of patient population and the various manifestations of heart failure (30).

Numerous mutagenesis studies of PLN have been carried out by the MacLennan, Jones, and Young groups, offering invaluable insight by identifying residues crucial to PLN's inhibitory ability (31-33). Although these studies served as a crucial starting point to understanding the effect of point mutations in PLN have on SERCA activity, they often did not identify the reasons for observed functional effects, i.e., whether the mutation induced a change to structural dynamics, altered the binding surface, decreased SERCA binding, etc. The data clearly demonstrate that the transmembrane domain is *Janus*-faced, with one side of the helix primarily involved in oligomerization and the other side binding to SERCA. Mutagenesis studies show that domain Ia and the loop are the optimum targets for designing loss-of-function (LOF) mutants. In contrast, mutations in

domain Ib and domain II yield varying results, but all known gain-of-function (GOF) and super-inhibitors are concentrated in those two domains.

The rationale of this study is to build on our previous success tuning the structural dynamics of PLN to control SERCA function by introducing a series of glycine residues to the loop domain. Our original hypothesis was that an increase in conformational dynamics in the loop would interrupt the structural coupling between the transmembrane helix, which is primarily responsible for SERCA inhibition, and the cytoplasmic helix, which contains the phosphorylation sites that dictate the inhibition state. To test this hypothesis, we sought to introduce single Gly mutations at the M20 site and Q22 site to investigate whether the LOF rendered by the P21G mutation was site-specific (**Figure 2**). Secondly, we determined the SERCA inhibition of the phosphorylated species to see if post-translational control of these single Gly-mutants of PLN still remains intact, a property which has been suggested to be crucial for therapeutic success (22). Thirdly, we expanded the Gly mutations into double and triple mutations: AFA-PLN$^{M20G\ P21G}$ and AFA-PLN$^{M20G\ P21G\ Q22G}$. To characterize the conformational dynamics of the various mutants and correlate with their functional state, we used nuclear magnetic resonance (NMR) spectroscopy that enables one to probe molecular motions of proteins at the atomic level (34).

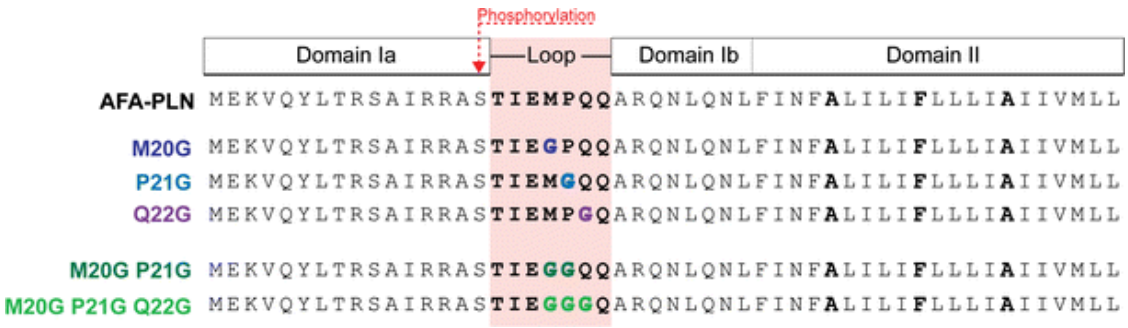

Figure 2. Primary structures of glycine mutants in this study*. The secondary structure motifs of PLN (helix, loop, helix) and dynamics domains are displayed above. Mutations are highlighted in the loop region*

Our results suggest that the structural dynamics of the glycine mutants can be tuned, resulting in varying degrees of fast timescale dynamics and degrees of SERCA inhibition. However, species where the mutation increased the conformational dynamics

past the threshold set by the phosphorylated species behave as the transmembrane helix alone. The mutants represent new templates for rational design of protein therapies using gene transfer approaches, modifying the effects of an inhibitor to control enzyme function.

8.2 Materials and methods

8.2.1 Cloning of PLN mutants

Primary sequences of the mutants cloned in this study are described in **Figure 2**. Cloning was performed using the Stratagene QuikChange protocol as previously described (22). For the AFA-PLN^{M20G}, AFA-PLN^{P21G}, and AFA-PLN^{Q22G} constructs, the pMal-c2E-TEV-AFA-PLN plasmid was used as a parental template, which expresses a maltose binding protein (MBP) PLN fusion protein with a tobacco etch virus (TEV) protease cleavage site encoded in-between. The forward primer for the AFA-PLN^{M20G} is as follows: 5′-ACC ATT GAA GGC CCG CAG CAG GCG CGC CAG AAC-3″. The forward primer for the AFA-PLN^{Q22G} is as follows: 5′-ACC ATT GAA ATG CCG GGC CAG GCG CGC CAG AAC-3″. The forward primer for the AFA-PLN$^{M20G\ P21G}$ is as follows: 5′-GGC AGC ACC ATT GAA GGC GGC CAG CAG GCG CGC CAG AAC CTG-3″. The cloning of GGG-PLN required two PCR reactions on the P21G PLN AFA background, first converting M20 to G and then Q22 to G. Pentameric mutants were cloned using the pMal-c2E-TEV-wtPLN plasmid as the parental template. PLN$^{M20G\ P21G}$ was cloned stepwise, using PLN^{P21G} as the initial template. Stepwise mutagenesis was necessitated due to the high T_m values of primers containing codons encoding for glycine, because of their high GC content. After mutagenesis was confirmed from EtBr stained agarose gels, the PCR reaction was transformed into DH5α cells and grown on ampicillin-agarose plates. Subsequent colonies were grown overnight in 5 mL Luria–Bertani media with 0.1 % ampicillin, and then spun down on a tabletop centrifuge at 13,000 rpm. The remaining pellet was resuspended and the plasmid was extracted from the pellet using the Qiagen Quick-Spin Miniprep kit. Constructs were confirmed through sequencing at the University of Minnesota Biomedical Genomics Center. Correct target constructs were then transformed into BL21 (DE3) *Escherichia coli* cells.

8.2.2 Protein preparations and ATPase activity assays

Protein expression and purification of all constructs were performed as previously described (8, 35). Phosphorylation of PLN samples at Ser16 was performed as previously described (17, 22, 36) using recombinantly expressed protein kinase A purified by an established protocol (37). Phosphorylation was confirmed by a band shift in the SDS-PAGE, and by MALDI-TOF mass spectrometry. The degree of SERCA inhibition by PLN analogs was determined using a coupled enzyme assay correlating the depletion in NADH absorbance to ATPase activity as previously described (22, 38). SERCA inhibition was measured in reconstituted lipid samples according to Reddy et al. (39). PLN variants were co-reconstituted with purified SERCA in lipid bilayer membranes (DOPC:DOPE, 4:1) at molar ratios of 10:1 PLN:SERCA and 700:1 lipids:SERCA. The calcium dependence of the ATPase activity was measured at 37 °C using a coupled enzyme assay, monitoring the consumption of NADH by the decrease in absorbance at 340 nm using a Spectromax microplate reader (Molecular Devices). Initial rate of SERCA (*V)* was measured as a function of calcium concentration (pCa), and data was fit to the Hill equation (39).

8.2.3 NMR studies

Unless otherwise noted, NMR samples were prepared with a buffer containing 20 mM Na_2HPO_4 (J.T. Baker), 120 mM NaCl (Malinkrodt), 0.1 % NaN_3, and 300 mM dodecylphosphocholine (DPC) (Avertec). Lyophilized PLN was weighed and added in increments to 300 µL buffer until the sample reached an approximate concentration of 1–1.5 mM protein. After addition of HPLC purified protein, all samples were adjusted to pH 6.0 with dilute NaOH to neutralize residual trifluoroacetic acid remaining in the protein powder. All [^{1}H, ^{15}N] heteronuclear single quantum coherence (HSQC) spectra were collected on a Varian spectrometer operating at a ^{1}H Larmor frequency of 600 MHz. Sample quality was assessed by signal-to-noise and resolution in the 2D spectrum with between 32 and 64 increments in the indirect dimension. Heteronuclear steady-state NOE spectra were collected as previously described (13, 22). Briefly, two spectra were collected using the established pulse sequence based on Farrow et al. (40) with a spectral width of 6,000 Hz in the indirect proton dimension and 1500 Hz in the indirect nitrogen dimension. 128 scans were done with 64 points in the indirect

dimension. The saturation spectrum was collected with a 3 s presaturation period on the proton frequency. Peak intensities were analyzed using NMRView5 software (41).

8.3 Results

Single Gly mutations were successfully cloned on a monomeric AFA-PLN background, yielding AFA-PLN^{M20G}, AFA-PLN^{P21G}, and AFA-PLN^{Q22G}. The species were expressed in *E. coli,* and subsequently isolated by affinity and HPLC chromatography. SERCA activity measurements served as the initial screen to assess the effects of the mutations. Functional assays were performed with SERCA reconstituted in lipids alone as the negative control, and also in the presence of AFA-PLN or the super-inhibitor mutant AFA-PLN^{N27A} as a positive control, giving a consistent ΔpK_{Ca} shift of 0.3 and 0.5 pCa units, respectively. **Figure 3a** displays a representative normalized ATPase activity curve which yields the pKCa shifts. **Figure 3b** shows the average ΔpK_{Ca} values for the three mutants as compared to the control AFA-PLN (filled bars). Compared to the AFA-PLN species, the AFA-PLN^{M20G}, AFA-PLN^{P21G}, and AFA-PLN^{Q22G} analogs reduced the PLN inhibition by approximately 0.1 pCa units. Therefore, irrespective of their positioning in the dynamic loop, the single site mutations manifested an LOF character. The extent of this effect is variable, with a gradient of SERCA inhibition ranging from ΔpK_{Ca} of 0.23 ± 0.01 for M20G to ΔpK_{Ca} of 0.16 ± 0.02 for Q22G. Remarkably, previous studies showed that Ala mutations of M20 or Q22 do not render LOF characteristics (4, 31).

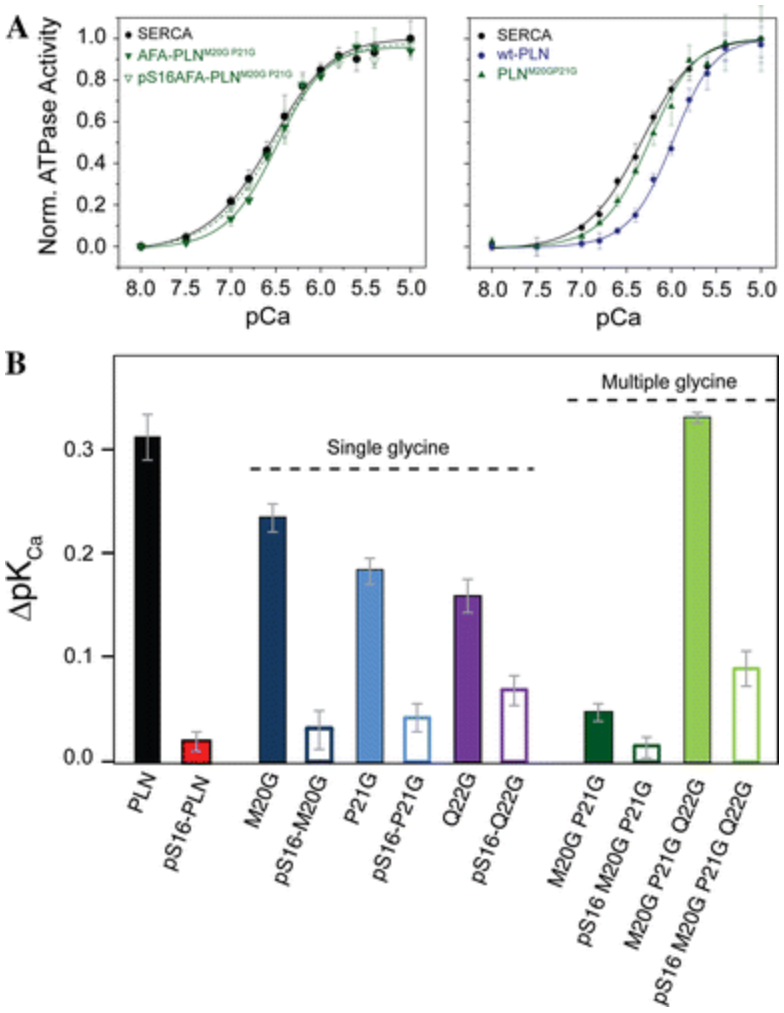

Figure 3. Functional measurements of SERCA in reconstituted lipids in the presence of PLN Gly loop mutants. *a. Coupled enzyme activity assay measurement of SERCA in absence (black circles) and presence of PLN species.Left panel unphosphorylated (closed green triangles) and phosphorylated (open green triangles) monomeric M20G P21G AFA-PLN. Specific activity of reconstituted SERCA averages 2.9 ± 1.4 IU as reported in Gustavsson et al. (2011b). Right panel wt-PLN (blue circles) and M20G P21G mutant on pentamer background (PLN^{M20GP21G}, green triangles). As in the monomeric conditions, the M20G P21G mutation in pentameric conditions is still severe LOF.* ***b****. Histogram of ΔpK_{Ca} measurements of all PLN species. Error bars are indicative of standard deviation from averaged values of ΔpK_{Ca}.*

To test their propensity to be phosphorylated by protein kinase A (PKA-C) and thereby reverse SERCA inhibition, the Gly mutants of PLN were incubated with catalytic amounts of the kinase and analyzed by gel shift assays. We found that all of the single

Gly PLN mutants were quantitatively phosphorylated in vitro by recombinant protein kinase A. Importantly, SERCA functional assays revealed that phosphorylation at Ser16 for each single Gly mutant was sufficient to reverse inhibition (**Figure 3b**, open bars).

To investigate whether the combination of two or more Gly mutations would increase the LOF effect, we cloned a double mutant, AFA-PLN$^{M20G\ P21G}$, and a triple Gly mutant, AFA-PLN$^{M20G\ P21G\ Q22G}$. We found that (1) the AFA-PLN$^{M20G\ P21G}$ species was a complete LOF mutant, and (2) AFA-PLN$^{M20G\ P21G\ Q22G}$ completely recovers the inhibitory function (**Figure 3b**). Based on these results, we speculate that combining the Gly at position M20 and P21 conferred even stronger LOF behavior, creating an additive effect in the double mutant. In contrast, a triple mutation eliminated the structural coupling between the cytoplasmic and transmembrane helix, resulting in a species that is similar to the transmembrane helix alone (14). Electrophoretic gel shift assays show that incubation of PKA with these double and triple mutants does result in a gel shift typically observed for the phosphorylated species, consistent with quantitative phosphorylation. These results were confirmed by mass spectrometry. The cytoplasmic helix contains the phosphorylation site, while the transmembrane helix is the principle domain responsible for inhibition. We sought to test the hypothesis that phosphorylation of the Gly mutants would not reverse the effects of inhibition, due to the possible breaking of the conformational coupling between these domains. Our results indicate that phosphorylation does reverse the effects of inhibition for PLN$^{M20G\ P21G}$ and also PLN$^{M20G\ P21G\ Q22G}$. **Figure 3b** shows the averaged SERCA activity measurements of several different samples of unphosphorylated (closed bars) and phosphorylated (open bars) of the double and triple glycine AFA-PLN loop mutations. Values of ΔpK_{Ca} are reported in Table 1.

Table 1. ΔpK_{Ca} values for all PLN species averaged over six measurements

	ΔpK_{Ca}	**ΔK_{Ca}, μM**
AFA-PLN	0.31 ± 0.02	0.46 ± 0.02
pSer16-AFA-PLN	0.025 ± 0.012	0.064 ± 0.037
AFA-PLN^{M20G}	0.23 ± 0.01	0.11 ± 0.09
pSer16-AFA-PLN^{M20G}	0.031 ± 0.018	0.012 ± 0.037

AFA-PLN^{P21G}	0.18 ± 0.01	0.18 ± 0.03
pSer16-AFA-PLN^{P21G}	0.042 ± 0.013	0.036 ± 0.038
AFA-PLN^{Q22G}	0.16 ± 0.02	0.053 ± 0.078
pSer16-AFA-PLN^{Q22G}	0.068 ± 0.014	0.020 ± 0.055
AFA-PLN$^{M20G\ P21G}$	0.047 ± 0.009	0.048 ± 0.024
pSer16-AFA-PLN$^{M20G\ P21G}$	0.015 ± 0.010	0.019 ± 0.022
AFA-PLN$^{M20G\ P21G\ Q22G}$	0.33 ± 0.01	0.29 ± 0.02
pSer16-AFA-PLN$^{M20G\ P21G\ Q22G}$	0.090 ± 0.017	0.047 ± 0.019

ΔpK_{Ca} values are calculated from as the *difference* in pK_{Ca} values from the fits of the SERCA activity curves in the absence and presence of PLN

A critical issue in the design of possible therapeutic mutations for delivery through gene therapy is the effect the species will have in vitro versus in vivo, particularly when dealing with possible functional effects that are the result of unknown protein–protein interactions and also interactions with the endogenous species. Hence, we studied the function of mutant with the most LOF character, AFA-PLN$^{M20G\ P21G}$ by comparison to the endogenous wild-type background sequence in order to determine whether the functional results may be due to altered oligomeric states. Functional results with SERCA in the presence of the PLN$^{M20G\ P21G}$ mutant show that this is a strong LOF mutant, with a ΔpK_{Ca} of 0.095 ± 0.021 (**Figure 3a**, right), confirming that the M20G P21G mutation results in a LOF species regardless of its monomeric or pentameric state.

To characterize the structural features of the mutations, AFA-PLN^{M20G}, AFA-PLN$^{M20G\ P21G}$, and AFA-PLN$^{M20G\ P21G\ Q22G}$ were expressed in ^{15}N isotopically labeled media, purified, and reconstituted in DPC micelles. The ^{1}H–^{15}N HSQC spectra of all three mutants were well resolved (**Figure S1a**) and assigned using 15N edited NOESY-HSQC experiments at short (70 ms) mixing times to identify short-range NOEs. Amide resonance assignments were correlated to the ^{1}H–^{15}N HSQC assignment for AFA-PLN

(**Figure S1b**). Most changes are localized near the mutation site. However, some distal changes, especially in domain Ib, are detected, specifically residues Arg25 and Asn27.

The structural dynamics of these mutations were characterized using nuclear spin relaxation measurements (34). R_1, R_2, and NOE values were measured for AFA-PLN^{M20G}, AFA-PLN$^{M20G\ P21G}$, and AFA-PLN$^{M20G\ P21G\ Q22G}$ (**Figure S2**) in DPC micelles. While the structure is largely intact, as evidenced by only minor perturbations in the $^{1}H–^{15}N$ HSQC spectrum compared to AFA-PLN, we do observe an increase in the fast (ps–ns) conformational dynamics of the backbone for all of the mutants examined. Increased motions are detected in the intervening loop and domains Ia and Ib. While domain Ib and the loop of the Gly mutants have conformational dynamics similar to that of pSer16 AFA-PLN, the phosphorylated species is significantly more mobile in domain Ia. Thus, introduction of the single or multiple Gly mutants change only the local motion and does not mimic the conformational dynamics found in the phosphorylated species (pSer16-AFA-PLN). A possible explanation is that the negatively charged phosphoserine interacts with the positively charged side chains of Arg13 and 14, forming transient salt bridges that affect the folding and dynamics of the entire cytoplasmic regions including domain Ia. In fact, the presence of the phosphoryl group shifts the conformational equilibrium of domain Ia of PLN from a folded (T state) to an unfolded (R state) (17, 19). The ^{15}N relaxation data do not support a significant T to R state transition upon Gly mutations. The latter was confirmed by $^{1}H–^{13}C$ HSQC experiments that image the side chains bearing methyl groups. Indeed, we found that the Gly mutations in the loop do not affect the T to R state equilibrium substantially, i.e. we observed only minor chemical shift changes for the domain Ia methyl groups (**Figure S3**). These findings indicate that the LOF character of the Gly mutants is not directly related to the T/R equilibrium of domain Ia, and that the Gly mutations in the intervening loop cause a local increase in backbone flexibility.

8.4 Discussion

We sought to expand on previously published results on tuning the function of SERCA by altering the conformational dynamics of the loop domain in PLN (22). Our previous results showed that AFA-PLN^{P21G} displayed similar structural dynamics to the pseudo-phosphorylated species PLN^{S16E}, which has shown promise in reversing heart failure in

animal models upon delivery via rAAV-mediated gene therapy (29). In addition to mimicking the structural dynamics of the pseudo-phosphorylated form, AFA-PLN^{P21G} also has the additional characteristic of being able to be post-translationally modified by phosphorylation at Ser16 by PKA, a regulatory feature which is crucial for maintaining Ca^{2+} homeostasis (42).

The functional results of AFA-PLN^{M20G}, AFA-PLN^{P21G}, and AFA-PLN^{Q22G} (**Figure 3, Table 1**) show that introduction of the Gly residue did not need to be specifically positioned at Pro 21 in order to have a LOF effect. Additionally, the in vitro phosphorylation results of the three species suggest that these mutants may still also be post-translationally modified in vivo. Remarkably, similar alanine mutations at M20 and Q22 did not show appreciable differences in SERCA inhibition (31, 43), demonstrating the sensitivity of SERCA activity on the PLN sequence. While all of the mutants resulted in LOF characteristics, they inhibited SERCA to different degrees, resulting in a gradient of function. This is an important factor when designing mutations to alter contractility. While introducing PLN mutants which are completely LOF would increase SERCA activity and activate diastole in the short term, constitutive activation of SERCA is known to promote hypertrophy (44) and a PLN null genotype is found in humans to result in heart failure (26, 28). Hence, development of mutations of PLN for use in gene therapy would necessitate mutants which sampled a wide array of levels in SERCA inhibition.

The results of AFA-PLN $^{M20G\ P21G}$ show that the LOF effects for the M20 and P21 site were additive, resulting in the least inhibitory mutant of this study. Phosphorylation of this species resulted in a ΔpK_{Ca} similar to that of pSer16 AFA-PLN. The NMR results show minimal differences in the average structures of the various mutants. In fact, comparison of the protein fingerprints ([^{1}H,^{15}N] HSQC spectra) of the AFA-PLN$^{M20G\ P21G}$ mutant and AFA-PLN show only some slight differences, especially in residues near the mutation site in the primary sequence. A few differences are also evident for residues located in the juxta membrane domain Ib (**Figure 1**). A map of the chemical shift changes upon increasing glycines in the loop did not follow the same trajectory that was seen for pseudo-phosphorylated mutants and the Ser16 phosphorylated species (17). Also, the NMR dynamic parameters (R_1, R_2 and heteronuclear NOE values) in domain Ia indicate that AFA PLN$^{M20G\ P21G}$ is significantly less dynamic than pSer16 AFA-PLN in this domain

(**Figure S2**). Still, AFA-PLN$^{M20G\ P21G}$ mimics pSer16-PLN functionally, which suggests that mutations in the loop leads to the reversal of SERCA inhibition by a different mechanism that an order-to-disorder transition of domain Ia, a mechanism that has been proposed for phosphorylated and pseudo-phosphorylated mutants of PLN (17). In contrast to domain Ia, the conformational dynamics of the loop and domain Ib of the Gly mutants are similar to that of pSer16 PLN and thus more mobile than AFA-PLN. Taken together with the chemical shift changes in domain Ib, this alteration of domain Ib conformational dynamics may be responsible for the functional effects associated with the Gly mutations.

Based on the data collected on these single, double, and triple Gly mutants, we hypothesize that the functional effects of the Gly mutations are related to a gradual structural uncoupling of the two helical domains of PLN: the inhibitory transmembrane domain and the regulatory cytoplasmic regions. A single Gly mutation increases the local dynamics and induces LOF character. Also, a double mutation augments the LOF character with concomitant increase of local dynamics. However, three sequential mutations cause a complete loss of the structural coupling between the regulatory cytoplasmic domain and *the inhibitory transmembrane domain*, rendering the mutant similar to the isolated transmembrane domain, which has an inhibitory potency similar to that of PLN (14). To support this hypothesis, we showed that single and double Gly mutants have increasing LOF character, while the inhibitory potency of the triple Gly mutant is virtually identical to that of AFA-PLN.

Interestingly, AFA-PLN$^{M20G\ P21G\ Q22G}$ can still be phosphorylated, reversing SERCA inhibition. The substitution of the three Gly residues in the loop does not prevent the signal of phosphorylation to be relayed from PLN to SERCA to reverse its inhibition. This suggests that phosphorylation is a more complex event that involves both structural and electrostatic changes in both binding partners, with a possible allosteric mechanism where interactions of the phosphorylated domain Ia lead to changes within SERCA that are relayed to domain II. The latter will be resolved when atomic resolution structural information on the SERCA/PLN will be available.

Although the original Ala-scanning experiments performed by (31) show Ala mutations in the loop region to be non-effectual on SERCA function (with the exception of P21A), Gly

mutations in the same region reveal that fairly conservative alterations in the loop region can have a significant impact on SERCA function. **Figure 4** shows a structural dynamics and function correlation between different species of PLN, and the blue triangle highlights the optimum area to target when designing LOF mutants to improve cardiac contractility by improving SERCA function. The results of this study are promising in revealing the loop region as an area to target for development of therapeutic PLN mutants, since the phosphorylation site remains intact. The results of studying PLN mutations have established that for a mutant to maintain proper function: (a) it must be able to be phosphorylated in order to relieve inhibition, and (b) the dynamic changes throughout domain Ia, the loop, and domain Ib can mimic the order-to-disorder transition induced by phosphorylation, but they should not exceed the dynamics of pSer16 PLN.

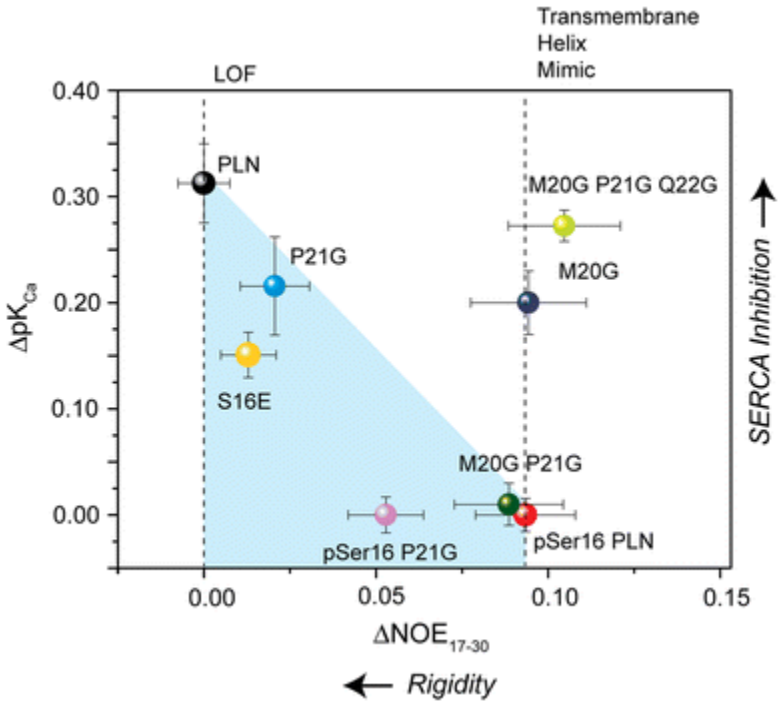

Figure 4. Stuctural dynamics-function correlation plot of PLN Gly mutants. *Left axis is degree of SERCA inhibition, with a larger ΔpK_{Ca} indicating more SERCA inhibition. ΔNOE is difference in average NOE values for each PLN species in the loop and domain Ib (residues 17–30) from AFA-PLN. Higher values in ΔNOE indicates more fast dynamics for that mutant. Blue triangle highlights optimum region for designing PLN mutants to improve cardiac contractility.*

8.5 References

1. Bers, D. M. 2002. Cardiac excitation-contraction coupling. Nature. 415, 198-205.

2. Kelly, E. M., Z. Hou, J. Bossuyt, D.M. Bers and S.L. Robia 2008. Phospholamban oligomerization, quaternary structure, and sarco(endo)plasmic reticulum calcium ATPase binding measured by fluorescence resonance energy transfer in living cells. J. Biol. Chem. 283, 12202-12211.

3. Haghighi, K., K.N. Gregory and E.G. Kranias 2004. Sarcoplasmic reticulum ca-ATPase-phospholamban interactions and dilated cardiomyopathy. Biochem. Biophys. Res. Commun. 322, 1214-1222.

4. MacLennan, D. H. and E.G. Kranias 2003. Phospholamban: A crucial regulator of cardiac contractility. Nat Rev Mol Cell Biol. 4, 566-77.

5. Toyoshima, C., M. Nakasako, H. Nomura and H. Ogawa 2000. Crystal structure of the calcium pump of sarcoplasmic reticulum at 2.6 A resolution. Nature. 405, 647-55.

6. Simmerman, H. K. and L.R. Jones 1998. Phospholamban: Protein structure, mechanism of action, and role in cardiac function. Physiol Rev. 78, 921-47.

7. Traaseth, N. J., K.N. Ha, R. Verardi, L. Shi, J.J. Buffy, L.R. Masterson and G. Veglia 2008. Structural and dynamic basis of phospholamban and sarcolipin inhibition of ca(2+)-ATPase. Biochemistry. 47, 3-13.

8. Veglia, G., K.N. Ha, L. Shi, R. Verardi and N.J. Traaseth 2010. What can we learn from a small regulatory membrane protein? Methods Mol. Biol. 654, 303-319.

9. Bers, D. M. 2008. Calcium cycling and signaling in cardiac myocytes. Annu. Rev. Physiol. 70, 23-49.

10. Traaseth, N. J., L. Shi, R. Verardi, D.G. Mullen, G. Barany and G. Veglia 2009. Structure and topology of monomeric phospholamban in lipid membranes determined by a hybrid solution and solid-state NMR approach. Proc. Natl. Acad. Sci. U. S. A. 106, 10165-10170.

11. Verardi, R., L. Shi, N.J. Traaseth, N. Walsh and G. Veglia 2011. Structural topology of phospholamban pentamer in lipid bilayers by a hybrid solution and solid-state NMR method. Proc Natl Acad Sci U S A. 108, 9101-9106.

12. Zamoon, J., A. Mascioni, D.D. Thomas and G. Veglia 2003. NMR solution structure and topological orientation of monomeric phospholamban in dodecylphosphocholine micelles. Biophys. J. 85, 2589-2598.

13. Metcalfe, E. E., J. Zamoon, D.D. Thomas and G. Veglia 2004. (1)H/(15)N heteronuclear NMR spectroscopy shows four dynamic domains for phospholamban reconstituted in dodecylphosphocholine micelles. Biophys. J. 87, 1205-1214.

14. Karim, C. B., C.G. Marquardt, J.D. Stamm, G. Barany and D.D. Thomas 2000. Synthetic null-cysteine phospholamban analogue and the corresponding transmembrane domain inhibit the ca-ATPase. Biochemistry. 39, 10892-7.

15. Karim, C. B., T.L. Kirby, Z. Zhang, Y. Nesmelov and D.D. Thomas 2004. Phospholamban structural dynamics in lipid bilayers probed by a spin label rigidly coupled to the peptide backbone. Proc Natl Acad Sci U S A. 101, 14437-42.

16. Chu, G., J.W. Lester, K.B. Young, W. Luo, J. Zhai and E.G. Kranias 2000. A single site (Ser16) phosphorylation in phospholamban is sufficient in mediating its maximal cardiac responses to beta -agonists. J. Biol. Chem. 275, 38938-38943.

17. Gustavsson, M., N.J. Traaseth, C.B. Karim, E.L. Lockamy, D.D. Thomas and G. Veglia 2011. Lipid-mediated Folding/Unfolding of phospholamban as a regulatory mechanism for the sarcoplasmic reticulum ca(2+)-ATPase. J. Mol. Biol. 408, 755-765.

18. Gustavsson, M., N.T. Traaseth and G. Veglia 2011. Probing ground and excited states of phospholamban in model and native lipid membranes by magic angle spinning NMR spectroscopy. Biochim. Biophys. Acta. 1818.

19. Masterson, L. R., T. Yu, L. Shi, Y. Wang, M. Gustavsson, M.M. Mueller and G. Veglia 2011. cAMP-dependent protein kinase A selects the excited state of the membrane substrate phospholamban. J. Mol. Biol. 412, 155-164.

20. Traaseth, N. J. and G. Veglia 2010. Probing excited states and activation energy for the integral membrane protein phospholamban by NMR CPMG relaxation dispersion experiments. Biochim. Biophys. Acta. 1798, 77-81.

21. Li, J., C.B. Boschek, Y. Xiong, C.A. Sacksteder, T.C. Squier and D.J. Bigelow 2005. Essential role for Pro21 in phospholamban for optimal inhibition of the ca-ATPase. Biochemistry. 44, 16181-16191.

22. Ha, K. N., N.J. Traaseth, R. Verardi, J. Zamoon, A. Cembran, C.B. Karim, D.D. Thomas and G. Veglia 2007. Controlling the inhibition of the sarcoplasmic Ca2+-ATPase by tuning phospholamban structural dynamics. J. Biol. Chem. 282, 37205-37214.

23. Hoshijima, M., Y. Ikeda, Y. Iwanaga, S. Minamisawa, M.O. Date, Y. Gu, M. Iwatate, M. Li, L. Wang, J.M. Wilson, Y. Wang, J. Ross Jr and K.R. Chien 2002. Chronic suppression of heart-failure progression by a pseudophosphorylated mutant of phospholamban via in vivo cardiac rAAV gene delivery. Nat. Med. 8, 864-871.

24. Kaye, D. M., A. Preovolos, T. Marshall, M. Byrne, M. Hoshijima, R. Hajjar, J.A. Mariani, S. Pepe, K.R. Chien and J.M. Power 2007. Percutaneous cardiac recirculation-mediated gene transfer of an inhibitory phospholamban peptide reverses advanced heart failure in large animals. J. Am. Coll. Cardiol. 50, 253-260.

25. Schmitt, J. P., M. Kamisago, M. Asahi, G.H. Li, F. Ahmad, U. Mende, E.G. Kranias, D.H. MacLennan, J.G. Seidman and C.E. Seidman 2003. Dilated cardiomyopathy and heart failure caused by a mutation in phospholamban. Science. 299, 1410-3.

26. Medeiros, A., D.G. Biagi, T.J. Sobreira, P.S. de Oliveira, C.E. Negrao, A.J. Mansur, J.E. Krieger, P.C. Brum and A.C. Pereira 2011. Mutations in the human phospholamban gene in patients with heart failure. Am. Heart J. 162, 1088-1095.e1.

27. Haghighi, K., F. Kolokathis, A.O. Gramolini, J.R. Waggoner, L. Pater, R.A. Lynch, G.C. Fan, D. Tsiapras, R.R. Parekh, G.W. Dorn 2nd, D.H. MacLennan, D.T. Kremastinos and E.G. Kranias 2006. A mutation in the human phospholamban gene, deleting arginine 14, results in lethal, hereditary cardiomyopathy. Proc. Natl. Acad. Sci. U. S. A. 103, 1388-1393.

28. Haghighi, K., F. Kolokathis, L. Pater, R.A. Lynch, M. Asahi, A.O. Garmolini, G. Fan, D. Tsiapras, H.S. Hahn, S. Adamopoulos, S.B. Liggett, G.W.I. Dorn, D.H. Mac Lennan, D.T. Kremastinos and E.G. Kranias 2003. Human phospholamban null results in lethal dilated cardiomyopathy revealing a critical difference between mouse and human. J Clin Invest. 111, 869-876.

29. Hoshijima, M., R. Knoll, M. Pashmforoush and K.R. Chien 2006. Reversal of calcium cycling defects in advanced heart failure toward molecular therapy. J. Am. Coll. Cardiol. 48, A15-23.

30. Ishikawa, K., L. Tilemann, K. Fish and R.J. Hajjar 2011. Gene delivery methods in cardiac gene therapy. J. Gene Med. 13, 566-572.

31. MacLennan, D. H., Y. Kimura and T. Toyofuku 1998. Sites of regulatory interaction between calcium ATPases and phospholamban. Ann N Y Acad Sci. 853, 31-42.

32. Simmerman, H. K., Y.M. Kobayashi, J.M. Autry and L.R. Jones 1996. A leucine zipper stabilizes the pentameric membrane domain of phospholamban and forms a coiled-coil pore structure. J Biol Chem. 271, 5941-6.

33. Trieber, C. A., M. Afara and H.S. Young 2009. Effects of phospholamban transmembrane mutants on the calcium affinity, maximal activity, and cooperativity of the sarcoplasmic reticulum calcium pump. Biochemistry. 48, 9287-9296.

34. Palmer, A. G.,3rd, C.D. Kroenke and J.P. Loria 2001. Nuclear magnetic resonance methods for quantifying microsecond-to-millisecond motions in biological macromolecules. Methods Enzymol. 339, 204-238.

35. Buck, B., J. Zamoon, T.L. Kirby, T.M. DeSilva, C. Karim, D. Thomas and G. Veglia 2003. Overexpression, purification, and characterization of recombinant ca-ATPase regulators for high-resolution solution and solid-state NMR studies. Protein Expr Purif. 30, 253-61.

36. Metcalfe, E. E., N.J. Traaseth and G. Veglia 2005. Serine 16 phosphorylation induces an order-to-disorder transition in monomeric phospholamban. Biochemistry. 44, 4386-4396.

37. Masterson, L. R., A. Mascioni, N.J. Traaseth, S.S. Taylor and G. Veglia 2008. Allosteric cooperativity in protein kinase A. Proc Natl Acad Sci U S A. 105, 506-511.

38. Fabiato, A. and F. Fabiato 1978. Calcium-induced release of calcium from the sarcoplasmic reticulum of skinned cells from adult human, dog, cat, rabbit, rat, and frog hearts and from fetal and new-born rat ventricles. Ann. N. Y. Acad. Sci. 307, 491-522.

39. Reddy, L. G., R.L. Cornea, D.L. Winters, E. McKenna and D.D. Thomas 2003. Defining the molecular components of calcium transport regulation in a reconstituted membrane system. Biochemistry. 42, 4585-92.

40. Farrow, N. A., R. Muhandiram, A.U. Singer, S.M. Pascal, C.M. Kay, G. Gish, S.E. Shoelson, T. Pawson, J.D. Forman-Kay and L.E. Kay 1994. Backbone dynamics of a free and phosphopeptide-complexed src homology 2 domain studied by 15N NMR relaxation. Biochemistry. 33, 5984-6003.

41. Johnson, B. A. 2004. Using NMRView to visualize and analyze the NMR spectra of macromolecules. Methods Mol. Biol. 278, 313-352.

42. Ha, K. N., L.R. Masterson, Z. Hou, R. Verardi, N. Walsh, G. Veglia and S.L. Robia 2011. Lethal Arg9Cys phospholamban mutation hinders Ca2+-ATPase regulation and phosphorylation by protein kinase A. Proc. Natl. Acad. Sci. U. S. A. 108, 2735-2740.

43. Kimura, Y., M. Asahi, K. Kurzydlowski, M. Tada and D.H. MacLennan 1998. Phospholamban domain ib mutations influence functional interactions with the Ca2+-ATPase isoform of cardiac sarcoplasmic reticulum. J Biol Chem. 273, 14238-41.

44. Shanmugam, M., S. Gao, C. Hong, N. Fefelova, M.C. Nowycky, L.H. Xie, M. Periasamy and G.J. Babu 2011. Ablation of phospholamban and sarcolipin results in cardiac hypertrophy and decreased cardiac contractility. Cardiovasc. Res. 89, 353-361.

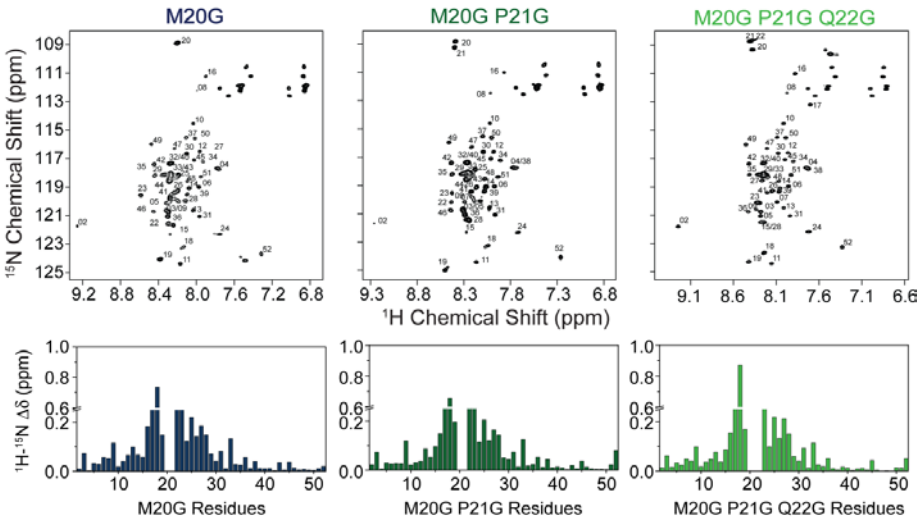

Figure S1. ^{1}H-^{15}N HSQC spectra *of AFA-PLN$_{M20G}$ (top left), AFA-PLN$_{M20G\ P21G}$ (top middle), AFAPLN$_{M20G\ P21G\ Q22G}$ (top right) and combined chemical shift perturbations between AFA-PLN and the M20Gmutant (bottom left, dark blue), M20G P21G mutant (bottom middle, evergreen), and M20G P21G Q22Gmutant (bottom right, lime).*

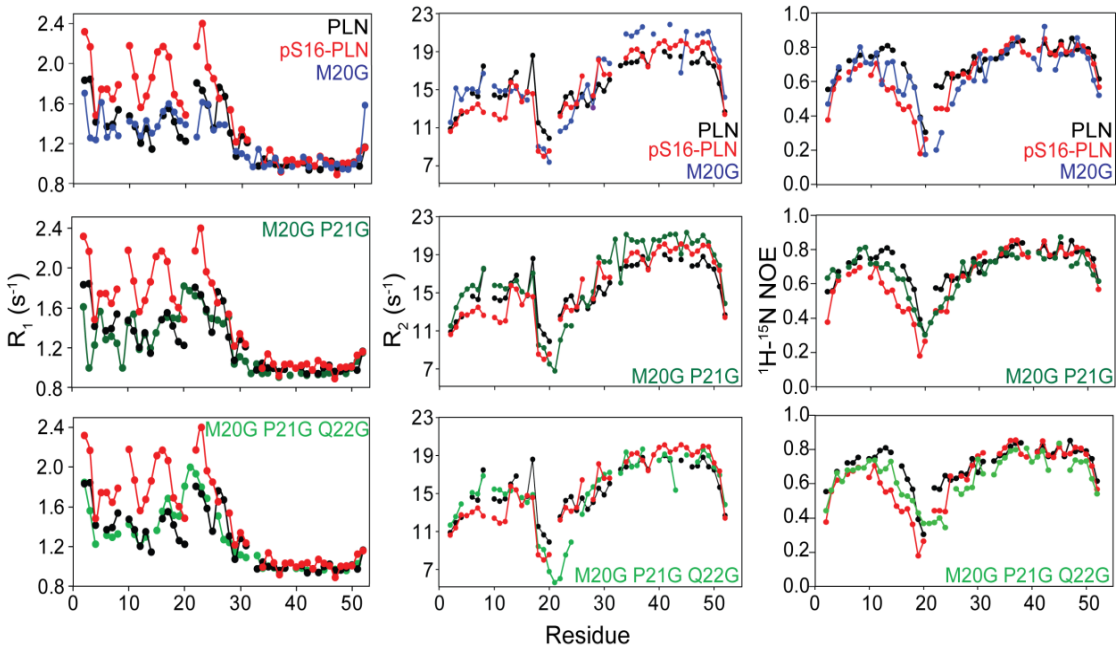

Figure S2. Fast amide backbone dynamics measurements by solution state NMR *of Gly PLN mutants. R_1 (left), R_2 (middle), and {^{1}H-^{15}N} steady state NOE measurements were done in 300 mM DPC micelles. AFAPLN (black) and pSer16-AFA-PLN (red) are plotted for comparison. Data for AFA-PLN and pSer16-AFAPLN are taken from Metcalfe, et. al. 2004 and 2005* (13, 36).

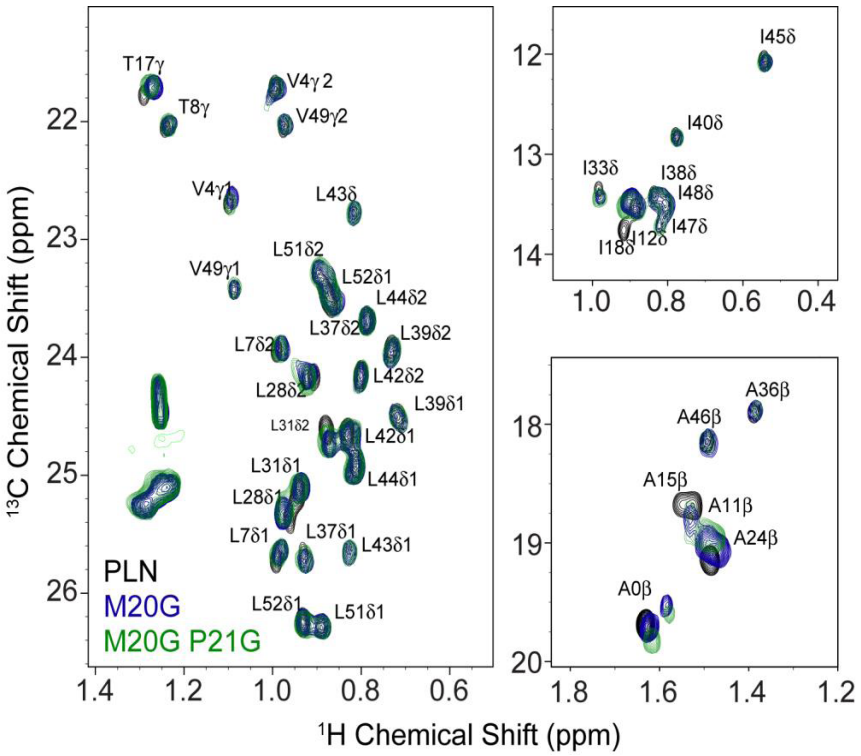

Figure S3. Overlay of [^{1}H-^{13}C] HSQC spectra *of AFA-PLN (black), AFA-PLN$_{M20G}$ (navy), and AFAPLN$_{M20GP21G}$ (dark green) in 300 mM DPC at 37 °C.*

Chapter 9 – Conclusions and future directions

In the last few years the field of membrane protein NMR has evolved to study larger systems under more native-like conditions. This has meant progressing from studies of single TM helices in detergent micelles or organic solvent to studies of large membrane-bound enzymes, channels, and receptors in bicelles, lipid vesicles or nanodiscs. In my initial studies I characterized the single-spanning membrane protein PLN in DPC micelles while my later studies have focused on the complex between PLN and the 110 kDa membrane-bound SERCA in native-like lipid bilayers. In this regard, the progression of my thesis has reflected the exciting development of the field.

Chapter 2 describes the characterization of the conformational equilibrium of PLN by NMR and concludes that the protein populates at least four different conformational states (T, T', R, and R'). Phosphorylation and pseudo-phosphorylation of PLN perturb the equilibrium by increasing the population of the partially unfolded R and R' states, which is correlated with less efficient inhibition of SERCA. The importance of the T and R states is further underscored in chapter 3, where we show that the R state but not the T state gets phosphorylated by PKA. A limitation with the two initial studies, as well as the study in chapter 4 where the high resolution structure of the T state in detergent micelles was determined, is that all NMR experiments were conducted in detergent micelles or isotropic bicelles. However, SERCA activity and inhibition of PLN is measured in lipid bilayers so to fully understand PLN function it was crucial to acquire NMR experiments at the same conditions. Chapter 5 describes the characterization of the conformational equilibrium of PLN by NMR in lipid vesicles. Importantly, this study showed that the structures of T and R states are conserved in lipids even if the relative populations of the two states are strongly lipid-dependent. In a parallel study, described in chapter 6, we also found that the function of SERCA and its inhibition by PLN can be modulated by the lipid composition of the bilayer. Chapter 7 describes how we utilized the foundation of sample preparation and NMR experiments that was built through chapters 2-6 to determine molecular details of the SERCA/PLN and the role of the R/T equilibrium in SERCA regulation. Through asymmetric spin labeling of SERCA, PLN and the lipid bilayer, we show that the R state has transient interactions with the cytoplasmic P and N domains of SERCA and that the T state remains bilayer-associated. This study

marks an unprecedented mapping of a membrane protein complex by solid state NMR spectropscopy. For example, this is the first time that PREs were used to probe the interaction between two membrane proteins in lipid bilayers. Another important aspect of our SERCA/PLN studies is the prospective of translating our in vitro results into in vivo studies to develop potential therapies against heart failure. In chapter 8 we find that by targeted mutagenesis in the loop region of PLN we can control SERCA function. Since mutations in the loop region do not interfere with PKA phosphorylation or SERCA binding, these mutants could be future candidates in the therapeutic efforts to treat heart failure.

From a SERCA/PLN perspective, the main conclusions from this thesis are

- The T and R states of PLN exist in all membrane-mimicking systems but the populations of the two states are very sensitive to lipid composition.
- The T/R state equilibrium of PLN is crucial to control SERCA function and for PKA phosphorylation and can be modulated by bilayer lipids.
- SERCA function is strongly dependent on lipid bilayer composition and SERCA is activated by PE and PS lipids.
- The cytoplasmic of PLN populates mutiple states in the SERCA/PLN complex: the T state is helical and bilayer associated, the R state is unfolded and membrane-dissociated and interacts transiently with the P and N domains of SERCA to form a “bound” state.
- In the bound state, interactions with the cytoplasmic domains of SERCA relieve PLN’s inhibition, forming a non-inhibitory complex.

Furthermore, our findings solidify the roles of the TM and cytoplasmic domains of PLN as inhibitory and regulatory modules, respectively. The regulatory cytoplasmic domain is transiently folded and interacts with a number of binding partners in different configurations. In fact, based on our data, this domain should be viewed as an

intrinsically disordered protein that can adapt its structure to its target of regulation. We have showed that this domain is unfolded in complex with both SERCA and PKA and helical when associated with the membrane bilayer. The cytoplasmic domain of PLN also interacts with HS-1–associated protein X-1 (HAX-1) (1) and A kinase anchoring protein 7 (AKAP7) (2). Even if the confirmation of PLN that interacts with these proteins remains to be determined it further underscores the versatile role of the cytoplasmic domain in PLN function.

The data presented here will provide a crucial foundation for the determination of high resolution structures of the complex between SERCA and the different PLN conformations. The structures could answer important questions of the molecular details of SERCA regulation. For example, even if we concluded that the cytoplasmic interactions between PLN and SERCA are non-inhibitory, we don't know if they are affecting ATP hydrolysis, Ca^{2+} transport or both. Also, because of the current inability to isotopically label SERCA, our NMR experiments have been limited to acquisitions of PLN signals and thus we are unable to directly detect the structural changes SERCA undergoes upon PLN interaction. By expression of SERCA in yeast or mammalian systems or by post-translational labeling, our solid state NMR methods could probe also the structure of SERCA. With detection of SERCA signals and extension of our asymmetric spin labeling approach to additional sites on both SERCA and PLN, solid-state NMR is in an excellent position to answer many of the longstanding questions about SERCA regulation by PLN. This knowledge could be of paramount importance in the development of heart failure novel therapies that target the SERCA/PLN complex.

In a broader perspective the results presented here have shown that:

- Membrane proteins, and particularly amphipathic helices, exist in multiple states and to understand protein function it is crucial to characterize all these conformations.
- Amphipathic helices are very sensitive to the membrane-mimicking environment (i.e detergent micelle, lipid bilayer).

- PREs are a powerful approach to map membrane protein interactions by solid-state NMR and can be applied to large membrane protein systems.

The conclusions are based on our results with PLN reconstituted into lipid bilayers, detergent micelles and bicelles, which were used to stabilize different states of PLN. Among these systems, lipid bilayers are undeniably the most native-like environment for a membrane protein, and a crucial development in the field of membrane protein structural biology will be to acquire experiments in native-like lipid bilayers or even complete cell membranes. To this end, solid-state NMR has found a niche in the study of biological systems such as membrane proteins and amyloid fibrils that are not amenable to solution NMR and X-ray crystallography in their native environment. With the current advancements in hardware design and sample preparation as well as novel techniques such as the application of dynamic nuclear polarization (DNP) (3) to biomolecules, solid-state NMR promises to be an even more powerful technique for studies of membrane proteins in the future.

9.1 References

1. Vafiadaki, E., D. Sanoudou, D.A. Arvanitis, D.H. Catino, E.G. Kranias and A. Kontrogianni-Konstantopoulos 2007. Phospholamban interacts with HAX-1, a mitochondrial protein with anti-apoptotic function. J. Mol. Biol. 367, 65-79.

2. Lygren, B., C.R. Carlson, K. Santamaria, V. Lissandron, T. McSorley, J. Litzenberg, D. Lorenz, B. Wiesner, W. Rosenthal, M. Zaccolo, K. Tasken and E. Klussmann 2007. AKAP complex regulates Ca2+ re-uptake into heart sarcoplasmic reticulum. EMBO Rep. 8, 1061-1067.

3. Maly, T., G.T. Debelouchina, V.S. Bajaj, K.N. Hu, C.G. Joo, M.L. Mak-Jurkauskas, J.R. Sirigiri, P.C. van der Wel, J. Herzfeld, R.J. Temkin and R.G. Griffin 2008. Dynamic nuclear polarization at high magnetic fields. J. Chem. Phys. 128, 052211.

Bibliography

Abu-Baker, S. and G.A. Lorigan 2006. Phospholamban and its phosphorylated form interact differently with lipid bilayers: A 31P, 2H, and 13C solid-state NMR spectroscopic study. Biochemistry. 45, 13312-13322.

Abu-Baker, S., J.X. Lu, S. Chu, C.C. Brinn, C.A. Makaroff and G.A. Lorigan 2007. Side chain and backbone dynamics of phospholamban in phospholipid bilayers utilizing (2)h and (15)n solid-state NMR spectroscopy. Biochemistry. 46, 11695-11706.

Ader, C., R. Schneider, S. Hornig, P. Velisetty, E.M. Wilson, A. Lange, K. Giller, I. Ohmert, M.F. Martin-Eauclaire, D. Trauner, S. Becker, O. Pongs and M. Baldus 2008. A structural link between inactivation and block of a K+ channel. Nat. Struct. Mol. Biol. 15, 605-612.

Ader, C., R. Schneider, K. Seidel, M. Etzkorn, S. Becker and M. Baldus 2009. Structural rearrangements of membrane proteins probed by water-edited solid-state NMR spectroscopy. J. Am. Chem. Soc. 131, 170-176.

Afara, M. R., C.A. Trieber, J.P. Glaves and H.S. Young 2006. Rational design of peptide inhibitors of the sarcoplasmic reticulum calcium pump. Biochemistry. 45, 8617-8627.

Al-Hashimi, H. M., P.J. Bolon and J.H. Prestegard 2000a. Molecular symmetry as an aid to geometry determination in ligand protein complexes. J. Magn. Reson. 142, 153-158.

Al-Hashimi, H. M., H. Valafar, M. Terrell, E.R. Zartler, M.K. Eidsness and J.H. Prestegard 2000b. Variation of molecular alignment as a means of resolving orientational ambiguities in protein structures from dipolar couplings. J. Magn. Reson. 143, 402-406.

Andronesi, O. C., S. Becker, K. Seidel, H. Heise, H.S. Young and M. Baldus 2005. Determination of membrane protein structure and dynamics by magic-angle-spinning solid-state NMR spectroscopy. J. Am. Chem. Soc. 127, 12965-12974.

Asahi, M., N.M. Green, K. Kurzydlowski, M. Tada and D.H. MacLennan 2001. Phospholamban domain IB forms an interaction site with the loop between transmembrane helices M6 and M7 of sarco(endo)plasmic reticulum Ca2+ ATPases. Proc Natl Acad Sci U S A. 98, 10061-6.

Asahi, M., E. McKenna, K. Kurzydlowski, M. Tada and D.H. MacLennan 2000. Physical interactions between phospholamban and sarco(endo)plasmic reticulum Ca2+-ATPases are dissociated by elevated Ca2+, but not by phospholamban phosphorylation, vanadate, or thapsigargin, and are enhanced by ATP. J Biol Chem. 275, 15034-8.

Bajaj, V. S., M.L. Mak-Jurkauskas, M. Belenky, J. Herzfeld and R.G. Griffin 2009. Functional and shunt states of bacteriorhodopsin resolved by 250 GHz dynamic nuclear polarization-enhanced solid-state NMR. Proc. Natl. Acad. Sci. U. S. A. 106, 9244-9249.

Bakheet, T. M. and A.J. Doig 2009. Properties and identification of human protein drug targets. Bioinformatics. 25, 451-457.

Baldwin, A. J., D.F. Hansen, P. Vallurupalli and L.E. Kay 2009. Measurement of methyl axis orientations in invisible, excited states of proteins by relaxation dispersion NMR spectroscopy. J. Am. Chem. Soc. 131, 11939-11948.

Battiste, J. L. and G. Wagner 2000. Utilization of site-directed spin labeling and high-resolution heteronuclear nuclear magnetic resonance for global fold determination of large proteins with limited nuclear overhauser effect data. Biochemistry. 39, 5355-5365.

Bax, A., G. Kontaxis and N. Tjandra 2001. Dipolar coupling in macromolecular structure determination. Methods in Enzymology. 339, 127-174.

Becucci, L., A. Cembran, C.B. Karim, D.D. Thomas, R. Guidelli, J. Gao and G. Veglia 2009. On the function of pentameric phospholamban: Ion channel or storage form? Biophys. J. 96, L60-2.

Bennett, A. E., C.M. Rienstra, M. Auger, K.V. Lakshmi and R.G. Griffin 1995. Heteronuclear decoupling in rotating solids. J Chem Phys. 103, 6951-8.

Berardi, M. J., W.M. Shih, S.C. Harrison and J.J. Chou 2011. Mitochondrial uncoupling protein 2 structure determined by NMR molecular fragment searching. Nature. 476, 109-113.

Bers, D. M. 2008. Calcium cycling and signaling in cardiac myocytes. Annu. Rev. Physiol. 70, 23-49.

Bers, D. M. 2002. Cardiac excitation-contraction coupling. Nature. 415, 198-205.

Bertelsen, E. B., L. Chang, J.E. Gestwicki and E.R. Zuiderweg 2009. Solution conformation of wild-type E. coli Hsp70 (DnaK) chaperone complexed with ADP and substrate. Proc. Natl. Acad. Sci. U. S. A. 106, 8471-8476.

Bertini, I., Y.K. Gupta, C. Luchinat, G. Parigi, M. Peana, L. Sgheri and J. Yuan 2007. Paramagnetism-based NMR restraints provide maximum allowed probabilities for the different conformations of partially independent protein domains. J. Am. Chem. Soc. 129, 12786-12794.

Bhabha, G., J. Lee, D.C. Ekiert, J. Gam, I.A. Wilson, H.J. Dyson, S.J. Benkovic and P.E. Wright 2011. A dynamic knockout reveals that conformational fluctuations influence the chemical step of enzyme catalysis. Science. 332, 234-238.

Bick, R. J., L.M. Buja, W.B. Van Winkle and G.E. Taffet 1998. Membrane asymmetry in isolated canine cardiac sarcoplasmic reticulum: Comparison with skeletal muscle sarcoplasmic reticulum. J. Membr. Biol. 164, 169-175.

Birmachu, W., F.L. Nisswandt and D.D. Thomas 1989. Conformational transitions in the calcium adenosinetriphosphatase studied by time-resolved fluorescence resonance energy transfer. Biochemistry. 28, 3940-3947.

Boehr, D. D., R. Nussinov and P.E. Wright 2009. The role of dynamic conformational ensembles in biomolecular recognition. Nat. Chem. Biol. 5, 789-796.

Bogdanov, M., P. Heacock, Z. Guan and W. Dowhan 2010. Plasticity of lipid-protein interactions in the function and topogenesis of the membrane protein lactose permease from escherichia coli. Proc. Natl. Acad. Sci. U. S. A. 107, 15057-15062.

Brini, M. and E. Carafoli 2009. Calcium pumps in health and disease. Physiol. Rev. 89, 1341-1378.

Buck, B., J. Zamoon, T.L. Kirby, T.M. DeSilva, C. Karim, D. Thomas and G. Veglia 2003. Overexpression, purification, and characterization of recombinant ca-ATPase regulators for high-resolution solution and solid-state NMR studies. Protein Expr Purif. 30, 253-61.

Buechler, J. A., J.A. Toner-Webb and S.S. Taylor 1991. Carbodiimides as probes for protein kinase structure and function. Methods Enzymol. 200, 487-500.

Buffy, J. J., N.J. Traaseth, A. Mascioni, P.L. Gor'kov, E.Y. Chekmenev, W.W. Brey and G. Veglia 2006. Two-dimensional solid-state NMR reveals two topologies of sarcolipin in oriented lipid bilayers. Biochemistry. 45, 10939-10946.

Cady, S. D., K. Schmidt-Rohr, J. Wang, C.S. Soto, W.F. Degrado and M. Hong 2010. Structure of the amantadine binding site of influenza M2 proton channels in lipid bilayers. Nature. 463, 689-692.

Caffrey, M. and G.W. Feigenson 1981. Fluorescence quenching in model membranes. 3. relationship between calcium adenosinetriphosphatase enzyme activity and the affinity of the protein for phosphatidylcholines with different acyl chain characteristics. Biochemistry. 20, 1949-1961.

Castellani, F., B. van Rossum, A. Diehl, M. Schubert, K. Rehbein and H. Oschkinat 2002. Structure of a protein determined by solid-state magic-angle-spinning NMR spectroscopy. Nature. 420, 98-102.

Chen, Z., B.L. Akin and L.R. Jones 2007. Mechanism of reversal of phospholamban inhibition of the cardiac Ca2+-ATPase by protein kinase A and by anti-phospholamban monoclonal antibody 2D12. J. Biol. Chem. 282, 20968-20976.

Cherezov, V., D.M. Rosenbaum, M.A. Hanson, S.G. Rasmussen, F.S. Thian, T.S. Kobilka, H.J. Choi, P. Kuhn, W.I. Weis, B.K. Kobilka and R.C. Stevens 2007. High-resolution crystal structure of an engineered human beta2-adrenergic G protein-coupled receptor. Science. 318, 1258-1265.

Chill, J. H., J.M. Louis, F. Delaglio and A. Bax 2007. Local and global structure of the monomeric subunit of the potassium channel KcsA probed by NMR. Biochim. Biophys. Acta. 1768, 3260-3270.

Chou, J. J., S. Gaemers, B. Howder, J.M. Louis and A. Bax 2001. Journal of Molecular Biology. 21, 377-382.

Chou, J. J., J.D. Kaufman, S.J. Stahl, P.T. Wingfield and A. Bax 2002. Micelle-induced curvature in a water-insoluble HIV-1 env peptide revealed by NMR dipolar coupling measurement in stretched polyacrylamide gel. J. Am. Chem. Soc. 124, 2450-2451.

Chu, G., J.W. Lester, K.B. Young, W. Luo, J. Zhai and E.G. Kranias 2000. A single site (Ser16) phosphorylation in phospholamban is sufficient in mediating its maximal cardiac responses to beta -agonists. J. Biol. Chem. 275, 38938-38943.

Chu, S., S. Abu-Baker, J. Lu and G.A. Lorigan 2010. (15)N solid-state NMR spectroscopic studies on phospholamban at its phosphorylated form at ser-16 in aligned phospholipid bilayers. Biochim. Biophys. Acta. 1798, 312-317.

Cierpicki, T., B. Liang, L.K. Tamm and J.H. Bushweller 2006. Increasing the accuracy of solution NMR structures of membrane proteins by application of residual dipolar couplings. high-resolution structure of outer membrane protein A. J. Am. Chem. Soc. 128, 6947-6951.

Clayton, J. C., E. Hughes and D.A. Middleton 2005. Spectroscopic studies of phospholamban variants in phospholipid bilayers. Biochem. Soc. Trans. 33, 913-915.

Clore, G. M. and J. Kuszewski 2003. Improving the accuracy of NMR structures of RNA by means of conformational database potentials of mean force as assessed by complete dipolar coupling cross-validation. J. Am. Chem. Soc. 125, 1518-1525.

Clore, M. G., M.A. Gronenborn and A. Bax 1998a. A robust method for determining the magnitude of the fully asymmetric alignment tensor of oriented macromolecules in the absence of structural information. Journal of Magnetic Resonance. 133, 216-221.

Clore, M. G., M.A. Gronenborn and N. Tjandra 1998b. Direct structure refinement against residual dipolar couplings in the presence of rhombicity of unknown magnitude. Journal of Magnetic Resonance. 131, 159-162.

Cook, P. F., M.E. Neville, K.E. Vrana , F.T. Hartl and R. Roskoshi 1982. Adenosine cyclic 3'5'-monophosphate dependent protein kinase: Kinetic mechanism for the bovine skeletal muscle catalytic subunit. Biochemistry. 21, 5794-5799.

Cornea, R. L., L.R. Jones, J.M. Autry and D.D. Thomas 1997. Mutation and phosphorylation change the oligomeric structure of phospholamban in lipid bilayers. Biochemistry. 36, 2960-7.

Cornea, R. L. and D.D. Thomas 1994. Effects of membrane thickness on the molecular dynamics and enzymatic activity of reconstituted ca-ATPase. Biochemistry. 33, 2912-2920.

Cornell, R. B. and S.G. Taneva 2006. Amphipathic helices as mediators of the membrane interaction of amphitropic proteins, and as modulators of bilayer physical properties. Curr. Protein Pept. Sci. 7, 539-552.

Cornilescu, G., F. Delaglio and A. Bax 1999. Protein backbone angle restraints from searching a database for chemical shift and sequence homology. J Biomol NMR. 13, 289-302.

Csermely, P., R. Palotai and R. Nussinov 2010. Induced fit, conformational selection and independent dynamic segments: An extended view of binding events. Trends Biochem. Sci. 35, 539-546.

Cui, Q. and M. Karplus 2008. Allostery and cooperativity revisited. Protein Sci. 17, 1295-1307.

Davis, J., M.V. Westfall, D. Townsend, M. Blankinship, T.J. Herron, G. Guerrero-Serna, W. Wang, E. Devaney and J.M. Metzger 2008. Designing heart performance by gene transfer. Physiol. Rev. 88, 1567-1651.

De Angelis, A. A., S.C. Howell, A.A. Nevzorov and S.J. Opella 2006. Structure determination of a membrane protein with two trans-membrane helices in aligned phospholipid bicelles by solid-state NMR spectroscopy. J. Am. Chem. Soc. 128, 12256-12267.

De Angelis, A. A., D.H. Jones, C.V. Grant, S.H. Park, M.F. Mesleh and S.J. Opella 2005. NMR experiments on aligned samples of membrane proteins. Methods Enzymol. 394, 350-82.

De Angelis, A. A. and S.J. Opella 2007. Bicelle samples for solid-state NMR of membrane proteins. Nat. Protoc. 2, 2332-2338.

de Planque, M. R., D.T. Rijkers, J.I. Fletcher, R.M. Liskamp and F. Separovic 2004. The alphaM1 segment of the nicotinic acetylcholine receptor exhibits conformational flexibility in a membrane environment. Biochim. Biophys. Acta. 1665, 40-47.

De Simone, A., B. Richter, X. Salvatella and M. Vendruscolo 2009. Toward an accurate determination of free energy landscapes in solution states of proteins. J. Am. Chem. Soc. 131, 3810-3811.

Dedmon, M. M., K. Lindorff-Larsen, J. Christodoulou, M. Vendruscolo and C.M. Dobson 2005. Mapping long-range interactions in alpha-synuclein using spin-label NMR and ensemble molecular dynamics simulations. J. Am. Chem. Soc. 127, 476-477.

del Monte, F., S.E. Harding, G.W. Dec, J.K. Gwathmey and R.J. Hajjar 2002. Targeting phospholamban by gene transfer in human heart failure. Circulation. 105, 904-907.

Delaglio, F., Grzesiek, S., Vuister, G. W., Zhu, G. Pfeifer, J., Bax,A. 1995. NMRPipe: A multidimensional spectral processing system based on UNIX pipes. J. Biomol. NMR. 6, 277-293.

Delaglio, F., S. Grzesiek, G.W. Vuister, G. Zhu, J. Pfeifer and A. Bax 1995. NMRPipe: A multidimensional spectral processing system based on UNIX pipes. J. Biomol. NMR. 6, 277-293.

Dominguez, C., R. Boelens and A.M. Bonvin 2003. HADDOCK: A protein-protein docking approach based on biochemical or biophysical information. J. Am. Chem. Soc. 125, 1731-1737.

D'Onofrio, M., L. Ragona, D. Fessas, M. Signorelli, R. Ugolini, M. Pedo, M. Assfalg and H. Molinari 2009. NMR unfolding studies on a liver bile acid binding protein reveal a global two-state unfolding and localized singular behaviors. Arch. Biochem. Biophys. 481, 21-29.

Douglas, S. M., J.J. Chou and W.M. Shih 2007. DNA-nanotube-induced alignment of membrane proteins for NMR structure determination. Proc. Natl. Acad. Sci. U. S. A. 104, 6644-6648.

Dowhan, W. and M. Bogdanov 2011. Lipid-protein interactions as determinants of membrane protein structure and function. Biochem. Soc. Trans. 39, 767-774.

Doyle, D. A., J.M. Cabral, R.A. Pfuetzner, A. Kuo, J.M. Gulbis, S.L. Cohen, B.T. Chait and R. Mackinnon 1998. The structure of the potassium channel : Molecular basis of K+ conduction and selectivity. Science. 280, 69-77.

Dyson, H. J. and P.E. Wright 2004. Unfolded proteins and protein folding studied by NMR. Chem. Rev. 104, 3607-3622.

Dyson, H. J. and P.E. Wright 2001. Nuclear magnetic resonance methods for elucidation of structure and dynamics in disordered states. Methods Enzymol. 339, 258-271.

Dyson, H. J. and P.E. Wright 1998. Equilibrium NMR studies of unfolded and partially folded proteins. Nat Struct Biol., 499-503.

Engelman, D. M. 2005. Membranes are more mosaic than fluid. Nature. 438, 578-580.

Engelman, D. M., Y. Chen, C.N. Chin, A.R. Curran, A.M. Dixon, A.D. Dupuy, A.S. Lee, U. Lehnert, E.E. Matthews, Y.K. Reshetnyak, A. Senes and J.L. Popot 2003. Membrane protein folding: Beyond the two stage model. FEBS Lett. 555, 122-125.

Espinoza-Fonseca, L. M. and D.D. Thomas 2011. Atomic-level characterization of the activation mechanism of SERCA by calcium. PLoS One. 6, e26936.

Fabiato, A. and F. Fabiato 1978. Calcium-induced release of calcium from the sarcoplasmic reticulum of skinned cells from adult human, dog, cat, rabbit, rat, and frog hearts and from fetal and new-born rat ventricles. Ann. N. Y. Acad. Sci. 307, 491-522.

Farias, R. N., B. Bloj, R.D. Morero, F. Sineriz and R.E. Trucco 1975. Regulation of allosteric membrane-bound enzymes through changes in membrane lipid compostition. Biochim. Biophys. Acta. 415, 231-251.

Farrow, N. A., R. Muhandiram, A.U. Singer, S.M. Pascal, C.M. Kay, G. Gish, S.E. Shoelson, T. Pawson, J.D. Forman-Kay and L.E. Kay 1994. Backbone dynamics of a free and phosphopeptide-complexed src homology 2 domain studied by 15N NMR relaxation. Biochemistry. 33, 5984-6003.

Ferrington, D. A., Q. Yao, T.C. Squier and D.J. Bigelow 2002. Comparable levels of ca-ATPase inhibition by phospholamban in slow-twitch skeletal and cardiac sarcoplasmic reticulum. Biochemistry. 41, 13289-13296.

Fersht, A. 1999. Structure and Mechanism in Protein Science. W.H. Freeman & Co., New York.

Fischer, M. W. F., J.A. Losonczi, J.L. Weaver and J.H. Prestegard 1999. Domain orientation and dynamics in multidomain proteins from residual dipolar couplings. Biochemistry. 38, 9013-9022.

Franzin, C. M., P. Teriete and F.M. Marassi 2007. Structural similarity of a membrane protein in micelles and membranes. J. Am. Chem. Soc. 129, 8078-8079.

Froud, R. J., C.R. Earl, J.M. East and A.G. Lee 1986. Effects of lipid fatty acyl chain structure on the activity of the (Ca2+ + Mg2+)-ATPase. Biochim. Biophys. Acta. 860, 354-360.

Fu, S., L. Yang, P. Li, O. Hofmann, L. Dicker, W. Hide, X. Lin, S.M. Watkins, A.R. Ivanov and G.S. Hotamisligil 2011. Aberrant lipid metabolism disrupts calcium homeostasis causing liver endoplasmic reticulum stress in obesity. Nature. 473, 528-531.

Goddard, T. D., Kneller,D.G. 1999. SPARKY 3.University of California.

Goddard, T. D. and D.G. Kneller SPARKY 3. University of California, San Francisco.

Gustavsson, M., N.J. Traaseth, C.B. Karim, E.L. Lockamy, D.D. Thomas and G. Veglia 2011a. Lipid-mediated Folding/Unfolding of phospholamban as a regulatory mechanism for the sarcoplasmic reticulum ca(2+)-ATPase. J. Mol. Biol. 408, 755-765.

Gustavsson, M., N.T. Traaseth and G. Veglia 2011b. Probing ground and excited states of phospholamban in model and native lipid membranes by magic angle spinning NMR spectroscopy. Biochim. Biophys. Acta. 1818.

Ha, K. N., L.R. Masterson, Z. Hou, R. Verardi, N. Walsh, G. Veglia and S.L. Robia 2011. Lethal Arg9Cys phospholamban mutation hinders Ca2+-ATPase regulation and phosphorylation by protein kinase A. Proc. Natl. Acad. Sci. U. S. A. 108, 2735-2740.

Ha, K. N., N.J. Traaseth, R. Verardi, J. Zamoon, A. Cembran, C.B. Karim, D.D. Thomas and G. Veglia 2007. Controlling the inhibition of the sarcoplasmic Ca2+-ATPase by tuning phospholamban structural dynamics. J. Biol. Chem. 282, 37205-37214.

Hadri, L. and R.J. Hajjar 2011. Calcium cycling proteins and their association with heart failure. Clin. Pharmacol. Ther. 90, 620-624.

Haghighi, K., K.N. Gregory and E.G. Kranias 2004. Sarcoplasmic reticulum ca-ATPase-phospholamban interactions and dilated cardiomyopathy. Biochem. Biophys. Res. Commun. 322, 1214-1222.

Haghighi, K., F. Kolokathis, A.O. Gramolini, J.R. Waggoner, L. Pater, R.A. Lynch, G.C. Fan, D. Tsiapras, R.R. Parekh, G.W. Dorn 2nd, D.H. MacLennan, D.T. Kremastinos and E.G. Kranias 2006. A mutation in the human phospholamban gene, deleting arginine 14, results in lethal, hereditary cardiomyopathy. Proc. Natl. Acad. Sci. U. S. A. 103, 1388-1393.

Haghighi, K., F. Kolokathis, L. Pater, R.A. Lynch, M. Asahi, A.O. Garmolini, G. Fan, D. Tsiapras, H.S. Hahn, S. Adamopoulos, S.B. Liggett, G.W.I. Dorn, D.H. Mac Lennan, D.T. Kremastinos and E.G. Kranias 2003. Human phospholamban null results in lethal dilated cardiomyopathy revealing a critical difference between mouse and human. J Clin Invest. 111, 869-876.

Haghighi, K., A.G. Schmidt, B.D. Hoit, A.G. Brittsan, A. Yatani, J.W. Lester, J. Zhai, Y. Kimura, G.W. Dorn 2nd, D.H. MacLennan and E.G. Kranias 2001. Superinhibition of sarcoplasmic reticulum function by phospholamban induces cardiac contractile failure. J. Biol. Chem. 276, 24145-24152.

Hakizimana, P., M. Masureel, B. Gbaguidi, J.M. Ruysschaert and C. Govaerts 2008. Interactions between phosphatidylethanolamine headgroup and LmrP, a multidrug transporter: A conserved mechanism for proton gradient sensing? J. Biol. Chem. 283, 9369-9376.

Hicks, M. J., M. Shigekawa and A.M. Katz 1979. Mechanism by which cyclic adenosine 3':5'-monophosphate-dependent protein kinase stimulates calcium transport in cardiac sarcoplasmic reticulum. Circ Res. 44, 384-91.

Hiller, S., R.G. Garces, T.J. Malia, V.Y. Orekhov, M. Colombini and G. Wagner 2008. Solution structure of the integral human membrane protein VDAC-1 in detergent micelles. Science. 321, 1206-1210.

Hohwy, M., C.M. Rienstra, C.P. Jaroniec and R.G. Griffin 1999. Fivefold symmetric homonuclear dipolar recoupling in rotating solids: Application to double quantum spectroscopy. J Chem Phys. 110, 7983-7992.

Hong, M., Y. Zhang and F. Hu 2012. Membrane protein structure and dynamics from NMR spectroscopy. Annu. Rev. Phys. Chem. 63, 1-24.

Hoshijima, M., Y. Ikeda, Y. Iwanaga, S. Minamisawa, M.O. Date, Y. Gu, M. Iwatate, M. Li, L. Wang, J.M. Wilson, Y. Wang, J. Ross Jr and K.R. Chien 2002. Chronic suppression of heart-failure progression by a pseudophosphorylated mutant of phospholamban via in vivo cardiac rAAV gene delivery. Nat. Med. 8, 864-871.

Hoshijima, M., R. Knoll, M. Pashmforoush and K.R. Chien 2006. Reversal of calcium cycling defects in advanced heart failure toward molecular therapy. J. Am. Coll. Cardiol. 48, A15-23.

Hou, Z., Z. Hu, D.J. Blackwell, T.D. Miller, D.D. Thomas and S.L. Robia 2012. 2-color calcium pump reveals closure of the cytoplasmic headpiece with calcium binding. PLoS One. 7, e40369.

Hubbard, J. A., L.K. MacLachlan, E. Meenan, C.J. Salter, D.G. Reid, P. Lahouratate, J. Humphries, N. Stevens, D. Bell and W.A. Neville 1994. Conformation of the cytoplasmic domain of phospholamban by NMR and CD. Mol. Membr. Biol. 11, 263-269.

Huggins, J. P. and P.J. England 1987. Evidence for a phosphorylation-induced conformational change in phospholamban from the effects of three proteases. FEBS Lett. 217, 32-36.

Hughes, E., J.C. Clayton and D.A. Middleton 2009. Cytoplasmic residues of phospholamban interact with membrane surfaces in the presence of SERCA: A new role for phospholipids in the regulation of cardiac calcium cycling? Biochim. Biophys. Acta. 1788, 559-566.

Hunter, G. W., S. Negash and T.C. Squier 1999. Phosphatidylethanolamine modulates ca-ATPase function and dynamics. Biochemistry. 38, 1356-1364.

Hus, J. C., L. Salmon, G. Bouvignies, J. Lotze, M. Blackledge and R. Bruschweiler 2008. 16-fold degeneracy of peptide plane orientations from residual dipolar couplings: Analytical treatment and implications for protein structure determination. J. Am. Chem. Soc. 130, 15927-15937.

Hwang, T. L., P.C. van Zijl and S. Mori 1998. Accurate quantitation of water-amide proton exchange rates using the phase-modulated CLEAN chemical EXchange (CLEANEX-PM) approach with a fast-HSQC (FHSQC) detection scheme. J. Biomol. NMR. 11, 221-226.

Inesi, G., A.M. Prasad and R. Pilankatta 2008. The Ca2+ ATPase of cardiac sarcoplasmic reticulum: Physiological role and relevance to diseases. Biochem. Biophys. Res. Commun. 369, 182-187.

Ishikawa, K., L. Tilemann, K. Fish and R.J. Hajjar 2011. Gene delivery methods in cardiac gene therapy. J. Gene Med. 13, 566-572.

James, P., M. Inui, M. Tada, M. Chiesi and E. Carafoli 1989. Nature and site of phospholamban regulation of the Ca2+ pump of sarcoplasmic reticulum. Nature. 342, 90-2.

Jensen, M. R. and M. Blackledge 2008. On the origin of NMR dipolar waves in transient helical elements of partially folded proteins. J. Am. Chem. Soc. 130, 11266-11267.

Jessup, M., B. Greenberg, D. Mancini, T. Cappola, D.F. Pauly, B. Jaski, A. Yaroshinsky, K.M. Zsebo, H. Dittrich, R.J. Hajjar and Calcium Upregulation by Percutaneous Administration of Gene Therapy in Cardiac Disease (CUPID) Investigators 2011. Calcium upregulation by percutaneous administration of gene therapy in cardiac disease (CUPID): A phase 2 trial of intracoronary gene therapy of sarcoplasmic reticulum Ca2+-ATPase in patients with advanced heart failure. Circulation. 124, 304-313.

Jha, A. K., A. Colubri, K.F. Freed and T.R. Sosnick 2005. Statistical coil model of the unfolded state: Resolving the reconciliation problem. Proc. Natl. Acad. Sci. U. S. A. 102, 13099-13104.

Johnson, B. A. 2004. Using NMRView to visualize and analyze the NMR spectra of macromolecules. Methods Mol. Biol. 278, 313-352.

Johnson, D. A., P. Akamine, E. Radzio-Andzelm, M. Madhusudan and S.S. Taylor 2001. Dynamics of cAMP-dependent protein kinase. Chem. Rev. 101, 2243-2270.

Johnson, J. E. and R.B. Cornell 1999. Amphitropic proteins: Regulation by reversible membrane interactions (review). Mol. Membr. Biol. 16, 217-235.

Johnson, L. N. 2009. The regulation of protein phosphorylation. Biochem. Soc. Trans. 37, 627-641.

Jones, L. R., R.L. Cornea and Z. Chen 2002. Close proximity between residue 30 of phospholamban and cysteine 318 of the cardiac Ca2+ pump revealed by intermolecular thiol cross-linking. J Biol Chem. 277, 28319-29.

Juretic, D., R.W. Hendler, F. Kamp, W.S. Caughey, M. Zasloff and H.V. Westerhoff 1994. Magainin oligomers reversibly dissipate delta microH+ in cytochrome oxidase liposomes. Biochemistry. 33, 4562-4570.

Kairouz, V., L. Lipskaia, R.J. Hajjar and E.R. Chemaly 2012. Molecular targets in heart failure gene therapy: Current controversies and translational perspectives. Ann. N. Y. Acad. Sci. 1254, 42-50.

Karim, C. B., T.L. Kirby, Z. Zhang, Y. Nesmelov and D.D. Thomas 2004. Phospholamban structural dynamics in lipid bilayers probed by a spin label rigidly coupled to the peptide backbone. Proc Natl Acad Sci U S A. 101, 14437-42.

Karim, C. B., C.G. Marquardt, J.D. Stamm, G. Barany and D.D. Thomas 2000. Synthetic null-cysteine phospholamban analogue and the corresponding transmembrane domain inhibit the ca-ATPase. Biochemistry. 39, 10892-7.

Karim, C. B., Z. Zhang, E.C. Howard, K.D. Torgersen and D.D. Thomas 2006. Phosphorylation-dependent conformational switch in spin-labeled phospholamban bound to SERCA. J. Mol. Biol. 358, 1032-1040.

Kawase, Y., D. Ladage and R.J. Hajjar 2011. Rescuing the failing heart by targeted gene transfer. J. Am. Coll. Cardiol. 57, 1169-1180.

Kay, L. E., E. Keifer and T. Saarinen 1992. Pure absorption gradient enhanced heteronuclear single quantum correlation spectroscopy with improved sensitivity. J. Am. Chem. Soc. 114, 10663-10665.

Kay, L. E., D.A. Torchia and A. Bax 1989. Backbone dynamics of proteins as studied by 15N inverse detected heteronuclear NMR spectroscopy: Application to staphylococcal nuclease. Biochemistry. 28, 8972-8979.

Kaye, D. M., M. Hoshijima and K.R. Chien 2008. Reversing advanced heart failure by targeting Ca2+ cycling. Annu. Rev. Med. 59, 13-28.

Kaye, D. M., A. Preovolos, T. Marshall, M. Byrne, M. Hoshijima, R. Hajjar, J.A. Mariani, S. Pepe, K.R. Chien and J.M. Power 2007. Percutaneous cardiac recirculation-mediated gene transfer of an inhibitory phospholamban peptide reverses advanced heart failure in large animals. J. Am. Coll. Cardiol. 50, 253-260.

Kelly, E. M., Z. Hou, J. Bossuyt, D.M. Bers and S.L. Robia 2008. Phospholamban oligomerization, quaternary structure, and sarco(endo)plasmic reticulum calcium ATPase binding measured by fluorescence resonance energy transfer in living cells. J. Biol. Chem. 283, 12202-12211.

Kern, D. and E.R. Zuiderweg 2003. The role of dynamics in allosteric regulation. Curr. Opin. Struct. Biol. 13, 748-757.

Ketchem, R. R., W. Hu and T.A. Cross 1993. High-resolution conformation of gramicidin A in a lipid bilayer by solid-state NMR. Science. 261, 1457-1460.

Kimura, Y., M. Asahi, K. Kurzydlowski, M. Tada and D.H. MacLennan 1998. Phospholamban domain ib mutations influence functional interactions with the Ca2+-ATPase isoform of cardiac sarcoplasmic reticulum. J Biol Chem. 273, 14238-41.

Kimura, Y., K. Kurzydlowski, M. Tada and D.H. MacLennan 1997. Phospholamban inhibitory function is activated by depolymerization. J Biol Chem. 272, 15061-4.

Kirby, T. L., C.B. Karim and D.D. Thomas 2004. Electron paramagnetic resonance reveals a large-scale conformational change in the cytoplasmic domain of phospholamban upon binding to the sarcoplasmic reticulum ca-ATPase. Biochemistry. 43, 5842-52.

Knighton, D. R., J. Zheng, L.F.T. Eyck, N.H. Xuong, S.S. Taylor and J.M. Sowadski 1991. Structure of a peptide inhibitor bound to the catalytic subunit of cyclic adenosine monophosphate-dependent protein kinase. Science. 253, 414-420.

Koshland, D. E.,Jr, G. Nemethy and D. Filmer 1966. Comparison of experimental binding data and theoretical models in proteins containing subunits. Biochemistry. 5, 365-385.

Krainev, A. G., D.A. Ferrington, T.D. Williams, T.C. Squier and D.J. Bigelow 1995. Adaptive changes in lipid composition of skeletal sarcoplasmic reticulum membranes associated with aging. Biochim. Biophys. Acta. 1235, 406-418.

Ladokhin, A. S. and S.H. White 1999. Folding of amphipathic alpha-helices on membranes: Energetics of helix formation by melittin. J. Mol. Biol. 285, 1363-1369.

Lakomek, N. A., T. Carlomagno, S. Becker, C. Griesinger and J. Meiler 2006. A thorough dynamic interpretation of residual dipolar couplings in ubiquitin. J. Biomol. NMR. 34, 101-115.

Lamberth, S., H. Schmid, M. Muenchbach, T. Vorherr, J. Krebs, E. Carafoli and C. Griesinger 2000. NMR solution structure of phospholamban. Helvetica Chimica Acta. 83, 2141-2151.

Lange, V., J. Becker-Baldus, B. Kunert, B.J. van Rossum, F. Casagrande, A. Engel, Y. Roske, F.M. Scheffel, E. Schneider and H. Oschkinat 2010. A MAS NMR study of the bacterial ABC transporter ArtMP. Chembiochem. 11, 547-555.

Langen, R., K.J. Oh, D. Cascio and W.L. Hubbell 2000. Crystal structures of spin labeled T4 lysozyme mutants: Implications for the interpretation of EPR spectra in terms of structure. Biochemistry. 39, 8396-8405.

Lee, A. G. 2003. Lipid-protein interactions in biological membranes: A structural perspective. Biochim. Biophys. Acta. 1612, 1-40.

Lee, A. G. 1998. How lipids interact with an intrinsic membrane protein: The case of the calcium pump. Biochim. Biophys. Acta. 1376, 381-390.

Lee, A. G. and J.M. East 1998. The effects of phospholipid structure on the function of a calcium pump. Biochem. Soc. Trans. 26, 359-365.

Levitt, M. H. 2001. Spin dynamics. John Wiley & sons, New York.

Levy, D., A. Gulik, A. Bluzat and J.L. Rigaud 1992. Reconstitution of the sarcoplasmic reticulum ca(2+)-ATPase: Mechanisms of membrane protein insertion into liposomes during reconstitution procedures involving the use of detergents. Biochim. Biophys. Acta. 1107, 283-298.

Li, J., C.B. Boschek, Y. Xiong, C.A. Sacksteder, T.C. Squier and D.J. Bigelow 2005. Essential role for Pro21 in phospholamban for optimal inhibition of the ca-ATPase. Biochemistry. 44, 16181-16191.

Li, J., Z.M. James, X. Dong, C.B. Karim and D.D. Thomas 2012. Structural and functional dynamics of an integral membrane protein complex modulated by lipid headgroup charge. J. Mol. Biol. 418, 379-389.

Li, P., I.R. Martins, G.K. Amarasinghe and M.K. Rosen 2008. Internal dynamics control activation and activity of the autoinhibited vav DH domain. Nat. Struct. Mol. Biol. 15, 613-618.

Liang, B., J.H. Bushweller and L.K. Tamm 2006. Site-directed parallel spin-labeling and paramagnetic relaxation enhancement in structure determination of membrane proteins by solution NMR spectroscopy. J. Am. Chem. Soc. 128, 4389-4397.

Lin, D., K.H. Sze, Y. Cui and G. Zhu 2002. Clean SEA-HSQC: A method to map solvent exposed amides in large non-deuterated proteins with gradient-enhanced HSQC. J. Biomol. NMR. 23, 317-322.

Linser, R., M. Dasari, M. Hiller, V. Higman, U. Fink, J.M. Lopez Del Amo, S. Markovic, L. Handel, B. Kessler, P. Schmieder, D. Oesterhelt, H. Oschkinat and B. Reif 2011.

Proton-detected solid-state NMR spectroscopy of fibrillar and membrane proteins. Angew. Chem. Int. Ed Engl. 50, 4508-4512.

Lockwood, N. A., R.S. Tu, Z. Zhang, M.V. Tirrell, D.D. Thomas and C.B. Karim 2003. Structure and function of integral membrane protein domains resolved by peptide-amphiphiles: Application to phospholamban. Biopolymers. 69, 283-92.

Lorieau, J., L. Yao and A. Bax 2008. Liquid crystalline phase of G-tetrad DNA for NMR study of detergent-solubilized proteins. J. Am. Chem. Soc. 130, 7536-7537.

Losonczi, J. A., M. Andrec, M.W. Fischer and J.H. Prestegard 1999. Order matrix analysis of residual dipolar coupling using singular value decomposition. Journal of Magnetic Resonance. 138, 334-342.

Luo, W., S.D. Cady and M. Hong 2009. Immobilization of the influenza A M2 transmembrane peptide in virus envelope-mimetic lipid membranes: A solid-state NMR investigation. Biochemistry. 48, 6361-6368.

Lygren, B., C.R. Carlson, K. Santamaria, V. Lissandron, T. McSorley, J. Litzenberg, D. Lorenz, B. Wiesner, W. Rosenthal, M. Zaccolo, K. Tasken and E. Klussmann 2007. AKAP complex regulates Ca2+ re-uptake into heart sarcoplasmic reticulum. EMBO Rep. 8, 1061-1067.

Ma, B. and R. Nussinov 2010. Enzyme dynamics point to stepwise conformational selection in catalysis. Curr. Opin. Chem. Biol. 14, 652-659.

Ma, C. and S.J. Opella 2000. Lanthanide ions bind specifically to an added "EF-hand" and orient a membrane protein in micelles for solution NMR spectroscopy. J. Magn. Reson. 146, 381-384.

Maclennan, D. H. 2004. Interactions of the calcium ATPase with phospholamban and sarcolipin: Structure, physiology and pathophysiology. J. Muscle Res. Cell. Motil. 25, 600-601.

MacLennan, D. H., Y. Kimura and T. Toyofuku 1998. Sites of regulatory interaction between calcium ATPases and phospholamban. Ann N Y Acad Sci. 853, 31-42.

MacLennan, D. H. and E.G. Kranias 2003. Phospholamban: A crucial regulator of cardiac contractility. Nat Rev Mol Cell Biol. 4, 566-77.

Mahaney, J. E., J.M. Autry and L.R. Jones 2000. Kinetics studies of the cardiac ca-ATPase expressed in Sf21 cells: New insights on ca-ATPase regulation by phospholamban. Biophys. J. 78, 1306-1323.

Maly, T., G.T. Debelouchina, V.S. Bajaj, K.N. Hu, C.G. Joo, M.L. Mak-Jurkauskas, J.R. Sirigiri, P.C. van der Wel, J. Herzfeld, R.J. Temkin and R.G. Griffin 2008. Dynamic nuclear polarization at high magnetic fields. J. Chem. Phys. 128, 052211.

Marsh, J. A. and J.D. Forman-Kay 2009. Structure and disorder in an unfolded state under nondenaturing conditions from ensemble models consistent with a large number of experimental restraints. J. Mol. Biol. 391, 359-374.

Mascioni, A., B.L. Eggimann and G. Veglia 2004. Determination of helical membrane protein topology using residual dipolar couplings and exhaustive search algorithm: Application to phospholamban. Chem. Phys. Lipids. 132, 133-144.

Mascioni, A., C. Karim, J. Zamoon, D.D. Thomas and G. Veglia 2002. Solid-state NMR and rigid body molecular dynamics to determine domain orientations of monomeric phospholamban. J. Am. Chem. Soc. 124, 9392-9393.

Mascioni, A. and G. Veglia 2003. Theoretical analysis of residual dipolar coupling patterns in regular secondary structures of proteins. J. Am. Chem. Soc. 125, 12520-12526.

Masterson, L. R., N. Bortone, T. Yu, K.N. Ha, E.C. Gaffarogullari, O. Nguyen and G. Veglia 2009. Expression and purification of isotopically labeled peptide inhibitors and substrates of cAMP-dependant protein kinase A for NMR analysis. Protein Expr. Purif. 64, 231-236.

Masterson, L. R., C. Cheng, T. Yu, M. Tonelli, A.P. Kornev, S.S. Taylor and G. Veglia 2010. Dynamics connect substrate recognition to catalysis in protein kinase A. Nat Chem Biol. 6, 821-828.

Masterson, L. R., A. Mascioni, N.J. Traaseth, S.S. Taylor and G. Veglia 2008. Allosteric cooperativity in protein kinase A. Proc Natl Acad Sci U S A. 105, 506-511.

Masterson, L. R., L. Shi, E. Metcalfe, J. Gao, S.S. Taylor and G. Veglia 2011a. Dynamically committed, uncommitted, and quenched states encoded in protein kinase A revealed by NMR spectroscopy. Proc. Natl. Acad. Sci. U. S. A. 108, 6969-6974.

Masterson, L. R., T. Yu, L. Shi, Y. Wang, M. Gustavsson, M.M. Mueller and G. Veglia 2011b. cAMP-dependent protein kinase A selects the excited state of the membrane substrate phospholamban. J. Mol. Biol. 412, 155-164.

Matsuzaki, K. 1999. Why and how are peptide-lipid interactions utilized for self-defense? magainins and tachyplesins as archetypes. Biochim. Biophys. Acta. 1462, 1-10.

McDermott, A. 2009. Structure and dynamics of membrane proteins by magic angle spinning solid-state NMR. Annu. Rev. Biophys. 38, 385-403.

McDermott, A. and T. Polenova 2007. Solid state NMR: New tools for insight into enzyme function. Curr. Opin. Struct. Biol. 17, 617-622.

Medeiros, A., D.G. Biagi, T.J. Sobreira, P.S. de Oliveira, C.E. Negrao, A.J. Mansur, J.E. Krieger, P.C. Brum and A.C. Pereira 2011. Mutations in the human phospholamban gene in patients with heart failure. Am. Heart J. 162, 1088-1095.e1.

Meier, S., M. Blackledge and S. Grzesiek 2008. Conformational distributions of unfolded polypeptides from novel NMR techniques. J. Chem. Phys. 128, 052204.

Mesleh, M. F. and S.J. Opella 2003. Dipolar waves as NMR maps of helices in proteins. J. Magn. Reson. 163, 288-299.

Mesleh, M. F., G. Veglia, T.M. DeSilva, F.M. Marassi and S.J. Opella 2002. Dipolar waves as NMR maps of protein structure. J. Am. Chem. Soc. 124, 4206-4207.

Metcalfe, E. E., N.J. Traaseth and G. Veglia 2005. Serine 16 phosphorylation induces an order-to-disorder transition in monomeric phospholamban. Biochemistry. 44, 4386-4396.

Metcalfe, E. E., J. Zamoon, D.D. Thomas and G. Veglia 2004. (1)H/(15)N heteronuclear NMR spectroscopy shows four dynamic domains for phospholamban reconstituted in dodecylphosphocholine micelles. Biophys. J. 87, 1205-1214.

Mills, F. D., V.C. Antharam, O.K. Ganesh, D.W. Elliott, S.A. McNeill and J.R. Long 2008. The helical structure of surfactant peptide KL4 when bound to POPC: POPG lipid vesicles. Biochemistry. 47, 8292-8300.

Mittag, T., L.E. Kay and J.D. Forman-Kay 2010. Protein dynamics and conformational disorder in molecular recognition. J. Mol. Recognit. 23, 105-116.

Moe, P. and P. Blount 2005. Assessment of potential stimuli for mechano-dependent gating of MscL: Effects of pressure, tension, and lipid headgroups. Biochemistry. 44, 12239-12244.

Moller, J. V., C. Olesen, A.M. Winther and P. Nissen 2010. The sarcoplasmic Ca2+-ATPase: Design of a perfect chemi-osmotic pump. Q. Rev. Biophys. 43, 501-566.

Monod, J., J. Wyman and J.P. Changeux 1965. On the nature of allosteric transitions: A plausible model. J Mol Biol. 12, 88-118.

Mori, S., J.M. Berg and P.C. van Zijl 1996. Separation of intramolecular NOE and exchange peaks in water exchange spectroscopy using spin-echo filters. J. Biomol. NMR. 7, 77-82.

Morris, G. A. and R.J. Freeman 1979. Enhancement of nuclear magnetic resonance signals by polarization transfer. J. Am. Chem. Soc. 101, 760-762.

Mrak, R. E. and S. Fleischer 1982. Lipid composition of sarcoplasmic reticulum from mice with muscular dystrophy. Muscle Nerve. 5, 439-446.

Mueller, B., C.B. Karim, I.V. Negrashov, H. Kutchai and D.D. Thomas 2004. Direct detection of phospholamban and sarcoplasmic reticulum ca-ATPase interaction in membranes using fluorescence resonance energy transfer. Biochemistry. 43, 8754-65.

Mueller, G. A., W.Y. Choy, D. Yang, J.D. Forman-Kay, R.A. Venters and L.E. Kay 2000. Global folds of proteins with low densities of NOEs using residual dipolar couplings: Application to the 370-residue maltodextrin-binding protein. J. Mol. Biol. 300, 197-212.

Nash, A. I., W.H. Ko, S.M. Harper and K.H. Gardner 2008. A conserved glutamine plays a central role in LOV domain signal transmission and its duration. Biochemistry. 47, 13842-13849.

Nesmelov, Y. E., C.B. Karim, L. Song, P.G. Fajer and D.D. Thomas 2007. Rotational dynamics of phospholamban determined by multifrequency electron paramagnetic resonance. Biophys. J. 93, 2805-2812.

Nodet, G., L. Salmon, V. Ozenne, S. Meier, M.R. Jensen and M. Blackledge 2009. Quantitative description of backbone conformational sampling of unfolded proteins at amino acid resolution from NMR residual dipolar couplings. J. Am. Chem. Soc. 131, 17908-17918.

Obara, K., N. Miyashita, C. Xu, I. Toyoshima, Y. Sugita, G. Inesi and C. Toyoshima 2005. Structural role of countertransport revealed in ca(2+) pump crystal structure in the absence of ca(2+). Proc. Natl. Acad. Sci. U. S. A. 102, 14489-14496.

Olesen, C., T.L. Sorensen, R.C. Nielsen, J.V. Moller and P. Nissen 2004. Dephosphorylation of the calcium pump coupled to counterion occlusion. Science. 306, 2251-2255.

Oxenoid, K. and J.J. Chou 2005. The structure of phospholamban pentamer reveals a channel-like architecture in membranes. Proc. Natl. Acad. Sci. U. S. A. 102, 10870-10875.

Palmer, A. G.,3rd, C.D. Kroenke and J.P. Loria 2001. Nuclear magnetic resonance methods for quantifying microsecond-to-millisecond motions in biological macromolecules. Methods Enzymol. 339, 204-238.

Park, S. H., B.B. Das, F. Casagrande, Y. Tian, H.J. Nothnagel, M. Chu, H. Kiefer, K. Maier, A.A. De Angelis, F.M. Marassi and S.J. Opella 2012. Structure of the chemokine receptor CXCR1 in phospholipid bilayers. Nature.

Park, S. H., S. Prytulla, A.A. De Angelis, J.M. Brown, H. Kiefer and S.J. Opella 2006. High-resolution NMR spectroscopy of a GPCR in aligned bicelles. J. Am. Chem. Soc. 128, 7402-7403.

Periasamy, M. and A. Kalyanasundaram 2007. SERCA pump isoforms: Their role in calcium transport and disease. Muscle Nerve.

Permi, P. and A. Annila 2000. Transverse relaxation optimised spin-state selective NMR experiments for measurement of residual dipolar couplings. J. Biomol. NMR. 16, 221-227.

Poget, S. F., S.M. Cahill and M.E. Girvin 2007. Isotropic bicelles stabilize the functional form of a small multidrug-resistance pump for NMR structural studies. J. Am. Chem. Soc. 129, 2432-2433.

Pollesello, P., A. Annila and M. Ovaska 1999. Structure of the 1-36 amino-terminal fragment of human phospholamban by nuclear magnetic resonance and modeling of the phospholamban pentamer. Biophys J. 76, 1784-95.

Prestegard, J. H. 1998. New techniques in structural NMR - anisotropic interactions. Nature Structural Biology., 517.

Prestegard, J. H., H.M. Al-Hashimi and J.R. Tolman 2000. NMR structures of biomolecules using field oriented media and residual dipolar couplings. Quarterly Review in Biophysics. 33, 371-424.

Qiang, W., Y. Sun and D.P. Weliky 2009. A strong correlation between fusogenicity and membrane insertion depth of the HIV fusion peptide. Proc. Natl. Acad. Sci. U. S. A. 106, 15314-15319.

Rand, R. P., N. Fuller, V.A. Parsegian and D.C. Rau 1988. Variation in hydration forces between neutral phospholipid bilayers: Evidence for hydration attraction. Biochemistry. 27, 7711-7722.

Rasmussen, S. G., H.J. Choi, D.M. Rosenbaum, T.S. Kobilka, F.S. Thian, P.C. Edwards, M. Burghammer, V.R. Ratnala, R. Sanishvili, R.F. Fischetti, G.F. Schertler, W.I. Weis and B.K. Kobilka 2007. Crystal structure of the human beta2 adrenergic G-protein-coupled receptor. Nature. 450, 383-387.

Reddy, L. G., R.L. Cornea, D.L. Winters, E. McKenna and D.D. Thomas 2003. Defining the molecular components of calcium transport regulation in a reconstituted membrane system. Biochemistry. 42, 4585-92.

Reddy, L. G., L.R. Jones, S.E. Cala, J.J. O'Brian, S.A. Tatulian and D.L. Stokes 1995. Functional reconstitution of recombinant phospholamban with rabbit skeletal ca(2+)-ATPase. J Biol Chem. 270, 9390-7.

Reddy, L. G., L.R. Jones and D.D. Thomas 1999. Depolymerization of phospholamban in the presence of calcium pump: A fluorescence energy transfer study. Biochemistry. 38, 3954-62.

Religa, T. L., A.M. Ruschak, R. Rosenzweig and L.E. Kay 2011. Site-directed methyl group labeling as an NMR probe of structure and dynamics in supramolecular protein systems: Applications to the proteasome and to the ClpP protease. J. Am. Chem. Soc. 133, 9063-9068.

Renault, M., R. Tommassen-van Boxtel, M.P. Bos, J.A. Post, J. Tommassen and M. Baldus 2012. Cellular solid-state nuclear magnetic resonance spectroscopy. Proc. Natl. Acad. Sci. U. S. A. 109, 4863-4868.

Roach, C., S.E. Feller, J.A. Ward, S.R. Shaikh, M. Zerouga and W. Stillwell 2004. Comparison of cis and trans fatty acid containing phosphatidylcholines on membrane properties. Biochemistry. 43, 6344-6351.

Robia, S. L., K.S. Campbell, E.M. Kelly, Z. Hou, D.L. Winters and D.D. Thomas 2007. Forster transfer recovery reveals that phospholamban exchanges slowly from pentamers but rapidly from the SERCA regulatory complex. Circ. Res. 101, 1123-1129.

Roger, V. L., A.S. Go, D.M. Lloyd-Jones, E.J. Benjamin, J.D. Berry, W.B. Borden, D.M. Bravata, S. Dai, E.S. Ford, C.S. Fox, H.J. Fullerton, C. Gillespie, S.M. Hailpern, J.A. Heit, V.J. Howard, B.M. Kissela, S.J. Kittner, D.T. Lackland, J.H. Lichtman, L.D. Lisabeth, D.M. Makuc, G.M. Marcus, A. Marelli, D.B. Matchar, C.S. Moy, D. Mozaffarian, M.E. Mussolino, G. Nichol, N.P. Paynter, E.Z. Soliman, P.D. Sorlie, N. Sotoodehnia, T.N. Turan, S.S. Virani, N.D. Wong, D. Woo, M.B. Turner and American Heart Association Statistics Committee and Stroke Statistics Subcommittee 2012. Executive summary: Heart disease and stroke statistics--2012 update: A report from the american heart association. Circulation. 125, 188-197.

Saito, H. and A. Naito 2007. NMR studies on fully hydrated membrane proteins, with emphasis on bacteriorhodopsin as a typical and prototype membrane protein. Biochim. Biophys. Acta. 1768, 3145-3161.

Saito-Nakatsuka, K., T. Yamashita, I. Kubota and M. Kawakita 1987. Reactive sulfhydryl groups of sarcoplasmic reticulum ATPase. I. location of a group which is most reactive with N-ethylmaleimide. J. Biochem. 101, 365-376.

Salmon, L., G. Nodet, V. Ozenne, G. Yin, M.R. Jensen, M. Zweckstetter and M. Blackledge 2010. NMR characterization of long-range order in intrinsically disordered proteins. J. Am. Chem. Soc. 132, 8407-8418.

Salvatella, X., B. Richter and M. Vendruscolo 2008. Influence of the fluctuations of the alignment tensor on the analysis of the structure and dynamics of proteins using residual dipolar couplings. J. Biomol. NMR. 40, 71-81.

Sammalkorpi, M. and T. Lazaridis 2007. Modeling a spin-labeled fusion peptide in a membrane: Implications for the interpretation of EPR experiments. Biophys. J. 92, 10-22.

Scarlata, S. and S.M. Gruner 1997. Role of phosphatidylethanolamine lipids in the stabilization of protein-lipid contacts. Biophys. Chem. 67, 269-279.

Schmidt, A. G., I. Edes and E.G. Kranias 2001. Phospholamban: A promising therapeutic target in heart failure? Cardiovasc Drugs Ther. 15, 387-96.

Schmidt, A. G., J. Zhai, A.N. Carr, M.J. Gerst, J.N. Lorenz, P. Pollesello, A. Annila, B.D. Hoit and E.G. Kranias 2002. Structural and functional implications of the phospholamban hinge domain: Impaired SR Ca2+ uptake as a primary cause of heart failure. Cardiovasc Res. 56, 248-59.

Schmitt, J. P., F. Ahmad, K. Lorenz, L. Hein, S. Schulz, M. Asahi, D.H. Maclennan, C.E. Seidman, J.G. Seidman and M.J. Lohse 2009. Alterations of phospholamban function can exhibit cardiotoxic effects independent of excessive sarcoplasmic reticulum Ca2+-ATPase inhibition. Circulation. 119, 436-444.

Schmitt, J. P., M. Kamisago, M. Asahi, G.H. Li, F. Ahmad, U. Mende, E.G. Kranias, D.H. MacLennan, J.G. Seidman and C.E. Seidman 2003. Dilated cardiomyopathy and heart failure caused by a mutation in phospholamban. Science. 299, 1410-3.

Schwieters, C. D., J.J. Kuszewski, N. Tjandra and G.M. Clore 2003. The xplor-NIH NMR molecular structure determination package. J. Magn. Reson. 160, 65-73.

Seidel, K., O.C. Andronesi, J. Krebs, C. Griesinger, H.S. Young, S. Becker and M. Baldus 2008. Structural characterization of ca(2+)-ATPase-bound phospholamban in lipid bilayers by solid-state nuclear magnetic resonance (NMR) spectroscopy. Biochemistry. 47, 4369-4376.

Selvaratnam, R., S. Chowdhury, B. VanSchouwen and G. Melacini 2011. Mapping allostery through the covariance analysis of NMR chemical shifts. Proc. Natl. Acad. Sci. U. S. A. 108, 6133-6138.

Sengupta, I., P.S. Nadaud, J.J. Helmus, C.D. Schwieters and C.P. Jaroniec 2012. Protein fold determined by paramagnetic magic-angle spinning solid-state NMR spectroscopy. Nat. Chem. 4, 410-417.

Shanmugam, M., S. Gao, C. Hong, N. Fefelova, M.C. Nowycky, L.H. Xie, M. Periasamy and G.J. Babu 2011. Ablation of phospholamban and sarcolipin results in cardiac hypertrophy and decreased cardiac contractility. Cardiovasc. Res. 89, 353-361.

Sharma, M., M. Yi, H. Dong, H. Qin, E. Peterson, D.D. Busath, H.X. Zhou and T.A. Cross 2010. Insight into the mechanism of the influenza A proton channel from a structure in a lipid bilayer. Science. 330, 509-512.

Shi, L., I. Kawamura, K.H. Jung, L.S. Brown and V. Ladizhansky 2011. Conformation of a seven-helical transmembrane photosensor in the lipid environment. Angew. Chem. Int. Ed Engl. 50, 1302-1305.

Shi, L., N.J. Traaseth, R. Verardi, A. Cembran, J. Gao and G. Veglia 2009. A refinement protocol to determine structure, topology, and depth of insertion of membrane proteins using hybrid solution and solid-state NMR restraints. J. Biomol. NMR. 44, 195-205.

Shi, L., N.J. Traaseth, R. Verardi, M. Gustavsson, J. Gao and G. Veglia 2011. Paramagnetic-based NMR restraints lift residual dipolar coupling degeneracy in multidomain detergent-solubilized membrane proteins. J Am Chem Soc. 133, 2232-2241.

Sigalov, A. B. 2011. Uncoupled binding and folding of immune signaling-related intrinsically disordered proteins. Prog. Biophys. Mol. Biol. 106, 525-536.

Simmerman, H. K., J.H. Collins, J.L. Theibert, A.D. Wegener and L.R. Jones 1986. Sequence analysis of phospholamban. identification of phosphorylation sites and two major structural domains. J Biol Chem. 261, 13333-41.

Simmerman, H. K. and L.R. Jones 1998. Phospholamban: Protein structure, mechanism of action, and role in cardiac function. Physiol Rev. 78, 921-47.

Simmerman, H. K., Y.M. Kobayashi, J.M. Autry and L.R. Jones 1996. A leucine zipper stabilizes the pentameric membrane domain of phospholamban and forms a coiled-coil pore structure. J Biol Chem. 271, 5941-6.

Singer, S. J. and G.L. Nicolson 1972. The fluid mosaic model of the structure of cell membranes. Science. 175, 720-731.

Smock, R. G. and L.M. Gierasch 2009. Sending signals dynamically. Science. 324, 198-203.

Sonntag, Y., M. Musgaard, C. Olesen, B. Schiott, J.V. Moller, P. Nissen and L. Thogersen 2011. Mutual adaptation of a membrane protein and its lipid bilayer during conformational changes. Nat. Commun. 2, 304.

Sorensen, T. L., J.V. Moller and P. Nissen 2004. Phosphoryl transfer and calcium ion occlusion in the calcium pump. Science. 304, 1672-1675.

Starling, A. P., K.A. Dalton, J.M. East, S. Oliver and A.G. Lee 1996. Effects of phosphatidylethanolamines on the activity of the ca(2+)-ATPase of sarcoplasmic reticulum. Biochem. J. 320 (Pt 1), 309-314.

Stevenson, L. W. 2003. Clinical use of inotropic therapy for heart failure: Looking backward or forward? part II: Chronic inotropic therapy. Circulation., 492-497.

Stokes, D. L. and N.M. Green 1990. Three-dimensional crystals of CaATPase from sarcoplasmic reticulum. symmetry and molecular packing. Biophys J. 57, 1-14.

Stokes, D. L., A.J. Pomfret, W.J. Rice, J.P. Glaves and H.S. Young 2006. Interactions between Ca2+-ATPase and the pentameric form of phospholamban in two-dimensional co-crystals. Biophys. J. 90, 4213-4223.

Su, Y., A.J. Waring, P. Ruchala and M. Hong 2010. Membrane-bound dynamic structure of an arginine-rich cell-penetrating peptide, the protein transduction domain of HIV TAT, from solid-state NMR. Biochemistry. 49, 6009-6020.

Szymanska, G., H.W. Kim and E.G. Kranias 1991. Reconstitution of the skeletal sarcoplasmic reticulum Ca2(+)-pump: Influence of negatively charged phospholipids. Biochim. Biophys. Acta. 1091, 127-134.

Tada, M. and M. Kadoma 1989. Regulation of the Ca2+ pump ATPase by cAMP-dependent phosphorylation of phospholamban. Bioessays. 10, 157-63.

Tada, M., T. Yamamoto and Y. Tonomura 1978. Molecular mechanism of active calcium transport by sarcoplasmic reticulum. Physiol. Rev. 58, 1-79.

Taffet, G. E., T.T. Pham, D.L. Bick, M.L. Entman, H.J. Pownall and R.J. Bick 1993. The calcium uptake of the rat heart sarcoplasmic reticulum is altered by dietary lipid. J. Membr. Biol. 131, 35-42.

Takegoshi, K., S. Nakamura and T. Terao 2001. 13C–1H dipolar-assisted rotational resonance in magic-angle spinning NMR. Chem. Phys. Lett. 344, 631.

Tang, C., J. Iwahara and G.M. Clore 2006. Visualization of transient encounter complexes in protein-protein association. Nature. 444, 383-386.

Tang, M., L.J. Sperling, D.A. Berthold, A.E. Nesbitt, R.B. Gennis and C.M. Rienstra 2011. Solid-state NMR study of the charge-transfer complex between ubiquinone-8 and disulfide bond generating membrane protein DsbB. J. Am. Chem. Soc. 133, 4359-4366.

Tjandra, N. and A. Bax 1997. Direct measurement of distances and angles in biomolecules by NMR in a dilute liquid crystalline medium. Science. 278, 1111-1114.

Tjandra, N., J. Marquardt and Clore M. G. 2000. Direct refinement against proton-proton dipolar coupling in NMR structure of macromolecules. Journal of Magnetic Resonance. 142, 393-396.

Tolman, J. R., J.M. Flanagan, M.A. Kennedy and J.H. Prestegard 1997. NMR evidence for slow collective motions in cyanometmyoglobin. Nat Struct Biol. 4, 292-7.

Tolman, J. R., J.M. Flanagan, M.A. Kennedy and J.H. Prestegard 1995. Nuclear magnetic dipole interactions in field-oriented proteins: Information for structure determination in solution. Proceedings Natinal Academy Science U S A. 92, 9279-9283.

Tolman, J. R. and K. Ruan 2006. NMR residual dipolar couplings as probes of biomolecular dynamics. Chem. Rev. 106, 1720-1736.

Tong, K. I., M. Yamamoto and T. Tanaka 2008. A simple method for amino acid selective isotope labeling of recombinant proteins in E. coli. J Biomol NMR. 42, 59-67.

Toyofuku, T., K. Kurzydlowski, M. Tada and D.H. MacLennan 1994. Amino acids lys-asp-asp-lys-pro-val-402 in the Ca2+-ATPase of cardiac sarcoplasmic reticulum are critical for functional association with phospholamban. Journal Biological Chemistry. 269, 22929-22932.

Toyoshima, C., M. Asahi, Y. Sugita, R. Khanna, T. Tsuda and D.H. MacLennan 2003. Modeling of the inhibitory interaction of phospholamban with the Ca2+ ATPase. Proc Natl Acad Sci U S A. 100, 467-72.

Toyoshima, C. and G. Inesi 2004. Structural basis of ion pumping by Ca2+-ATPase of the sarcoplasmic reticulum. Annu. Rev. Biochem. 73, 269-292.

Toyoshima, C., M. Nakasako, H. Nomura and H. Ogawa 2000. Crystal structure of the calcium pump of sarcoplasmic reticulum at 2.6 A resolution. Nature. 405, 647-55.

Toyoshima, C. and H. Nomura 2002. Structural changes in the calcium pump accompanying the dissociation of calcium. Nature. 418, 605-11.

Traaseth, N. J., J.J. Buffy, J. Zamoon and G. Veglia 2006. Structural dynamics and topology of phospholamban in oriented lipid bilayers using multidimensional solid-state NMR. Biochemistry. 45, 13827-13834.

Traaseth, N. J., K.N. Ha, R. Verardi, L. Shi, J.J. Buffy, L.R. Masterson and G. Veglia 2008. Structural and dynamic basis of phospholamban and sarcolipin inhibition of ca(2+)-ATPase. Biochemistry. 47, 3-13.

Traaseth, N. J., L. Shi, R. Verardi, D.G. Mullen, G. Barany and G. Veglia 2009. Structure and topology of monomeric phospholamban in lipid membranes determined by a hybrid solution and solid-state NMR approach. Proc. Natl. Acad. Sci. U. S. A. 106, 10165-10170.

Traaseth, N. J., D.D. Thomas and G. Veglia 2006. Effects of Ser16 phosphorylation on the allosteric transitions of phospholamban/Ca(2+)-ATPase complex. J. Mol. Biol. 358, 1041-1050.

Traaseth, N. J. and G. Veglia 2010. Probing excited states and activation energy for the integral membrane protein phospholamban by NMR CPMG relaxation dispersion experiments. Biochim. Biophys. Acta. 1798, 77-81.

Traaseth, N. J. and G. Veglia 2009. Probing excited states and activation energy for the integral membrane protein phospholamban by NMR CPMG relaxation dispersion experiments. Biochim. Biophys. Acta.

Traaseth, N. J., R. Verardi, K.D. Torgersen, C.B. Karim, D.D. Thomas and G. Veglia 2007. Spectroscopic validation of the pentameric structure of phospholamban. Proc. Natl. Acad. Sci. U. S. A. 104, 14676-14681.

Traaseth, N. J., R. Verardi and G. Veglia 2008. Asymmetric methyl group labeling as a probe of membrane protein homo-oligomers by NMR spectroscopy. J. Am. Chem. Soc. 130, 2400-2401.

Trieber, C. A., M. Afara and H.S. Young 2009. Effects of phospholamban transmembrane mutants on the calcium affinity, maximal activity, and cooperativity of the sarcoplasmic reticulum calcium pump. Biochemistry. 48, 9287-9296.

Trieber, C. A., J.L. Douglas, M. Afara and H.S. Young 2005. The effects of mutation on the regulatory properties of phospholamban in co-reconstituted membranes. Biochemistry. 44, 3289-3297.

Tsai, C. J., A. Del Sol and R. Nussinov 2009. Protein allostery, signal transmission and dynamics: A classification scheme of allosteric mechanisms. Mol. Biosyst. 5, 207-216.

Tugarinov, V. and L.E. Kay 2004. An isotope labeling strategy for methyl TROSY spectroscopy. J Biomol NMR. 28, 165-72.

Tugarinov, V. and L.E. Kay 2003. Ile, leu, and val methyl assignments of the 723-residue malate synthase G using a new labeling strategy and novel NMR methods. J Am Chem Soc. 125, 13868-78.

Tycko, R., F.J. Blanco and Y. Ishii 2000. Alignment of biopolymers in strained gels: A new way to create detectable dipole-dipole couplings in high-resolution biomolecular NMR. Journal of the American Chemical Society. 122, 9340-9341.

Tzeng, S. R. and C.G. Kalodimos 2009. Dynamic activation of an allosteric regulatory protein. Nature. 462, 368-372.

Vafiadaki, E., D. Sanoudou, D.A. Arvanitis, D.H. Catino, E.G. Kranias and A. Kontrogianni-Konstantopoulos 2007. Phospholamban interacts with HAX-1, a mitochondrial protein with anti-apoptotic function. J. Mol. Biol. 367, 65-79.

Vallurupalli, P., D.F. Hansen, E. Stollar, E. Meirovitch and L.E. Kay 2007. Measurement of bond vector orientations in invisible excited states of proteins. Proc. Natl. Acad. Sci. U. S. A. 104, 18473-18477.

Van den Berg, B., W.M. Clemons Jr, I. Collinson, Y. Modis, E. Hartmann, S.C. Harrison and T.A. Rapoport 2004. X-ray structure of a protein-conducting channel. Nature. 427, 36-44.

Van Horn, W. D., H.J. Kim, C.D. Ellis, A. Hadziselimovic, E.S. Sulistijo, M.D. Karra, C. Tian, F.D. Sonnichsen and C.R. Sanders 2009. Solution nuclear magnetic resonance structure of membrane-integral diacylglycerol kinase. Science. 324, 1726-1729.

van Meer, G., D.R. Voelker and G.W. Feigenson 2008. Membrane lipids: Where they are and how they behave. Nat. Rev. Mol. Cell Biol. 9, 112-124.

Vandecaetsbeek, I., M. Trekels, M. De Maeyer, H. Ceulemans, E. Lescrinier, L. Raeymaekers, F. Wuytack and P. Vangheluwe 2009. Structural basis for the high Ca2+ affinity of the ubiquitous SERCA2b Ca2+ pump. Proc. Natl. Acad. Sci. U. S. A. 106, 18533-18538.

Vangheluwe, P., K.R. Sipido, L. Raeymaekers and F. Wuytack 2006. New perspectives on the role of SERCA2's Ca2+ affinity in cardiac function. Biochim. Biophys. Acta. 1763, 1216-1228.

Veglia, G., K.N. Ha, L. Shi, R. Verardi and N.J. Traaseth 2010. What can we learn from a small regulatory membrane protein? Methods Mol. Biol. 654, 303-319.

Veglia, G. and S.J. Opella 2000. Journal of the American Chemical Society., 11733-11734.

Veglia, G., A.C. Zeri, C. Ma and S.J. Opella 2002. Deuterium/hydrogen exchange factors measured by solution nuclear magnetic resonance spectroscopy as indicators of the structure and topology of membrane proteins. Biophys. J. 82, 2176-2183.

Velyvis, A., Y.R. Yang, H.K. Schachman and L.E. Kay 2007. A solution NMR study showing that active site ligands and nucleotides directly perturb the allosteric equilibrium in aspartate transcarbamoylase. Proc. Natl. Acad. Sci. U. S. A. 104, 8815-8820.

Verardi, R., L. Shi, N.J. Traaseth, N. Walsh and G. Veglia 2011. Structural topology of phospholamban pentamer in lipid bilayers by a hybrid solution and solid-state NMR method. Proc Natl Acad Sci U S A. 108, 9101-9106.

Volkov, A. N., J.A. Worrall, E. Holtzmann and M. Ubbink 2006. Solution structure and dynamics of the complex between cytochrome c and cytochrome c peroxidase determined by paramagnetic NMR. Proc. Natl. Acad. Sci. U. S. A. 103, 18945-18950.

von Heijne, G. 2011. Introduction to theme "membrane protein folding and insertion". Annu. Rev. Biochem. 80, 157-160.

von Heijne, G. 2006. Membrane-protein topology. Nat. Rev. Mol. Cell Biol. 7, 909-918.

Wallin, E. and G. von Heijne 1998. Genome-wide analysis of integral membrane proteins from eubacterial, archaean, and eukaryotic organisms. Protein Sci. 7, 1029-1038.

Walsh, J. D. and Y.X. Wang 2005. Periodicity, planarity, residual dipolar coupling, and structures. J. Magn. Reson. 174, 152-162.

Warren, J. J. and P.B. Moore 2001. A maximum likelihood method ofr determining da and R for sets of dipolar coupling data. Journal of Magnetic Resonance. 149, 271-275.

Wegener, A. D., H.K. Simmerman, J.P. Lindemann and L.R. Jones 1989. Phospholamban phosphorylation in intact ventricles. phosphorylation of serine 16 and threonine 17 in response to beta-adrenergic stimulation. Journal Biological Chemistry. 264, 11468-11474.

White, S. H. and W.C. Wimley 1999. Membrane protein folding and stability : Physical principles. Annual Review Biophysics Biomolecular Structures. 28, 319-365.

Wimley, W. C. 2003. The versatile beta-barrel membrane protein. Curr. Opin. Struct. Biol. 13, 404-411.

Winters, D. L., J.M. Autry, B. Svensson and D.D. Thomas 2008. Interdomain fluorescence resonance energy transfer in SERCA probed by cyan-fluorescent protein fused to the actuator domain. Biochemistry. 47, 4246-4256.

Wohnert, J., K.J. Franz, M. Nitz, B. Imperiali and H. Schwalbe 2003. Protein alignment by a coexpressed lanthanide-binding tag for the measurement of residual dipolar couplings. J. Am. Chem. Soc. 125, 13338-13339.

Wright, P. E. and H.J. Dyson 2009. Linking folding and binding. Curr. Opin. Struct. Biol. 19, 31-38.

Yao, X., M.K. Rosen and K.H. Gardner 2008. Estimation of the available free energy in a LOV2-J alpha photoswitch. Nat. Chem. Biol. 4, 491-497.

Yonemoto, W. M., M.L. McGlone, L.W. Slice and S.S. Taylor 1991. Prokaryotic expression of catalytic subunit of adenosine cyclic monophosphate-dependent protein kinase. Methods Enzymol. 200, 581-596.

Young, H. S., L.R. Jones and D.L. Stokes 2001. Locating phospholamban in co-crystals with ca(2+)-ATPase by cryoelectron microscopy. Biophys J. 81, 884-94.

Young, H. S., L.G. Reddy, L.R. Jones and D.L. Stokes 1998. Co-reconstitution and co-crystallization of phospholamban and ca(2+)-ATPase. Ann. N. Y. Acad. Sci. 853, 103-115.

Young, H. S., J.L. Rigaud, J.J. Lacapere, L.G. Reddy and D.L. Stokes 1997. How to make tubular crystals by reconstitution of detergent-solubilized Ca2(+)-ATPase. Biophys. J. 72, 2545-2558.

Zamoon, J., A. Mascioni, D.D. Thomas and G. Veglia 2003. NMR solution structure and topological orientation of monomeric phospholamban in dodecylphosphocholine micelles. Biophys. J. 85, 2589-2598.

Zamoon, J., F. Nitu, C. Karim, D.D. Thomas and G. Veglia 2005. Mapping the interaction surface of a membrane protein: Unveiling the conformational switch of phospholamban in calcium pump regulation. Proc. Natl. Acad. Sci. U. S. A. 102, 4747-4752.

Zech, S. G., A.J. Wand and A.E. McDermott 2005. Protein structure determination by high-resolution solid-state NMR spectroscopy: Application to microcrystalline ubiquitin. J. Am. Chem. Soc. 127, 8618-8626.

Zhang, H., S. Neal and D.S. Wishart 2003. RefDB: A database of uniformly referenced protein chemical shifts. J. Biomol. NMR. 25, 173-195.

Zhao, X., S. Hu, J. Li, Y. Mou, K. Bian, J. Sun and Z. Zhu 2008. rAAV-asPLB transfer attenuates abnormal sarcoplasmic reticulum Ca2+-ATPase activity and cardiac dysfunction in rats with myocardial infarction. European Journal of Heart Failure,. 10, 47-54.

Zhou, Y., T. Cierpicki, R.H. Jimenez, S.M. Lukasik, J.F. Ellena, D.S. Cafiso, H. Kadokura, J. Beckwith and J.H. Bushweller 2008a. NMR solution structure of the integral membrane enzyme DsbB: Functional insights into DsbB-catalyzed disulfide bond formation. Mol. Cell. 31, 896-908.

Zhou, Y., T. Cierpicki, R.H. Jimenez, S.M. Lukasik, J.F. Ellena, D.S. Cafiso, H. Kadokura, J. Beckwith and J.H. Bushweller 2008b. NMR solution structure of the integral membrane enzyme DsbB: Functional insights into DsbB-catalyzed disulfide bond formation. Mol. Cell. 31, 896-908.